Ghent University
Faculty of Sciences
Department of Plant Biotechnology and Genetics
Department of Applied Mathematics and
Computer Science

MODELING AUXIN FEEDBACK SIGNALING FOR POLARIZED AUXIN TRANSPORT IN PLANT DEVELOPMENT

Krzysztof Teodor Wabnik

Promotors: Willy Govaerts and Jiří Friml

17th of June 2011

Thesis submitted in partial fulfillment of
the requirements for the degree of
Doctor (Ph.D.) in Biotechnology
Academic year 2010-2011

The CD-ROM accompaning this thesis, contains the Supplementary
Movies (Chapters 2-5) in QuickTime file format and electronic version of this thesis (PDF format).

Research presented in this thesis was
performed at the University of Ghent,
VIB, Department of Plant Systems Biology

Promotors:

Prof. Willy Govaerts
Department of Applied Mathematics and Computer Science, Ghent University
Krijgslaan 281 -S9
B-9000 Gent, Belgium
Phone: +32 (0)9 264 48 93
Willy.Govaerts@UGent.be

Prof. Jiří Friml
Department of Plant Biotechnology and Genetics, Ghent University
Department of Plant Systems Biology, VIB
Technologiepark 927
B - 9052 Gent, Belgium
Phone: +32 (0)9 33 13 913
jifri@psb.vib-ugent.be

Examination commision:

Prof. Ann Depicker (chair)
Department of Plant Biotechnology and Genetics, Ghent University
Department of Plant Systems Biology, VIB
Technologiepark 927
B - 9052 Gent, Belgium
Phone: + 32 (0)9 33 13 940
anpic@psb.vib-ugent.be

Dr. Jürgen Kleine-Vehn
1. Department of Plant Biotechnology and Genetics, Ghent University
Department of Plant Systems Biology, VIB
Technologiepark 927
B - 9052 Gent, Belgium
2. Institute of Applied Genetics and Cell Biology (IAGZ)
Muthgasse 18
A-1190, Wien, Austria
Phone: +32 (0)9 33 13946
jurgen.kleine-vehn@psb.vib-ugent.be, juergen.kleine-vehn@boku.ac.at

Prof. Tom Beeckman
Department of Plant Biotechnology and Genetics, Ghent University
Department of Plant Systems Biology, VIB

Technologiepark 927
B - 9052 Gent, Belgium
Phone: + 32 (0)9 33 13 930
tobee@psb.vib-ugent.be

Dr. Eva Benková
Department of Plant Biotechnology and Genetics, Ghent University
Department of Plant Systems Biology, VIB
Technologiepark 927
B - 9052 Gent, Belgium
Phone: +32 (0)9 33 13 871
evben@psb.vib-ugent.be

Asst. Prof. Dr. Eric Kramer
Physics Department, Bard College at Simons Rock,
Great Barrington, MA 01230, USA
Phone: 413-528-7476
ekramer@simons-rock.edu

Asst. Prof. Dr. Richard S. Smith
Department of Plant Sciences, University of Bern
Altenbergrain 21
CH-3013, Bern
Phone: +41 31 631 5223
richard.smith@ips.unibe.ch

Prof. Marnix Van Daele
Ghent University
Department of Applied Mathematics and Computer Science, Ghent University
Krijgslaan 281 -S9
B-9000 Gent, Belgium
Phone: +32 9 264 48 09
Marnix.VanDaele@UGent.be

"A scientist in his laboratory is not a mere technician: he is also a child confronting natural phenomena that impress him as though they were fairy tales."

-Marie Curie

Contents

Preface

"Plants are extraordinary. For instance ... if you pinch a leaf of a plant you set off an electrical impulse. You can't touch a plant without setting off an electrical impulse ... There is no question that plants have all kinds of sensitivities. They do a lot of responding to an environment. They can do almost anything you can think of."

— Barbara McClintock

Plants are fascinating biological systems with a great potential for adaption of their developmental programs to environmental cues. In contrast to animals, plants cannot run away and thus they had to develop specialized mechanisms to react to rapid changes in the environment. These plant-specific mechanisms including light perception, tropism and developmental reprogramming (*de novo* organ formation, tissue re-shaping), represent highly dynamic regulatory processes that are linked and intertwined on the molecular, cellular and tissue levels. The ultimate communication between these different levels is the key to understand how plants realize their developmental decisions. Cell signaling, tissue polarization, directional transport of signaling molecules within tissues are among those biological processes that allow for such multilevel organization in plant development. Nevertheless our understanding of these processes remains largely elusive.

This doctoral thesis demonstrates the results of multidisciplinary studies at the interface between several scientific disciplines, including mathematics, computer science (under supervision of Prof. Willy Govaerts) and cell and developmental biology (under guidance of Prof. Jiří Friml). Therefore, I will utilize state-of-the-art mathematical and computational techniques combined with the most recent biological data to address cell and tissue polarities as well as graded distribution patterns of the plant phytohormone auxin, in the context of plant developmental flexibility. The main goal of the research presented herein was to explore general principles of auxin feedback regulation and its outstanding roles in auxin-driven plant development. A special focus was given to the combination of local auxin signaling cues (inside and outside of the cell), subcellular dynamics (trafficking of auxin carriers) and cell-type specific factors (spatial patterns of gene activity) to account for the developmental patterns observed *in planta* such as canalization of auxin transport, leaf venation patterning, tissue regeneration and establishment and maintenance of cell and tissue polarities. The core of the thesis will start with a general introduction to the models for auxin-mediated plant development and will be followed by presentation of various scientific results and their potential implications for hopefully better understanding of patterning mechanisms in plants. Finally, the summarizing chapter of this thesis aims to translate the results of these various studies to the more general concept of the local auxin feedback regulation in plants.

The research presented in this thesis has been gathered over the last 2 years of my doctoral training. The results of my first two years of research are not directly related to the main results presented in this thesis. Therefore, I decided to not enclose them in this book. Instead, I refer to the publication list in Chapter - General remarks.

Brief summary

Multiscale modeling frameworks aim to integrate multiple levels of biological organization (molecular, cellular and tissue scale) to investigate how the cross-regulation of these levels leads to fascinating beauty of biological patterning. Importantly, they allow us to make predictions which can often be translated back to the laboratory to stimulate further experimental research. Here, we utilize theoretical and modeling approaches grounded on the experimental data on auxin transport, auxin signaling and trafficking mechanisms of PIN auxin efflux carrier to predict, analyze and understand PIN polarization and auxin distribution patterns during auxin-mediated plant development. The comprehensive introduction to the research topic is presented in **Chapter 1**.

Chapter 1 contains a comprehensive review of recent theoretical and experimental insights into mechanisms underlying PIN polar distributions in cells during auxin-driven plant development. These models for PIN polarization are confronted with the latest experimental insights into PIN trafficking processes. We highlight the ongoing evolution and adaptation of theoretical concepts for PIN polarization to better support experimental observations.

"A key question of developmental biology relates to a fundamental issue in cell and tissue polarities, namely, how an individual cell in a polarized tissue senses the polarities of its neighbors and its position within tissue" - an attempt to address this intriguing question is one of the major challanges of developmental biology. A special focus was given to a novel concept: the synergistic coupling of intracellular and extracellular auxin signaling pathways to address PIN polarization events during plant development (**Chapter 2**). The results and implications of our modeling investigation of this novel PIN polarization framework are presented in **Chapter 2**. Remarkably, our model predictions were used to investigate the potential role of extracellular auxin signaling on PIN trafficking (Robert *et al*., 2010), highlighting not only the explanatory but also the predictive power of the proposed PIN polarization concept.

In **Chapter 3** of this doctoral thesis, we investigate in depth and reveal experimentally and theoretically, the complex mechanism underlying the maintenance of PIN polarization in plant cells. We discuss individual roles of PIN trafficking processes in the establishment and maintenance of cell polarity in plant cells, highlighting essential differences to those mechanisms that operate in animal or yeast cells. We found that spatially restricted internalization of PIN proteins and reduced lateral diffusion of PIN proteins in the plasma membrane of the cell are crucial for the maintenance of polar domains in plants. Moreover, we suggest that the mechanism for spatially defined PIN internalization could involve a positive feedback loop such as that presented in **Chapter 2** of this thesis.

In the following **Chapter 4**, we travel back in time by focusing on the evolution of polar auxin transport. We stimulate an open debate on the function of polar auxin transport in non-vascular plant such as mosses that are evolutionarily older that flower-

ing plant species. We propose a novel plausible model for ancient auxin transport in the moss *Physcomitrella patens (Bryophyta)* that could be an alternative to known polar transport mechanisms in the flowering plant *A. thaliana*. We also speculated in depth, on the evolutionarily plausible scenario that the translocations of PIN auxin carriers and receptor-based auxin signaling from the lumen of Endoplasmic reticulum (ER) to the plasma membrane could not only be evolutionarily but also functionally connected.

Finally, in **Chapter 5,** we suggest the novel mechanism for a gradient-guided auxin pattering in the root meristem that utilizes the synergy of PIN-dependent polar auxin transport and a feedback loop between auxin accumulation in the root and the activity of the master organizer of root stem cells. The multilevel feedback model provides a conceptual framework for how an auxin maximum is spatially restricted to the root quiescent centre (QC) cells and robustly maintained during growth and developmental patterning of the root. We propose that similar conserved mechanisms could operate during embryogenesis and the patterning of plant shoot meristems.

In conclusion, this thesis presents new insights into mechanisms underlying polarized auxin transport and auxin-driven patterning in plants. We demonstrate that associated auxin gradients can be coordinated, synchronized and maintained in the tissue context from the concerted action of polar auxin transport, local feedback auxin signalling and cell type-specific factors. Moreover, this thesis aims to link evolution and function of feedback mechanisms underlying auxin patterning in the development of land plant species. Finally, the summarizing discussion that connects different studies shown in this thesis is presented in **Chapter 6** (Conclusions and perspectives).

Chapter 1

Feedback models for polarized auxin transport:

an emerging trend

"The sciences do not try to explain, they hardly even try to interpret, they mainly make models. By a model is meant a mathematical construct which, with the addition of certain verbal interpretations, describes observed phenomena. The justification of such a mathematical construct is solely and precisely that it is expected to work—that is, correctly to describe phenomena from a reasonably wide area."

— **John von Neumann**

FEEDBACK MODELS FOR POLARIZED AUXIN TRANSPORT
AN EMERGING TREND

Krzysztof Wabnik[1,2,4], Willy Govaerts[4] , Jiří Friml[1,2] and Jürgen Kleine-Vehn[1,2,3]

Molecular Biosystems, 2011, in press

[1]Department of Plant Systems Biology, VIB, 9052 Gent, Belgium
[2]Department of Plant Biotechnology and Genetics, Ghent University, 9052 Gent, Belgium
[3]Department of Applied Genetics and Cell Biology, University of Applied Life Sciences and Natural Resources (BOKU), 1190 Vienna, Austria
[4]Department of Applied Mathematics and Computer Science, Ghent University, 9000 Gent, Belgium

ABSTRACT

The phytohormone auxin is vital to plant growth and development. A unique property of auxin among all other plant hormones is its cell-to-cell polar transport that requires activity of polarly localized PIN-FORMED (PIN) auxin efflux transporters. Despite the substantial molecular insight into the cellular PIN polarization, the mechanistic understanding for developmentally and environmentally regulated PIN polarization is scarce. The long-standing belief that auxin modulates its own transport by means of a positive feedback mechanism has inspired both experimentalists and theoreticians for more than two decades. Recently, theoretical models for auxin-dependent patterning in plants include the feedback between auxin transport and the PIN protein localization. These computer models aid to assess the complexity of plant development by testing and predicting plausible scenarios for various developmental processes that occur *in planta.* Although the majority of these models rely on purely heuristic principles, the most recent mechanistic models tentatively integrate biologically testable components into known cellular processes that underlie the PIN polarity regulation. The existing and emerging computational approaches to describe PIN polarization are presented and discussed in the light of recent experimental data on the PIN polar targeting.

1.1 INTRODUCTION

Auxin is a small plant signaling molecule that coordinates plant growth and patterning. Charles and Francis Darwin's pioneering work on phototropic bending of canary grass (*Phalaris canariensis*) and oat (*Avena sativa*) coleoptiles led finally to the discovery of this plant hormone (Darwin and Darwin, 1880). Darwin's experiments envisioned the existence of a mobile, signaling substance that allows the flexible growth of plants that was later isolated and designated auxin (from the Greek "auxein" for to grow) (Kögl and Kostermans, 1934; Went, 1974). Numerous experimental studies indicated dose-dependent auxin responses, including growth promotion (Haagen-Smit *et al.*, 1946; Jones *et al.*, 1998; Jones *et al.*, 2009; Xu *et al*., 2010), axis formation during embryogenesis (De Smet and Jürgens, 2007; Friml *et al.*, 2003), *de novo* organ positioning (Heisler *et al.*, 2005; Kuhlemeier, 2007; Reinhardt *et al.*, 2003) and tropism (Abas *et al.*, 2006; Ding *et al.*, 2011; Friml *et al.*, 2002b; Kleine-Vehn *et al.*, 2010). Local auxin distributions (auxin gradients) are established and maintained by local auxin metabolism (biosynthesis, conjugation and degradation) and cell-to-cell polar auxin transport and appear to serve as biological signals to instruct morphogenesis, generate developmental outputs and determine cellular fates (Benková *et al.*, 2003; Blilou *et al.*, 2005; Friml *et al.*, 2002a; Grieneisen *et al.*, 2007; Ljung *et al.*, 2005; Sabatini *et al.*, 1999; Sorefan *et al.*, 2009; Stepanova *et al.*, 2008).

In 1969, Tsvi Sachs proposed the canalization hypothesis that describes the feedback between auxin and its own transport within tissues (Sachs, 1969). Sachs assumed that high auxin flux across cells enhances their capacity for polar auxin transport and subsequently leads to the formation of vascular strands. By using a subset of elegant experimental approaches, including local auxin applications during vascular development and regeneration in plants, Sachs was able to demonstrate the feasibility of his hypothesis (Sachs, 1969; Sachs, 1981). These highly inspirational studies resulted in the formulation of the pioneering mathematical feedback models for auxin transport-driven patterning in plant development (Mitchison, 1980; Mitchison, 1981). Interestingly, these first models forecasted the existence of polarly localized, putative auxin efflux carriers (Goldsmith *et al.*, 1981; Mitchison, 1981; Raven, 1975; Rubery and Sheldrak.Ar, 1974) and opened a new research direction in the auxin biology.

By means of forward genetics, the PIN auxin efflux carriers (Wiśniewska *et al.*, 2006) have been discovered that display the predicted polar localization at the plasma membrane (Berleth and Sachs, 2001; Galweiler *et al.*, 1998; Lomax *et al.*, 1995; Okada *et al.*, 1991). PIN polarization is crucial to facilitate the direction of the intercellular auxin transport (Petrášek *et al.*, 2006; Zhang *et al.*, 2010) and, thus, to maintain the auxin gradients within tissues (Benjamins and Scheres, 2008). PIN polarization and abundance at the plasma membrane depend on various vesicle transport-dependent processes, such

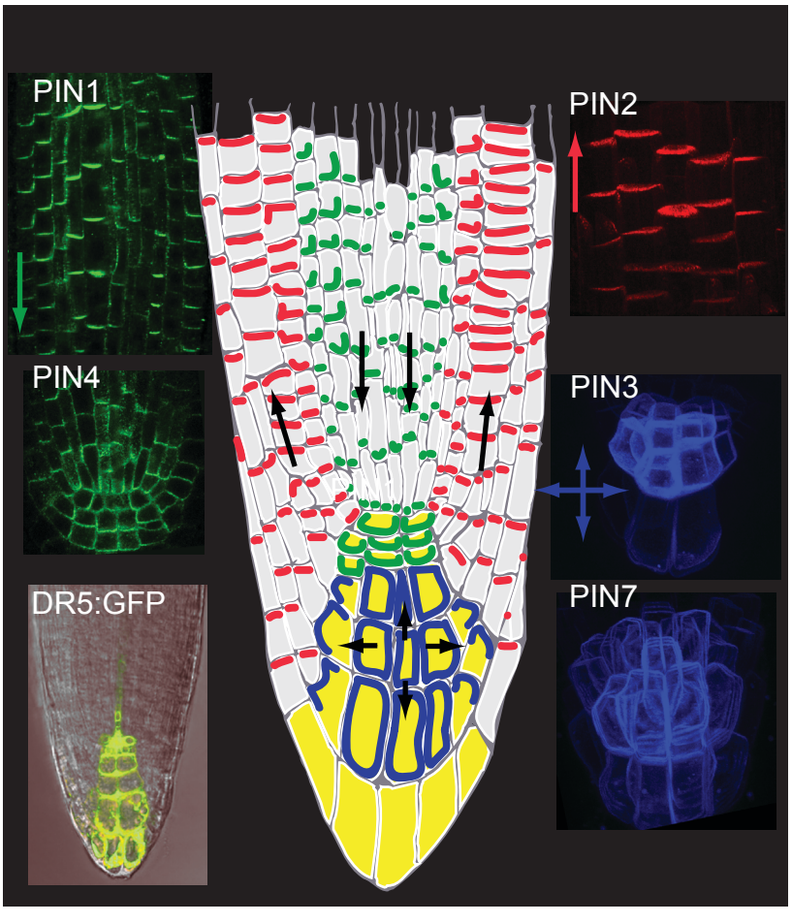

Figure 1 PIN protein and auxin distributions in the *Arabidopsis* root

Schematic and localization of PIN protein distribution in the root meristem. The auxin gradient in the root tip is shown in yellow. PIN1 and PIN4 (in green) direct acropetal auxin flow in the root stele (black arrows). PIN2 is shown in red and mediates basipetal auxin flow through the root epidermis (black arrows). PIN3 and PIN7 (in blue) are mainly expressed in root columella cells and display largely non-polar localizations.The root tip-associated auxin maximum is demonstrated with the synthetic auxin response reporter (DR5:GFP).

as the constitutive cycling of PIN proteins (Dhonukshe *et al.*, 2007; Geldner *et al.*, 2001; Kleine-Vehn *et al.*, 2008a; Kleine-Vehn *et al.*, 2009; Paciorek *et al.*, 2005; Robert *et al.*, 2010; Tanaka *et al.*, 2009), *de novo* protein secretion (Dhonukshe *et al.*, 2008; Heisler *et al.*, 2005; Vieten *et al.*, 2005) and protein degradation in lytic vacuoles (Abas *et al.*, 2006; Kleine-Vehn *et al.*, 2008b; Laxmi *et al.*, 2008).

Interestingly, recent studies demonstrated that the member of PIN protein family PIN5 does not localize to the plasma membrane, but to the Endoplasmic reticulum (ER) where it regulates auxin transport from the cytosol into the ER lumen, being instructive for intracellular auxin homeostasis (Mravec *et al.*, 2009). PIN5 might furthermore control the cytosolic availability of auxin for the export from cells (Friml and Jones, 2010).

Despite the substantial molecular insight into the regulation of the PIN targeting (for an in depth review, see Grunewald and Friml, 2010), the unifying mechanism to explain the PIN polarization in response to developmental and environmental cues is still elusive. Although thanks to these recent experimental discoveries, several theoretical concepts have evolved and been adapted.

Experimentally inspired, hypothesis-driven computer models can generate verifiable predictions that could guide the design of wet-lab experiments. Here, we summarize and discuss the simultaneous advances of experimental and computational approaches addressing the PIN polarity in auxin-driven plant development.

1.2 PIN POLARITY AND THE CONCEPTUAL PROBLEM

PIN proteins determine the rate and direction of the polar auxin transport (Petrášek *et al.*, 2006; Wiśniewska *et al.*, 2006). Therefore, the most of computational models for polar auxin transport mechanisms concentrated largely on the PIN-dependent formation of conductive auxin channels. However, during simultaneously occurring processes, such as the PIN1 polarization during phyllotaxis (positioning of leaves and flowers around plant meristems) and leaf vascular development, PIN proteins often display a diverse behavior (Bayer *et al.*, 2009; Heisler *et al.*, 2005; Reinhardt *et al.*, 2003). The PIN1 protein can polarize either towards or away from the auxin accumulation site during phyllotaxis (up-the-auxin gradient polarization) and during the venation patterning (with-the-flow polarization), respectively. Analogously, PIN1 and PIN2 polarize towards and away from the auxin maxium in the root vasculature and root epidermis, respectively, directing the acropetal and basipetal auxin flows in the root (Benjamins and Scheres, 2008; Blilou *et al.*, 2005; Grieneisen *et al.*, 2007; Kleine-Vehn and Friml, 2008) (Figure 1).

Currently, there is no mechanistic explanation for these striking phenomena of adverse PIN polarizations. Hence, theoretical models to test the whole spectrum of possible scenarios have been developed with the common assumption of a positive feedback between auxin and the PIN protein activity.

1.3 MULTIPLE LEVELS OF AUXIN FEEDBACK ON THE PIN PROTEIN ACTIVITY

The concept of a positive auxin feedback mechanism for the regulation of the polar auxin transport has a deep-rooted history in auxin research (Leyser, 2006). The transcription of PIN auxin carriers is under the direct control of auxin (Heisler *et al.*, 2005; Scarpella *et al.*, 2006; Vieten *et al.*, 2005). Hence, auxin-induced PIN transcription (Vieten *et al.*, 2005) could represent the important component of positive feedback loop for the auxin

canalization (Heisler *et al*., 2005; Scarpella *et al*., 2006; Vieten *et al*., 2005), namely via its binding to the nuclear auxin receptors TRANSPORT INHIBITOR RESPONSE 1/ AUXIN SIGNALLING F-BOX (TIR1/AFB) (Chapman and Estelle, 2009).

Auxin-inducible gene expression is generally facilitated by the auxin response factors (ARFs), a family of auxin-responsive transcription factors (Gray *et al*., 2001) and the auxin/indole-3-acetic acid (Aux/IAA) transcriptional repressors (Tan *et al*., 2007). Upon auxin binding, nuclear TIR1/AFB auxin receptors release the Aux/IAA-dependent repression of auxin responses by targeting the Aux/IAA proteins for proteasome-dependent degradation (Dharmasiri *et al*., 2005; Kepinski and Leyser, 2005a; Kepinski and Leyser, 2005b). The auxin transcriptional responses occur within 15 minutes to 2 hours and, thus, provide a means for the slow feedback signaling on the auxin carrier levels in cells (Chapman and Estelle, 2009).

Yet another level of auxin feedback on PIN activity has been proposed (Paciorek *et al*., 2005; Robert *et al*., 2010), namely that auxin enhances its own efflux by the modulation of the PIN protein trafficking (Paciorek *et al*., 2005). Remarkably, this auxin-mediated inhibition of the PIN protein internalization from the plasma membrane occurs within minutes (fast response) and is independent of the TIR1/AFB-dependent pathways (Robert *et al*., 2010).

A good candidate for the auxin-mediated inhibition of PIN internalization is the putative auxin receptor AUXIN BINDING PROTEIN1 (ABP1) (Napier *et al*., 2002). ABP1 has been suggested to reside in the lumen of the endoplasmic reticulum and to be partially secreted to the cell walls (Napier *et al*., 2002; Tromas *et al*., 2010) where it is physiologically active (Leblanc *et al*., 1999; Steffens *et al*., 2001), but its function in the auxin signaling remained an open question (Tromas *et al*., 2010). ABP1 appears to be a positive regulator of clathrin-dependent internalization of plasma membrane proteins, including the PIN proteins (Robert *et al*., 2010). Intriguingly, auxin binding to ABP1 presumably inhibits the action of ABP1 on the clathrin machinery (Robert *et al*., 2010).

These experimental data illustrate that the proposed auxin feedback mechanisms for the formation of conductive auxin channels may rely on auxin-dependent control of the PIN abundance via both the regulation of PIN transcription and PIN trafficking.

1.4 FEEDBACK MODELS FOR POLARIZED AUXIN TRANSPORT

1.4.1 WITH-THE-FLOW MODELS

Inspired by the complex beauty of vascular patterns in plant leaves, Tsvi Sachs proposed the theoretical feedback mechanism by which auxin transport could be self-enhanced by the dominant auxin flux in the tissues (Sachs, 1981).

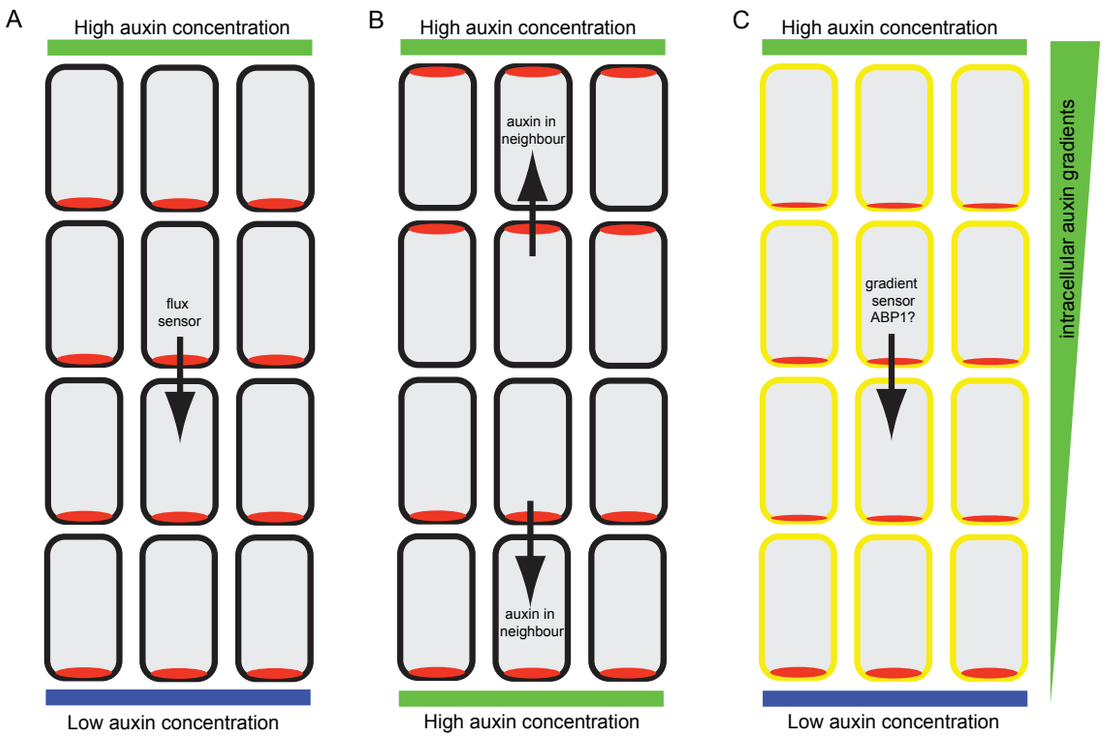

Figure 2 Overview of the theoretical mechanisms for the PIN polarization

(A) Classical canalization hypothesis (Mitchison, 1981; Rolland-Lagan and Prusinkiewicz, 2005; Sachs, 1981). Feedback mechanism for the PIN polarization incorporates a flux-sensing component. The with-the-flow models utilize this, yet to be identified, flux sensor to measure ongoing auxin fluxes across the plasma membrane (black arrow). In cells, the PIN proteins polarize along these fluxes (red), eventually leading to the formation of conductive auxin channels and connecting an auxin source (green) to an auxin sink (blue). **(B)** The up-the-gradient mechanism (Jönsson *et al.*, 2006; Smith *et al.*, 2006) Intercellular signaling for sensing auxin concentrations in neighboring cells (black arrow) is incorporated indirectly. Cells are polarized (PIN proteins in red) towards the adjacent cell with the highest auxin concentration (green). This hypothesis was based on the live-imaging of the PIN polarity and DR5 auxin reporter during the *de novo* organization of leaves and flowers on the surface of shoot meristems (Heisler *et al.*, 2005; Reinhardt *et al.*, 2003). **(C)** Gradient-based model for PIN polarization (Kramer, 2009). Internal auxin concentrations gradients (green) are included as a cell-autonomous signal to polarize the PIN proteins (red). These intracellular auxin gradients could be sensed by a dedicated auxin receptor, i.e. the ABP1 protein. PIN proteins are aligned to the side of the cell where the auxin concentration is the lowest (black arrow). This coordination of PIN polarity in cells starts near the auxin sink (blue) and proceeds towards the auxin source (green). Polarized cells in the conductive channels maintain high auxin concentrations by the AUX/LAX-dependent auxin import into these cells (orange).

This scenario is analogous with that of a water stream draining channels into the river systems (thus the name canalization). The Mitchison's computer model of venation patterning (Mitchison 1980, 1981) proposes that auxin canalization could be realized either through facilitated diffusion mechanism or by a hypothetical flux-sensing component that is crucial for the coordination of polarized auxin transport routes (Mitchison 1981). The flux sensor was abstracted in a pioneer mathematical model for vascular patterning (Mitchison 1981), in which the capacity of the auxin transport mediated by putative polar efflux transporters is assumed to increase nonlinearly with the auxin flux measured in cells. *In silico*, such a scenario results in auxin canalization into discrete channels (Mitchison, 1981), similarly to those observed during vascular development in plant leaves (Sachs, 1981; Scarpella *et al.*, 2006).

After the PIN proteins had been identified and characterized, the canalization-based, also termed with-the-flow models, have been adapted to incorporate a theoretical, positive feedback between the auxin flux and the allocation of the PIN proteins at the plasma membrane (Feugier *et al.*, 2005; Fujita and Mochizuki, 2006; Rolland-Lagan and Prusinkiewicz, 2005). However, the constitutive PIN recycling mechanism (Dhonukshe *et al.*, 2007; Geldner *et al.*, 2001) had rarely been integrated into these models (Feugier *et al.*, 2005).

The with-the-flow models (reviewed in Rolland-Lagan and Prusinkiewicz, 2005) (Figure 2A) are capable of reproducing the unprecedented range of leaf venations and shoot branching patterns that occur *in planta* (Berleth and Sachs, 2001; Prusinkiewicz *et al.*, 2009; Scarpella *et al.*, 2006), including connected veins, first-order vein loops and discontinuous vascular strands in mutants (Rolland-Lagan and Prusinkiewicz, 2005; Sauer *et al.*, 2006; Scarpella *et al.*, 2006). Computer simulations of these models predict narrow domains of the PIN expression in provascular cells, faithfully reproducing/predicting experimental findings (Sauer *et al.*, 2006; Scarpella *et al.*, 2006).

Classical with-the-flow models predict the appearance of low auxin concentrations in developing veins (Fujita and Mochizuki, 2006; Rolland-Lagan and Prusinkiewicz, 2005) in contradiction with the experimental observations of high auxin content in leaf veins (Scarpella *et al.*, 2006). To assess these shortcomings of the model, a fixed number of PIN proteins *per* cell and the competition of cell sides for intracellular pool of PINs were assumed that led to high auxin concentrations in fully developed veins (Feugier *et al.*, 2005). Another model, in which the AUX/LAX auxin influx carriers (Bennett *et al.*, 1996) were proposed to facilitate the accumulation of auxin in the provascular cells (Kramer, 2004). The progression of the basal PIN1 polarization in provascular cells that is predicted by with-the-flow models (Rolland-Lagan and Prusinkiewicz, 2005) can start either from the auxin sink (preexisting vasculature) or from the auxin source, reproducing experimental observations (Reinhardt *et al.*, 2003; Sauer *et al.*, 2006; Scarpella *et al.*, 2006).

PIN1 proteins have a diverse behavior during phyllotaxis and midvein formation that occur simultaneously (Bayer *et al.*, 2009; Reinhardt *et al.*, 2003). During midvein formation, the PIN proteins show a basal polarization in provascular cells as already mentioned, but in surrounding tissues they polarize towards the adjacent cells with high auxin concentrations (Reinhardt *et al.*, 2003). This converse PIN polarization could not be predicted with with-the-flow models. Recently, the with-the-flow model has been revised by postulating weak and strong regimes of auxin feedback on the PIN protein distribution (Stoma *et al.*, 2008). The weak regime was used together with the hypothetical assumption of an auxin sink, at the side of the auxin accumulation (also called auxin convergence point) to predict the PIN1 orientation upwards in the auxin gradient, whereas the strong regime was used to explain the PIN1 polarization in the leaf vasculature (Stoma *et al.*, 2008). Although with-the-flow models faithfully predicted the auxin canalization during vascular development, these canalization models failed to describe the PIN1 polarization observed in leaves and flowers (Bayer *et al.*, 2009; Reinhardt *et al.*, 2003), hinting at the possibility of alternative feedback and/or cell-type specific mechanisms.

1.4.2 UP-THE-GRADIENT MODELS

A concentration-based mechanism for the PIN polarization (Jönsson *et al.*, 2006; Smith *et al.*, 2006) was inspired by the experimental observation of PIN polarization during phyllotaxis (Reinhardt *et al.*, 2003). In the so-called up-the-gradient model the PIN proteins preferentially orient toward the cell side that faces the neighboring cell with the highest auxin concentration (Jönsson *et al.*, 2006; Smith *et al.*, 2006) (Figure 2B). This model assumes the existence of a hypothetical short-range intercellular signaling pathway for gathering of information on auxin content in surrounding tissues (Jönsson *et al.*, 2006; Smith *et al.*, 2006). This non-cell autonomous sensing of auxin concentrations is utilized to regulate the PIN protein abundance at the plasma membrane. Unlike the with-the-flow models (Rolland-Lagan and Prusinkiewicz, 2005), several versions of the up-the-gradient model implemented the constitutive recycling of PIN proteins between plasma membrane and internal cellular compartments (Ibañes *et al.*, 2009; Jönsson *et al.*, 2006; Merks *et al.*, 2007; Sahlin *et al.*, 2009).

The up-the-gradient model (Figure 2B) simulations on growing tissue layouts faithfully and robustly reproduced a stunning variety of phyllotactic patterns. These simulations largely reproduced *in planta* patterning, including spiral, distichous, decussate, and tricussate phyllotaxis (Kuhlemeier, 2007; Smith *et al.*, 2006). The apparent switch from one phyllotactic pattern to the other could be obtained solely by manipulating the model parameters (Smith *et al.*, 2006). Interestingly, the up-the-gradient models

suggested that if the amount of PIN proteins in the cells were not fixed but gradually increased with auxin concentrations, the predicted auxin convergence points could be unstable (Heisler and Jonsson, 2006), hinting at possible role of auxin influx carriers in the stabilization of phylotactic patterns (Bainbridge *et al*., 2008). In addition, an unifying mechanism for the PIN polarization has been recently proposed (Merks *et al*., 2007). An auxin-induced PIN expression has been incorporated in the up-the-gradient model to predict the PIN polarization events during phylotaxis and midvein formation (Merks *et al*., 2007), giving an intriguing explanation for auxin flow canalization. However, this predicted phenomenon, namely the wave-causing movement of auxin inside vascular tissues of leaves, has not yet been experimentally demonstrated.

Generally, up-the-gradient models tend to be more robust than the with-the-flow (canalization) models with a flux sensor, especially in the view of perturbations of model parameters.

1.4.3 COMBINED POLARIZATION MECHANISMS

To reconcile both PIN polarization towards and away from an auxin maxima, the with-the-flow and up-the-gradient models for the PIN polarization were integrated (Bayer *et al*., 2009). In the combined model, cells are able to sense both auxin fluxes and auxin concentrations to polarize the PIN proteins. The dominating mechanism is activated based on the actual auxin content of particular cells (Bayer *et al*., 2009). Accordingly, cells with low auxin concentrations follow the "up-the-gradient" mode, whereas cells with high auxin concentration utilize the "with-the-flow" mechanism (Bayer *et al*., 2009). Remarkably, the combined model represents the first computational approach that has been able to reproduce in details the whole spectrum of PIN polarization events observed during simultaneous processes of phyllotaxis and leaf vein patterning. The model predicts the basal PIN polarization in provascular cells and the inner-lateral PIN polarization in tissues that circumvent vasculature to facilitate auxin accumulation in veins (Bayer *et al*., 2009). The common shortcoming of the with-the-flow models implemented on the realistic cellular tissues is that they tend to fail connecting auxin source to an auxin sink. To address this model limitation Bayer *et al* (Bayer *et al*., 2009) proposed in their model the hypothetical diffusible substances to guide the propagation of a developing vein towards the auxin sink (preexisting vasculature). Although, the presence of cell-type specific factors that control vein progression might be plausible, it requires further experimental investigation.

The with-the-flow (Feugier *et al*., 2005; Fujita and Mochizuki, 2006; Mitchison, 1981; Rolland-Lagan and Prusinkiewicz, 2005; Stoma *et al*., 2008), up-the-gradient models (Ibañes *et al*., 2009; Jönsson *et al*., 2006; Merks *et al*., 2007; Sahlin *et al*., 2009;

Smith *et al.*, 2006) and their recent combination (Bayer *et al.*, 2009) need the integration of hypothetical molecular components to realize auxin-sensing mechanisms. In the with-the-flow models, a molecular component for flux sensors has not been identified yet, whereas in up-the-gradient models, an elaborate intercellular signaling pathways have recently been suggested (Bilsborough *et al.*, 2011; Heisler *et al.*, 2010), namely a hypothetical biomechanical sensor that acts upstream of the PIN1 localization and microtubule array orientation (Heisler *et al.*, 2010). As high auxin concentrations could contribute to strong cell wall acidification and subsequent relaxation in local cell walls, the PIN proteins would polarize according to biomechanical tensions towards the cell wall with the highest auxin levels (Heisler *et al.*, 2010).

Another computational model to particularly describe leaf margin development (Bilsborough *et al.*, 2011) incorporates two auxin feedback mechanisms that work in concert: the first feedback is realized by the up-the-gradient model for the PIN polar localization (Bilsborough *et al.*, 2011), whereas the second mechanism consists of the negative feedback signaling on the expression of the *CUP-SHAPED COTYLEDON2* (*CUC2*) transcription factor (Bilsborough *et al.*, 2011). This conceptually novel combination of the auxin signaling could account for stable leaf serration patterns (Bilsborough *et al.*, 2011).

The formulation of combined polarization mechanism resulted in stunning insights and greatly stimulated wet lab research activities (Bayer *et al.*, 2009; Heisler *et al.*, 2010; Bilsborough *et al.*, 2011).

1.4.4 GRADIENT-BASED PIN POLARIZATION

The common shortcoming of all PIN polarization models discussed so far is the lack of molecular components for the respective PIN polarization mechanisms. To address this issue, the polar signal for PIN proteins was proposed to be generated by directional sensing of a intracellular auxin gradient (Kramer, 2009) (initially indicated by Mitchison, 1980, 1981) (Figure 2C). This model implies that PIN proteins are presumably targeted to the cell side with the lowest cytoplasmic auxin concentration. As the model includes the recycling of PIN proteins between the plasma membrane and the intracellular compartments, the process of PIN polarization might be facilitated by resorting of the PIN proteins to the given cell side (Kramer, 2009). This model has been successfully applied to leaf venation patterning and suggests that ABP1 might be a gradient sensor inside the cell (Kramer, 2009). In such a scenario, auxin would bind to ABP1 inside the cell and promote PIN translocation from the region of high auxin concentrations to that of low auxin concentrations (Kramer, 2009) (Figure 2C). This mechanistic gradient-based model explicitly integrates the local activity of auxin influx trans-

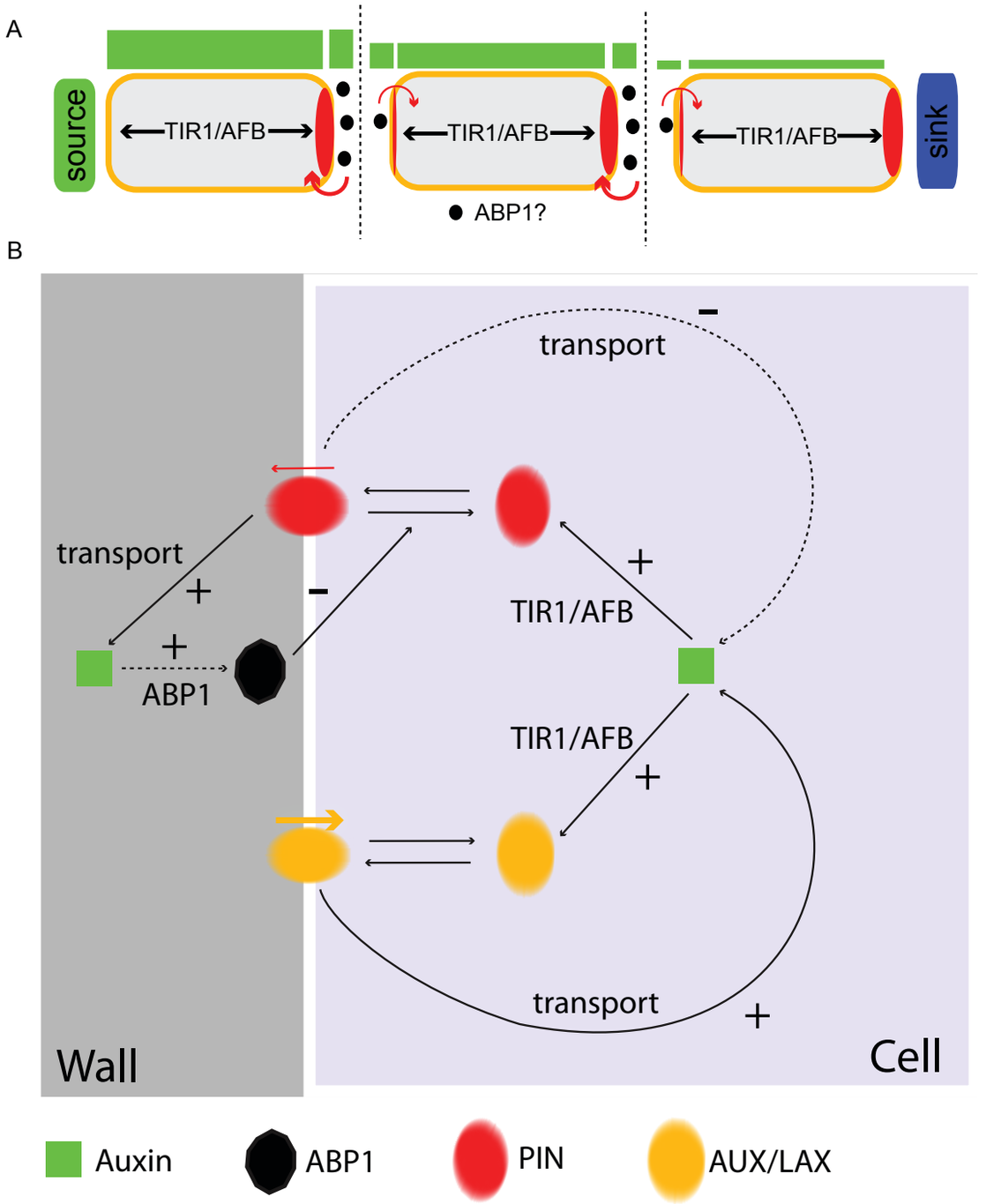

Figure 3 Synergy of intracellular and extracellular auxin signaling for PIN polarization

(A) Schematic extracellular receptor-based polarization (ERP) model (Wabnik *et al.*, 2010). The model integrates the intracellular TIR-dependent auxin signaling for the regulation of the PIN expression and presumably the ABP1-dependent extracellular auxin signaling for the inhibition of the PIN protein internalization (PIN proteins at the plasma membrane in red; extracellular ABP1 in black). The concerted alignment of the PIN polarity within tissues results from local differences in auxin signaling in the cell wall (red arrows) and *de novo* PIN synthesis (black arrows). Asymmetry in the extracellular auxin signaling is generated by the competitive utilization

of ABP1 receptors in the cell wall. The dashed black line separates symbolically near proximities of neighboring cells. Green bars mimic extracellular auxin gradients. "Source" and "Sink" terms represent auxin source and auxin sink, respectively. **(B)** The interaction of the three feedback loops inside and outside of the cell generates the polar signal for PIN proteins in the ERP model (Wabnik *et al*., 2010). Coupled intracellular feedbacks on auxin transport involve TIR1-dependent regulation of auxin carrier expression; In turn, auxin carrier activity induce positive feedback (+) through AUX1/LAX proteins (auxin uptake) and negative feedback (-) through PIN (auxin efflux) activity. The positive feedback (+) located in the cell wall integrates the auxin-modulated inhibition of PIN endocytosis through the extracellular auxin receptor. i.e. ABP1, leading to reduced intracellular auxin concentration due to enhanced PIN-dependent efflux.

porters (AUX/LAX) to reproduce the high auxin accumulation in developing veins (Kramer, 2009) (Figure 2C).

However, the preferential localization of ABP1 in the lumen of the endoplasmic reticulum and the outer surface of the plasma membrane questions whether ABP1 could be an intracellular receptor for the cytosolic auxin (Napier *et al*., 2002; Tromas *et al*., 2010). It also remains to be tested whether this model (Kramer, 2009) could unify with-the-flow and up-the-gradient PIN polarization.

This concept of gradient sensor in the model for the polar auxin transport (Kramer, 2009) has been suggested as a possible alternative to flux sensors (Mitchison, 1981). From this initial concept, a new class of gradient-based feedback models for the PIN polarization was generated.

1.4.5 EXTRACELLULAR RECEPTOR-BASED POLARIZATION

Theoretical models for polarized auxin transport often neglect the auxin transport to the extracellular space (apoplast) (reviewed in (Kramer, 2008). Although, the influence of the apoplastic auxin on plant patterning is not clear (Sahlin *et al*., 2009; Santos *et al*., 2010), the putative auxin receptor ABP1 has been reported to be secreted into the apoplast (Napier *et al*., 2002; Tromas *et al*., 2010). Therefore, the cell wall might be an important compartment for the auxin signaling, but the apoplast as a plausible site for local auxin signaling had not been included explicitly in previous models.

An alternative model for the PIN polarization integrates not only the auxin transport to the apoplast but also an extracellular feedback mechanism for auxin-modulated PIN polarity (Wabnik *et al*., 2010). The heart of this extracellular receptor-based polarization (ERP) mechanism is the competitive utilization of the extracellular auxin receptors in the cell wall for the spatial regulation of the PIN protein internalization (Figure 3A). In addition, the ERP model includes the well-characterized intracellular TIR-de-

pendent auxin signaling on the production of PIN and AUX/LAX proteins (Figure 3A).

Computer simulations demonstrated that a synergy of the intracellular and extracellular auxin signaling could lead to the coordinated PIN polarity alignment within the tissue (Wabnik *et al.*, 2010). This emergence of the PIN polarization in the model depends on and contributes to the establishment of local auxin gradients in the apoplast (Wabnik *et al.*, 2010) (Figure 3A). In the ERP model, the symmetry-breaking cues for PIN polar distribution are generated via the competitive signaling in the apoplast which enables to uncouple the regulation of PIN polarization from the actual auxin concentration. Subsequently, this PIN polarization is reinforced by competition between carrier-dependent auxin influx and auxin efflux activities, leading to steeper auxin gradients in the apoplast (Wabnik *et al.*, 2010).

The plausibility of the ERP model was tested by computer simulations of various auxin-related processes, including *de novo* vascularization, venation patterning, vein loop formation, vein attraction/repulsion, competitive canalization and tissue regeneration on various tissue layouts and under growth conditions (Wabnik *et al.*, 2010). Interestingly, the ERP model was able to reproduce realistic PIN polarization and auxin distribution patterns that are associated with vascular development (Wabnik *et al.*, 2010) (Figure 3B-I) and vascular regeneration (Wabnik *et al.*, 2010). The mathematical analysis of the model demonstrated that it could unify contrasting PIN polar behaviors, such as PIN polarization with-the-flow, up-the-gradient and bipolarity (Wabnik *et al.*, 2010). Nevertheless, the model prediction should be evaluated for potential plausibility in other systems such as roots, embryos and apical meristems. The ERP model predicts the self-emergence of extracellular auxin gradient as a consequence of local feedback regulation in the cell wall. This apparent prediction of the model simulations could by validated or discarded by future experiments.

The ABP1 protein represents a suitable candidate as putative extracellular auxin receptor in the ERP model (Wabnik *et al.*, 2010). A recent experimental study might support the model prediction by invoking the role of ABP1 in regulating the internalization of plasma membrane proteins (Robert *et al.*, 2010). However, these recent experimental insights in the regulation of PIN trafficking proposed that ABP1 is a positive regulator of overall clathrin-dependent endocytosis and auxin binding to ABP1 inhibits this promoting effect (Robert *et al.*, 2010). In contrast, the ERP model incorporates an auxin receptor that upon auxin binding negatively signals solely on PIN internalization (Wabnik *et al.*, 2010). However, the non polar AUX1/LAX localization is crucial for the model performance (Wabnik *et al.*, 2010). Even though, general principles of the ERP model stand, this model should be reevaluated with the data on the positive impact of ABP1 on internalization of both PIN and AUX/LAX proteins.

In the ERP model (Wabnik *et al.*, 2010), an extracellular auxin gradient is sensed by the competitive utilization of auxin signaling components to polarize the PIN proteins

and to direct auxin fluxes within the tissue, highlighting the possibility for a mechanistic explanation for the auxin flow canalization (Sachs, 1969; Sachs, 1981).

1.5 CONCLUDING REMARKS

The plant-specific signaling molecule auxin is a versatile developmental trigger for embryogenesis, postembryonic *de novo* organ formation, and tropism. The PIN-dependent cell-to-cell polar auxin transport directly connects cell polarity to developmental patterning processes in plants. A long-standing belief that auxin could feed back on its transport from cells has been a great inspiration for both theoreticians and experimentalists, but the molecular and cellular components realizing such a feedback mechanism have remained unknown for a long time. The recent advances in experimental and theoretical understanding of plausible mechanisms underlying the PIN polarization events have led to a computational evolution in PIN polarization models for the auxin transport in plant development.

Here, we reviewed and evaluated these theoretical concepts for the PIN polarization. We pinpoint both the advantages and shortcomings of each modeling approach by challenging them with recent experimental insights into PIN polarization and auxin distribution. The ongoing evolution of various modeling methodologies to describe the PIN polarization is illustrated from initially simple, purely conceptual models to more recent mechanistic approaches that allow the formulation of testable hypotheses on molecular and cellular mechanisms underlying the PIN polarization. The future adaptation and realistic validation of current models for PIN polarization will require a strong experimental input, especially considering the biophysical parameters attributed to these models and the identification of upstream molecular components for the regulation of the PIN polarity.

Beside polar PIN-dependent auxin transport, also the intracellular carrier-dependent auxin transport could contribute to auxin transport-driven patterning in early land plant such as mosses, highlighting the possibility for alternative or prototype mechanisms for auxin transport (Wabnik *et al*., 2011, in press). Therefore, the integration of the PIN5-type carrier-dependent regulation of subcellular auxin compartmentalization (Mravec *et al.*, 2009) might be functionally important for auxin-dependent plant development and, hence, should be also integrated into models describing auxin-driven pattering in higher plants.

We have demonstrated that predictions from theoretical models not only can increase our understanding of plant developmental processes, but also, most importantly, guide and stimulate wet-lab experiments in a meaningful fashion. We believe that the joint efforts of experimental and modeling techniques will accelerate the research out-

come on the PIN polarization, ultimately bringing us closer to understand the auxin-dependent plant development.

ACKNOWLEDGMENTS

We are greatful to M. De Cock for help in preparing the manuscript. This work was supported by grants from the Research Foundation-Flanders (Odysseus to J.F. and project no. 3G006507 to W.G.), the EMBO Young Investigator Program (to J.F), and the Vienna Science and Technology Fund (to J.K.-V.). We apologize to our colleagues whose work have been inadvertently omitted or could not be reviewed in depth.

CHAPTER 2

EMERGENCE OF TISSUE POLARIZATION FROM SYNERGY OF INTRACELLULAR AND EXTRACELLULAR AUXIN SIGNALING

"Not only do the various components of the cells form a living system, in which the capacity to live, react, and reproduce is dependent on the interactions of all the members of the system; but this living system is identical with the genetic system. The form of life is determined not only by the specific nature of the hereditary units but also by the structure and arrangement of the system. The whole system is more than the sum of its parts, and the effect of each of the components depends on and is influenced by all previous reactions, whose sequence is in turn determined by the whole idiotype."

— Peter Michaelis

EMERGENCE OF TISSUE POLARIZATION FROM SYNERGY OF INTRACELLULAR AND EXTRACELLULAR AUXIN SIGNALING

Krzysztof Wabnik[1,2,3,8] Jürgen Kleine-Vehn[1,2,8] Jozef Balla[4], Michael Sauer[1,2,6], Satoshi Naramoto[1,2], Vilém Reinöhl[4], Roeland M.H. Merks[1,2,7,] Willy Govaerts[3] and Jiří Friml[1,2,5]

Contribution: Computation modeling work has been handled by K. Wabnik

Molecular Systems Biology **6:** 447 (2010)

[1] Department of Plant Systems Biology, VIB, 9052 Gent, Belgium, [2] Department of Plant Biotechnology and Genetics, Ghent University, 9052 Gent, Belgium, [3] Department of Applied Mathematics and Computer Science, Ghent University, 9000 Gent, Belgium, [4] Department of Plant Biology, Mendel University, 613 00 Brno, Czech Republic, [5] Department of Experimental Biology, Masaryk University, 601 77 Brno, Czech Republic [6] Present address: Departamento de Genética Molecular de Plantas, Centro Nacional de Biotecnología, Consejo Superior de Investigaciones Científicas, 28049 Madrid, Spain. [7] Present address: Centrum Wiskunde & Informatica, 1098 XG Amsterdam, and Netherlands Consortium for Systems Biology, 1098 XG Amsterdam, The Netherlands [8] These authors contributed equally to this work

ABSTRACT

Plant development is exceptionally flexible as manifested by its potential for organogenesis and regeneration, which are processes involving rearrangements of tissue polarities. Fundamental questions concern how individual cells can polarize in a coordinated manner to integrate into the multicellular context. In canalization models, the signaling molecule auxin acts as a polarizing cue and feedback on the intercellular auxin flow is key for synchronized polarity rearrangements. We provide a novel mechanistic framework for canalization, based on up-to-date experimental data and minimal, biologically plausible assumptions. Our model combines the intracellular auxin signaling for expression of PINFORMED (PIN) auxin transporters and the theoretical postulation of extracellular auxin signaling for modulation of PIN subcellular dynamics. Computer simulations faithfully and robustly recapitulated the experimentally observed patterns of tissue polarity and asymmetric auxin distribution during formation and regeneration of vascular systems and during the competitive regulation of shoot branching by apical dominance. Additionally, our model generated new predictions that could be experimentally validated, highlighting a mechanistically conceivable explanation for the PIN polarization and canalization of the auxin flow in plants.

2.1 INTRODUCTION

A key question in developmental biology relates to the fundamental issue of how an individual cell in a polarized tissue senses the polarities of its neighbors and its position within the tissue. In plant development, this issue is of pronounced importance, because plants have the remarkable ability to redefine cell and tissue polarities in different developmental programs, such as embryogenesis, postembryonic organogenesis, vascular tissue formation, and tissue regeneration (Kleine-Vehn and Friml, 2008).

In 1880, Charles Darwin predicted that a growth-stimulating molecule directionally moves within plant tissues (Darwin and Darwin, 1880). This growth regulator was later on termed auxin and represents the first isolated phytohormone. Intercellular auxin transport in conjunction with local auxin biosynthesis are postulated to define auxin gradients during embryonic and postembryonic development, giving positional cues for primordium formation, organ patterning, and tropistic growth (Friml *et al.*, 2002; Benková *et al.*, 2003; Reinhardt *et al.*, 2003; Heisler *et al.*, 2005; Scarpella *et al.*, 2006; Dubrovsky *et al.*, 2008). The direction of the auxin transport depends largely on the polar subcellular localization of PINFORMED (PIN) proteins at the plasma membrane (Petrášek *et al.*, 2006; Wiśniewska *et al.*, 2006). As the molecular basis of the PIN polarization in plants remains unexplored, theoretical and experimental insights into mechanisms that regulate the PIN polarity are of outstanding interest to plant biologists.

PIN proteins recycle between the plasma membrane and the intracellular endosomal compartments (Geldner *et al.*, 2001; Dhonukshe *et al.*, 2007). This recycling modulates PIN-dependent auxin efflux rates and enables rapid changes in PIN polarity (Dhonukshe *et al.*, 2008; Kleine-Vehn *et al.*, 2008a). Additionally, auxin interferes with the PIN recycling by inhibiting the PIN protein internalization (Paciorek *et al.*, 2005).

At the tissue level, polarization of PIN proteins in individual cells has been suggested to be coordinated in the surrounding cells by a positive feedback between auxin and its directional transport (Mitchison, 1980; Sauer *et al.*, 2006). As the molecular mechanism for PIN polarization still needs to be unraveled, numerous theoretical studies have been applied to test various hypotheses. In the canalization hypothesis (Sachs, 1981), an underlying positive feedback loop exists between the auxin-flux and auxin-transport capacity of cells, ultimately canalizing auxin progressively into discrete channels. It incorporates a hypothetical flux sensor component as an essential part of the auxin feedback mechanism for PIN polarization (Mitchison, 1980) and is widely exploited in so-called flux-based models to study PIN-dependent developmental processes, such as venation patterning in leaves (Rolland-Lagan and Prusinkiewicz, 2005; Sauer *et al.*, 2006; Scarpella *et al.*, 2006). Based on the experimental observation of adverse PIN polarization during phyllotactic patterning in vegetative shoot apical meristems (Reinhardt *et al.*, 2003), PIN proteins have been proposed to orient to the side of the cell that faces

the neighboring cell with the highest auxin concentration (Jönsson *et al.*, 2006; Smith *et al.*, 2006). This alternative hypothesis integrates an unknown short-range intercellular signal transmitting the auxin concentration of its direct neighbors (Sahlin *et al.*, 2009). Concentration-based models can reproduce various phyllotactic patterns occurring in planta (Reinhardt *et al.*, 2003; Jönsson *et al.*, 2006; Smith *et al.*, 2006) and initiation of the primary leaf vein (Merks *et al.*, 2007).

The flux-based (Mitchison, 1980; Rolland-Lagan and Prusinkiewicz, 2005) and concentration-based models (Merks *et al.*, 2007) provide conceptually different frameworks for PIN polarization during venation patterning in plants. Unless additional assumptions are included (Feugier *et al.*, 2005), these models predict the low auxin concentration in vein precursors, which contradicts the experimental observations of high auxin signaling in developing veins (Scarpella *et al.*, 2006).

To assess this issue, flux-based and concentration-based models were combined into a dual polarization model, in which the dominating mechanism depends on the actual auxin content of the cells (Bayer *et al.*, 2009). This model generates the simultaneous appearance of high auxin concentration in emerging veins and recapitulates PIN polarization and auxin transport during early midvein formation and phyllotaxis.

Nevertheless, biological evidence for a hypothetical flux sensor (Mitchison, 1980; Rolland-Lagan and Prusinkiewicz, 2005; Bayer *et al.*, 2009) and/or a short-range signal (Jönsson *et al.*, 2006; Smith *et al.*, 2006; Merks *et al.*, 2007; Bayer *et al.*, 2009) for PIN polarization remains difficult to identify. To overcome this problem, individual cells have been suggested to read-out hypothetical intracellular auxin gradients to polarize PIN proteins by a yet to be clarified perception mechanism (Kramer, 2009). Based solely on the steepness of this internal auxin gradient (independently of the overall auxin concentrations) PIN proteins would polarize toward the side of the cell with the lowest intracellular auxin concentration (Kramer, 2009). This model predicts that a conductive auxin channel originates from an auxin sink instead of an auxin source whereas experimental observations suggest the opposite (Sauer *et al.*, 2006).

Here, we propose a novel, biologically plausible model for PIN polarization that combines intracellular and extracellular auxin signaling as a unifying approach for tissue polarization during auxin canalization in plants. The model integrates experimental data, such as auxin feedback on PIN transcription (Peer *et al.*, 2004; Heisler *et al.*, 2005) via a nuclear auxin signaling pathway (Chapman and Estelle, 2009) and auxin feedback on PIN endocytosis (Paciorek *et al.*, 2005) via the hypothetical, yet conceivable assumption of extracellular auxin perception. The extracellular receptor-based polarization (ERP) model faithfully reproduces PIN polarization and auxin distribution patterns during vascularization, tissue regeneration, vein connection, generation of leaf vein loops, and competitive auxin canalization for axillary bud outgrowth. The detailed analysis of our model revealed new mechanistic insights into initiation, maintenance, and robust-

ness of PIN polarization during venation patterning and tissue regeneration. Remarkably, the ERP model generated new predictions that were experimentally validated. The versatility and accuracy of model predictions highlight the importance and plausibility of dual auxin perception for PIN polarization and auxin-driven plant development.

2.2 ASSUMPTIONS OF THE MODEL

Tissue polarization requires cell-to-cell communication, but, in plants, a biologically conceivable mechanism for PIN polarization was elusive. Therefore, we assumed that the extracellular space (apoplast) provides a relatively easy mean for a direct and simple cell-to-cell communication by the competitive utilization of one or more signaling components (i.e., receptors). Notably, the first isolated auxin-binding protein (ABP1) has been proposed to be secreted and to be active in the apoplast (for review, see Napier *et al.*, 2002; Tromas *et al.*, 2009), indicating the possibility for extracellular auxin signaling.

Auxin exerts its action to a large extent by modulating gene expression via binding to the well-characterized nuclear auxin receptor TIR1 (reviewed in Chapman and Estelle, 2009). Here, we explored the simplest, yet biologically plausible, scenario in which auxin would act both intracellularly on PIN expression and extracellularly on the subcellular dynamics of PIN proteins via receptor-mediated signaling pathways.

The computational approach to model the PIN polarization integrated available molecular and cell biological data. Biological data (I) and hypothetical assumptions (II) were incorporated into a computer model for auxin transport and PIN polarization (for model details, see Model description).

(I) The auxin fluxes were modelled between discrete cells and cell wall compartments by using the chemiosmotic hypothesis (Goldsmith *et al.*, 1981) (Figure 1A). Accordingly, auxin slowly diffused and was actively transported by the AUX/LAX family of auxin influx carriers into the cell (Swarup *et al.*, 2005) (Figure 1A). To exit the cell, auxin required an active transport mediated by the PIN auxin efflux carriers (Petrášek *et al.*, 2006) (Figure 1A). The auxin diffusion between discrete wall compartments was also taken into account, because of its importance for auxin transport (Swarup *et al.*, 2005; Kramer *et al.*, 2007). Moreover, we considered that the diffusion of auxin was significantly reduced in the apoplast (Kramer *et al.*, 2007). On the single cell level, the ERP model incorporated an auxin-dependent carrier expression (Peer *et al.*, 2004; Heisler *et al.*, 2005; Vieten *et al.*, 2005) that is mediated intracellularly (Figure 1B) by the nuclear TIR1-dependent pathway (Kepinski and Leyser, 2005; Dharmashiri *et al.*, 2005). In the model, auxin carriers undergo constitutive degradation in lytic vacuoles (Abas *et al.*, 2006; Kleine-Vehn *et al.*, 2008b) (Figure 1B). The auxin influx carriers (AUX/LAX) were uniformly distributed at the plasma membranes and their targeting mechanisms are

considered to be distinct from the PIN proteins (Kleine-Vehn *et al.*, 2006) (Figure 1C). The dynamics of PIN recycling allowed the translocation of proteins between different cell sides and rapid changes in PIN polarity as well in response to various external and internal signals (Benková *et al.*, 2003; Dhonukshe *et al.*, 2008; Friml *et al.*, 2002, 2003; Heisler *et al.*, 2005; Kleine-Vehn *et al.*, 2008a).

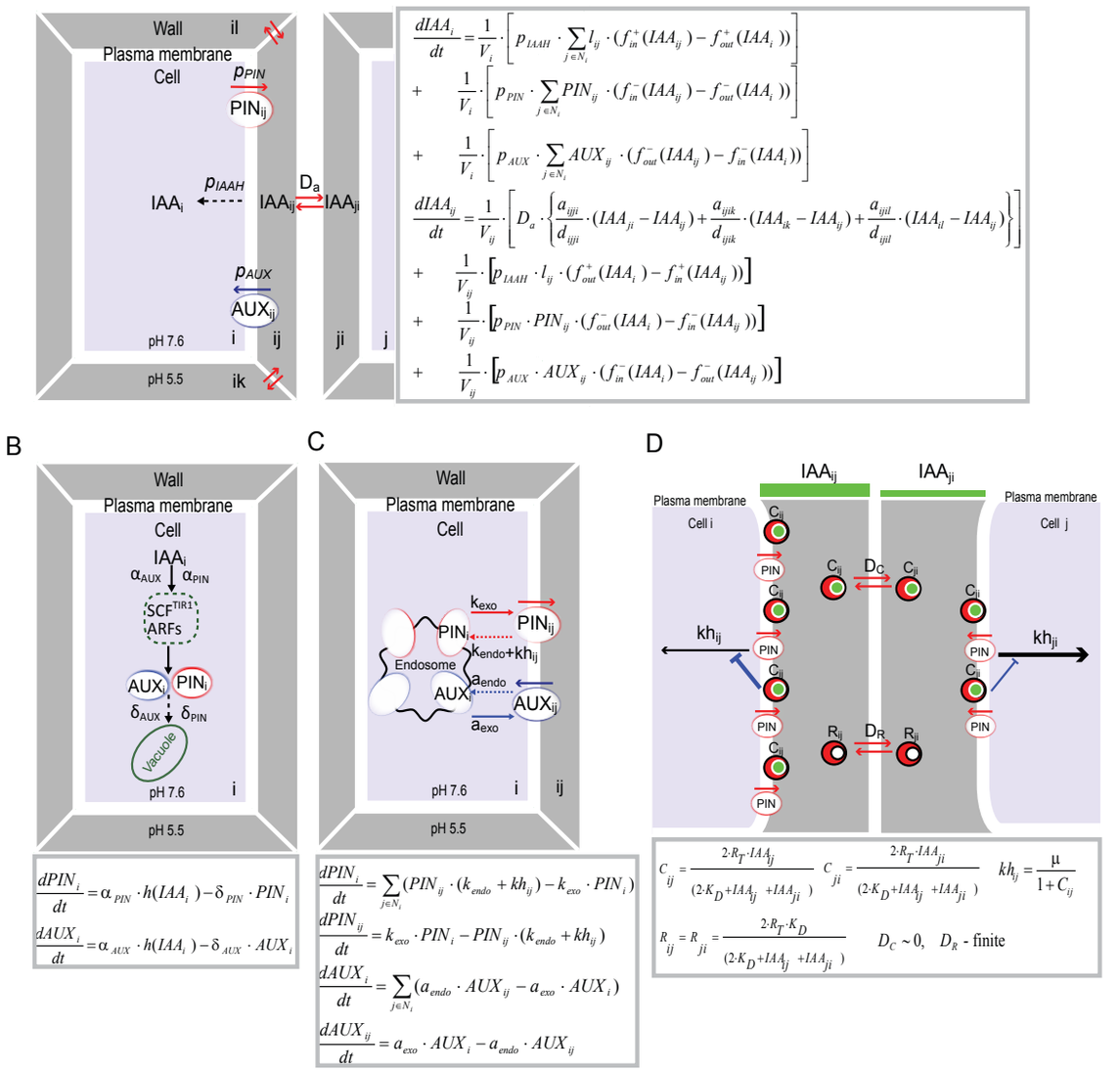

$$\frac{dIAA_i}{dt} = \frac{1}{V_i}\cdot\left[p_{IAAH}\cdot\sum_{j\in N_i} l_{ij}\cdot(f_{in}^{+}(IAA_{ij}) - f_{out}^{+}(IAA_i))\right] + \frac{1}{V_i}\cdot\left[p_{PIN}\cdot\sum_{j\in N_i} PIN_{ij}\cdot(f_{in}^{-}(IAA_{ij}) - f_{out}^{-}(IAA_i))\right] + \frac{1}{V_i}\cdot\left[p_{AUX}\cdot\sum_{j\in N_i} AUX_{ij}\cdot(f_{out}^{-}(IAA_{ij}) - f_{in}^{-}(IAA_i))\right]$$

$$\frac{dIAA_{ij}}{dt} = \frac{1}{V_{ij}}\cdot\left[D_a\cdot\left\{\frac{a_{ijji}}{d_{ijji}}\cdot(IAA_{ji} - IAA_{ij}) + \frac{a_{ijik}}{d_{ijik}}\cdot(IAA_{ik} - IAA_{ij}) + \frac{a_{ijil}}{d_{ijil}}\cdot(IAA_{il} - IAA_{ij})\right\}\right] + \frac{1}{V_{ij}}\cdot\left[p_{IAAH}\cdot l_{ij}\cdot(f_{out}^{+}(IAA_i) - f_{in}^{+}(IAA_{ij}))\right] + \frac{1}{V_{ij}}\cdot\left[p_{PIN}\cdot PIN_{ij}\cdot(f_{out}^{-}(IAA_i) - f_{in}^{-}(IAA_{ij}))\right] + \frac{1}{V_{ij}}\cdot\left[p_{AUX}\cdot AUX_{ij}\cdot(f_{in}^{-}(IAA_i) - f_{out}^{-}(IAA_{ij}))\right]$$

B

$$\frac{dPIN_i}{dt} = \alpha_{PIN}\cdot h(IAA_i) - \delta_{PIN}\cdot PIN_i$$

$$\frac{dAUX_i}{dt} = \alpha_{AUX}\cdot h(IAA_i) - \delta_{AUX}\cdot AUX_i$$

C

$$\frac{dPIN_i}{dt} = \sum_{j\in N_i}(PIN_{ij}\cdot(k_{endo} + kh_{ij}) - k_{exo}\cdot PIN_i)$$

$$\frac{dPIN_{ij}}{dt} = k_{exo}\cdot PIN_i - PIN_{ij}\cdot(k_{endo} + kh_{ij})$$

$$\frac{dAUX_i}{dt} = \sum_{j\in N_i}(a_{endo}\cdot AUX_{ij} - a_{exo}\cdot AUX_i)$$

$$\frac{dAUX_{ij}}{dt} = a_{exo}\cdot AUX_i - a_{endo}\cdot AUX_{ij}$$

D

$$C_{ij} = \frac{2\cdot R_T\cdot IAA_{ij}}{(2\cdot K_D + IAA_{ij} + IAA_{ji})} \qquad C_{ji} = \frac{2\cdot R_T\cdot IAA_{ji}}{(2\cdot K_D + IAA_{ij} + IAA_{ji})} \qquad kh_{ij} = \frac{\mu}{1 + C_{ij}}$$

$$R_{ij} = R_{ji} = \frac{2\cdot R_T\cdot K_D}{(2\cdot K_D + IAA_{ij} + IAA_{ji})} \qquad D_C \sim 0, \quad D_R \text{ - finite}$$

Figure 1 Schematic and mathematical representations of the main model assumptions

(A) Schematic and mathematical representations of auxin transport between cells (*i, j*) and cell wall interfaces (*ij*, *ji*, *ik*, and *il*). IAA_i describes the mean auxin concentration in the i-th cell; whereas IAA_{ij} and IAA_{ji} determine the auxin concentrations in discrete wall compartments (*ij* and *ji*). The functions f_{in}^{+}/f_{in}^{-} and f_{out}^{+}/f_{out}^{-} are used to evaluate the fractions of auxin in the cell and in the cell wall. Dashed arrows indicate the rate of passive auxin diffusion into the cell and p_{IAAH} describes the membrane permeablility for protonated auxin. D_a is the diffusion coefficient of auxin between neighboring wall compartments. p_{PIN}

and p_{AUX} are parameters that determine PIN- and AUX/LAX-dependent efflux and influx of auxin across the plasma membrane, respectively. PIN_{ij}/PIN_{ji} and AUX_{ij}/AUX_{ji} are PIN (red) and AUX/LAX (blue) levels in neighboring plasma membranes. **(B)** Schematic and mathematical representations of intracellular auxin perception: auxin-induced carrier synthesis (solid black arrows) and basic carrier degradation (dashed black arrows). The α_{PIN} and α_{AUX} are the rates of auxin-dependent PIN and AUX/LAX expression, respectively. The degradation rates of PIN and AUX/LAX proteins are given by parameters δ_{PIN} and δ_{AUX}. **(C)** Schematic and mathematical representations of auxin carrier trafficking. The rates of endo- and exocytosis affect carrier abundance at the plasma membrane. PIN_i corresponds to the PIN level of the *i*-th cell (red arrows) and AUX_i determines the AUX/LAX level (blue arrows) in the *i*-th cells. The base rates for PIN exocytosis and PIN endocytosis are k_{exo} and k_{endo}, whereas aexo and aendo similarly correspond to AUX/LAX recycling rates. The component khij determines the inhibitory effect of auxin on the PIN internalization at a given cell side. **(D)** Schematic and mathematical representations of extracellular receptor-based auxin signaling pathway for modulation of PIN trafficking. Two adjacent cells share a common pool of extracellular auxin receptors denoted as $2R_T = C_{ij} + C_{ji} + R_{ij} + R_{ji}$, where C_{ij} and C_{ji} represent the levels of the auxin-bound receptor in the discrete wall compartments facing the surfaces of the adjacent cells *i* and *j*. R_{ij} and R_{ji} correspond to the levels of free receptors that undergo diffusion between common wall compartments (D_R). The auxin receptors are activated by auxin via direct binding at the cell surface and transfer an inhibitory signal to regulate PIN internalization rates (kh_{ij} and kh_{ji}) that is linked with their temporal immobilization at a given side of the cells ($D_C \sim 0$). The green bars represent auxin concentrations in the discrete cell wall compartments.

Similarly to most recent models (Sahlin *et al.*, 2009; Ibañes *et al.*, 2009), we included this dynamics of PIN recycling and assumed the auxin-dependent regulation of PIN internalization (Paciorek *et al.*, 2005) (Figure 1C).

(II) In our model, the concentration-dependent effect of auxin on PIN internalization (Paciorek *et al.*, 2005) involved the extracellular receptor-based signaling pathway at the cell surface (Figure 1D), the extracellular pools of hypothetical auxin receptors were shared by each pair of neighboring cells, and the competitive utilization of these auxin receptors allowed direct cell-to-cell communication (Figure 1D). We assumed that auxin binding to the receptor induced signals to inhibit PIN internalization, leading to differential PIN protein retention at different cell sides. Although the direct mode of the signal transfer is unknown, we speculated that bound receptors might be recruited and, hence, temporarily immobilized, to the plasma membrane (or alternatively to cell wall components) for signal transfer, which is modeled by the reduced diffusion of receptors involved in the auxin signaling (Figure 1D). Simultaneously, free receptors from the intercellular pools underwent free diffusion (Figure 1D). To reduce the model complexity, auxin binding to the receptors immediately imposed an inhibitory signal to the nearest cell (Figure 1D). To model the spatial proximity of receptor-based signal transfer to the nearest cell side, we divided the apoplast in two discrete compartments suitable for com-

putational reasons (Figure 1D). The strength of auxin signaling was determined by the amount of auxin-bound receptors present in these discrete wall compartments (Figure 1D).

Analysis of our model revealed that differences in diffusion rates of bound auxin and free receptors are crucial for the model performance. This competitive utilization mechanism enabled cell-to-cell communication in the model, leading to receptor enrichment at the site of increased auxin concentration (Supplementary Figure 1).

We propose that the implementation of these biological data (I) and hypothetical assumptions (II) are sufficient to generate PIN polarity in a given tissue. The model generates initially a weak, diffusion-driven auxin gradient in the apoplast that leads to asymmetric PIN retention at neighboring cell sides (Figure 2A). The competitive utilization of the auxin signaling components and subsequent auxin influx/efflux activities reinforce the asymmetry in PIN internalization rate in the neighboring cells, leading to the alignment of PIN polarity.

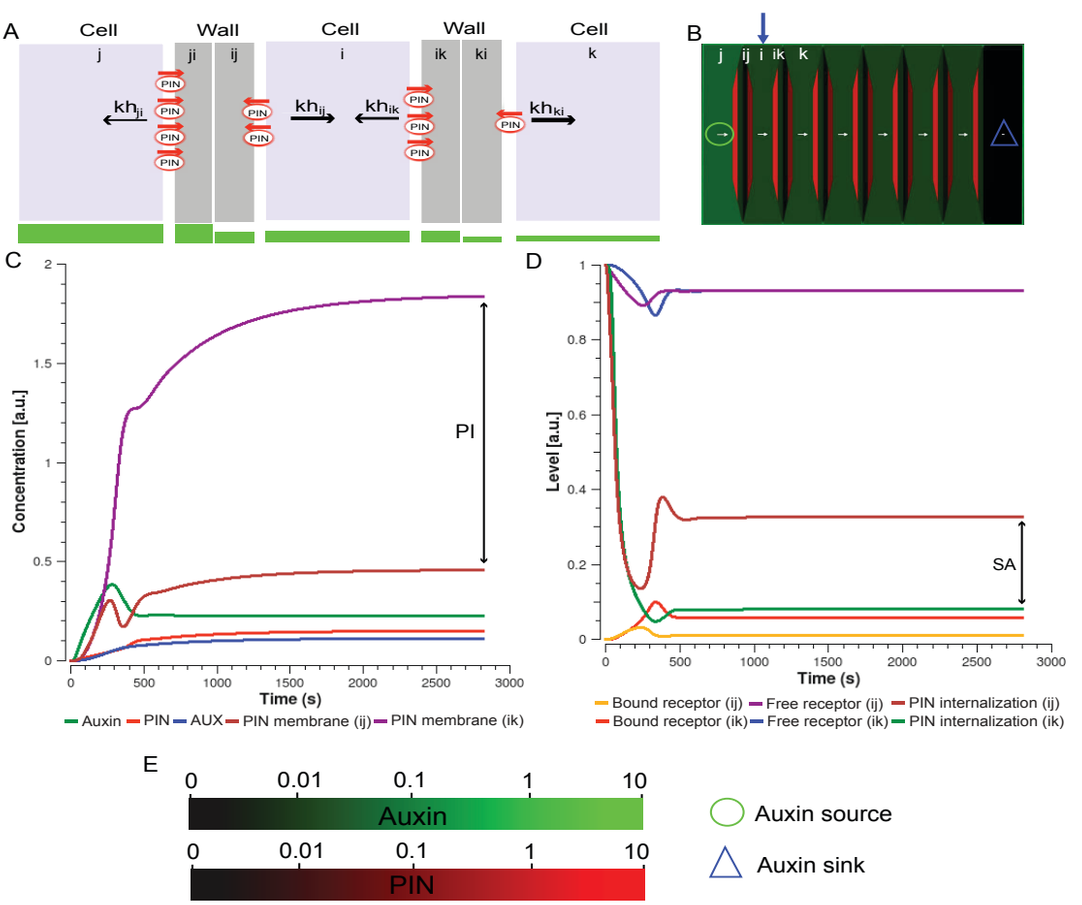

Figure 2 Global polar signal in the cell file produced by the synergy of the local extracellular auxin signaling

(A) Schematic representation of a cell file separated by discrete cell wall compartments. Indexes *i*, *j*, and *k* correspond to the three depicted cells. The wall compartments between adjacent pairs of cells are rep-

resented by indexes *ji/ij* (between cells *i* and *j*) and *ik*/*ki* (between cells *i* and *k*). The component *kh* with the corresponding index determines the effective rate of the PIN internalization at the given cell side, as described in Figure 1D. PIN (red) abundance at the plasma membrane presumably correlates with the profile of the auxin gradient (green bars). **(B)** *In silico* model simulation on the cell file predicting PIN polarization and canalization of auxin flow. Red and green depict PIN proteins and auxin distribution, respectively. The blue arrow marks the position of the monitored cell in the cell file. **(C)** Time-course profiles of auxin concentration, intracellular PIN and AUX/LAX levels (PIN_i and AUX_i), and PIN membrane levels (PIN_{ij} and PIN_{ik}). **(D)** Time-course profiles of bound (C_{ij} and C_{ik}) and free receptor (R_{ij} and R_{ik}). The levels are normalized by total amount of receptors in the pool (R_T); khij and khik are the corresponding PIN internalization rates. The Polarization Index (PI) indicates asymmetry and represents the ratio between PIN levels at the *ik*-th plasma membrane and those of the *ij*-th membrane (C). The Signaling Asymmetry (SA) depicts difference in extracellular auxin signaling between *ik*-th and *ij*-th sides of the cell *i* (D). PI and SA are associated with different states of the cell polarization: no polarization (PI ~0, SA ~ 0), initiation of polarization (PI and SA increased), and maintenance of polarization (PI and SA saturated). (E) Color coding schemes for auxin concentrations and PIN levels used in all model simulations. Auxin concentrations can vary from 0 (black) to 10 (bright green). PIN levels at the plasma membrane may change from 0 (black) to 10 (bright red). White arrows point in the direction of preferential PIN polarity and the arrow size indicates the relative strength of the PIN expression in the cell. Green circle (source) and blue triangle (sink) illustrate the positions of auxin source and auxin sink on the tissue template.

Indeed, the synergy of the local auxin signaling between each pair of competing cells promoted tissue polarization (Figure 2B). Intriguingly, this feedback regulation of polar auxin transport contributed to formation of steeper extracellular auxin gradient (Figures 2A and 2B). In conclusion, the PIN polarization and polar auxin transport both depended on and contributed to the establishment of a differential auxin signaling (Figures 2C and 2D). Such feedback loop led ultimately to the alignment of PIN polarization within a tissue (Figure 2B).

2.3 THE ERP MODEL ROBUSTLY REPRODUCES PIN1 POLARITY DURING VASCULAR DEVELOPMENT

To test whether the ERP model could reproduce the PIN1 polarity patterns observed in vivo during vein formation, we used a tissue grid layout and applied minimal assumptions, such as the presence of an auxin source and a distal sink (Figure 3). After auxin application, the simulation revealed that PIN1 polarized away from an auxin source, confirming our theoretical expectations (see above). PIN1 expression was initially broad (Figures 3A and 3C), but converged over time to a single cell file with strong PIN1 ex-

pression and polarization (Figure 3B). This simulation recapitulated the experimental observations during vein formation that PIN1 expression was initially broad with poorly defined polarity (Figure 3E). The addition of an auxin sink was not essential to polarize the PIN proteins (data not shown), but imposed directionality on the developing vein that ultimately linked the auxin source and sink by a PIN-dependent conductive auxin channel.

To analyze behavior, sensitivity, and robustness of the ERP model, we tested the contribution of model components for predicted PIN polarity and auxin distribution patterns. These components include extracellular receptor-based auxin perception and competitive utilization of receptors by neighboring cells (Supplementary Figures 1-3), auxin-mediated carrier expression (Supplementary Figures 4 and 5), PIN- and AUX\LAX-dependent polar transport (Supplementary Figures 6 and 7), and auxin diffusion (Supplementary Figures 8 and 9).

Our model predictions were robust with respect to altered source or sink locations (Supplementary Figure 10) or intracellular auxin gradients (Supplementary Figure 11). The ERP model provided a robust mechanism for canalization of auxin flow (Supplementary Figure 10). Additionally, this model is able to capture conflicted PIN behaviors including PIN polarization with or against the auxin gradient (Supplementary Figures 12-16). During midvein formation, neighboring cells at the advancing edge of the forming vein display transient PIN polarization toward each other (Bayer *et al.*, 2009). Intriguingly, the ERP model reproduced this PIN polarization pattern: cells at the growing edge of the forming conductive channel polarized the PIN proteins toward the auxin channel (Figure 3C). In the simulations, the initially weak apoplastic auxin gradient between these cells led to relatively high auxin-dependent inhibition of the PIN endocytosis at the plasma membrane of both cells and, consequently, PIN proteins in neighboring cells became polarized toward each other. However, because differences in the auxin transport rates of these neighboring cells (derived from auxin-dependent regulation of auxin carrier expression and polarity) progressively enhanced the extracellular auxin gradient, an enhanced asymmetry in the local auxin signaling was created. The competitive utilization of auxin receptors in the apoplast was necessary for this propagation of differential extracellular auxin signaling and the coordination of PIN polarity within the tissue (Supplementary Figures 1-3). Interestingly, the complete removal of auxin-induced carrier expression from the ERP model did not caused the loss of PIN polarity and auxin canalization in the model simulations (although polarization patterns were less realistic), but only when either the high amount of carriers in the initial pool (Supplementary Figures 4A-4L) or high auxin-independent carrier expression (Supplementary Figures 5A-5L) were integrated in the model. Next, we tested the ERP model on a more natural tissue layout in which cell shape varied (Figures 3D and 3G). The model accurately predicted the PIN1 polarization in the natural tissue layout (Figure 3H), reca-

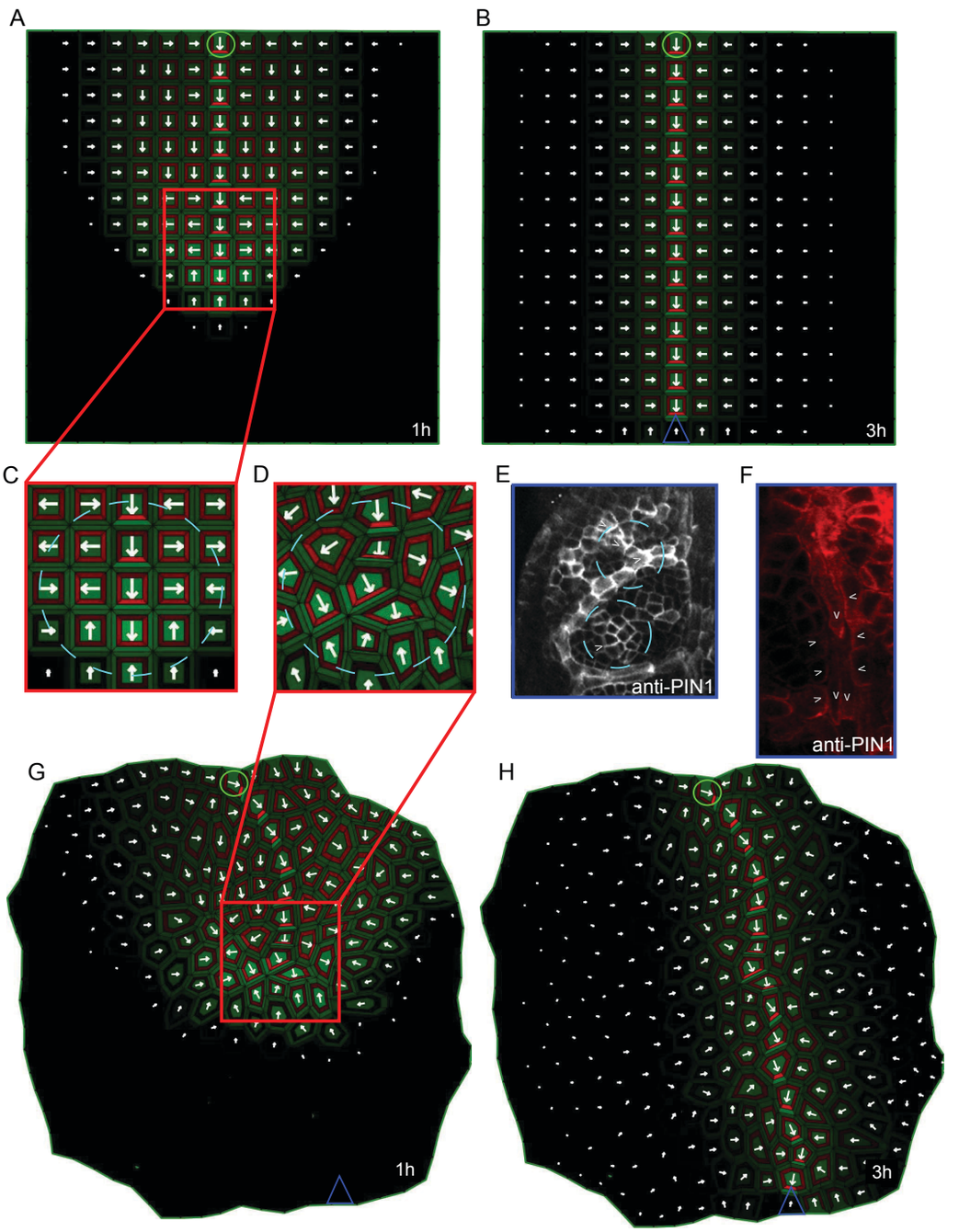

Figure 3 Experimental and simulated PIN-dependent auxin canalization

(A-C) Simulations of the ERP model on a grid tissue layout. Initially, a broad PIN1 expression domain was predicted (A, C), originating from the site of auxin application (green circle). Subsequently, this expression domain became narrowed to a single cell file, and, finally, produced a conductive auxin channel that connected the auxin source to the distal auxin sink (blue triangle) (B). **(D, E)** The broad PIN1 expression domain predicted by the model simulation using the cellular layout (D) and reported *in vivo* in *Arabidopsis* during leaf venation patterning with PIN1 immunolocalization (E). **(F)** PIN polarization during primary vein initiation in young leaves as reported by the PIN1 antibody. Provascular cells show basal PIN1 polarization while the surrounding cells are polarized toward them. **(G, H)** ERP model simulation using the cellular tissue layout. The initial, broad PIN1 expression domain (G) becomes reduced to a narrow domain

of strong PIN expression (H). The cells adjacent to the vascular strand are polarized toward it (H), as observed in planta (F). In the simulations (see Supplementary Movies 1 and 2), the PIN proteins are indicated in red and the auxin distribution in green. Arrowheads show preferential PIN polarization.

pitulating primary vein formation as observed in leaves (Figure 3F).
For both virtual tissues, the model reproduced the basal PIN1 polarization in provascular cells and lateral PIN1 polarization, pointing toward the conductive auxin channel, in adjacent cells (Figures 3B and 3G). Interestingly, this observation of lateral PIN1 polarization was absent from the predictions of flux-based models (Mitchison, 1980; Feugier *et al.*, 2005; Rolland-Lagan and Prusinkiewicz, 2005). In our model due to the high auxin concentrations, the auxin carrier expression is stronger in the conductive channel compared to the adjacent tissues. Furthermore, the PIN-driven efflux is strongly oriented towards the basal cell side of provascular cells while auxin influx remains uniform. This leads to stronger auxin influx compared to auxin efflux at the lateral side of the provascular cell, ultimately triggering the carrier-driven formation of a weak horizontal auxin gradient. In response to this gradient, PIN1 in the neighboring tissues polarized toward the conductive channel. Surprisingly, we found that the activity of the AUX/LAX proteins buffered the motility of auxin in the wall and largely contributed to the maintenance of PIN polarization and auxin gradients in the tissues (Supplementary Figure 7). This finding is consistent with a role of AUX/LAX proteins in phyllotactic patterning (Bainbridge *et al.*, 2008).

2.4 THE ERP SIMULATIONS PREDICTS DIVERSE PIN POLARIZATION AND HIGH AUXIN CONCENTRATION IN VEINS

Simulations with the ERP model on tissue layouts predicted PIN1 polarization during the formation of the conductive auxin channel (vein precursor). Other single mechanism-based models, such as flux-based (Mitchison, 1980; Rolland-Logan and Prusinkiewicz, 2005) and concentration-based models (Merks *et al.*, 2007), anticipate low auxin concentrations in the developing veins, which is in contradiction with experimental observations (Scarpella *et al.*, 2006). However, several solutions for this problem have been suggested, such as enhanced AUX/LAX-dependent uptake (Kramer, 2004; Swarup *et al.*, 2005) or constant total carrier protein abundance (Feugier *et al.*, 2005). On the other hand, the ERP model reproduces auxin canalization patterns, involving the dynamic changes in auxin-dependent carrier expression. The auxin concentrations in our model simulations were higher in the emerging veins than in those of surrounding tissues (Figure 4A). An elevation of auxin concentration was observed in pro-vascular cells, whereas neighboring cells showed a steep decrease in auxin concentrations (Figure 4B). This

observation might be conceptualized as the balance between PIN1-dependent auxin export from adjacent cells toward the vein precursors and the active drainage of auxin from lateral tissues by AUX/LAX-dependent influx into the provascular cells.

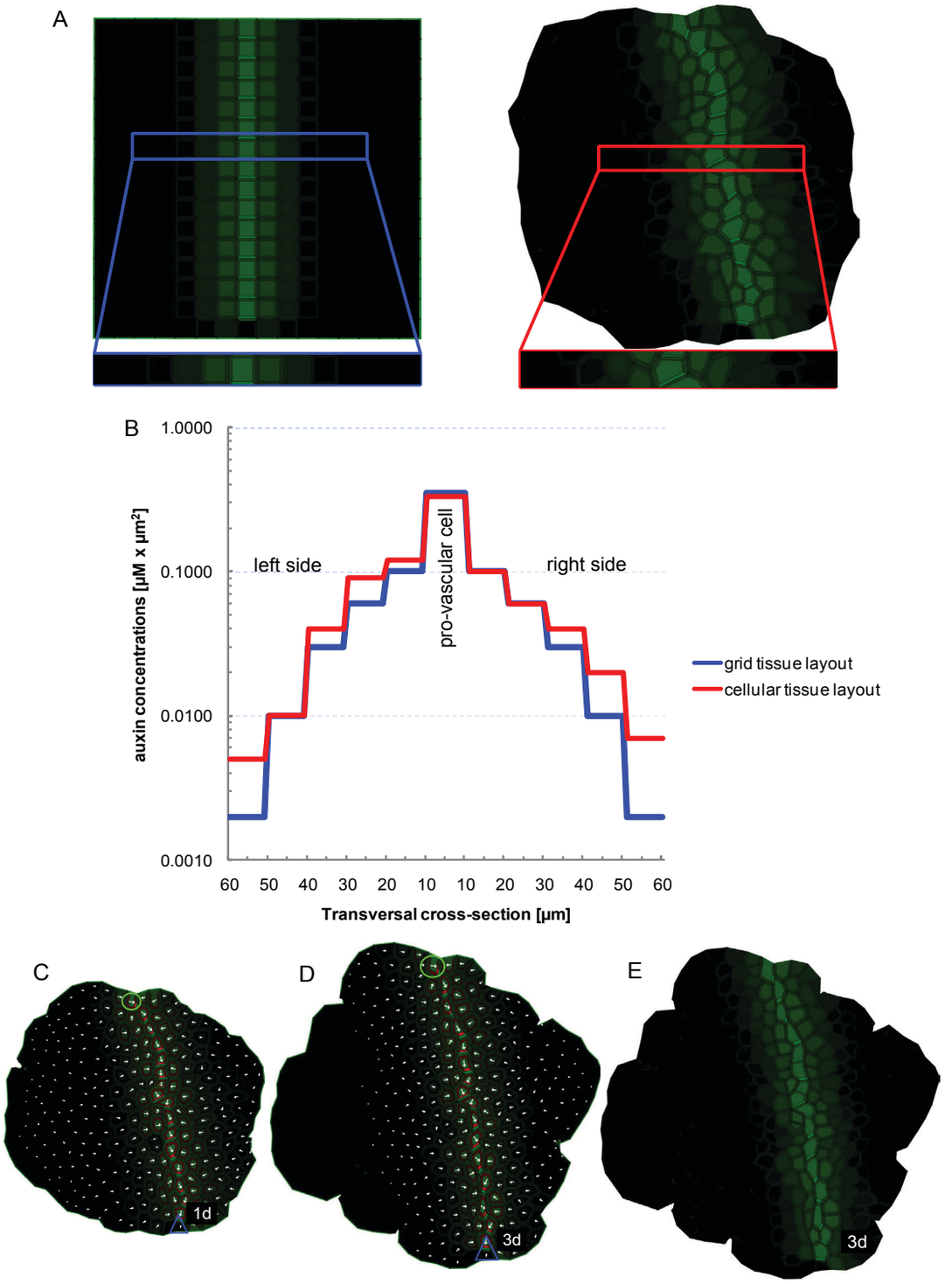

Figure 4 Steady-state auxin distribution patterns during vein propagation and robustness of vein pattern toward tissue growth

(A) Steady-state auxin distribution patterns for grid and cellular tissue layouts. **(B)** Examination of the auxin concentrations in cross sections of the tissue layouts showing that the auxin concentration is 10-fold higher in the provascular cells than in the surrounding tissues. **(C, D)** Simulation of auxin canalization during dynamic tissue growth (see Supplementary Movie 3). The vein pattern is not altered due to tissue growth. The model predicts PIN1 polarity pattern (C) as observed *in vivo* in *Arabidopsis* (Figures 3E and 3F). The auxin distribution pattern during tissue growth **(E)** corresponds to that in the non-growing tissue (A).

The *in silico* predictions of our model illustrate that high auxin concentrations and high auxin fluxes can simultaneously guide venation patterning, as suggested experimentally (Scarpella *et al.*, 2006). Importantly, the ERP model predicted PIN1 polarization not only away from the auxin source, but also toward provascular cells with high auxin levels; thus, through a single mechanism, the model recapitulates diverse cell polarization events both away from and toward an auxin maximum.

2.5 THE ERP MODEL IS ROBUST WITH RESPECT TO TISSUE GROWTH

We successfully utilized the ERP model to reproduce PIN1 polarity in a tissue grid and a more natural tissue layout. To investigate the flexibility and robustness of the model, we additionally imposed a dynamic growth simulation onto the natural tissue layout by assuming that the tissue consecutively expanded and subdivided as the cells changed their size and gave rise to daughter cells (Figure 4C). The growth simulations of the ERP model revealed that (following auxin source and sink application) discrete PIN-dependent auxin channels were maintained within growing cells and, moreover, were re-established after cell division (Figures 4D and 4E). Under these assumptions, the dynamic interplay of intracellular and extracellular auxin signaling might explain the robust adaptation of vascular patterning to tissue growth.

2.6 THE ERP MODEL REPRODUCES VEIN CONNECTIONS

The ERP model simulations faithfully reproduced vein formation and progression. Beside single vein formations, plants have evolved a complex network of connected vasculature. Classical experiments had revealed that preexisting vasculature attracts *de novo* established veins, allowing vein connections to be made (Sachs, 1981; Roland-Lagan and Prusinkiewicz, 2005), but the underlying mechanism of these inspiring observations remained to be solved.

To study whether the ERP model could provide a theoretical framework to assess the mechanisms underlying these classical experiments, the ERP model was simulated on grid tissue layout and, initially, a single vein pattern was induced by introducing an auxin source and a distal sink. Next, secondary auxin sources were introduced adjacent to the primary vein (Figure 5A). The simulation showed that a new conductive auxin channel was formed, which originated from the lateral auxin source and ultimately connected to the preexisting vein (Figure 5B). Both *in planta* and *in silico* it was observed that PIN proteins in the cells that surrounded a conductive auxin channel were polarized towards that channel (Figure 3). In our simulations, it is this preferential lateral polarization towards the auxin-containing channels that leads to the attraction of secondary veins.

2.7 THE ERP MODEL RECAPITULATES VEIN LOOP PATTERNS

Although complex vein networks in leaves are not fully understood, PIN-dependent auxin transport at the leaf margin and auxin biosynthesis appear to initiate vein loop formation (Roland-Lagan and Prusinkiewicz, 2005; Scarpella *et al.*, 2006). To test whether these complex vascular patterns could emerge by using the ERP model, the cellular tissue layout was simulated with an auxin-induced single vein pattern (Figures 5C-5H). As a bipolar PIN1 localization at the side of the vein loop initiation had been observed experimentally (Scarpella *et al.*, 2006), we tested whether a bipolar PIN1 signal would be triggered by the sequential introduction of lateral auxin sources in pairs of neighboring cells within the tissue surrounding the main vasculature. Within these pairs of cells, a bipolar PIN1 localization occurred that led to an auxin flow in two directions from the auxin sources, leaving a trace of polarized cells. Over time, the emerging veins were attracted by the main vein and, finally, formed closed vascular strands (vein loop precursors) (Figures 5C-5F). The leaf vein loop precursors produced by the simulation contained high auxin concentrations (Figure 5H) and displayed a narrow PIN1 expression domain (Figures 5C-5F). These predicted patterns were consistent with the PIN and auxin distribution patterns observed in developing leaves (Figures 5G and 5H). Additionally, we found that the distance of the lateral auxin sources from the main vasculature might determine the shape, radius, and length of the secondary vein (data not shown).

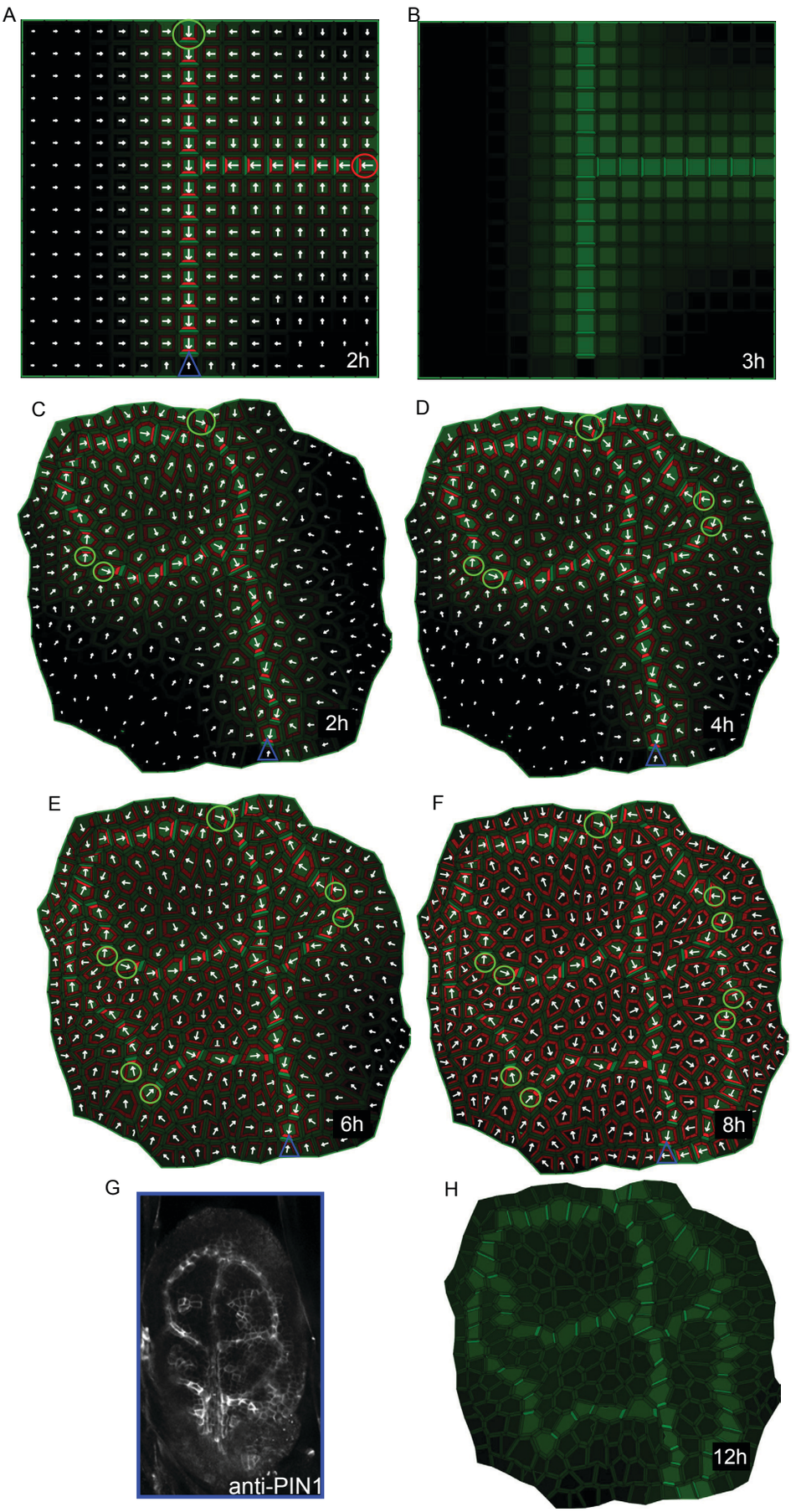
A
2h
B
3h
C
2h
D
4h
E
6h
F
8h
G
anti-PIN1
H
12h

Figure 5. Experimental and simulated auxin distributions and PIN polarization patterns during vein attraction and vein loop formation

(A, B) In silico experiment with the induction of a strong lateral auxin source (red). The main vein attracts the secondary vein, leading to a vascular connection (A). (B) Corresponding steady-state auxin distribution pattern. **(C-F)** Simulation of sequential application of lateral auxin sources (C, D, E, and F)(Supplementary Movie 4). Sequential addition of lateral auxin sources resulting in a complex vein loop pattern (D) with a predicted PIN1 distribution pattern that is similar to that detected by PIN1 immunolocalization in Arabidopsis leaves **(G)**. **(H)** Corresponding steady-state auxin concentration pattern revealing high auxin concentration accumulation in vein loops, as observed in planta (Scarpella *et al.*, 2006).

2.8 THE ERP MODEL PREDICTS COMPETITIVE CANALIZATION DURING SHOOT BRANCHING

The ERP model simulations predict that vein connections occur when the lateral auxin source is either comparable to or stronger than the primary auxin source (data not shown). This finding suggests that the interconnection of vascular systems might depend on the actual auxin concentration ratio between competing auxin sources, a relation reminiscent to a process proposed to regulate shoot branching. Auxin production and auxin flow in the primary shoot impose an apical dominance over lateral buds and inhibit their outgrowth (Thimann and Skoog, 1933). The removal of the apical auxin source, for instance by decapitation, leads to bud outgrowth. A competitive auxin transport mechanism between the dormant bud and stem vasculature has been proposed to regulate bud outgrowth (Prusinkiewicz *et al.*, 2009; Balla *et al.*, 2011). Accordingly, dormant buds fail to polarize PIN proteins and establish a PIN-dependent auxin flow and vein connection to the main vein in the stem, limiting their developmental progression.

To investigate whether the temporal supremacy of the primary auxin source in the system might be the actual reason for the inhibition of vein connection, we simulated the ERP model on grid tissue layout (stem representation) with a dominant apical auxin source and a distal auxin sink to induce a primary vein. Subsequently, we reduced the strength of the primary auxin source, which could correspond to virtual stem decapitation (Figure 6A). Afterward, we introduced a secondary lateral auxin source (Figure 6B). Over time, vein connection was observed from the lateral auxin source, following PIN1 polarization toward the primary vein (Figures 6C-6E). To verify the model outcome experimentally, we studied the PIN1 localization by immunolocalization with a PIN1 antibody in pea (*Pisum sativum*) stems. After stem decapitation (Figure 6F), exogenous application of auxin to the lateral site of the stem resulted in PIN1 expression at the site of application and polarization of PIN1 toward the preexisting vasculature (Figures 6G and 6H). To substantiate this finding, we reactivated the primary auxin source after stem decapitation (Figures 6I and

6J), before the virtual application of the secondary auxin source (Figure 6K). Under this condition, the lateral auxin source failed to connect to the primary vasculature (Figures 6L and 6M), which could be validated by performing PIN1 immunolocalizations on pea stems to which an apical auxin source had been applied after decapitation (Figures 6N-6P).

The observations from the model simulations and experiments imply that the temporal supremacy of primary over secondary auxin sources is presumably determined by the relative strength of the sources. To support this conclusion, we analyzed the behavior of the ERP model under the variable strength of auxin input in the system (Supplementary Figure 12). The dynamic instabilities characterized by periodic oscillations of PIN polarization in the presence of a weak auxin source corresponded to the absence of vein connection (vein repulsion) (Supplementary Figures 12M-12P). In contrast, an increase of the overall auxin concentrations in the tissue due to the presence of an enhanced auxin source led to the stable formation of vein patterns (Supplementary Figures 12E-12L). These findings are in agreement with experimental and theoretical observations based on PIN-dependent auxin transport (Prusinkiewicz *et al.*, 2009).

The ERP simulations revealed simple, yet important, mechanistic insights into this type of competitive inhibition that had initially been proposed to explain branching patterns in plants (Prusinkiewicz *et al.*, 2009). Our simulations faithfully reproduced PIN polarization toward the existing conductive auxin channel and preferential PIN polarization toward the newly forming auxin channel. However, the pattern of PIN polarization at the growing tip of the channel led to adverse PIN polarization in the proximity of the main vein (Figure 6I). Accordingly, the auxin concentration in the emerging lateral vein precursor needed to be comparable to or higher than that in the main vein to break this adverse polarization and to establish a vein connection (Figure 6D and Supplementary Figure 12). Thus, our modeling and experimental results provide a strong support for the hypothesis of competitive auxin canalization (Prusinkiewicz *et al.*, 2009) proposed for shoot branching in plants.

2.9 SELF-ORGANIZATION OF THE ERP MODEL EXPLAIN PIN POLARITY REARRANGEMENTS DURING VASCULAR REGENERATION

The ERP model accounted for vascular patterning processes, such as vein formation and propagation, competitive vein attraction/repulsion, and vein loop formation. Next, we studied another interesting aspect of vascular patterning linked to the regeneration of plant vasculature after local tissue wounding. Local wounding during tissue regeneration stimulates rearrangements in the polar localization of PIN proteins, thus providing plants with a flexible developmental adaptation (Benková *et al.*, 2003; Sauer *et al.*, 2006).

We tested the ERP model for changes in PIN polarity and auxin distribution associated with the regeneration of vasculature after wounding.

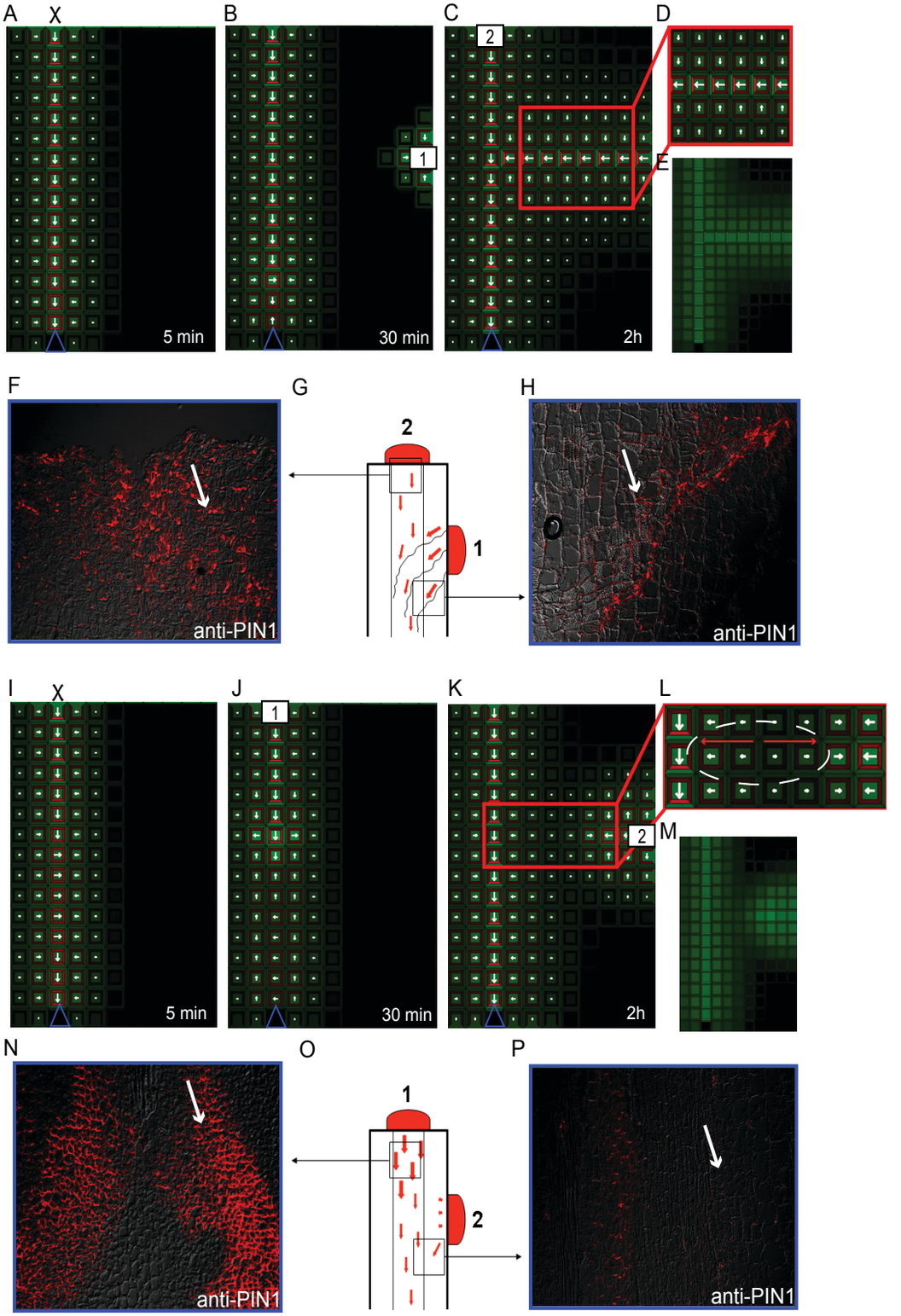

Figure 6 Experimental and simulated auxin distributions and PIN polarization patterns during branching activation and inhibition

(A-E) Simulation of a virtual stem cut (A) and subsequent virtual auxin applications, first to the lateral site (B) and second to the apical site (C). (D) Unilateral PIN1 polarity in the proximity of the main vein and canalization from the lateral auxin source as predicted by ERP model (E)(Supplementary Movie 5). **(F-H)** PIN1 immunolocalization in pea stems after decapitation (F and H). Auxin was applied first laterally and then apically (G). Canalization from the lateral source occurs analogously to that from a secondary auxin source (F and H). **(I-M)** Simulations of a virtual stem cut (I) and subsequent virtual auxin application, first to the apical site (J) and second to the lateral side of the tissue (K). (L) Bipolar PIN1 polarity in the cells between the main vein and the lateral source resulting in the lack of vein connection (M). **(N-P)** PIN1 immunolocalization in pea stems after decapitation and subsequent auxin application (N and P). Auxin was applied first to the apical site and then to the lateral site (O). Canalization from the lateral source did not occur (P)(Supplementary Movie 6).

First, we simulated an apical auxin source and distal auxin sink to establish an initial steady-state vein pattern. Subsequently, we disrupted this pattern by introducing virtual wounding (cell ablation) (Figures 7A-7C). A few minutes after wounding, auxin accumulated above the wound (Figure 7D), after which the PIN1 proteins were re-polarized. These flexible polarity rearrangements led to the regeneration of a conductive auxin channel circumventing the ablated cells (Figure 7E) (Sauer *et al.*, 2006). Additionally, the model simulation suggested a transient down-regulation of the PIN1 expression below the ablated cells (Figure 7F) that had not been reported previously.

To test these observations experimentally, we used a PIN1 antibody to study PIN1 distribution after wounding in pea stems. Tissue ablation resulted in a reduction in PIN1 expression just below the wound (Figure 7G). The PIN polarity pattern observed after *de novo* vascular regeneration (Figure 7G) was very similar to that predicted by the ERP model (Figure 7H and 7I).

The whole sequence of events predicted by the model, including auxin accumulation above the wound and PIN polarization around the wound, are consistent with previous experimental findings (Sauer *et al.*, 2006). The model forecasts that the ectopic accumulation of auxin (new sources) above the wound and the decrease in auxin content below the wound (new sinks) is the actual trigger for vein regeneration. Accordingly, high auxin above the wound functions as a new auxin source that leads to PIN polarization toward the tissues with low auxin concentration below the wound. Concomitantly, the auxin-induced carrier expression integrated in the ERP model was necessary to facilitate this PIN re-polarization during vein regeneration (Supplementary Figures 4M-4P and 5M-5P), suggesting a temporal down-regulation of PIN expression in the surroundings of the ablated region, ectopic auxin accumulation above the wound, and *de novo* PIN synthesis facilitate re-arrangement of PIN polarity and guide the regeneration of

tissues.

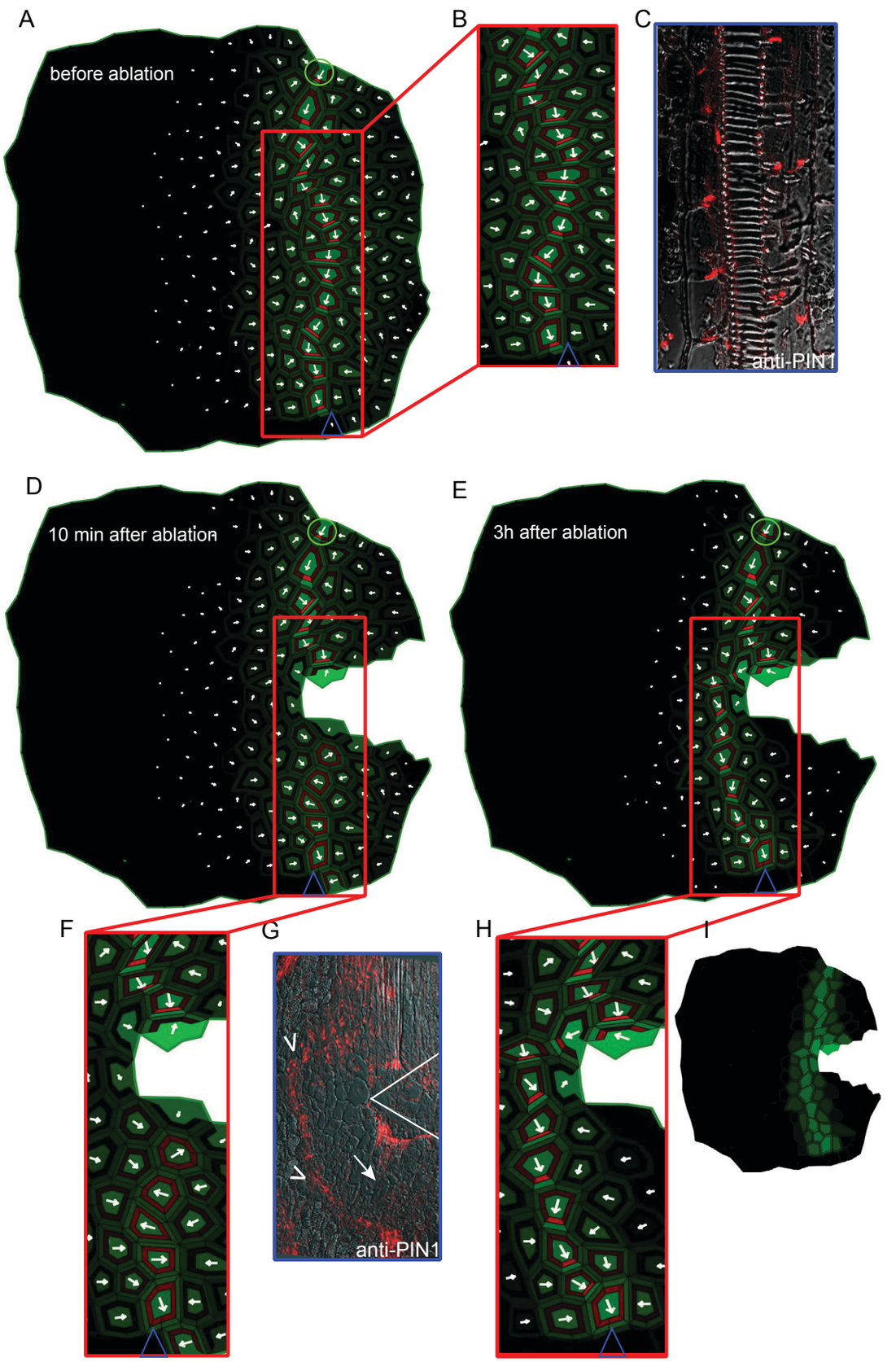
A
before ablation
B
C
anti-PIN1
D
10 min after ablation
E
3h after ablation
F
G
anti-PIN1
H
I

Figure 7 Experimental and simulated rearrangement of PIN polarity after wounding

(A-C) PIN1 polarization pattern in the model simulation (A and B)(Supplementary Movie 7) and in a *pea* stem (C) before tissue ablation. **(D)** Down-regulation of PIN1 expression below the wound apparent immediately after wounding. **(E)** Restoration of the vascular pattern by circumvention of the ablated cells. **(F-H)** Enlarged views of the wound site. PIN1 down-regulation in response to wounding in the model simulation (F), and in the *pea* wounding experiment (G), as reported with the PIN1 antibody (white arrow). The predicted PIN polarization pattern after vein regeneration (H) is similar to that observed in the pea stem (G) as indicated by the white arrowheads. **(I)** Auxin distribution pattern revealing the auxin accumulation site just above the ablated cells.

2.10 DISCUSSION

A unique feature of auxin among the plant hormones is its tightly regulated, cell-to-cell polar transport that allows auxin to convey positional and directional signals between cells and to contribute to tissue polarization and patterning. Here, we validate a conceptually novel mecha-nism for polarization of auxin transport in plant tissues. Our computer model integrates up-to-date cell biological data and a minimal theoretical framework for an auto-regulatory positive feedback loop between auxin and its polar redistribution of PIN auxin transporters. The subcellular dynamics of auxin carriers and auxin feedback on carrier expression that have been reported experimentally are both integrated into our model. Additionally, the model provides a mechanistically plausible framework for extracellular receptor-based auxin regulation for spatio-temporal synchronization and coordination of cell polarity, which, to our knowledge, had never been exploited in previous theoretical or experimental studies.

We propose that plants cell compete for extracellular auxin receptors to establish their polarities within tissues. Neither the auxin gradients in the cell wall nor the competitive utilization of receptors in the extracellular space had been so-far considered for spatial-temporal regulation of the PIN abundance at the plasma membrane (Sahlin *et al.*, 2009).

We demonstrated the plausibility of the ERP model for various processes, including *de novo* vascularization, venation patterning, and tissue regeneration in computer simulations performed with only minimal initial assumptions, namely a discrete auxin source and a distal sink. Moreover, these simulations were robust with respect to variable conditions, such as tissue growth, membrane permeability, auxin diffusion and auxin carrier expression levels, and position of auxin sources with respect to the auxin sink position.

The ERP model reproduces the very detailed PIN polarization events that occur during primary vein initiation (Scarpella *et al.*, 2006), such as basal PIN polarity

in provascular cells, transient adverse PIN polarization in neighboring cells during the alignment of tissue polarization, and inner-lateral polarity displayed by the tissues surrounding a conductive auxin channel.

Additionally, the ERP model generates high auxin concentration and high auxin flux simultaneously in emerging veins, revising the classical canalization models (Mitchison, 1980; Rolland-Lagan and Prusinkiewicz, 2005). Importantly, all the simulations support the claim that the ERP model represents the first single approach that faithfully reproduces the PIN polarization both with the auxin gradient (basal PIN1 polarity in provascular cells) and against the auxin gradient (transient adverse PIN1 polarization in neighboring cells surrounding the provascular bundle) as well as producing the corresponding auxin distribution patterns during auxin canalization.

Interestingly, the ERP model predicts that minimal assumptions, such as the regulated position and strength of auxin sources, are sufficient to explain (i) the source-to-sink guided organization of complex venation patterns (loops) at the base of a leaf solely by the read out of localized auxin concentration spots (Scarpella *et al.*, 2006) and (ii) the actual magnitude of auxin sources as a self-reliant signal to control mutual auxin source competition for vascular connection, for instance during the auxin transport regulation of shoot branching. The model simulations revealed that the generation of these complex and often transient PIN polarities is a self-emerging property of the ERP model. Importantly, the stability of these complex polarities is regulated by auxin in a concentration-dependent manner that provides a new explanation for vein attraction and repulsion phenomena.

Finally, we have demonstrated that the self-organizing dynamics of the ERP model produce a system that is able to adapt to external disruptions and provide a mechanistic framework for processes such as vascular tissue regeneration (Sauer *et al.*, 2006). By guiding a switch in PIN polarization and creating the associated temporal changes in auxin accumulation, a flexible pattern was created that allows the plant to adapt. The model analysis revealed the necessity of tight regulation of carrier expression by auxin for vascular patterning and regeneration after wounding. The ERP model simulations also illustrate how macroscopically different developmental processes, such as vascular tissue formation and apical dominance-controlled shoot branching, can be unified by a single mechanism derived through the combination of intracellular auxin feedback on carrier expression and extracellular perception-based regulation of the auxin carrier trafficking.

Here, we propose that extracellular auxin signaling facilitated by high-affinity binding of auxin to its extracellular receptor is essential to account for coordinated polarization of PIN proteins and auxin canalization during vascular development. The putative candidate for extracellular auxin receptor is ABP1 that resides in the lumen of the endoplasmic reticulum and is secreted to the cell wall (Napier *et al.*, 2002) where it is

physiologically active (Leblanc *et al.*, 1999; Steffens *et al.*, 2001). Auxin inhibits clathrin-dependent PIN internalization via binding to ABP1 (Robert *et al.*, 2010). However, ABP1 and its contribution to coordinated tissue polarity still needs to be experimentally investigated (Tromas *et al.*, 2010). Such extracellular fraction of ABP1 (or yet to be identified auxin-binding proteins) could correspond to the intercellular pools of extracellular auxin receptors in the ERP model. It still remains to be tested whether the ERP model could account for complex PIN polarity and auxin distribution patterns associated with embryogenesis, root system maintenance, and *de novo* organ formation.

2.11 COMPUTATIONAL METHODS

For model description, parameters, sensitivity analysis, and simulation insets, we refer to Supplementary Material. The model was based on a version of VirtualLeaf (Merks *et al.*, 2007; Merks *et al.*, 2011) (http://code.google.com/p/virtualleaf), a cell-based simulation tool for modeling plant development. All simulations were run until steady-state patterns emerged. All figures were processed in Adobe Illustrator. Figures 3-7 and Supplementary movies 1-7 are screenshots from the model simulations.

2.12 EXPERIMENTAL METHODS

Whole-mount immunolocalizations in *Arabidopsis thaliana* (L.) Heyhn. leaves were carried out as described (Friml *et al.*, 2003) and in pea (Pisum sativum) on 5-mm longitudinal epicotyl sections according to the method established and described for Arabidopsis stems (Friml *et al.*, 2003). The anti-Arabidopsis PIN1 antibody recognized also a polarly localized homologous PIN protein in pea (Sauer *et al.*, 2006). The following antibodies and dilutions were used: anti-PIN1 (1:500), FITC- and CY3-conjugated anti-rabbit (1:500), or anti-mouse (1:500). For wounding experiments, pea seedlings were used 5 days after germination. Incisions to 70%–80% of the stem diameter were made on epicotyls between the cotyledons and the first axillary bud. Wounded tissue was separated with plastic film. At least 20 epicotyls from two independent experiments were analyzed. After the treatments, epicotyl sections were fixed, embedded in paraffin, and processed for anti-PIN1 immunocytochemistry as described (Friml *et al.*, 2003).

Specimens were viewed under a confocal laser scanning microscope TCS SP2 AOBS (Leica; www.leica-microsystems.com) with a 10x/0.4, 20x/0.7, or 63x/1.4 objective at room temperature or with Fluoview 200 (Olympus; www.olympusfluoview.com) and a 20/0.50 objective at room temperature. Images were acquired with the Leica confocal software 2.00 or Fluoview 5.1 software, saved as TIF files, processed with Adobe Photoshop 7.0 (www.adobe.com), and adjusted for brightness and contrast.

2.13 MODEL DESCRIPTION

2.13.1 AUXIN TRANSPORT

According to the classical chemiosmotic hypothesis proposed by Raven and Goldsmith (Raven, 1975; Goldsmith *et al.*, 1981), in the presence of high cytoplasmic pH (7.2-7.6), auxin is almost completely de-protonated and requires polar transport mediated by PINs to move across the plasma membrane (with permeability pPIN) and consequently to leave the cell. In the apoplast at acidic pH (5.5), fractions of protonated and ionic auxin can either enter the cell via passive diffusion (with permeability pIAAH) and is enhanced by the activity of influx carriers (AUX/LAX) (with permeability pAUX). The model explicitly includes the movement of auxin within the apoplast (Mitchison, 1980) determined by diffusion coefficient $D_{a.}$ The auxin movement between cells and within cell wall is given by:

$$\begin{aligned}
\frac{dIAA_i}{dt} &= \frac{1}{V_i}\cdot\left[p_{IAAH}\cdot\sum_{j\in N_i} l_{ij}\cdot\left(f_{in}^{+}(IAA_{ij})-f_{out}^{+}(IAA_i)\right)\right] \\
&+ \frac{1}{V_i}\cdot\left[p_{AUX}\cdot\sum_{j\in N_i} AUX_{ij}\cdot\left(f_{out}^{-}(IAA_{ij})-f_{in}^{-}(IAA_i)\right)\right] \\
&+ \frac{1}{V_i}\cdot\left[p_{PIN}\cdot\sum_{j\in N_i} PIN_{ij}\cdot\left(f_{in}^{-}(IAA_{ij})-f_{out}^{-}(IAA_i)\right)\right]
\end{aligned} \tag{1}$$

$$\begin{aligned}
\frac{dIAA_{ij}}{dt} &= \frac{1}{V_{ij}}\cdot\left[D_a\cdot\left\{\frac{a_{ijji}}{d_{ijji}}\cdot(IAA_{ji}-IAA_{ij})+\frac{a_{ijik}}{d_{ijik}}\cdot(IAA_{ik}-IAA_{ij})+\frac{a_{ijil}}{d_{ijil}}\cdot(IAA_{il}-IAA_{ij})\right\}\right] \\
&+ \frac{1}{V_{ij}}\cdot\left[p_{IAAH}\cdot l_{ij}\cdot\left(f_{out}^{+}(IAA_i)-f_{in}^{+}(IAA_{ij})\right)\right] \\
&+ \frac{1}{V_{ij}}\cdot\left[p_{PIN}\cdot PIN_{ij}\cdot\left(f_{out}^{-}(IAA_i)-f_{in}^{-}(IAA_{ij})\right)\right] \\
&+ \frac{1}{V_{ij}}\cdot\left[p_{AUX}\cdot AUX_{ij}\cdot\left(f_{in}^{-}(IAA_i)-f_{out}^{-}(IAA_{ij})\right)\right]
\end{aligned} \tag{2}$$

with

$$\begin{aligned}
&f_{in}^{+}(IAA_{ij}) = \frac{IAA_{ij}}{1+10^{pHwall-pK}}, \quad f_{out}^{+}(IAA_i) = \frac{IAA_i}{1+10^{pHcell-pK}}, \\
&f_{in}^{-}(IAA_{ij}) = \frac{\Phi_{influx}}{1+10^{-pHwall+pK}}\cdot\frac{IAA_{ij}}{k_t+IAA_{ij}}, \quad f_{in}^{-}(IAA_i) = \frac{\Phi_{influx}}{1+10^{-pHcell+pK}}\cdot\frac{IAA_i}{k_t+IAA_i}, \\
&f_{out}^{-}(IAA_{ij}) = \frac{\Phi_{efflux}}{1+10^{-pHwall+pK}}\cdot\frac{IAA_{ij}}{k_t+IAA_{ij}}, \quad f_{out}^{-}(IAA_i) = \frac{\Phi_{efflux}}{1+10^{-pHcell+pK}}\cdot\frac{IAA_i}{k_t+IAA_i}
\end{aligned} \tag{3}$$

where IAA_i is the mean auxin concentration in the *i*-th cell and IAA_{ij}, IAA_{ji}, IAA_{ik}, IAA_{il}, are the mean auxin concentrations in adjacent wall compartments (Figure 1, main text), V_i and V_{ij} are the dimensions of the cell and wall compartment, respectively. N_i denotes the number of direct neighbors of cell *i*. The PIN_{ij} and AUX_{ij} variables determine the average level of PINs and AUX/LAXs carriers at the *i*-th plasma membrane facing cell *j*. The parameter k_t defines the saturation constant of polar auxin transport. The parameter D_a describes auxin diffusion between the neighboring wall compartments. p_{IAAH}, p_{PIN}, p_{AUX} are the membrane permeabilities for passive diffusion and carrier mediated transport, respectively. The pH differs between cytoplasm and extracellular space (pH_{cell}, pH_{wall}) leading to different auxin fractions inside/outside of the cell: $f_{in}^{+}(IAA_{ij})$, $f_{in}^{-}(IAA_{ij})$, $f_{in}^{-}(IAA_t)$, $f_{out}^{+}(IAA_t)$, $f_{out}^{-}(IAA_{ij})$, $f_{out}^{-}(IAA_t)$ (Figure 1). Each wall compartment (*ij*) is considered to have three neighbors, left and right neighbors (*il*, *ik*) connected to the same cell *i* and one neighbor (*ji)* "connected" to the neighboring cell *j*. The crossing area between neighboring cytoplasm and membrane/wall compartments (for passive transport) is denoted as l_{ij}, crossing areas between neighboring wall compartments is a_{ijji}, a_{ijik}, a_{ijil} and distances between neighboring wall compartments used in the diffusion terms are given by d_{ijji}, d_{ijik}, d_{ijil}. For simplicity we used the constant value of a = 0.25 μm corresponding to cell wall thickness of 500 nm. In addition, the model assumes that the active auxin transport mediated by PINs and AUX/LAXs proteins depends on the electrochemical gradient between cytoplasm and the apoplast. The Φ_{influx} and Φ_{efflux} parameters (eq. 3) describe the membrane potential:

$$\Phi_{influx} = \Phi_{efflux} \cdot e^{\frac{zVF}{RT}} = \frac{zVF}{RT} \cdot \frac{e^{\frac{zVF}{RT}}}{e^{\frac{zVF}{RT}} - 1} \tag{4}$$

where $V = -100\ mV$, $F = 9.6 \times 10^4\ mol^{-1}$, $R = 8.3\ Jmol^{-1}K^{-1}$, $T = 300K$.

2.13.2 AUXIN CARRIER PRODUCTION AND BREAKDOWN

We model the expression of AUX/LAX and PIN proteins in the cell as follows:

$$\frac{dPIN_i}{dt} = \alpha_{PIN} \cdot h(IAA_i) - \delta_{PIN} \cdot PIN_i \tag{5}$$

$$\frac{dAUX_i}{dt} = \alpha_{AUX} \cdot h(IAA_i) - \delta_{AUX} \cdot AUX_i \tag{6}$$

$$h(IAA_i) = \frac{IAA_i}{k_m + IAA_i} \tag{7}$$

where PIN_i and AUX_i are the total intracellular concentrations of PIN and AUX/LAX in cell i, α_{PIN} and α_{AUX} define the rates of auxin-induced PIN and AUX/LAX synthesis (Heisler *et al*., 2005; Vieten *et al*., 2005; Scarpella *et al*., 2006) and δ_{PIN} and δ_{AUX} determine decay rates of PIN and AUX/LAX proteins. IAA_i expresses the mean auxin concentration in the i-th cell and k_m is a Michaelis–Menten constant for auxin-dependent carrier production ($h(IAA_i)$, Figure 1B).

2.13.3 AUXIN CARRIER RECYCLING

Auxin carriers recycle between endosomes and plasma membrane (Steinmann *et al*., 1999; Geldner *et al*., 2001) with the base rates a_{exo}, k_{exo} and a_{endo}, k_{endo} for AUX/LAX and PIN exocytosis (trafficking from endosomes to the plasma membrane) and their internalization (trafficking from plasma membrane to the endosomes), respectively. AUX/LAX transporters are distributed evenly on the cell membrane and show non-polar subcellular localization.
The AUX/LAX carriers are allocated in the plasma membrane in each time step as follows:

$$\frac{dAUX_{ij}}{dt} = a_{exo} \cdot AUX_i - a_{endo} \cdot AUX_{ij} \tag{8}$$

where AUX_{ij} represents the average amount of AUX/LAX proteins at the plasma membrane, and AUX_i is a total intracellular level of AUX/LAX in cell i and a_{exo} and a_{endo} are the rates of AUX/LAX exocytosis and internalization, respectively.
The corresponding change in intracellular AUX/LAX levels in *ith* cell is described as follows:

$$\frac{dAUX_i}{dt} = \sum_{j \in N_i} (a_{endo} \cdot AUX_{ij} - a_{exo} \cdot AUX_i) \tag{9}$$

The polar, subcellular localization of PIN auxin efflux facilitators in the model is determined by differential PIN retention at a given cell side (Dhonukshe *et al*., 2008) as a result of an auxin-dependent inhibition of PIN internalization (Paciorek *et al*., 2005) and an intracellular competition of cell membranes for auxin efflux transporters (Figure 1C, main text).
PIN allocation in the plasma membrane changes according to the following formula:

$$\frac{dPIN_{ij}}{dt} = k_{exo} \cdot PIN_i - PIN_{ij} \cdot (k_{endo} + kh_{ij}) \tag{10}$$

where PIN_{ij} are the PIN level on *ij*-th plasma membrane, and PIN_i is the total intracellular PIN level in *i*-th cell. The parameter k_{exo} determines the rate of PIN exocytosis, and k_{endo} is a base rate for PIN endocytosis whereas kh_{ij} determines the auxin-dependent effect on PIN internalization.

The corresponding change in intracellular PIN level in *ith* cell is given by:

$$\frac{dPIN_i}{dt} = \sum_{j \in N_i} (PIN_{ij} \cdot (k_{endo} + kh_{ij}) - k_{exo} \cdot PIN_i) \tag{11}$$

2.13.4 AUXIN EFFECT ON PIN INTERNALIZATION

We assumed in our model that two neighboring cells share the intercellular pool of auxin receptors which we denote as $2R_T$. These extracellular receptors bind to auxin to form an active auxin-receptor complex (recruited receptor) whereas remaining free receptors from intercellular pool freely diffuse from one side of the cell to the closest side of adjacent cell.

Because the amount of auxin receptors remains is conserved in the extracellular space between two neighboring cells, the mass conservation law is written as:

$$2R_T = R_{ij} + R_{ji} + C_{ij} + C_{ji} \tag{12}$$

where R_{ij} and R_{ji} are unbound/free solution receptors in the adjacent wall compartments, respectively and C_{ij} and C_{ji} are the active auxin-receptor complexes. The kinetics of the reversible auxin-receptor binding is given by:

$$IAAij + Rij \xleftrightarrow{kf,kr} Cij, \quad IAAji + Rji \xleftrightarrow{kf,kr} Cji \tag{13}$$

where k_f and k_r are forward and backward rates of receptor cycling between active and inactive states, respectively. Then a dissociation constant of auxin-receptor complex (K_D) is determined as:

$$K_D = \frac{kr}{kf} \tag{14}$$

Next the relative changes in the amount of bound and unbound receptors are governed by following ODE system:

$$\frac{dC_{ij}}{dt} = IAA_{ij} \cdot R_{ij} - K_D \cdot C_{ij} + D_c \cdot (C_{ji} - C_{ij}) \tag{15}$$

$$\frac{dC_{ji}}{dt} = IAA_{ji} \cdot R_{ji} - K_D \cdot C_{ji} - D_c \cdot (C_{ji} - C_{ij}) \tag{16}$$

$$\frac{dR_{ij}}{dt} = -IAA_{ij} \cdot R_{ij} + K_D \cdot C_{ij} + D_R \cdot (R_{ji} - R_{ij}) \tag{17}$$

$$\frac{dR_{ji}}{dt} = -IAA_{ji} \cdot R_{ji} + K_D \cdot C_{ji} - D_R \cdot (R_{ji} - R_{ij}) \tag{18}$$

where D_R is a free-receptor diffusion coefficient and D_C denotes the diffusion of the auxin-receptor complex. For simplicity we assume that auxin-receptor complexes and free receptors in *ij*-th and *ji*-th discrete wall compartments are practically in dynamic equilibrium (quasi-steady state) due to the fast kinetic reactions. In our model we considered the intercellular pools of extracellular receptor per each pair of neighboring cells such that the total amount of receptors in each intercellular pool is conserved. Therefore, the transversal diffusion of receptors can be negligible. To express that one puts the right side of equations (15)-(17) to zero whereas equation (18) can be replaced by equation (12). By solving the linear system of equations (12), (15)-(17) for *Cij*, $C_{ji,,}$ R_{ij} and $R_{ji,}$ one obtains the following relations:

$$C_{ij} = \frac{2 \cdot R_T \cdot \left(\sqrt{\alpha \cdot \beta} \cdot (IAA_{ij} + IAA_{ji}) + IAA_{ij} \cdot (\alpha \cdot IAA_{ji} + K_D)\right)}{K_D \cdot (2 \cdot K_D + IAA_{ij} + IAA_{ji}) + 2 \cdot \sqrt{\alpha \cdot \beta} \cdot (IAA_{ij} + IAA_{ji} + 2 \cdot K_D) + \alpha \cdot (2 \cdot IAA_{ij} \cdot IAA_{ji} + IAA_{ij} \cdot K_D + IAA_{ji} \cdot K_D)} \tag{19}$$

$$C_{ji} = \frac{2 \cdot R_T \cdot \left(\sqrt{\alpha \cdot \beta} \cdot (IAA_{ij} + IAA_{ji}) + IAA_{ji} \cdot (\alpha \cdot IAA_{ij} + K_D)\right)}{K_D \cdot (2 \cdot K_D + IAA_{ij} + IAA_{ji}) + 2 \cdot \sqrt{\alpha \cdot \beta} \cdot (IAA_{ij} + IAA_{ji} + 2 \cdot K_D) + \alpha \cdot (2 \cdot IAA_{ij} \cdot IAA_{ji} + IAA_{ij} \cdot K_D + IAA_{ji} \cdot K_D)} \tag{20}$$

$$R_{ij} = \frac{2 \cdot R_T \cdot K_D (K_D + 2 \cdot \sqrt{\alpha \cdot \beta} + \alpha \cdot IAA_{ji})}{K_D \cdot (2 \cdot K_D + IAA_{ij} + IAA_{ji}) + 2 \cdot \sqrt{\alpha \cdot \beta} \cdot (IAA_{ij} + IAA_{ji} + 2 \cdot K_D) + \alpha \cdot (2 \cdot IAA_{ij} \cdot IAA_{ji} + IAA_{ij} \cdot K_D + IAA_{ji} \cdot K_D)} \tag{21}$$

$$R_{ji} = \frac{2 \cdot R_T \cdot K_D (K_D + 2 \cdot \sqrt{\alpha \cdot \beta} + \alpha \cdot IAA_{ji})}{K_D \cdot (2 \cdot K_D + IAA_{ij} + IAA_{ji}) + 2 \cdot \sqrt{\alpha \cdot \beta} \cdot (IAA_{ij} + IAA_{ji} + 2 \cdot K_D) + \alpha \cdot (2 \cdot IAA_{ij} \cdot IAA_{ji} + IAA_{ij} \cdot K_D + IAA_{ji} \cdot K_D)} \tag{22}$$

where

$$\alpha = \frac{D_C}{D_R}$$

and

$$\beta = D_C \cdot D_R$$

We assumed that the active auxin-receptor complexes are recruited with the highest probability to the nearest cell. Because recruited receptors transfer a signal to the plasma membrane they could be temporally immobilized at the cell surface (represented by

discrete wall compartment) presumably due to its interaction with plasma membrane or its conformational changes. Therefore, the diffusion of free receptor in the apoplast becomes much larger than the diffusion of auxin-bound recptors ($D_C << D_R$) which then implicates $\alpha \sim 0$ and $\beta \sim 0$ for finite values of D_R and D_C. In this case of $D_C = 0$ and $D_R \to \infty$ the equations (19)-(22) simplify to:

$$C_{ij} = \frac{2 \cdot RT \cdot IAA_{ij}}{(2 \cdot K_D + IAA_{ij} + IAA_{ji})} \tag{23}$$

$$C_{ji} = \frac{2 \cdot RT \cdot IAA_{ji}}{(2 \cdot K_D + IAA_{ij} + IAA_{ji})} \tag{24}$$

$$R_{ij} = R_{ji} = \frac{2 \cdot RT \cdot K_D}{(2 \cdot K_D + IAA_{ij} + IAA_{ji})} \tag{25}$$

In our model we assume that the recruited receptors signal on PIN internalization. Taking into account equations (23)-(25) one derives the formula that describes the auxin-dependent inhibition of PIN internalization at the *(ij)* side of the *i*-th cell:

$$kh_{ij} = \frac{\mu}{1 + C_{ij}} \tag{26}$$

where kh_{ij} expresses the effective rate of PIN endocytosis (μ) repressed by the amount of active signalling components at *ijth* side of the cell as presented in Figures 1D and 2A.

2.13.5 TISSUE LAYOUT

Two representations of a longitudinal section of the shoot apical meristem, including a two-dimensional grid and a cellular template with irregular cell topology, were used to simulate auxin transport during auxin canalization, vein loop formation, and tissue wounding. Depending on the specific case simulated, a single cell is either a square (grid representation) or an arbitrary polygon (longitudinal meristem section). Each cell was surrounded by wall compartments that included plasma membranes and the apoplast (extracellular space). A cell volume of 100 μm^2 and a wall length of 10 μm in the two-dimensional were adopted in the grid tissue layout. The intracellular gradients in the grid tissue layout (Supplementary Figure 11) were modeled as follows: The single cell box was divided in four identical triangular compartments each associated with the one side of the cell and the cell center. In this case, intracellular auxin freely diffuses within intracellular compartments following Fick's law:

$$J_{1->2} = -D \cdot \frac{c_1 - c_2}{L} \tag{27}$$

where $J_{1->2}$ is the net flux from compartment 1 to compartment 2, c_j is the concentration of intracellular auxin in compartment j for j=1,2, and D is the diffusion coefficient of auxin in the cell, and L is a distance between compartments.
In the cellular templates, the cell volume and cell wall length varied, but were, on average, approximately 98 μm^2 and 9 μm, respectively. For simplicity, cell wall thickness was set at 0.5 μm.

2.13.6 BOUNDARY CONDITIONS

In the computer simulations of auxin canalization and tissue wounding (Figures 3, 4, and 7), the auxin source was represented by a cell that produced auxin at a rate of 0.0015 $\mu M\ \mu m^{-2}\ s^{-1}$. The auxin sink was placed at the bottom-most part of the tissue (grid and cellular tissue layouts) and to the right-most cell in simulations on the file of cells and corresponded to the site of the tissue where auxin was evacuated from the system (sink preserves near zero auxin concentration). For the remaining tissue borders in all model simulations, zero-flux boundary conditions were used. Virtual wounding (Figure 7) was represented by cell ablation (simply by removing cells from the tissue layout). For the simulations of vein loop patterns (Figure 5), the primary source was as above (Figures 3 and 4), and the secondary auxin sources were sites of enhanced auxin production at the rate of 0.001 $\mu M\ \mu m^{-2}\ s^{-1}$ (each source). In competitive canalization simulations (Figure 6), the pea stem decapitation corresponded to a strong reduction of strength of the primary auxin source by 10-fold but not its complete removal which would result in the suppression of stable PIN polarization pattern (Supplementary Figure 12). Most of the auxin biosynthesis is indeed coming from the decapitated region, however also the vascular tissue is the site of local auxin biosynthesis. Therefore we reduced the auxin level, which is likely to reflect *in planta* situation. The weak and strong auxin sources were represented by auxin-producing cells at rates of 0.0002 $\mu M\ \mu m^{-2}\ s^{-1}$ and 0.002 $\mu M\ \mu m^{-2}\ s^{-1}$, respectively.

2.13.7 PARAMETERS

The general parameters for tissue layout and model simulations are shown in Supplementary Table 1. The parameters for auxin transport dynamics are presented in Supplementary Table 2, and were mainly derived from the literature (Goldsmith *et al*., 1981; Mitchison, 1980a; Swarup *et al*., 2005; Kramer, 2006; Kramer *et al*., 2007). The quantitative parameters for PIN and AUX/LAX recycling, production and degradation remain to a large extent unknown and were chosen to assert that auxin carriers recycling is a much faster process than an auxin carrier expression. They are presented in Supplemen-

tary Table 3.

2.13.8 CELL EXPANSION AND CELL DIVISION

Cellular growth was described by cell expansion and was regulated by auxin in a concentration-dependent manner (Chen *et al*., 2001) and subsequent cell division**.** The tissue dynamics encompassed threshold of cell size above which cells start to divide. The arbitrary division threshold was set at 1000 μm^2. For simplicity in the model, the provascular cells undergo the auxin-dependent differentiation to mature cells. Once those cells *reached maturity they* lose their capability to divide (Ye, 2002). We assumed that high auxin concentrations in the tissue promote vascular differentiation (Ye, 2002). Simulations of growing tissue (Figure 4C-4E) were carried out over 3 CPU time days, which corresponds to 259,200 simulation steps.

2.13.9 NUMERICAL AND SIMULATION METHODS

The dynamic cell-based simulations of auxin transport were done by numerical computations of coupled ODE systems, with an adaptive-size, fifth-order Runge-Kutta method with monitoring of local truncation error to ensure accuracy and adjustment of the step size. A time step was adjusted in each iteration to minimize local calculation errors. If the local truncation error was small enough, the method gave the output for the defined time interval and then proceeded to the next time step. A maximum time step of 1 s was used, but other values were also tested without significant changes in the qualitative results of the simulations. For the sensitivity and bifurcation analysis of the stationary solutions (Supplementary Figures 13-16), we used MATCONT - graphical Matlab package for numerical bifurcation analysis (Dhooge *et al*., 2003).

2.13.10 MODEL SENSITIVITY ANALYSIS

We analyzed the importance of each component of the ERP model for general model behavior, sensitivity and robustness. Our model analysis was divided in four parts; each part treats about one structural component of the ERP model. For instance, we investigated the altered dynamics of extracellular receptor-based auxin signalling mechanism by modifying diffusion rates of bound and unbound receptors, the amount of receptors in the intercellular pools and specificity of auxin binding (receptor recruitment) (Supplementary Figures 1-3). We concluded that the competitive utilization of auxin receptors in the apoplast determined by their respective motility is the actual trigger for initiation of PIN polarization. Therefore, we found that auxin-mediated carrier expression plays a crucial role in generating realistic PIN polarization patterns during vascularization and tissue regeneration (Supplementary Figures 4 and 5). Also

the *in silico* interference with the main components of polar auxin transport system that includes PIN and AUX/LAX transporters led to the surprising observations (Supplementary Figures 6 and 7). In particular, the contribution of AUX/LAX-dependent transport to PIN polarization maintenance has been revealed (Supplementary Figure 7). Also the general role of polar auxin transport in buffering auxin diffusion in the apoplast to maintain cell polarities has been suggested (Supplementary Figures 8 and 9). Then we tested the robustness of the ERP model with respect to the auxin source/sink translocation and presence of intracellular diffusion-driven auxin gradients (Supplementary Figures 10 and 11). We also found that auxin biosynthesis plays a crucial role in stabilizing PIN polarization and polar auxin transport in the tissue (Supplementary Figure 12) and their spatio-temporal regulation may be linked to phenomena such as vascular attraction/repulsion and competitive canalization of auxin flow in shoot branching. To investigate model behavior, we analyzed the sensitivity and robustness of stationary solutions with respect to perturbations in model parameters (Supplementary Figures 13-16). We identified the parameter regimes for which our model exhibits particular type of behavior (Supplementary Figures 13-16).

2.14 SUPPLEMENTARY TABLES

Supplementary Table 1 General parameters for tissue layout and model simulations

Parameter	Cell file	Grid layout	Cellular layout	Cellular growth	Units
Cell area (V_i)	100	100	98*	variable	μm^2
Wall area (V_{ij})	0.1 x V_i	0.1 x V_i	0.1 x V_i*	variable	μm^2
Wall length (l_{ij})	10	10	9.8*	variable	µm
Wall thickness term (a_{ijji}/d_{ijji})	0.025	0.025	0.025	0.025	µm
Time step	1	1	1	1	s
Growth step	-	-	-	1	min
Cell expansion rate	-	-	-	0.01	-
Cell division threshold	-	-	-	1000	μm^2

* Mean cell and wall volumes and mean wall length for cellular tissue layout

Supplementary Table 2 Auxin transport parameters

Parameter	Fig. 2,3,4,5,6,7 and Supp Fig. 2,4,5,10,12	Supp Fig. 1	Supp Fig. 3	Supp Fig. 6	Supp Fig. 7	Supp Fig. 8	Supp Fig. 9	Supp Fig. 11	Units
Apoplastic diffusion (D_a)	100	100	100, 10	100	100	100, 10	500, 20	100	$\mu m^2 s^{-1}$
Free receptor diffusion (D_R)	1	1, 0.1, 10 ,100	1	1	1	1	1	1	$\mu m^2 s^{-1}$
Auxin-receptor complex diffusion (D_C)	0	0, 0.001, 0.1, 1	0	0	0	0	0	0	$\mu m^2 s^{-1}$
IAAH permeability (p_{IAAH})	10	10	10	10	100, 10	10	50, 10	10	$\mu m\, s^{-1}$
PIN permeability (p_{PIN})	30	30	30	300, 30, 1	30	30	150, 30	30	$\mu m\, s^{-1}$
AUX/LAX permeability (p_{AUX})	30	30	30	30	300, 30, 1	30	150, 30	30	$\mu m\, s^{-1}$
pH in wall (pH_{wall})	5.5	5.5	5.5	5.5	5.5	5.5	5.5	5.5	-
pH in cell (pH_{cell})	7.6	7.6	7.6	7.6	7.6	7.6	7.6	7.6	-
Dissociation constant (pK)	5	5	5	5	5	5	5	5	-
Saturation constant for auxin transport (k_t)	1	1	1	1	1	10, 1	1	1	µM
Intracellular auxin diffusion (D)	-	-	-	-	-	-	-	600, 300, 100, 50, 10	$\mu m^2 s^{-1}$

Supplementary Table 3 PIN and AUX/LAX dynamics

Parameter	Fig. 2,3,4,5,6,7 and Supp Fig. 1,6,7,8,9,10,11,12	Supp Fig. 2	Supp Fig. 3	Supp Fig. 4 and 5	Units
PIN exocytosis base rate (k_{exo})	1	1	1	1	s^{-1}
PIN internalization base rate (k_{endo})	0.001	0.001	0.001	0.001	s^{-1}
Effective PIN internalization (μ)	1	1, 0.1	1	1	s^{-1}
AUX/LAX exocytosis base rate (a_{exo})	1	1	1	1	s^{-1}
AUX/LAX internalization base rate (a_{endo})	0.1	0.1	0.1	0.1	s^{-1}
PIN production rate (α_{PIN})	1	1	1	1, 0.1, 0.01, 0	s^{-1}
PIN degradation rate (δ_{PIN})	0.03	0.03	0.03	0.03, 0.001, 0	s^{-1}
AUX/LAX production rate (α_{AUX})	1	1	1	1, 0.1, 0.01, 0	s^{-1}
AUX/LAX degradation rate (δ_{AUX})	0.05	0.05	0.05	0.05, 0.001, 0	s^{-1}
Saturation of auxin-induced PIN and AUX/LAX production (k_m)	100	100	100	100	μM
Receptor dissociation constant (K_D)	1	1	10, 1, 0.1	1	μM
The number of extracellular auxin receptors (R_T)	100	10000, 100, 1	100	100	-

2.15 SUPPLEMENTARY FIGURES

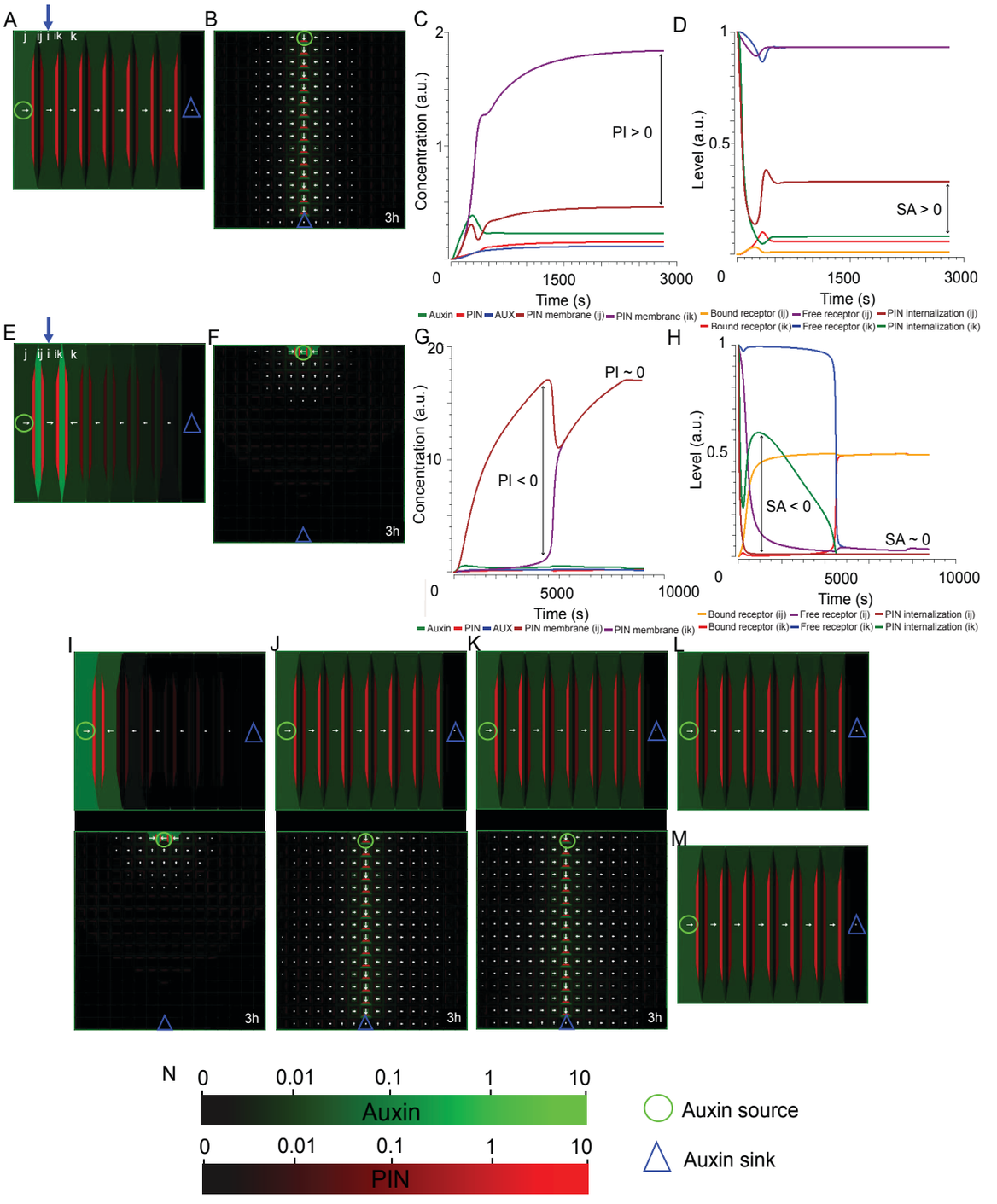

Supplementary Figure 1 Model sensitivity with respect to diffusion rates of free and bound auxin receptor

(A-D) *In silico* 'WT' control simulation **-** Model simulations on the file of cells (A) and on the cellular grid (B) showed PIN polarization and canalization of auxin flow from an auxin source towards a distal auxin sink. Diffusion rate of free receptor (D_R) was set at 1 $\mu m^2 s^{-1}$ and diffusion of bound auxin receptor (D_C) was assumed negligible (~0). **(C)** Time-course profiles of auxin concentration, intracellular PIN and AUX/LAX levels (PIN_i and AUX_i), and PIN membrane levels (PIN_{ij} and PIN_{ik}). **(D)** Time-course profiles of bound (C_{ij} and C_{ik}) and free receptor (R_{ij} and R_{ik}) levels normalized by total amount of receptors in the pool (R_T); and corresponding PIN internalization rates (kh_{ij} and kh_{ik}). Polarization Index (PI) and Signaling Asymmetry (SA) are given to evalutate asymmetry (see also Figure legend 2 for description). **(E-H)** Model simulations on the file of cells (E) and on the cellular grid (F) are presented for diffusion rates of bound and unbound receptor that were equivalent (D_R=D_C=1 $\mu m^2 s^{-1}$). In this case, neither PIN polarization towards an auxin sink nor canalization of auxin flow were observed. This model simulation predicted that neighboring cells tend to pump auxin out to the common cell wall (E, F). Initially, PI and SA were negative, suggesting that more PINs and higher auxin signaling was present at *ij*-th side of the cell. In time they both approach zero which is reflected in non-polar cell behavior (G, H). **(I)** Model simulations on the file of cells and on the cellular grid are presented and diffusion rates of bound and unbound receptor were D_R=1 $\mu m^2 s^{-1}$, D_C=0.1 $\mu m^2 s^{-1}$, **(J)** D_R=1 $\mu m^2 s^{-1}$, D_C=0.001 $\mu m^2 s^{-1}$,**(K)** D_R=0.1 $\mu m^2 s^{-1}$, D_C=0 $\mu m^2 s^{-1}$, **(L)** D_R=10 $\mu m^2 s^{-1}$, D_C=0 $\mu m^2 s^{-1}$, **(M)** D_R=100 $\mu m^2 s^{-1}$, D_C=0 $\mu m^2 s^{-1}$.

A ratio of bound/unbound receptor mobility, denoted as $\alpha = D_C/D_R$ (equations 19-22) directly reflects the asymmetry of signaling on PIN internalization (SA). The lower this ratio is the higher SA becomes. Here, we demonstrated that our model predicts PIN polarization patterns if the diffusion rate of recruited receptors (D_C) is assumed to be at least an order of magnitude lower than the diffusion rate of free soluble receptors (D_R). **(N)** Color coding and symbols are as in Figure 2E and apply to all model simulations.

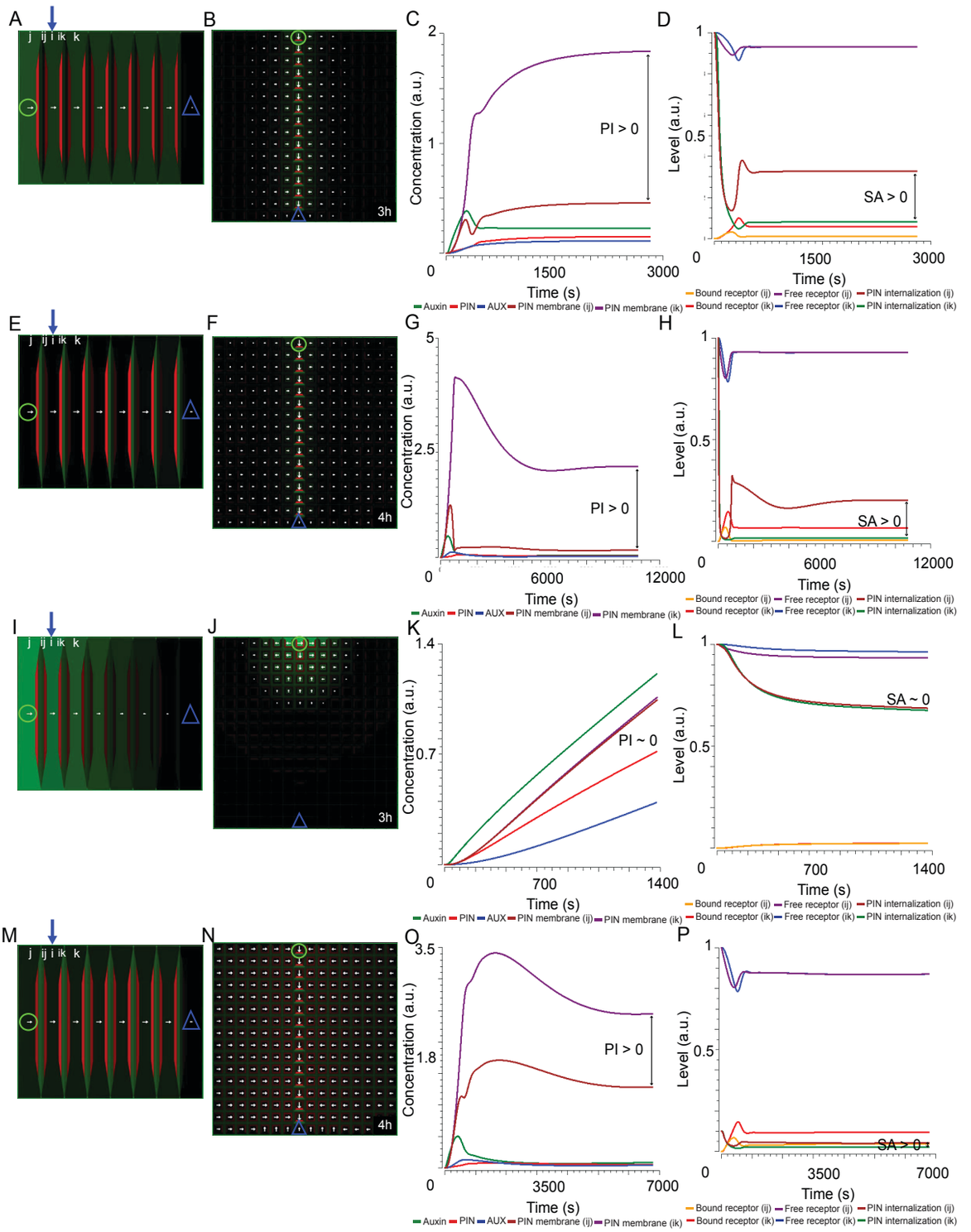
A
B
C
D
j ij i ik k
3h
Concentration (a.u.)
PI > 0
Time (s)
Level (a.u.)
SA > 0
Auxin PIN AUX PIN membrane (ij) PIN membrane (ik)
Bound receptor (ij) Free receptor (ij) PIN internalization (ij)
Bound receptor (ik) Free receptor (ik) PIN internalization (ik)
E
F
G
H
4h
I
J
K
L
PI ~ 0
SA ~ 0
M
N
O
P

Supplementary Figure 2 Model sensitivity with respect to abundance of extracellular auxin receptors **(A-D)** *In silico* 'WT' control simulation - Model simulations on the file of cells (A) and on the cellular grid (B) showed PIN polarization and canalization of auxin flow from an auxin source towards a distal auxin sink. The amount of receptors in the intercellular pools was: R_T = 100 (virtually the same as control simulation presented in Supplementary Figure 1A-D). **(E-H)** Model simulations on the file of cells (E) and on the cellular grid (F) are presented for R_T = 10000. The predicted vascular pattern by model simulation had dropped auxin concentrations (G) presumably due to high levels of extracellular auxin signaling (H), more PINs at the plasma membranes and thus more PIN-dependent auxin transport in the tissue (G). Note that steady-state values of PI and SA were slightly increased (G, H) compared to those in control simulation (C, D) **(I-L)** Model simulations on the file of cells (I) and on the cellular grid (J) are presented for R_T = 1. Here, R_T parameter was significantly reduced which was reflected in over-accumulation of auxin in the cell (K) and the high PIN internalization rates (L). Note that both PI and SA were practically 0. However, the reduction of effective rate of PIN internalization ($\mu = 1\ s^{-1}$) by a 10-fold was sufficient to reestablish differential auxin signaling (increased SA) **(O, P)**, trigger PIN polarization (PI > 0) and reproduce vein pattern **(M, N).** These findings indicate parameter μ is limiting parameter for PIN recycling. Inset of parameter μ allows in our model to increase or decrease PIN levels at the plasma membrane to modulate a sensitivity of feedback mechanism to the amount of extracellular receptors available in the intracellular pool. Polarization Index (PI) and Signaling Asymmetry (SA) are introduced in Figure 2. For symbols and color code, see Figures 2E and Supplementary Figure 1N.

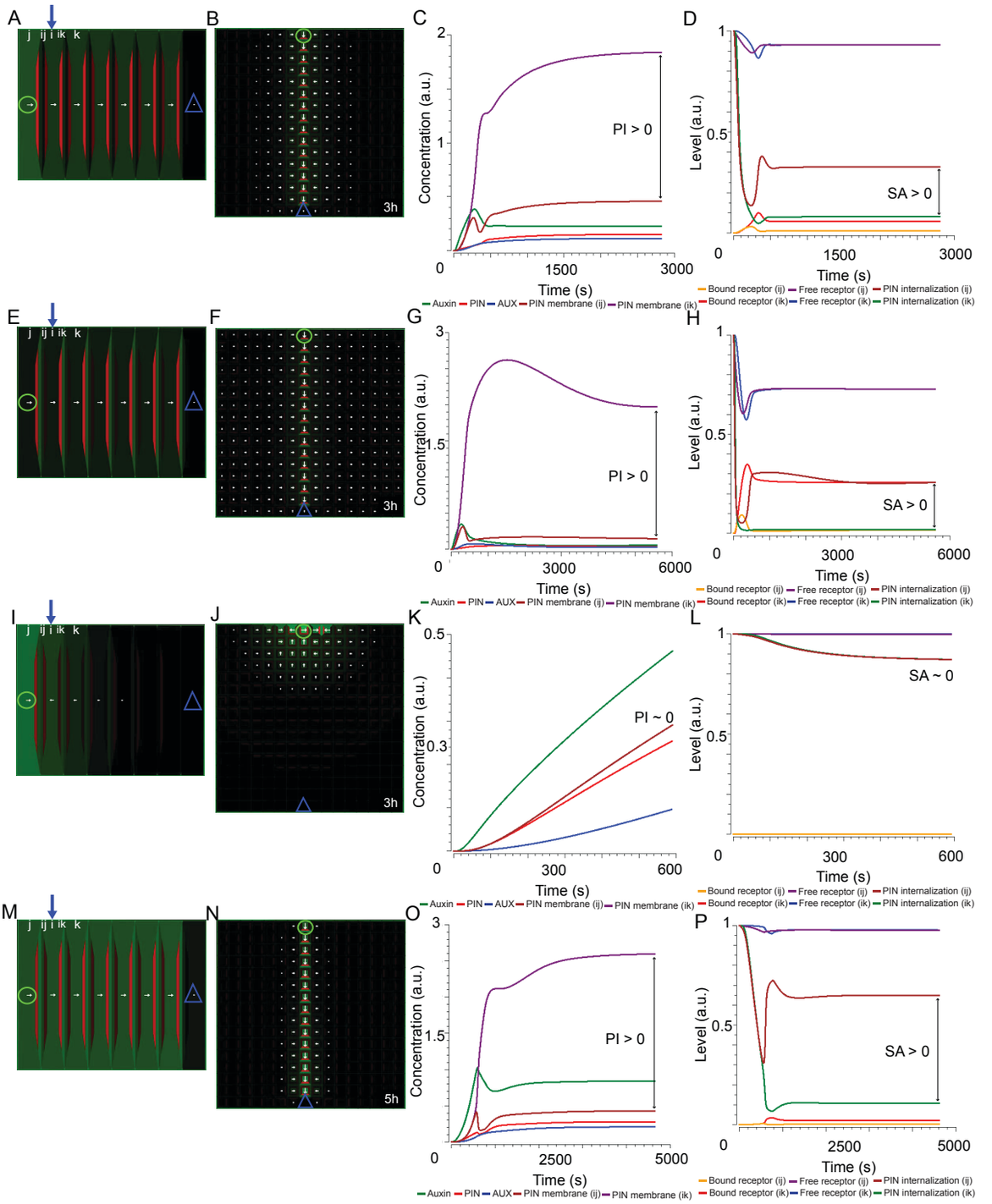
A
B
C
D
j ij i ik k
3h
Concentration (a.u.)
PI > 0
Time (s)
Level (a.u.)
SA > 0
Auxin PIN AUX PIN membrane (ij) PIN membrane (ik)
Bound receptor (ij) Free receptor (ij) PIN internalization (ij)
Bound receptor (ik) Free receptor (ik) PIN internalization (ik)
E
F
G
H
I
J
K
L
PI ~ 0
SA ~ 0
M
N
O
P
5h

Supplementary Figure 3 Model sensitivity with respect to extracellular receptor recycling

(A-D) *In silico* 'WT' control simulation - Model simulations on the file of cells (A) and on the cellular grid (B) reproduced PIN polarization and canalization of auxin flow from an auxin source towards a distal auxin sink. The dissociation constant of extracellular receptor (represented by the ratio between forward and backward rates of receptor cycling, equation 14) was: K_D = 1 μM (virtually the same as control simulation presented in Supplementary Figure 1A-D). **(E-H)** Model simulations on the file of cells (E) and on the cellular grid (F) are presented for K_D = 0.1 μM. This model simulation predicted the vascular pattern with lower auxin concentrations in the channel due to appearance of more PINs at the plasma membrane and higher auxin transport in the cells (G). However, the appearance of low auxin concentrations in this model simulation resulted in saturated auxin signaling (higher SA (H) compared to control simulation (D)). Also a strong PIN polarity was observed (increased PI) (G). **(I-L)** Model simulations on the file of cells (I) and on the cellular grid (J) are presented for K_D = 10 μM. Due to low affinity rate (high K_D) receptor-based auxin signaling was partially blocked (SA ~ 0) (L) and no PIN polarization (PI ~ 0) was predicted by the model (K). Interestingly, a 10-fold decrease of diffusion of auxin in the apoplast **(M-P)** resulted in increased SA (P) and strong PIN polarization (increased PI) yet enough to canalise auxin flow (M, N). Notably, the time point at the initiation of PIN polarization (for PI > 0) was delayed (~500s, O, P) compared to that in the control simulation (~250s, C, D). This finding implicates that auxin binding to extracellular receptor should occur fast (K_D < 10 μM) to balance the effect of free auxin diffusion in the cell wall. Interestingly, the putative auxin binding protein (ABP1) - a candidate for extracellular auxin receptor, has high affinity and specificity to auxin (K_D ranges from 0.05 μM to 5 μM) for pH of 5.5 (Tromas *et al*., 2010).

Polarization Index (PI) and Signaling Asymmetry (SA) are introduced in Figure 2. For symbols and color code, see Figures 2E and Supplementary Figure 1N.

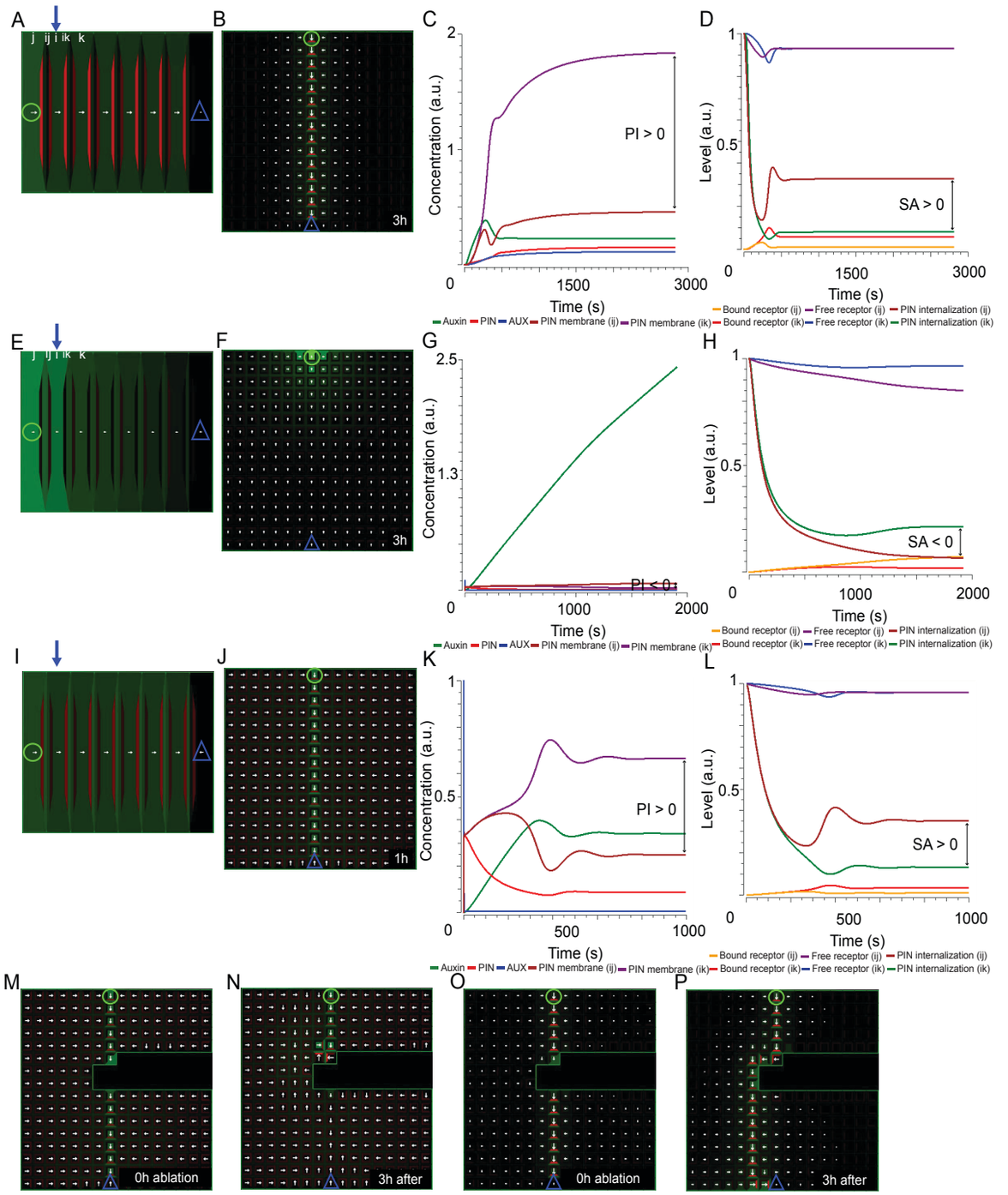
A
B
C
D
j ij i ik k
3h
Concentration (a.u.)
PI > 0
Level (a.u.)
SA > 0
Time (s)
Auxin PIN AUX PIN membrane (ij) PIN membrane (ik)
Bound receptor (ij) Free receptor (ij) PIN internalization (ij)
Bound receptor (ik) Free receptor (ik) PIN internalization (ik)
E
F
G
H
PI < 0
SA < 0
I
J
K
L
1h
M
N
O
P
0h ablation
3h after

Supplementary Figure 4 The role of auxin-dependent carrier expression in vascular patterning and tissue regeneration

(A-D) *In silico* 'WT' control simulation - Model simulations on the file of cells (A) and on the cellular grid (B) predicted PIN polarization and canalization of auxin flow from an auxin source towards a distal auxin sink. The auxin-dependent carrier expression rates were: α_{PIN}=0.1, α_{AUX}=0.1, and carrier degradation terms: δ_{PIN}=0.003, δ_{AUX}=0.003 (equations 5-7, virtually the same as control simulation presented in Supplementary Figure 1A-D). **(E-H)** Simulations on the file of cells (E) and on the cellular grid (F) are presented for the model conditions that do not include auxin-induced carrier expression. Initially, the fixed pool of auxin carriers was assigned to each cell and set at 0.1 a.u. (arbitrary units). Under this condition, auxin canalization could not be reproduced by the ERP model simulations (E, F). The observed values of PI and SA were negative which resulted in the adverse PIN polarization (towards auxin source) in our model simulations (G, H). **(I-L)** Model simulations on the file of cells (I) and on the cellular grid (J) are presented. The amount of auxin carriers in the pool was set at 1 (K, L). The positive values of both PI and SA were associated with PIN polarization from and an auxin source (I, J). Although, the steady-state patterns of PIN polarization were obtained after approx. 16 min (K, L) which was faster than in control simulation (~50 min) (C, D). This results clearly indicate that PIN proteins are important components of the model and thus the sufficient level of PINs (>= 1 a.u.) has to be associated with each cell when carrier expression is turned off. **(M-P)** Simulations of tissue regeneration on the regular cellular grid. (M, N) Fixed pool of carriers in each cell was set at 1 a.u. and no regeneration of vascular pattern was observed (N). (O, P) 'WT' control simulation – model with auxin-induced carrier expression and fixed carrier degradation predicts dynamic re-polarization of cells in direct surrounding of ablated region, down regulation of PINs below the wound and consequently vein regeneration (P).

These results of the model simulations suggest that both PIN degradation and a dynamic regulation of PIN expression by auxin are necessary to narrow down PIN expression domains below the ablated region, and subsequent for *de novo* polarization of PINs (P).

Polarization Index (PI) and Signaling Asymmetry (SA) are introduced in Figure 2. For symbols and color code, see Figures 2E and Supplementary Figure 1N.

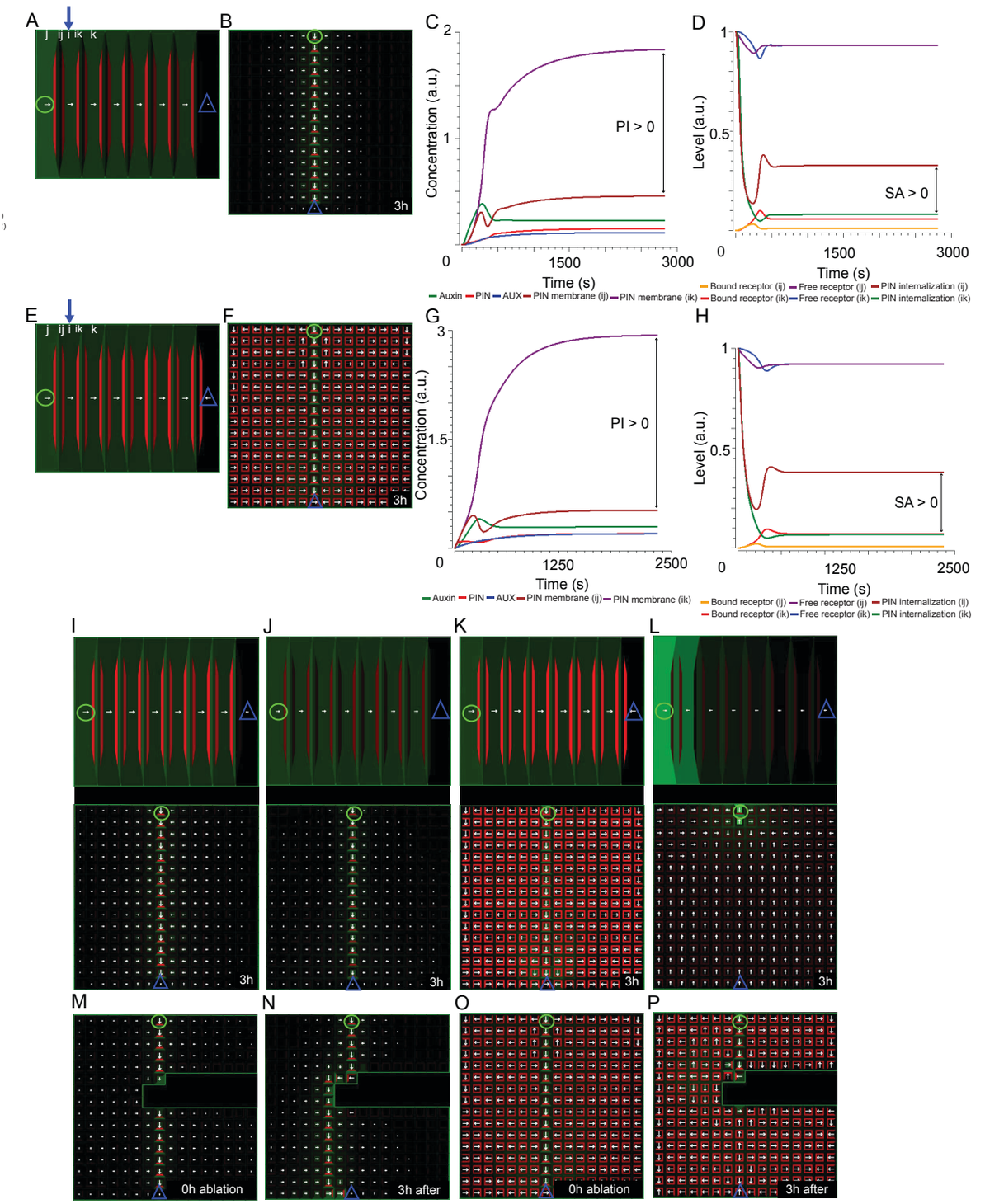
A
B
C
D
j ij i ik k
3h
Concentration (a.u.)
PI > 0
Time (s)
Level (a.u.)
SA > 0
Auxin PIN AUX PIN membrane (ij) PIN membrane (ik)
Bound receptor (ij) Free receptor (ij) PIN internalization (ij)
Bound receptor (ik) Free receptor (ik) PIN internalization (ik)
E
F
G
H
I
J
K
L
M
N
O
P
0h ablation
3h after

Supplementary Figure 5 Auxin-dependent versus auxin-independent carrier expression in vascular patterning and tissue regeneration

(A-D) *In silico* 'WT' control simulation - Model simulations on the file of cells (A) and on the cellular grid (B) predicted PIN polarization and canalization of auxin flow from an auxin source towards a distal auxin sink. The auxin-dependent carrier expression rates were: α_{PIN}=0.1, α_{AUX}=0.1, and carrier degradation terms: δ_{PIN}=0.003, δ_{AUX}=0.003 (equations 5-7, virtually the same as control simulation presented in Supplementary Figure 1A-D). **(E-H)** Model simulations on the file of cells (E) and on the cellular grid (F) are presented for the model with an auxin-independent carrier expression. The rates of fixed carrier expression were: α_{PIN}=0.01, α_{AUX}=0.01, and carrier degradation terms: δ_{PIN}=0.003, δ_{AUX}=0.003. The ERP model predicted the canalization of auxin flow and basal PIN polarization in pro-vascular cells (E, F). Note that PI and SA were slightly increased (G, H) compared to those in control simulation (C, D) presumably due to higher PIN signal at the plasma membrane of each cell. Notably, this model simulation predicted the adverse PIN polarization in the cells that surrounded pro-vascular channel, and only broad, uniform and strong PIN expression was observed in the whole tissue (F). **(I-J)** Simulations on the file of cells and on the cellular grid for the ERP model with auxin-dependent carrier expression rates that were: α_{PIN}=1, α_{AUX}=1 (I) and α_{PIN}=0.01, α_{AUX}=0.01 (J). **(K-L)** Model simulations on the file of cells and on the cellular grid with fixed carrier expression rates: α_{PIN}=0.1, α_{AUX}=0.1 (K) and α_{PIN}=0.001, α_{AUX}=0.001 (L) are presented. Note that low levels of carrier expression in the model resulted in patterning defects (L). **(M-P)** 'WT' control simulation – the model with an auxin-induced carrier expression allows for dynamic re-polarization of cells in direct surrounding of ablated region, down regulation of PINs below the wound and consequently vein regeneration (M, N). The model with fixed carrier expression (α_{PIN}=0.01, α_{AUX}=0.01) was not able to reproduce PIN polarization during vein regeneration (O, P).

In agreement with results presented in Supplementary Figure 4, these model simulations demonstrated the importance of auxin-dependent regulation of PIN expression for generating realistic, narrowed and flexible PIN polarization patterns during auxin canalization and vascular regeneration.

Polarization Index (PI) and Signaling Asymmetry (SA) are introduced in Figure 2. For symbols and color code, see Figures 2E and Supplementary Figure 1N.

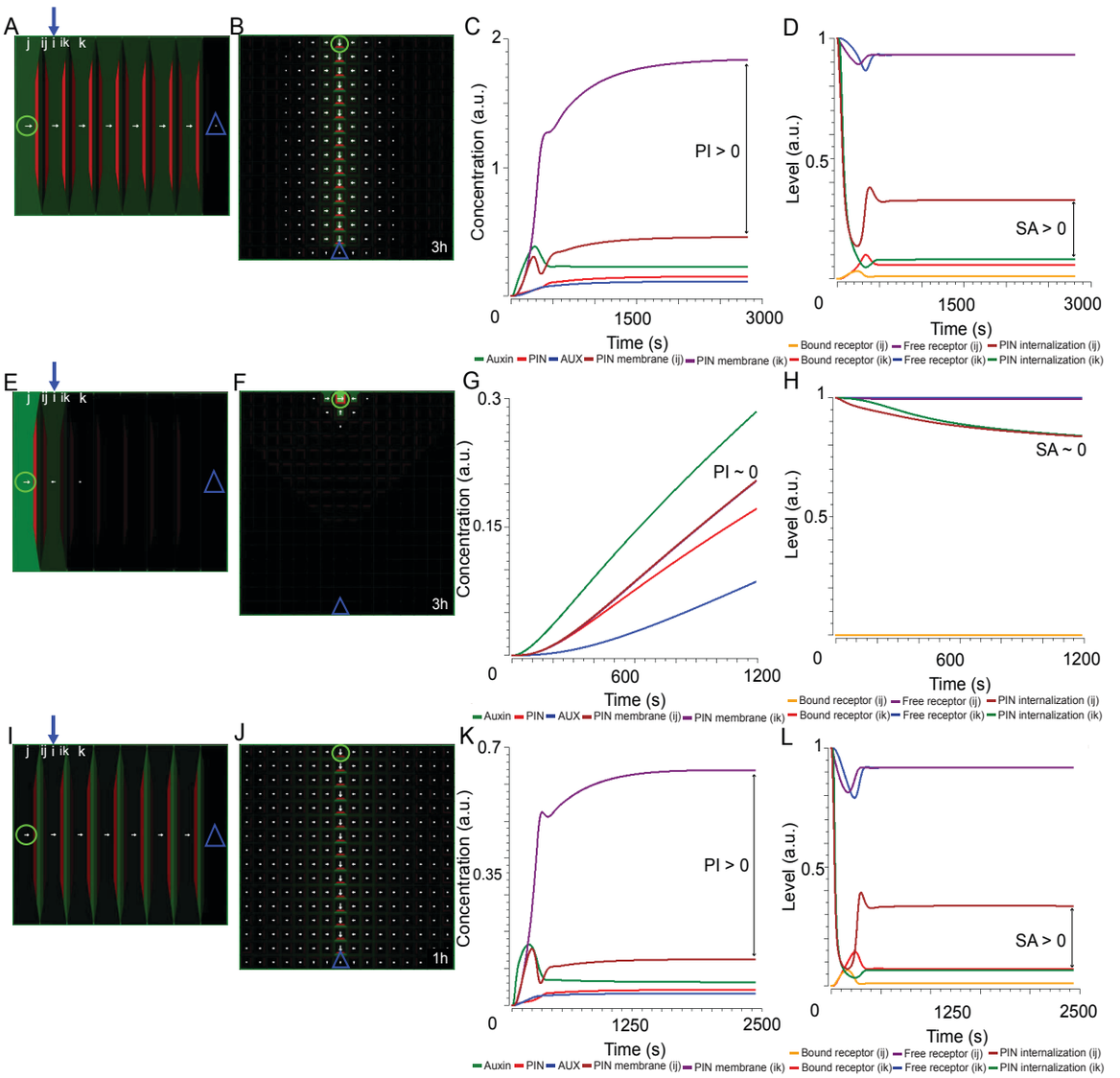
A
j ij i ik k
B
3h
C
Concentration (a.u.)
PI > 0
Time (s)
Auxin PIN AUX PIN membrane (ij) PIN membrane (ik)
D
Level (a.u.)
SA > 0
Time (s)
Bound receptor (ij) Free receptor (ij) PIN internalization (ij)
Bound receptor (ik) Free receptor (ik) PIN internalization (ik)
E
F
3h
G
PI ~ 0
H
SA ~ 0
I
J
1h
K
PI > 0
L
SA > 0

Supplementary Figure 6 Model robustness with respect to the efficiency of PIN-dependent auxin transport

(A-D) 'WT' control simulation **-** Model simulations on the file of cells (A) and on the cellular grid (B) showed PIN polarization and canalization of auxin flow from an auxin source towards a distal auxin sink. The permeability of PIN-dependent transport (p_{PIN}) was set at 30 μms^{-1} (virtually the same as control simulation presented in Supplementary Figure 1A-D). **(E-H)** Model simulations on the file of cells (E) and on the cellular grid (F) are presented for parameter p_{PIN}=1 μms^{-1} which mimic *pin* mutants (practically the lack of PIN-dependent transport). In this simulation, the canalization of auxin flow did not occur (E, F). Moreover, model predicted accumulation of auxin in the tracked cell (G) which resulted in the lack of PIN polarization (PI ~ 0) (G) and no visible asymmetry in extracellular auxin signaling (SA ~ 0) (H). **(I-L)**. Model simulations on the file of cells (I) and on the cellular grid (J) are presented for parameter p_{PIN}=300. In this case the capacity of PIN-dependent auxin transport (p_{PIN}) was set a 10-fold higher than that in control simulation (A-D). No qualitative change of model behavior was observed (K, L) compared to control simulation (C, D). Additionally, auxin concentrations were lower in the channel (I, J) than those reported in the control simulation (A, B). These model simulations suggest that the capacity of PIN-dependent auxin transport (p_{PIN}) is crucial parameter for the model to reproduce venation patterning and its inset should be higher than the weak "background" permeability of 1 μms^{-1} (E, H).

Polarization Index (PI) and Signaling Asymmetry (SA) are introduced in Figure 2. For symbols and color code, see Figures 2E and Supplementary Figure 1N.

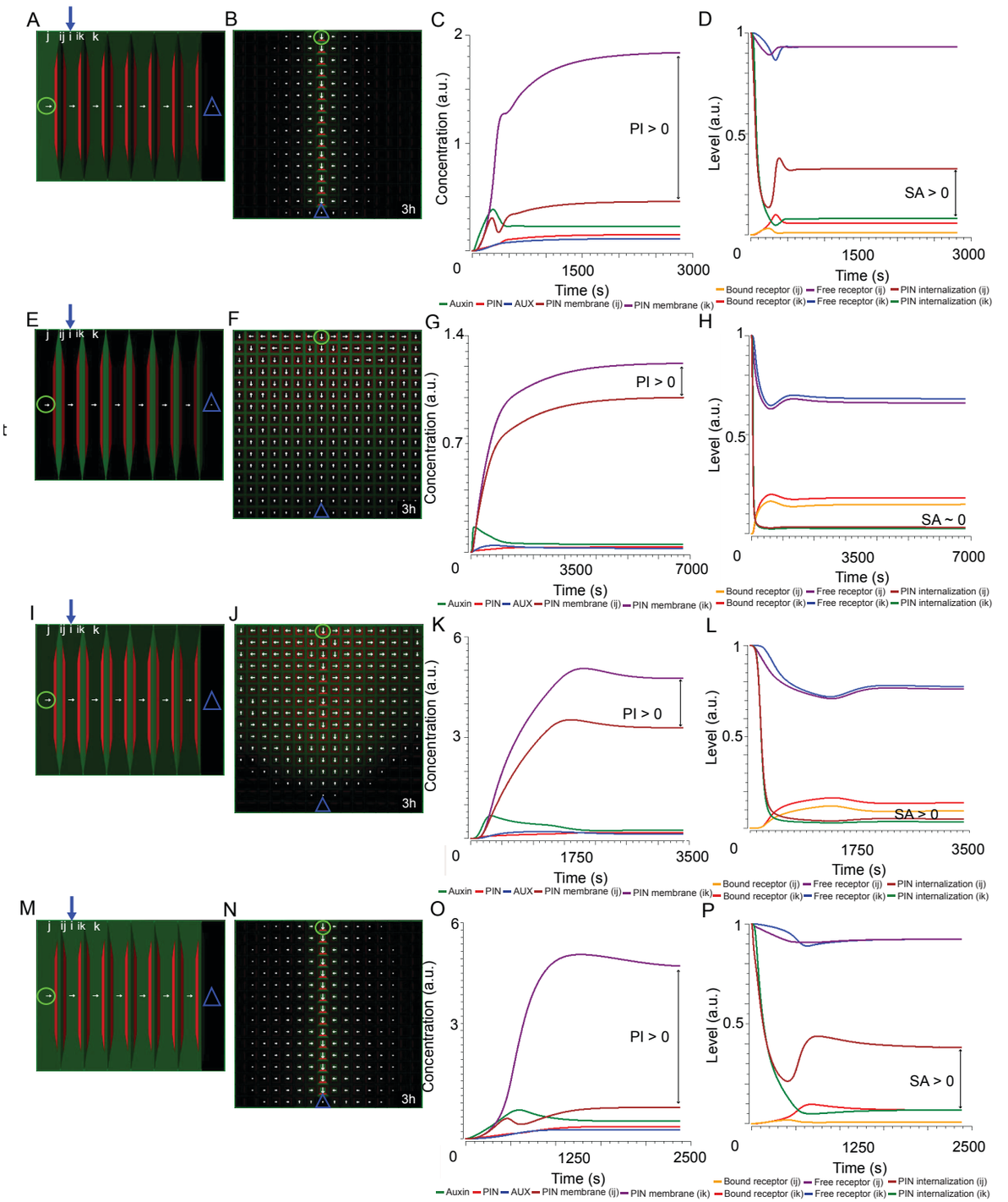
A
B
C
D
j ij i ik k
3h
Concentration (a.u.)
Level (a.u.)
PI > 0
SA > 0
Time (s)
Auxin PIN AUX PIN membrane (ij) PIN membrane (ik)
Bound receptor (ij) Free receptor (ij) PIN internalization (ij)
Bound receptor (ik) Free receptor (ik) PIN internalization (ik)
E
F
G
H
SA ~ 0
I
J
K
L
M
N
O
P

Supplementary Figure 7 Model sensitivity with respect to the efficiency of AUX/LAX-dependent auxin transport

(A-D) 'WT' control simulation **-** Model simulations on the file of cells (A) and on the cellular grid (B) showed PIN polarization and canalization of auxin flow from an auxin source towards a distal auxin sink. The permeability of AUX/LAX-dependent transport (p_{AUX}) was set at 30 μms^{-1} (virtually the same as control simulation presented in Supplementary Figure 1A-D). **(e-h)** Model simulations on the file of cells (E) and on the cellular grid (F) are reported for parameter p_{AUX}=1 μms^{-1}. Here, the canalization of auxin flow was not predicted by model simulations as well as strong basal PIN polarization in pro-vascular cells and lateral polarization of surrounding tissues (E, F). A very weak difference in PIN levels between *ik*-th and *ij*-th plasma membranes was established (small PI) (G). However, this weak PIN polarization did not get enhanced and maintained presumably due to a shallow difference in extracellular auxin signaling across the cell wall (SA ~ 0) (H). **(I-L)** Model simulations on the file of cells (I) and on the cellular grid (J) are presented for parameter p_{AUX} set at 1 μms^{-1} and for a 10-fold higher inset of p_{IAAH}. Note that *in silico* AUX/LAX phenotype (E-H) was virtually rescued as predicted by model simulation (I, J). Nevertheless, the basal PIN polarization in the pro-vascular cells was not maintained (small PI) and thus an auxin source did not connect to a distal auxin sink (J). Interestingly, this model simulation predicted no delay in the initiation of PIN polarization (K, L) compared to control simulation (C, D). This suggests that a diffusion-based auxin influx into cell (p_{IAAH}) tends to delay, but does not balance the auxin efflux from cell (K). Consequently, auxin was trapped in the extracellular space in high concentrations and thus no significant asymmetry in extracellular auxin signaling was generated (SA ~ 0) (L). Our model simulations indicate that the contribution of AUX/LAX carriers to the dynamic drainage of auxin from the apoplast is central to the maintenance of basal PIN polarization in the pro-vascular cells and lateral PIN polarization of surrounding tissues (A, B). **(M-P)** Model simulations on the file of cells (M) and on the cellular grid (N) are presented for parameter p_{AUX}=300 μms^{-1}. The capacity of AUX/LAX-dependent auxin transport was a 10-fold higher than that in control simulation (A-D). Model predicted that auxin efflux from the cell is balanced by active AUX/LAX influx resulting in increased PI (O) and increased SA (P).

Polarization Index (PI) and Signaling Asymmetry (SA) are introduced in Figure 2. For symbols and color code, see Figures 2E and Supplementary Figure 1N.

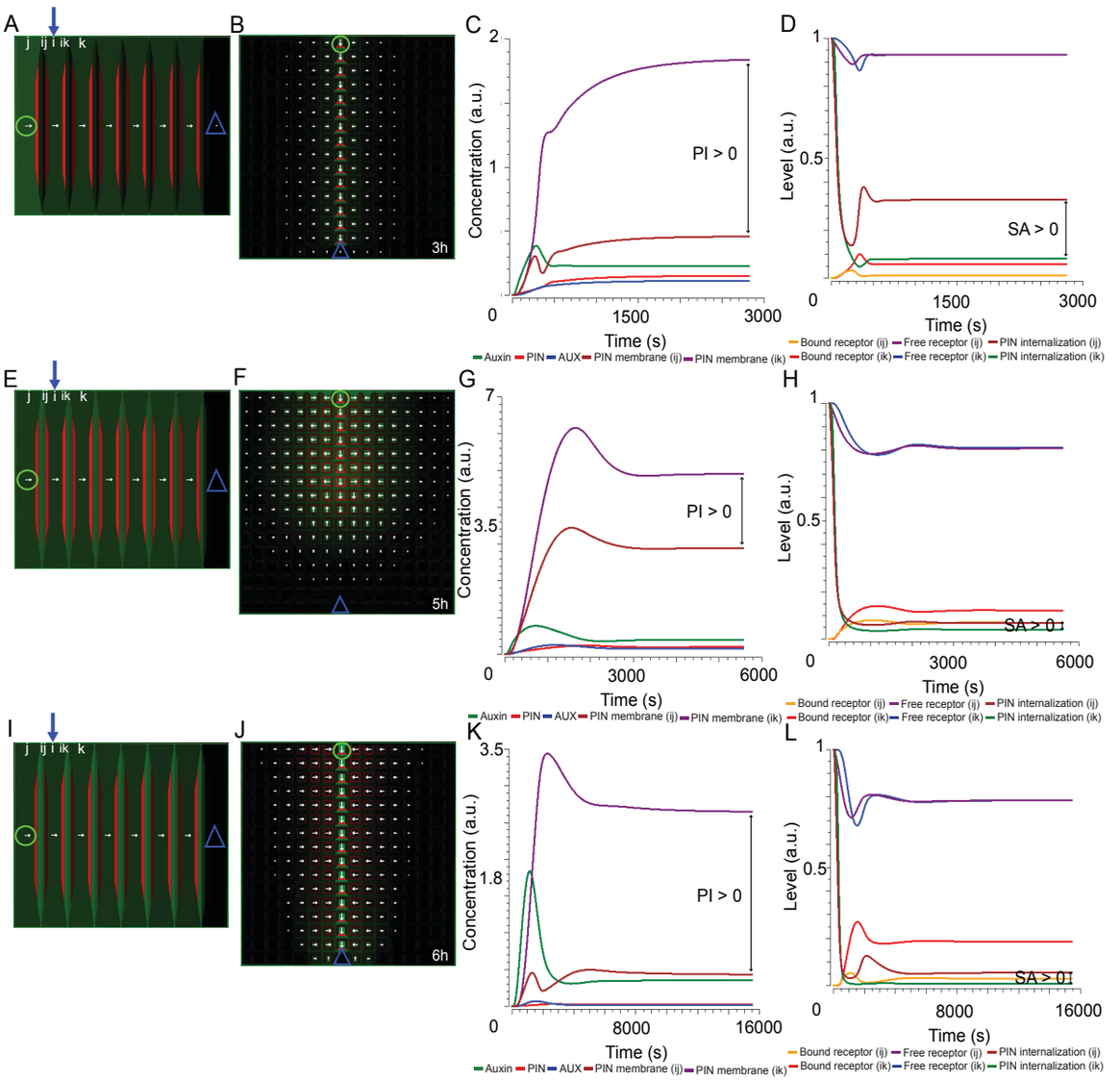
A
j ij i ik k
B
3h
C
Concentration (a.u.)
PI > 0
Time (s)
Auxin PIN AUX PIN membrane (ij) PIN membrane (ik)
D
Level (a.u.)
SA > 0
Time (s)
Bound receptor (ij) Free receptor (ij) PIN internalization (ij)
Bound receptor (ik) Free receptor (ik) PIN internalization (ik)
E
F
5h
G
H
I
J
6h
K
L

Supplementary Figure 8 Model sensitivity with respect to the speed of polar auxin transport

(A-D) 'WT' control simulation - Model simulations on the file of cells (A) and on the cellular grid (B) showed PIN polarization and canalization of auxin flow from an auxin source towards a distal auxin sink. The saturation of polar auxin transport (k_t) was set at 1 μM (virtually the same as control simulations presented in Supplementary Figure 1A-D). **(E-H)** Model simulations on the file of cells (E) and on the cellular grid (F) are presented for parameter k_t=10 μM. The initiation of PIN polarization was observed (PI > 0) (G), however, no significant difference in extracellular auxin signaling was reported (low SA) (H). The model simulations predicted a transient basal PIN polarization in pro-vascular cells and no lateral polarization of surrounding tissues (E, F). In this case the low capacity of polar auxin transport provided no means to counteract apoplastic auxin diffusion and consequently, PIN polarization associated with the positive value of PI could not be sufficiently maintained (G, H). **(I-L)** Model simulations on the file of cells (I) and on the cellular grid (J) are presented for parameter k_t=10 μM, and a 10-fold decrease of auxin diffusion in the apoplast (D_a) compared to that used in control simulations (D_a = 100 $\mu m^2 s^{-1}$). (I, J) Model predicted virtual rescue of *in silico* phenotype (E-H). Notably, the simulation demonstrated a transient maximum of PI associated with PIN polarization that was a 10-fold stronger (K) than that observed in control simulation (C). Similarly, this reduction in apoplastic diffusion (D_a) in our model resulted in an increase of SA (L). This indicates that the speed of carrier-dependent auxin transport system has to be comparable or faster than passive movement of auxin within the cell wall.

Polarization Index (PI) and Signaling Asymmetry (SA) are introduced in Figure 2. For symbols and color code, see Figures 2E and Supplementary Figure 1N.

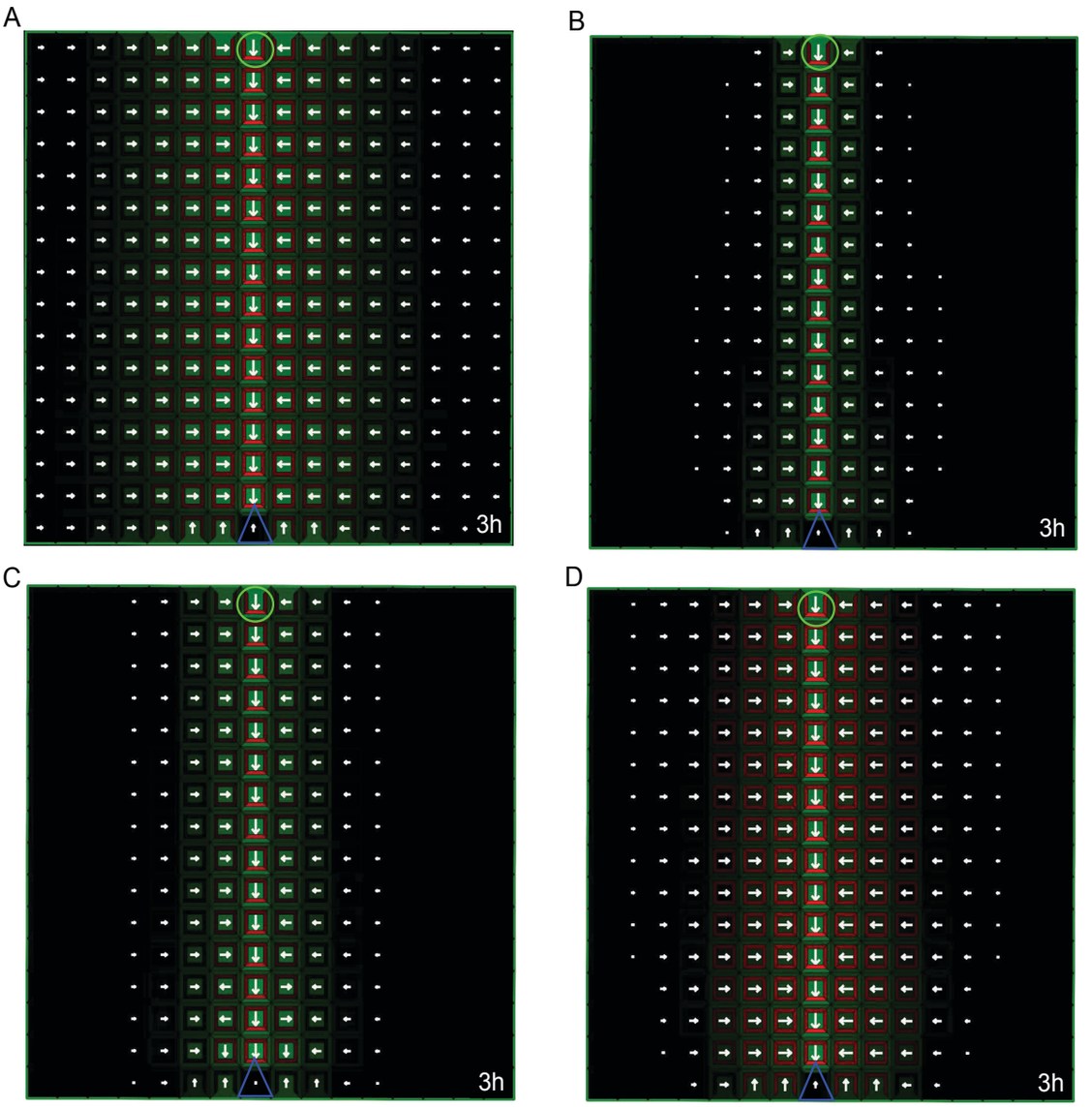
A
3h
B
3h
C
3h
D
3h

Supplementary Figure 9 Model robustness with respect to diffusion and permeability rates

(A) PIN polarity and auxin distribution patterns for a 5-fold increase of apoplastic auxin diffusion (D_a) that was originally set at 100 $\mu m^2 s^{-1}$. **(B)** A sharp auxin distribution pattern was observed in the model simulation with a 5-fold decrease of D_a. The ERP model with the values of apoplastic auxin diffusion from range of 10 $\mu m^2 s^{-1}$ up to 500 $\mu m^2 s^{-1}$ which covers the variety of measurement of apoplastic auxin diffusion in plants [11]-[13]. **(C)** A 5-fold increase in the total membrane permeability values (p_{PIN} and p_{AUX}) had no visible impact on PIN polarization and the canalization of auxin flow. **(D)** Cell polarity and auxin distribution patterns in model simulation with a 5-fold decrease in the total permeability values: $p_{PIN}=p_{AUX}=6\ \mu m s^{-1}$.

For symbols and color code, see Figures 2E and Supplementary Figure 1N.

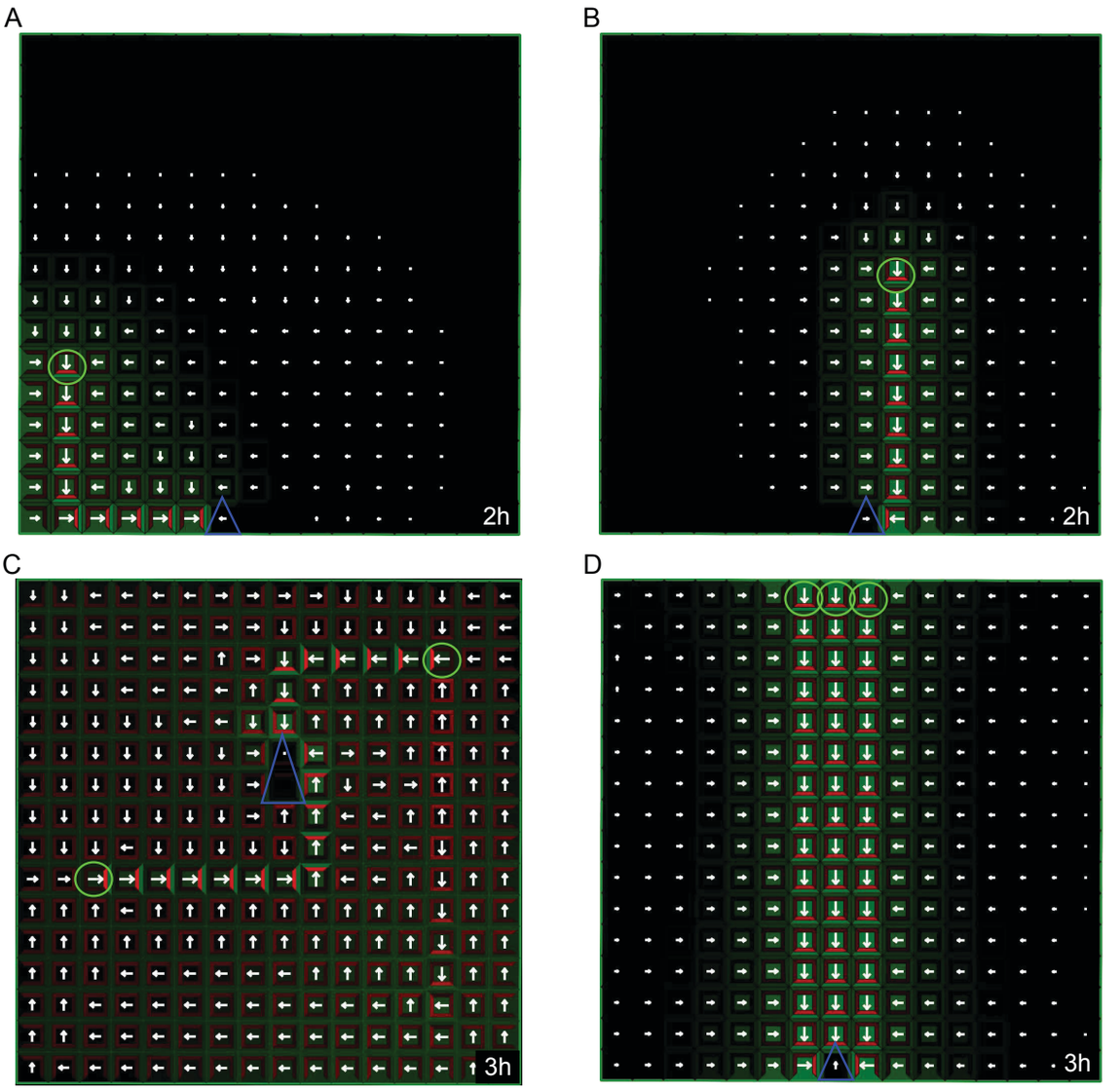
A
2h
B
2h
C
3h
D
3h

Supplementary Figure 10 Model sensitivity with respect to altered boundary conditions

(A) Model simulation of auxin canalization on regular grid with an auxin source that was placed against the boundary. The strength of auxin source was set at 0.001 μM μm^{-2} s^{-1}. Auxin canalization was observed in this ERP model simulation (A). Interestingly, the predicted auxin channel was not stringent to tissue boundary compared with the observations from predictions of classical canalization models suggesting that the ERP model faithfully and robustly reproduces auxin canalization patterns. (**B)** Auxin canalization on the regular grid predicted by the ERP mechanism with randomly chosen spot of the auxin biosynthesis. **(C)** The ERP model provides the robust sink finder mechanism for auxin canalization. An auxin sink was set at the random position on the cellular grid and two, equivalent in strength auxin sources (0.001 μM μm^{-2} s^{-1}) were introduced at the same time on the grid tissue layout. The shortest path from each auxin source to an auxin sink was robustly found in the ERP model simulation (C). **(D)** The widening of auxin channel in the ERP model simulation. The single-cell auxin source located in the center of the top cell layer of a grid tissue layout was extended to the two adjacent cells which resulted in the formation of broad auxin channel (D).

For symbols and color code, see Figures 2E and Supplementary Figure 1N.

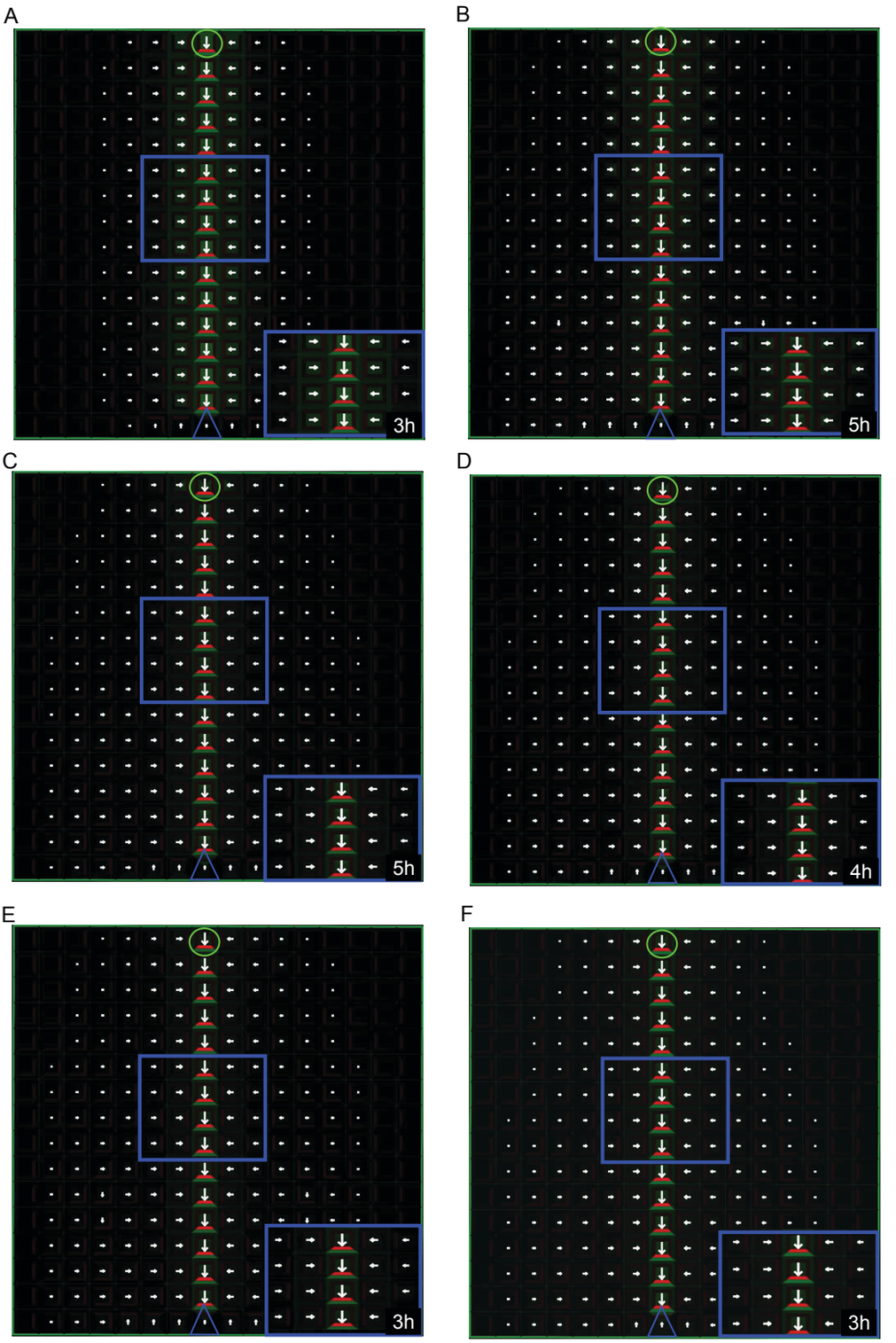
A
3h
B
5h
C
5h
D
4h
E
3h
F
3h

Supplementary Figure 11 The ERP model with intracellular auxin diffusion

(A) Model simulations on the file of cells (A) and on the cellular grid (B) showed PIN polarization and canalization of auxin flow from an auxin source towards a distal auxin sink. Each cell is represented by a rectangular square with the mean auxin concentration in the cytoplasm (A) (the model inset was the same as simulation presented in Figure 3A and 3B). (**B)** The square box representing one cell was divided in four identical intracellular compartments and each component associated with the one side of the cell and the cell center. Here our model additionally integrated an intracellular auxin diffusion between these intracellular compartments that was described by Fick's law -equation (27). **(B)** The diffusion coefficient D was set at 10 $\mu m^2 s^{-1}$, **(C)** D = 50 $\mu m^2 s^{-1}$, **(D)** D = 100 $\mu m^2 s^{-1}$, **(E)** D = 300 $\mu m^2 s^{-1}$, **(F)** D = 600 $\mu m^2 s^{-1}$. These model simulations that include intracellular auxin diffusion were performed for a wide range of diffusion rates (B-F) and were yielded qualitatively similar predictions as the control simulations with no intracellular auxin diffusion (A).

Polarization Index (PI) and Signaling Asymmetry (SA) are introduced in Figure 2. For symbols and color code, see Figures 2E and Supplementary Figure 1N.

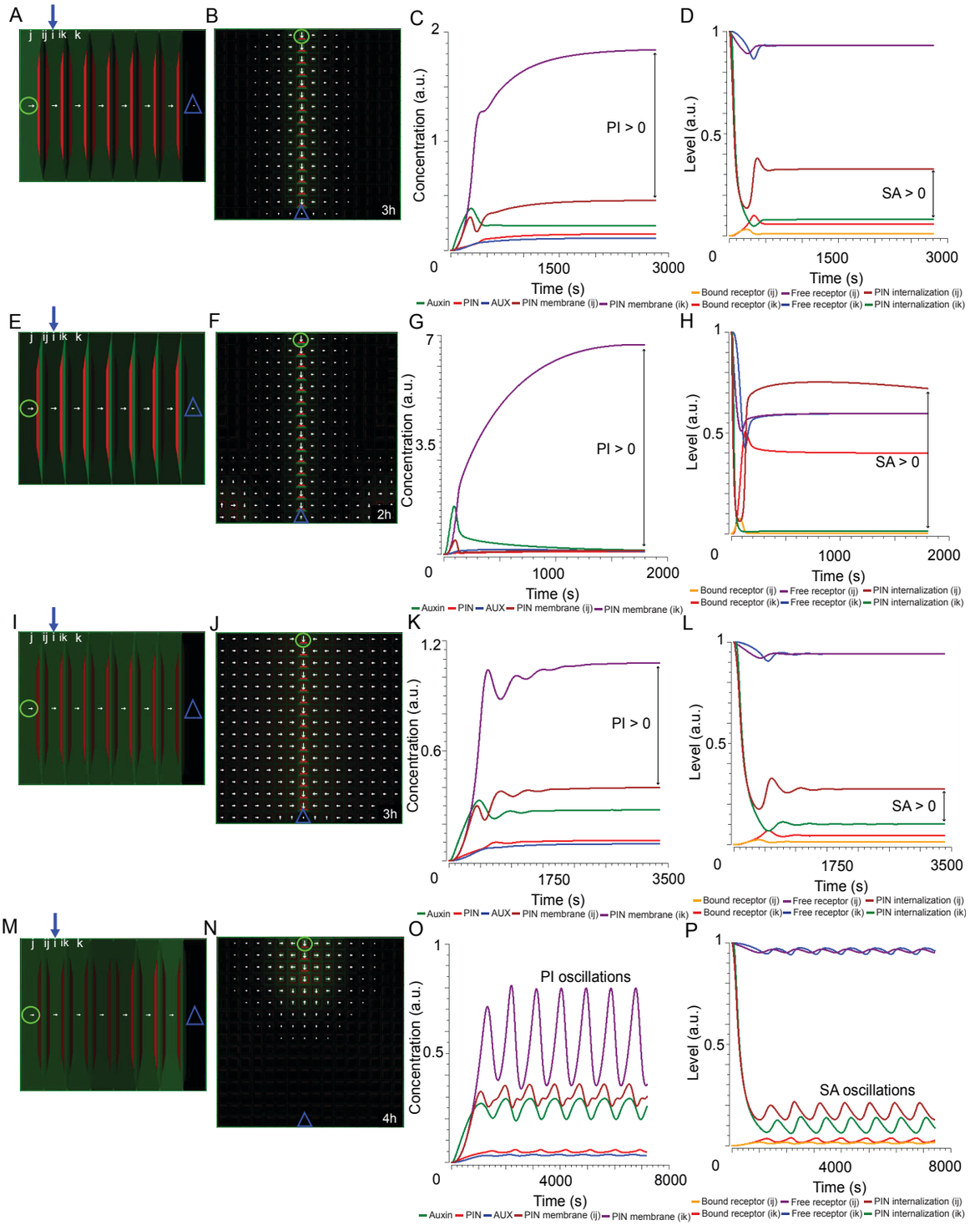
A
B
C
D
j ij i ik k
3h
Concentration (a.u.)
PI > 0
Time (s)
Level (a.u.)
SA > 0
Auxin PIN AUX PIN membrane (ij) PIN membrane (ik)
Bound receptor (ij) Free receptor (ij) PIN internalization (ij)
Bound receptor (ik) Free receptor (ik) PIN internalization (ik)
E
F
G
H
2h
I
J
K
L
M
N
O
P
4h
PI oscillations
SA oscillations

Supplementary Figure 12 Auxin concentration is a main polarizing signal

(A-D) 'WT' control simulation **-** Model simulations on the file of cells (A) and on the cellular grid (B) predicted PIN polarization and canalization of auxin flow from an auxin source towards a distal auxin sink. The auxin source was set to 0.001 μM μm^{-2} s^{-1} (virtually the same as control simulation presented in Supplementary Figure 1A-D). **(E-H).** Model simulations on the file of cells (E) and on the cellular grid (F) with auxin source set to 0.01 μM μm^{-2} s^{-1} and a distal auxin sink are presented. The auxin concentration threshold sufficient causing increase of the PI was reached nearly two times faster (G) compared to that presented in control simulation (C). Notably, the model predicted a steep difference in extracellular auxin signaling on both sides of *i*-th cell that was associated with the high positive value of SA (H). The PIN levels on *ik*-th membrane were a 7-fold higher than those on *ij*-th membrane (high PI) (G). **(I-L)** Model simulations on the file of cells (I) and on the cellular grid (J) with auxin source set to 0.0005 μM μm^{-2} s^{-1} and a distal auxin sink are presented. The establishment of PIN polarization was delayed (K) in comparison with control simulation (C), by about 100s. This is presumably due to a longer time of auxin accumulation in the cell (K). Interestingly, in the presence of this weak auxin source, our model predicted fluctuations (oscillations) in the steady-state values of chemicals, that were damped over time resulting with stable PIN polarization pattern (K, L). Note that PI and SA – measures of PIN polarization and auxin signaling were also oscillating **(M-P)** Model simulations on the file of cells (M) and on the cellular grid (N) with an auxin source set to 0.0001 μM μm^{-2} s^{-1} and a distal auxin sink are presented. In this model simulation, the establishment of PIN polarization was considerably delayed by about 1000 s (O) if compared to predictions from control simulation (C). Also here oscillations of values of PI and SA were observed and those corresponded to similar fluctuations in chemical levels (O, P). In summary, our model predicted unstable PIN polarity resulting in the lack of vascular connection (M, N).

We demonstrated that hot spots of auxin production (auxin sources) mediate the stability of PIN polarization patterns and thus provide means for auxin-regulated processes such as vascular formation/connection (Figures 3, 4, 5, 6A-6E) and vascular repulsion (Figure 6I-6M).

Polarization Index (PI) and Signaling Asymmetry (SA) are introduced in Figure 2. For symbols and color code, see Figures 2E and Supplementary Figure 1N.

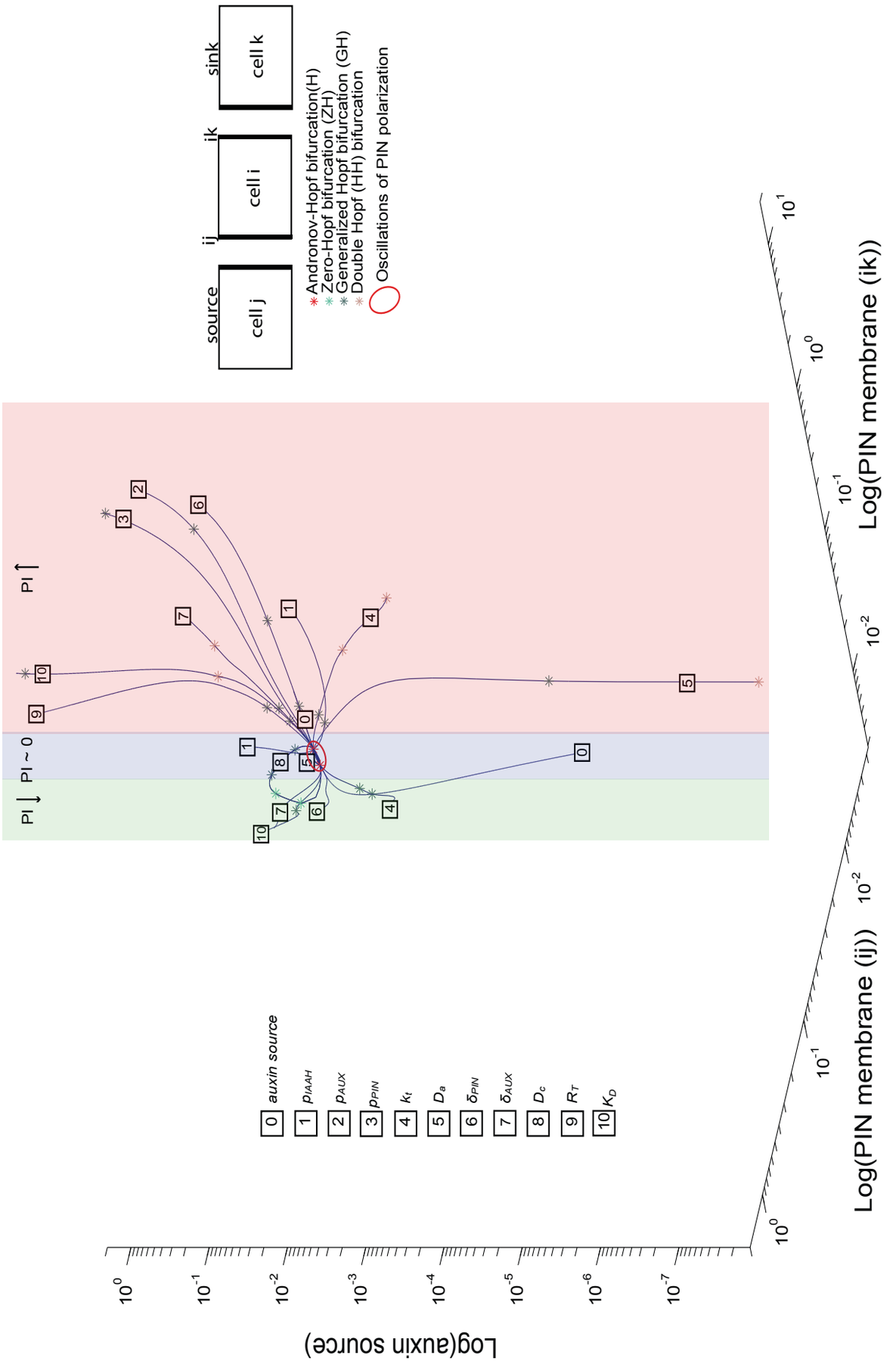
source
cell j
ij
cell i
ik
sink
cell k
Andronov-Hopf bifurcation(H)
Zero-Hopf bifurcation (ZH)
Generalized Hopf bifurcation (GH)
Double Hopf (HH) bifurcation
Oscillations of PIN polarization
PI ↑
PI ~ 0
PI ↓
0 auxin source
1 p_{IAAH}
2 p_{AUX}
3 p_{PIN}
4 k_t
5 D_a
6 δ_{PIN}
7 δ_{AUX}
8 D_c
9 R_T
10 K_D
Log(auxin source)
Log(PIN membrane (ij))
Log(PIN membrane (ik))

Supplementary Figure 13 The evolution of stationary equilibrium under variation of model parameters
A bifurcation diagram represents the family of stationary solutions for varying source strength (0). Two Hopf-points (H) were detected using numerical continuation of the equilibrium. These points indicate the appearance of supercritical Andronov-Hopf bifurcation with stable limit cycle (first Lapunov coefficients were negative, a pair of purely imaginary eigenvalues). The curve connecting H points corresponds to the parameter regime for which oscillations of PIN polarization occur. The equilibrium curves (1-10) describe the families of stationary solutions for the variation of auxin source strength and one additional model parameter. Note that several additional bifurcations were detected including Generalized Hopf (GH), Zero-Hopf (ZH) (one zero eigenvalue) and Hopf-Hopf (HH) bifurcations. The schematic colorized planes describe three different model behaviors (green, blue, red) which are associated with:
"Up-the-gradient" PIN polarization (green plane) associated with decreasing Polarization Index (PI)
Unstable PIN polarization or no PIN polarization (blue plane) when PI is crossing zero.
"With-the-gradient" PIN polarization (red plane) associated with increasing value of PI.
Each of these model behaviors correspond to different phenomena occurring during canalization of auxin flow in our model simulations that includes vein connection ($PI > 0$), vein repulsion ($PI \sim 0$) and PIN polarization towards an auxin source ($PI < 0$). Polarization Index (PI) is described in Figure 2.

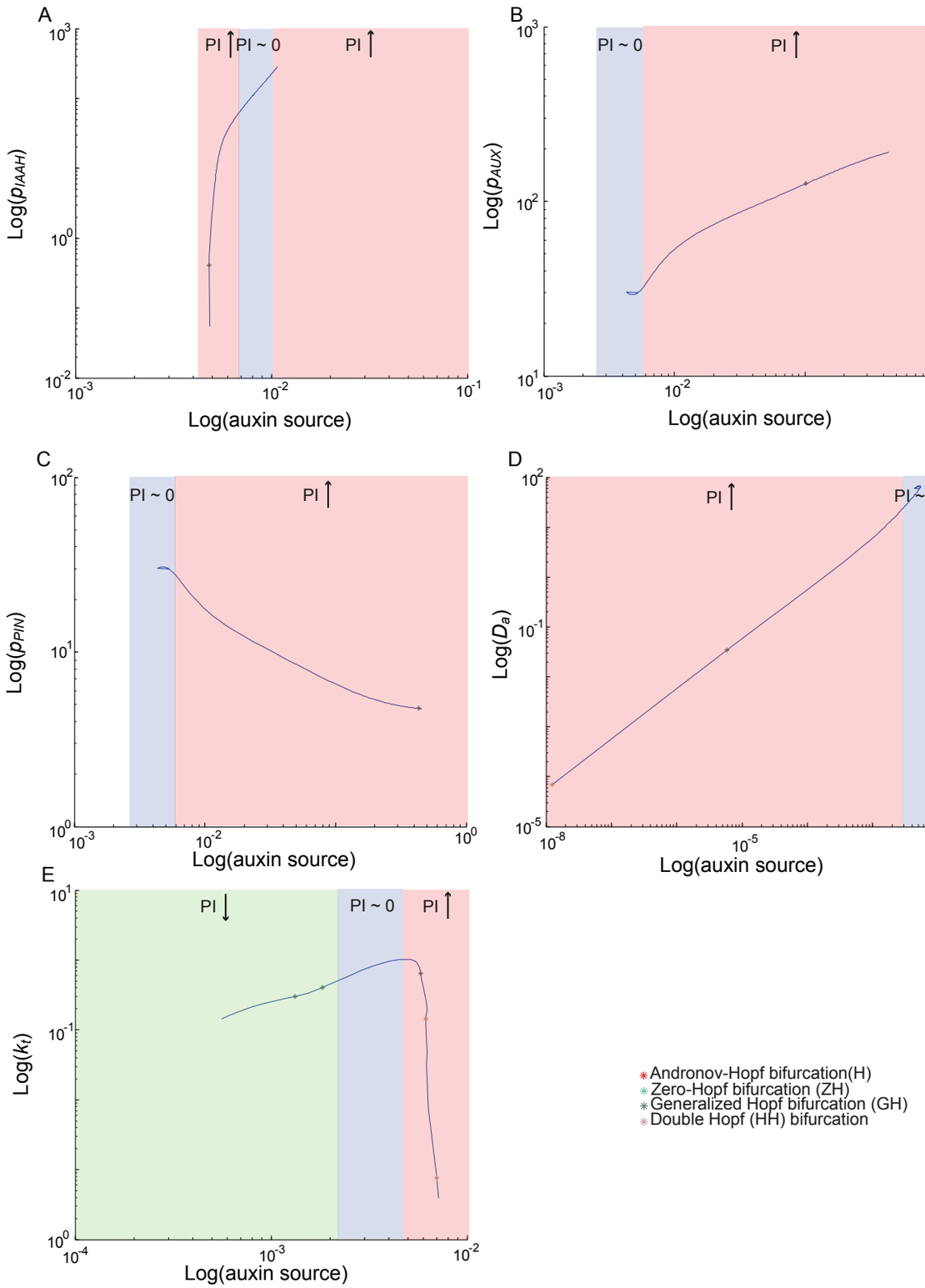
A
PI ↑
PI ~ 0
PI ↑
Log(p_{IAAH})
Log(auxin source)
B
PI ~ 0
PI ↑
Log(p_{AUX})
Log(auxin source)
C
PI ~ 0
PI ↑
Log(p_{PIN})
Log(auxin source)
D
PI ↑
PI ~ 0
Log(D_a)
Log(auxin source)
E
PI ↓
PI ~ 0
PI ↑
Log(k_t)
Log(auxin source)
Andronov-Hopf bifurcation(H)
Zero-Hopf bifurcation (ZH)
Generalized Hopf bifurcation (GH)
Double Hopf (HH) bifurcation

Supplementary Figure 14 Two-dimensional bifurcation diagrams for equilibrium curves (1-5) presented in Supplementary Figure 13

Analysis of model sensitivity and model behaviors associated with Polarization index (PI) are presented for the subsequent variation in strength of auxin source and one additional parameter: **(A)** passive auxin influx into cell (p_{IAAH}), **(B)** efficiency of AUX/LAX- dependent transport (p_{AUX}), **(C)** efficiency of PIN-dependent transport (p_{PIN}), **(D)** auxin diffusion in the cell wall (D_a), **(E)** saturation of polar auxin transport(k_t). Polarization Index (PI) is described in Figure 2. The sign of PI corresponds to different model behavior (Supplementary Figure 13).

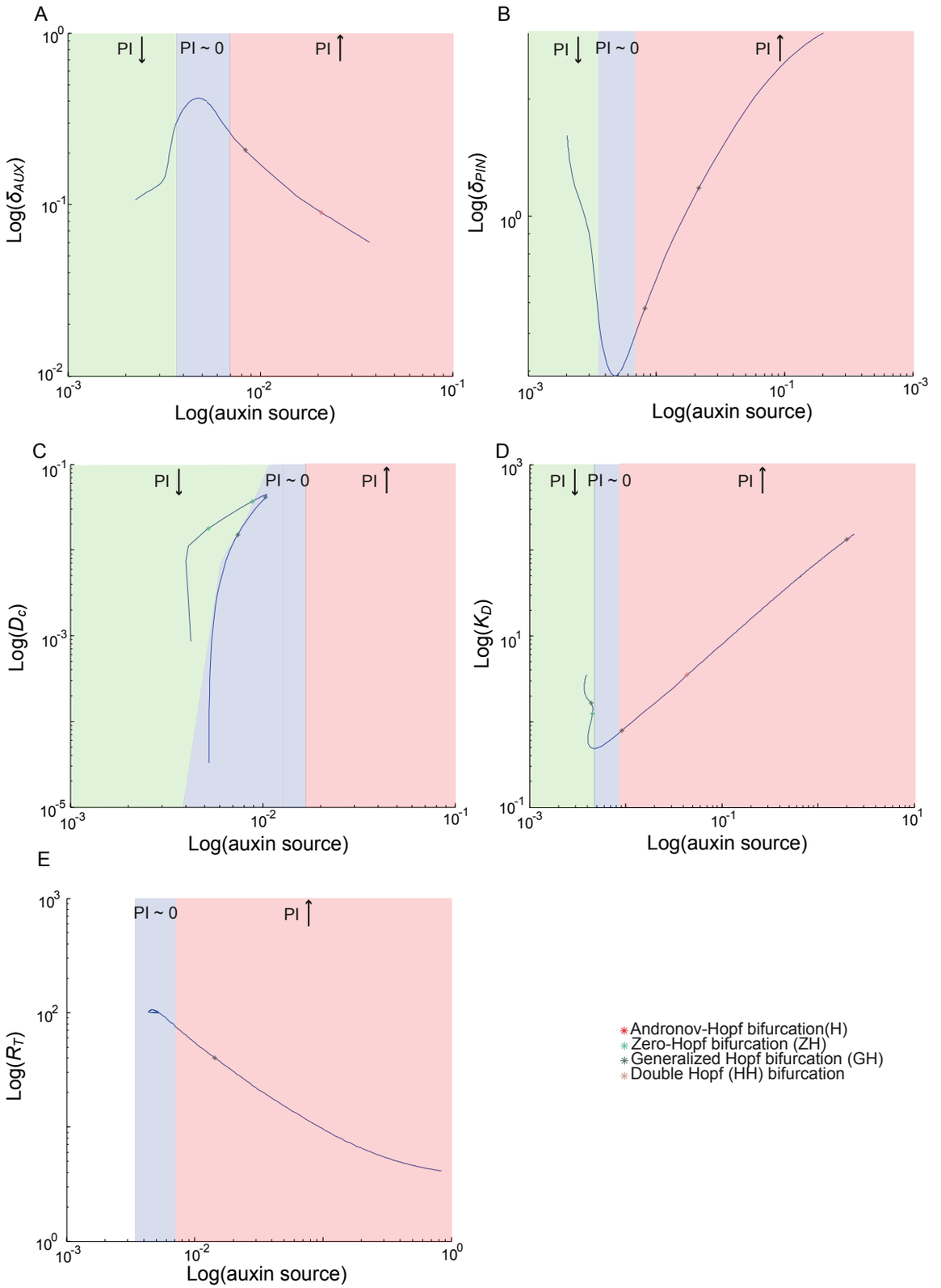
A
PI ↓
PI ~ 0
PI ↑
Log(δAUX)
Log(auxin source)
B
PI ↓
PI ~ 0
PI ↑
Log(δPIN)
Log(auxin source)
C
PI ↓
PI ~ 0
PI ↑
Log(Dc)
Log(auxin source)
D
PI ↓
PI ~ 0
PI ↑
Log(KD)
Log(auxin source)
E
PI ~ 0
PI ↑
Log(RT)
Log(auxin source)
Andronov-Hopf bifurcation(H)
Zero-Hopf bifurcation (ZH)
Generalized Hopf bifurcation (GH)
Double Hopf (HH) bifurcation

Supplementary Figure 15 Two-dimensional bifurcation diagrams for equilibrium curves (6-10) presented in Supplementary Figure 13

Analysis of model sensitivity and model behaviors associated with Polarization index (PI) are presented for the subsequent variation in strength of auxin source and one additional parameter: **(A)** degradation of auxin influx carriers (δ_{AUX}), **(B)** degradation of auxin efflux carriers (δ_{PIN}), **(C)** diffusion of auxin-bound receptors in the cell wall (D_c), **(D)** receptor dissociation constant (K_D), **(E)** Amount of extracellular auxin receptors in the intercellular pools (R_T).

Polarization Index (PI) is described in Figure 2. The sign of PI corresponds to different model behavior (Supplementary Figure 13).

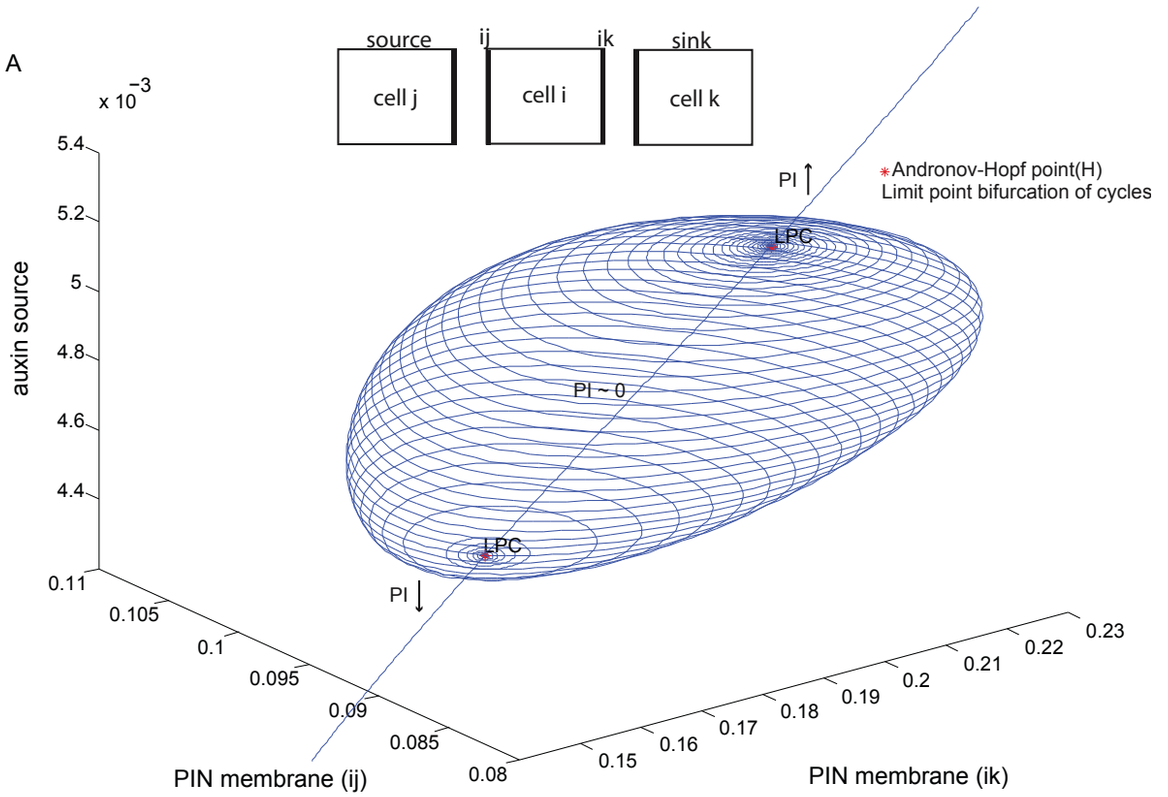
A
source
ij
ik
sink
cell j
cell i
cell k
x 10^-3
auxin source
5.4
5.2
5
4.8
4.6
4.4
PI
Andronov-Hopf point(H)
Limit point bifurcation of cycles
LPC
PI ~ 0
LPC
PI
0.11
0.105
0.1
0.095
0.09
0.085
0.08
PIN membrane (ij)
0.15
0.16
0.17
0.18
0.19
0.2
0.21
0.22
0.23
PIN membrane (ik)

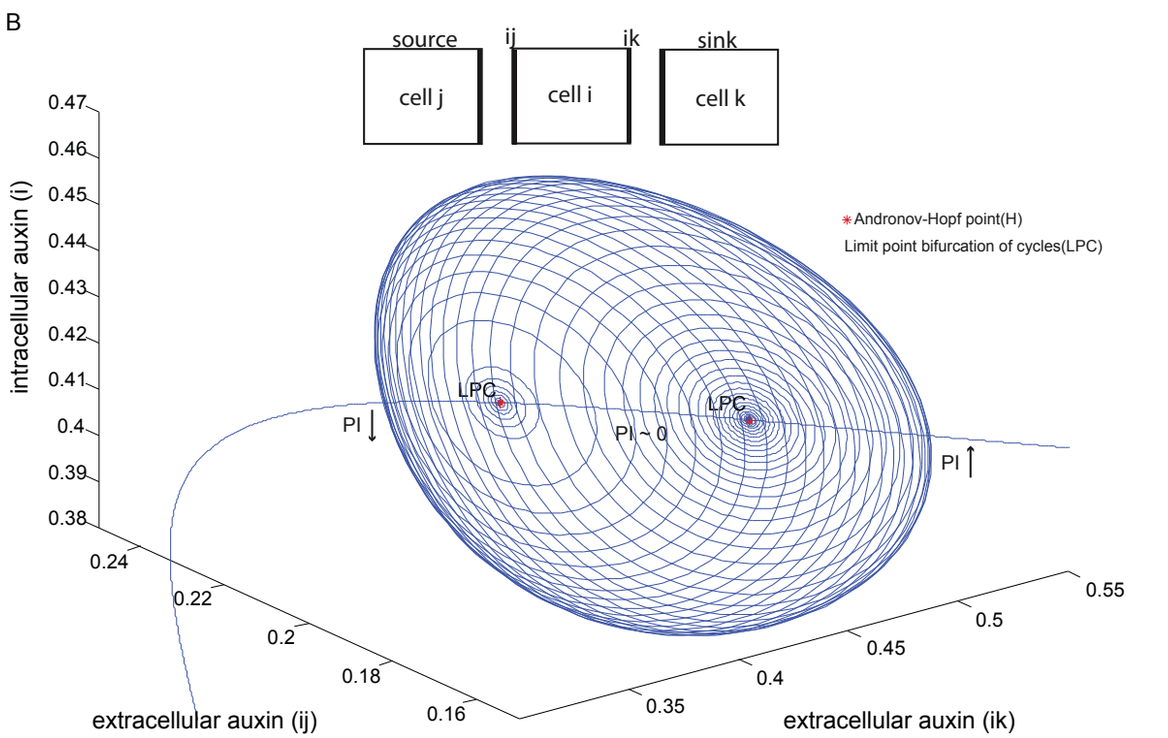
B
source
ij
ik
sink
cell j
cell i
cell k
intracellular auxin (i)
0.47
0.46
0.45
0.44
0.43
0.42
0.41
0.4
0.39
0.38
Andronov-Hopf point(H)
Limit point bifurcation of cycles(LPC)
LPC
LPC
PI
PI ~ 0
PI
0.24
0.22
0.2
0.18
0.16
extracellular auxin (ij)
0.35
0.4
0.45
0.5
0.55
extracellular auxin (ik)

Supplementary Figure 16 The periodic orbits of PIN and auxin levels correspond to stable limit cycle emerging from Hopf bifurcation

(A) Stable limit cycle (LPC) connects two Hopf points (H). The variation of auxin source strength yielded the appearance of either oscillatory (PI ~ 0) or stable PIN polarization in the model (PI <> 0). **(B)** Phase portrait showing the borders between either oscillating (PI ~ 0) or stable (PI <> 0) auxin levels, inside and outside of the cell.

Polarization Index (PI) is described in Figure 2. The sign of PI corresponds to different model behavior (Supplementary Figure 13).

2.16 SUPPLEMENTARY MOVIES

Supplementary Movie 1

The file contains Supplementary Movie 1 displaying the PIN-dependent auxin canalization on grid layout (simulation of Figure 3A-3C). Color coding schemes for auxin concentrations and PIN levels that were used in the model simulations as described in Figure 3I. Auxin concentrations can vary from 0 (black) to 10 (bright green). PIN levels at the plasma membrane may change from 0 (black) to 10 (bright red). White arrows point in the direction of the preferential PIN polarity, and arrow size indicates the relative strength of PIN expression in the cell.

Supplementary Movie 2

The file contains Supplementary Movie 2 showing the PIN-dependent auxin canalization on cellular layout (simulation of Figure 3D, 3G and 3H). Color coding schemes for auxin concentrations and PIN levels that were used in the model simulations as described in Figure 3I. Auxin concentrations can vary from 0 (black) to 10 (bright green). PIN levels at the plasma membrane may change from 0 (black) to 10 (bright red). White arrows point in the direction of the preferential PIN polarity, and arrow size indicates the relative strength of PIN expression in the cell.

Supplementary Movie 3

The file contains Supplementary Movie 3 showing PIN polarity and auxin distribution associated with auxin canalization during dynamic cellular growth over 3 CPU days (simulation of Figure 4C-4E). Color coding schemes for auxin concentrations and PIN levels that were used in the model simulations as described in Figure 3I. Auxin concentrations can vary from 0 (black) to 10 (bright green). PIN levels at the plasma membrane may change from 0 (black) to 10 (bright red). White arrows point in the direction of the preferential PIN polarity, and arrow size indicates the relative strength of PIN expression in the cell.

Supplementary Movie 4

The file contains Supplementary Movie 4 displaying the formation of vein loop pattern (simulation of Figure 5C-5H). Auxin concentrations can vary from 0 (black) to 10 (bright green). PIN levels at the plasma membrane may change from 0 (black) to 10 (bright red). White arrows point in the direction of the preferential PIN polarity, and arrow size indicates the relative strength of PIN expression in the cell.

Supplementary Movie 5

The file contains Supplementary Movie 5 addressing competitive canalization and lateral bud release (simulation of Figure 6A-6E). Auxin concentrations can vary from 0 (black) to 10 (bright green). PIN levels at the plasma membrane may change from 0 (black) to 10 (bright red). White arrows point in the direction of the preferential PIN polarity, and arrow size indicates the relative strength of PIN expression in the cell.

Supplementary Movie 6

The file contains Supplementary Movie 6 showing competitive canalization and apical dominance (simulation of Figure 6I-6M). Auxin concentrations can vary from 0 (black) to 10 (bright green). PIN levels at the plasma membrane may change from 0 (black) to 10 (bright red). White arrows point in the direction of the preferential PIN polarity, and arrow size indicates the relative strength of PIN expression in the cell.

Supplementary Movie 7

The file contains Supplementary Movie 7 illustrating the vascular tissue regeneration after wounding (simulation of Figure 7). Color coding schemes for auxin concentrations and PIN levels that were used in the model simulations as described in Figure 3I. Auxin concentrations can vary from 0 (black) to 10 (bright green). PIN levels at the plasma membrane may change from 0 (black) to 10 (bright red). White arrows point in the direction of the preferential PIN polarity, and arrow size indicates the relative strength of PIN expression in the cell.

ACKNOWLEDGEMENTS

We thank Angharad Jones for critical reading of the manuscript, more particularly Przemyslaw Prusinkiewicz for fruitful discussions and comments, and Martine De Cock for help in preparing it. This work was supported by grants from the Research Foundation-Flanders (Odysseus) and the EMBO Young Investigator Program to J.F., the Research Foundation Flanders (project no. 3G006507) to W.G., Marie Curie European Reintegration Grant 230974 to R.M., and Czech Min-

istry of Education LC06034 to J.B. This work was co-financed by the Netherlands Consortium for Systems Biology (NCSB), which is part of the Netherlands Genomics Initiative/Netherlands Organization for Scientific Research. *Author contributions*: JF, JKV, KW, RHM, WG designed the experiments; KW, JKV, MS, JB, SN performed the experiments; VR, JB and MS provided biological material; KW, JKV and JF, wrote the paper.

CHAPTER 3

MECHANISTIC FRAMEWORK FOR GENERATION AND MAINTENANCE OF PIN AUXIN EFFLUX CARRIER POLARITY IN PLANT CELLS

"The physicist's problem is the problem of ultimate origins and ultimate natural laws. The biologist's problem is the problem of complexity."

—Richard Dawkins

MECHANISTIC FRAMEWORK FOR GENERATION AND MAINTENANCE OF PIN AUXIN EFFLUX CARRIER POLARITY IN PLANT CELLS

Jürgen Kleine-Vehn[1,2,3,9], Krzysztof Wabnik[1,2,4,9], Alexandre Martinière[5], Łukasz Łangowski[1,2], Hirokazu Tanaka[1,2,6], Katrin Willig[7], Satoshi Naramoto[1,2], Johannes Leitner[6], Stefan Jakobs[7], Stephanie Robert,[1,2,8], Christian Luschnig[3], Willy Govaerts[4], Stefan Hell[7], John Runions[5], and Jiří Friml[1,2]

under review, (2011)

Contribution: Computation modeling work has been done by K. Wabnik

[1]Department of Plant Systems Biology, VIB, 9052 Gent, Belgium

[2]Department of Plant Biotechnology and Genetics, Ghent University, 9052 Gent, Belgium

[3]Department of Applied Genetics and Cell Biology, University of Applied Life Sciences and Natural Resources (BOKU), 1190 Vienna, Austria

[4]Department of Applied Mathematics and Computer Science, Ghent University, 9000 Gent, Belgium

[5]School of Life Sciences, Oxford Brookes University, Gipsy Lane, Oxford OX3 0BP, UK.

[6]Department of Biological Science, Graduate School of Science, Osaka University, Osaka 560-0043, Japan

[7]Department of NanoBiophotonics and DFG-Research Center for Molecular Physiology of the Brain, Max Planck Institute for Biophysical Chemistry, 37077 Göttingen, Germany

[8]Umeå Plant Science Centre, Department of Forest Genetics and Plant Physiology, Swedish University of Agricultural Sciences, Umeå University, SE-90 183 Umeå, Sweden.

[9]These authors contributed equally to this work

ABSTRACT

Cell polarity reflected by asymmetric distribution of proteins at the plasma membrane is a fundamental feature of unicellular and multicellular organisms. It remains conceptually unclear how cell polarity is achieved in cell wall-encapsulated plant cells without cellular junctions. We have used super-resolution and semi-quantitative live-cell imaging in combination with pharmacological, genetic and computational approaches to reveal unexpected insights into the mechanism behind generation and maintenance of cell polarity in *Arabidopsis thaliana*. We show that polar-competent PIN transporters for the phytohormone auxin are delivered to the centre of polar domains by a super-polar exocytosis. Within polar domains, PINs are recruited into non-mobile membrane clusters, which dramatically reduce their lateral diffusion and ensures longer polar retention. At the circumventing edges of the polar domain, spatially defined internalization of escaped cargos occurs by clathrin-dependent endocytosis. Our *in silico* simulations confirm that the combination of these processes provides a robust mechanism for polarity maintenance in plant cells. Moreover, our study suggests that the regulation of lateral diffusion and spatially defined endocytosis, but not super polar exocytosis have primary importance for PIN polarity maintenance.

3.1 INTRODUCTION

Cell polarity is fundamental to many aspects of cell and developmental biology in both unicellular and multi-cellular organisms. In animals, the deposition of remarkably conserved polarity (Crumbs, Scribble and PAR) modules ensures the formation and maintenance of cell polarity (Chen *et al*., 2010; Humbert *et al.*, 2006; Lu and Bilder, 2005; Tepass *et al*., 2001; Wells *et al*., 2006). However, compared to animal and yeast cells, the underlying mechanisms that maintain cell polarity in plants are until now unknown. Notably, the molecular components of animal polarity protein complexes are absent in plants (Geldner, 2009).

In plants, PIN proteins are prominent polar cargos that determine the direction and rate of cellular export and intercellular transport of the plant growth substance auxin (Petrášek *et al*., 2006; Wiśniewska *et al*., 2006). The phytohormone auxin coordinates many growth and developmental processes in plants, which to a large extent is modulated via a dynamic control of cellular PIN polarity and its effects on directionality of auxin fluxes (Vanneste and Friml, 2009). At the molecular level, polar PIN targeting depends on cell type- and PIN sequence-specific factors (Wiśniewska *et al*., 2006). PIN proteins constitutively cycle between the plasma membrane and an endosomal pool (Dhonukshe *et al*., 2007; Geldner *et al*., 2001). The function of this cycling is unclear but it might serve as a mean to mediate polarity establishment and rapid polarity alteration (Dhonukshe *et al*., 2008; Friml *et al*., 2002; Kleine-Vehn *et al*., 2008). PIN internalization (endocytosis) from the plasma membrane depends on the clathrin machinery (Dhonukshe *et al*., 2007). In a positive feedback mechanism, auxin itself inhibits the clathrin-dependent endocytosis of PINs (Paciorek *et al*., 2005; Robert *et al*., 2010) and appears to contribute by this mechanism to a self-organizing, auxin-mediated tissue polarization (Sachs, 1981; Scarpella *et al*., 2006; Wabnik *et al*., 2010).

Mechanisms underlying apical and basal polar PIN deposition appear to be molecularly distinct (Kleine-Vehn *et al.,* 2006; Wiśniewska *et al.,* 2006) and recruitment into these pathways depends on the phosphorylation status of PIN proteins (Dhonukshe *et al.,* 2010; Friml *et al.,* 2004; Huang *et al.,* 2010; Kleine-Vehn *et al.,* 2009; Zhang *et al.,* 2010). The serine/threonine protein kinase PINOID (PID) catalyzes PIN phosphorylation (Michniewicz *et al.,* 2007), leading to basal-to-apical polarity switches by PIN recruitment to a ARF-GEF GNOM independent pathway (Kleine-Vehn *et al.,* 2009). The phosphatase PP2A counteracts PINOID action on PIN phosphorylation and preferentially promotes GNOM-dependent basal PIN localization (Kleine-Vehn *et al.,* 2009; Michniewicz *et al.,* 2007).

Besides PIN-dependent auxin transport mechanism, polar vesicle trafficking also contributes to other often diverse cellular functions, such as polar tip growth, nutrition uptake, root soil interface establishment and pathogen response (Alassimone *et al.,* 2010;

Kwon *et al.,* 2008; Łangowski *et al.,* 2010; Takano *et al.,* 2010; Takeda *et al.,* 2008).

Despite this wealth of molecular clues into polar targeting and subcellular dynamics of PIN proteins, the trafficking mechanisms underlying the maintenance of polar distribution of PIN proteins or other polar cargos in plant cells are unknown, so far. Establishing semi-quantitative and subdiffraction resolution fluorescence imaging for living plant cells have provided us with unexpected insights into the mechanisms underlying polarity generation and maintenance. We illustrate (*i*) presumably endosome guided super-polar targeting of PIN proteins to the centre of polar domains, (*ii*) PIN recruitment to immobile membrane clusters that reduce lateral PIN mobility and (*iii*) an PIN protein retrieval at the lateral cell side by spatially defined clathrin-dependent endocytosis. *In silico* model simulations are consistent with these experimental observations and reveal the individual roles of these cellular processes in the formation and maintenance of sharply defined polar plasma membrane domains.

3.2 EVALUATION OF PIN POLARITY ESTABLISHMENT IN PLANT CELLS

In order to obtain further insight into the polar targeting mechanism in plants, we investigated prominent polar plant cargos of the PIN phytohormone auxin efflux carrier family (Figiure 1A). In root epidermal cells PIN2 proteins localize mainly to the apical plasma membrane domain, but to a lesser extent also to other sides of the cell (Supplementary Figure 1A-1C). We applied a semi-quantitative confocal microscopy technique to visualize relative fluorescence intensity of PIN2-GFP (Figure 1A) or endogenous PIN2 (Figure 1B), enabling us to address the ratio of polar PIN distribution within the plasma membrane. 3D imaging (x,y,z) combined with colour-coded fluorescence intensity profiling revealed that the majority of PIN2-reporter indeed localized to the apical cell side with a remarkably steep decrease in intensity at the edges of the apical domain (Figure 1A and 1B).

3.3 PREFERENTIAL PIN1 AND PIN2 TARGETING TO THE CENTRE OF THE POLAR PLASMA MEMBRANE DOMAIN

To address the so far elusive mechanism of cell polarity maintenance in plant cells, we initially addressed polar deposition of PIN2 in the apical cell side. We performed z-stack imaging (0.5-µm steps) of whole root epidermal cells and calculated 3D projections to obtain a detailed representation of PIN2-GFP fluorescence intensity within the apical cell side.

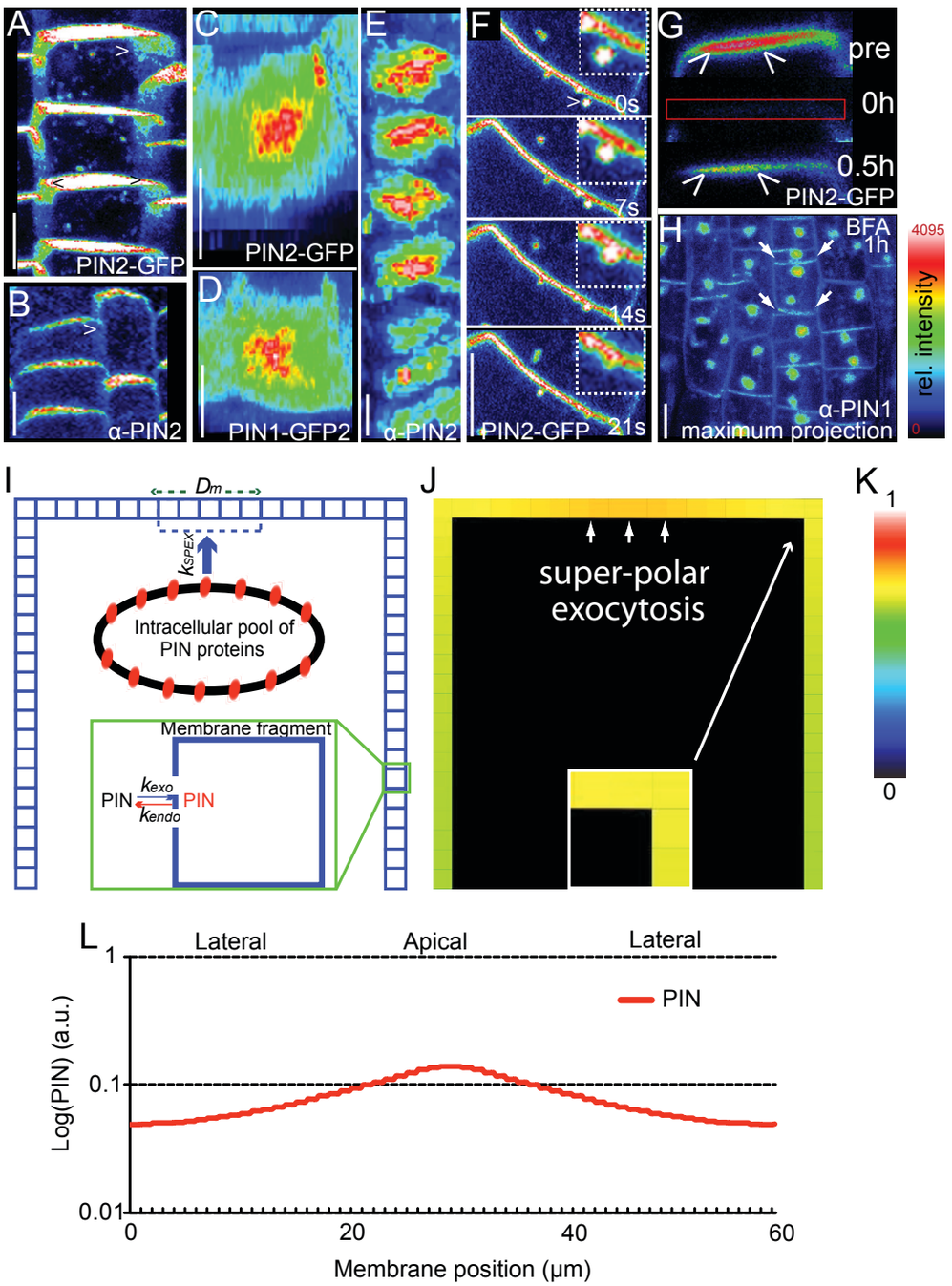

Figure 1 Super-polar PIN2 targeting

(A, B) Maximum projection of epidermal PIN2-GFP (12 sections at 1 µm step size) (A) and endogenous PIN2 (6 sections at 2µm step size) (B) reveals preferential apical PIN2 localization and steep decrease at the lateral cell side. Arrowheads depict the steep decrease in lateral PIN2 localisation. **(C-E)** Top view of the apical cell surface by 3D xyz-projection (30 sections at 0.5 µm size) of a epidermal cell expressing PIN2:PIN2-GFP (C) and PIN2:PIN1-GFP2. (D) Apical PIN2-GFP and basal PIN1-GFP2 signal intensity is highest in the center and gradually gets weaker towards the cell edges. (E) PIN2 antibody staining depicts

7 consecutive cells (45° angle). **(F)** Timelapse of PIN2-GFP containing endosome at the apical cell surface (see arrowhead and inset). **(G)** Medial, single scan sections of PIN2-GFP expressing root epidermal cells. Pre bleached cell shows preferential super polar PIN2 localization and preferential super polar recovery (0.5h) after photobleaching (see arrowheads and also Supplementary Figure 2). **(H)** BFA [50 µM] treatment for 1 h results in PIN1 (antibody) accumulation in BFA compartments in root stele cells (z-stack maximum projection). BFA compartments reside close to the basal or apical cell side. Arrows indicate preferential polar distribution of PIN1 at the basal cell side. **(I)** Schematics of the computer model. Intracellular space is abstracted by a single endosomal compartment that contains the common intracellular pool of PIN proteins. PIN proteins recycle between the endosomal compartment and each discrete plasma membrane fragment at the constant basal PIN turnover rates kexo and kendo (blue and red arrows). PIN proteins are delivered by the super-polar exocytosis (k_{SPEX}; thick blue arrow) to the center of the polar plasma membrane domain. D_m describes the free lateral diffusion of PIN proteins in the plasma membrane. **(J-L)** Computer model simulations with spatially restricted polar delivery of PIN proteins (I, white arrow) predicted the loss of apical PIN polarization in root epidermis cell due to lateral diffusion (Supplementary Movie 1) (L). (K) Color coding scheme for model simulations (log scale). (L) Steady-state PIN distribution pattern. Graph depicts nearly uniform distributions of PIN proteins in all cell sides.
Fluorescence intensity from 0 (black) to 4095 (brightest/white) is represented by the color code shown beneath the figure (A-H). Scale bar: 5 µm

Highest PIN2-GFP fluorescence intensities could be detected in an inner core of the apical plasma membrane that we have designated the super apical domain (Figure 1C). Endogenous PIN2 proteins also displayed localization predominantly restricted to the super apical domain (see inset in Figure 1E). Notably, this super polar PIN2 localization was not observed in all epidermal cells and appears to be less pronounced in younger epidermal root cells (Figure 1E).

Next we investigated PIN2:PIN1-GFP2 transgenic lines that preferentially show basal PIN1 localization in root epidermal cells (Wiśniewska *et al*., 2006). The stronger PIN1-GFP2 localization was present in the inner core of the basal cell sides (Figure 1D). In contrast, non polar plasma membrane marker BRI1-GFP did not show comparable enrichments in the basal or apical cell sides (Supplementary Figure 1), indicating specific polar targeting mechanisms for PIN proteins.

To address whether super-polar PIN2 targeting is linked to its enhanced delivery to the apical cell side, we specifically photobleached the entire apical cell side and recorded its recycling based recovery within 15-30 minutes. In the majority of cells (n=33; 66%) displaying super-polar PIN2 localization, stronger PIN2 recovery in the inner core of the apical cell side was observed (Figure 1G; Supplementary Figure 2). This finding suggests that the super-polar PIN2 localization requires a defined polar exocytosis/deliv-

ery mechanism.

Notably, PIN cargos containing endomembranes (hereafter defined as endosomes) are frequently observed beneath the plasma membrane. PIN2-GFP enrichment in the apical plasma membrane correlates with endosomal occurrence beneath (Figure 1F). One can speculate that endosomal positioning beneath the plasma membrane and subsequent spatially defined exocytosis or fusion might enable highly defined "super-polar" deposition of PIN proteins (Figure 1F; Supplementary Figure 1D-1F).

3.4 SUPER POLAR PIN DELIVERY IS NOT SUFFICIENT FOR DEFINED PIN POLARITY MAINTENANCE

To test whether super-polar delivery of PIN to the polar domain is sufficient to explain PIN polarity establishment, we used computer model simulations (Figure 1I-1L).

The apical and neighboring lateral sides of root epidermis cell were modeled explicitly. We represented the plasma membrane as a sequence of discrete membrane fragments each of 1x1 micron size (Figure 1I). Each fragment was associated with either the apical or one of the two lateral cell sides (Figure 1I). The intracellular membranes were approximated by one single endosomal compartment that represented the common intracellular pool of PIN proteins (Figure 1I). The redistribution of PIN proteins between membrane fragments and endosomal compartments was determined by the basis of the PIN turnover rates (k_{exo} and k_{endo}) (Figure 1I, thin blue and red arrows). This basal exo- and endocytosis rates are set to be constant for all cell sides. We considered that PIN proteins display lateral diffusion (D_m) within the plasma membrane (Figure 1I).

The super polar delivery of PIN proteins occurs to a central region within one side of the cell, presumably via endosomal trafficking mechanisms and subsequent spatially defined protein recycling. We modeled this process by assuming an increased rate of PIN delivery (k_{SPEX}) to the center of the polar domain (Figure 1I, thick blue arrow). However, even the assumption of a highly defined, super polar PIN deposition did not lead to a pronounced PIN polarization in our model (Figure 1I-1L). In accordance, the pharmacological inhibition of GNOM-dependent PIN1 exocytosis to the basal cell side did not lead to the total loss of preferential PIN localisation (Figure 1H; Supplementary Figure 1G). These findings indicate that polar PIN delivery is not sufficient to explain the defined PIN polarization.

3.5 PIN PROTEINS DISPLAY REDUCED LATERAL DIFFUSION WITHIN THE PLASMA MEMBRANE

Once proteins are deposited at the plasma membrane, the fluidity of the membrane allows their lateral diffusion. Notably, polar competent PIN proteins have been suggested to display reduced lateral diffusion in the plasma membrane compared to non-polar markers, such as PLASMA MEMBRANE INTRINSIC2 (PIP2) or LOW-TEMPERATURE-INDUCED6b (LTI6) (Dhonukshe *et al.*, 2008; Men *et al.*, 2008).

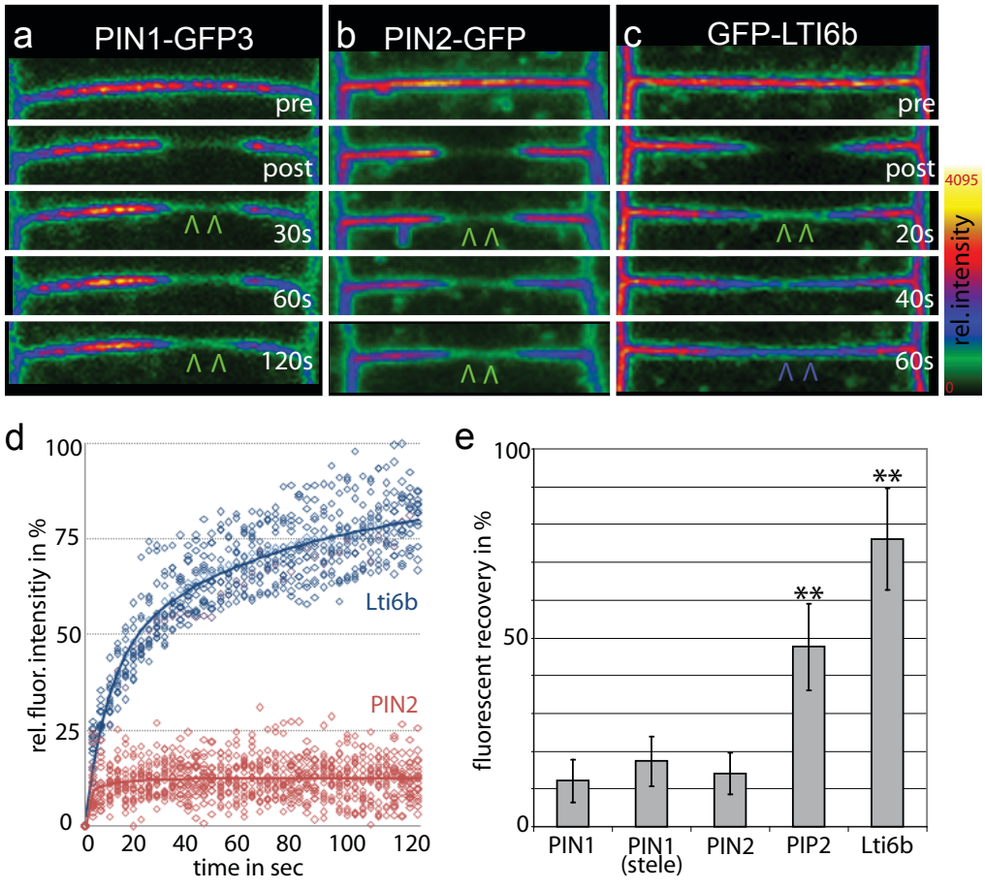

Figure 2 PIN proteins reside in a non-mobile membrane fraction

(A, B) PIN1-GFP (A) or PIN2 (B) display only weak fluorescence recovery after photobleaching (FRAP) within 2 minutes as visualized by colour based fluorescence intensity coding. In contrast, the non-polar plasma membrane marker GFP-LTI6b (C) displays rapid and substantial recovery within 1 minute. **(D, E)** Fluorescence recovery kinetics of PIN2-GFP and GFP-LTI6b FRAP experiment (D). Maximum fluorescence recoveries of the non-polar plasma membrane markers PIP2-GFP (47.6%; n=23) and LTI6b-GFP (76.1%; n=20 cells) are significantly higher (E) than is the recovery of epidermal PIN2-GFP (14%; n=27 cells) and PIN2:PIN1-GFP3 (12.1%; n=12) and PIN1:PIN1-GFP (17.3%; n=14) in stele (* indicate $p<0.001$). Error bars represent standard deviation.

Fluorescence intensity from 0 (black) to 4095 (brightest) is represented by the color code shown beneath the figure (A-C). Scale bar: 5 µm.

We utilized the combination of fluorescence recovery after photobleaching (FRAP) (Chen *et al*., 2006) and a confocal-based semi-quantitative imaging approach to address lateral diffusion of plasma membrane proteins. PIN1 and PIN2 short term, diffusion-based recovery in root epidermal cells was visibly weaker than LTI6b-GFP recovery (Figure 2A-2C). The fluorescence PIN2-GFP recovery was largely abolished after the whole plasma membrane was bleached (n=15; mean recovery: 4,1%; SD: 1,8%); indicating that recovery within 2 minutes was due to lateral diffusion and is largely independent of secretion. This finding is in agreement with previous inhibitors-based demonstration of lateral diffusion of plasma membrane proteins (Men *et al*., 2008). Next, we analyzed the kinetics of PIN2 and LTI6b fluorescent recovery. The GFP-LTI6b showed rapid (maximum of 76%) recovery of initial fluorescence within 2 minutes after photobleaching (Figure 2D) whereas the recovery of PIN2-GFP was only about 14% (Figure 2C and 2D), suggesting that only a small fraction of the PIN proteins can freely diffuse laterally within the plasma membrane, and the majority of PINs appears to be non-mobile. Notably, the lateral diffusion of PIN2 was not only reduced in the center of the apical cell side (n=27; mean recovery: 14,0%; SD: 5,6%), but also in peripheral and apical cell sides (n=11; mean recovery: 12,7%; SD: 5,3%; p-value: 0,76).

Similar to PIN2, PIN1 in root epidermal and stele cells showed severely reduced lateral diffusion (Figure 2E), indicating a general mechanism for PIN protein immobilization. The aquaporin PIP2;1 had a relatively high non-mobile fraction in the plasma membrane (Figure 2E). Nevertheless, the lateral mobility of PIP2;1 was significantly higher than that of PIN2, but lower than Lti6b (Figure 2E), indicating complex regulation of lateral diffusion of different plasma membrane proteins.

Our data suggest that the reduced lateral diffusion behavior of PIN proteins (Dhonukshe *et al*., 2008; Men *et al*., 2008) might not be due to slower diffusion rates, but rather relate to a mechanism that immobilizes a large fraction of PIN proteins in the plasma membrane.

3.6 PIN PROTEINS LOCALIZE TO MEMBRANE CLUSTERS WITHIN THE PLASMA MEMBRANE

Reduced lateral PIN mobility within the plasma membrane might be regulated by membrane heterogeneity; therefore, we analyzed the PIN protein distribution within the plasma membrane.

Semi-quantitative confocal and super-resolution microscopy revealed that PIN1 and PIN2 auxin efflux carriers are not evenly distributed in the plasma membrane but that they accumulate in distinct “clusters” (Figure 3A-3C).

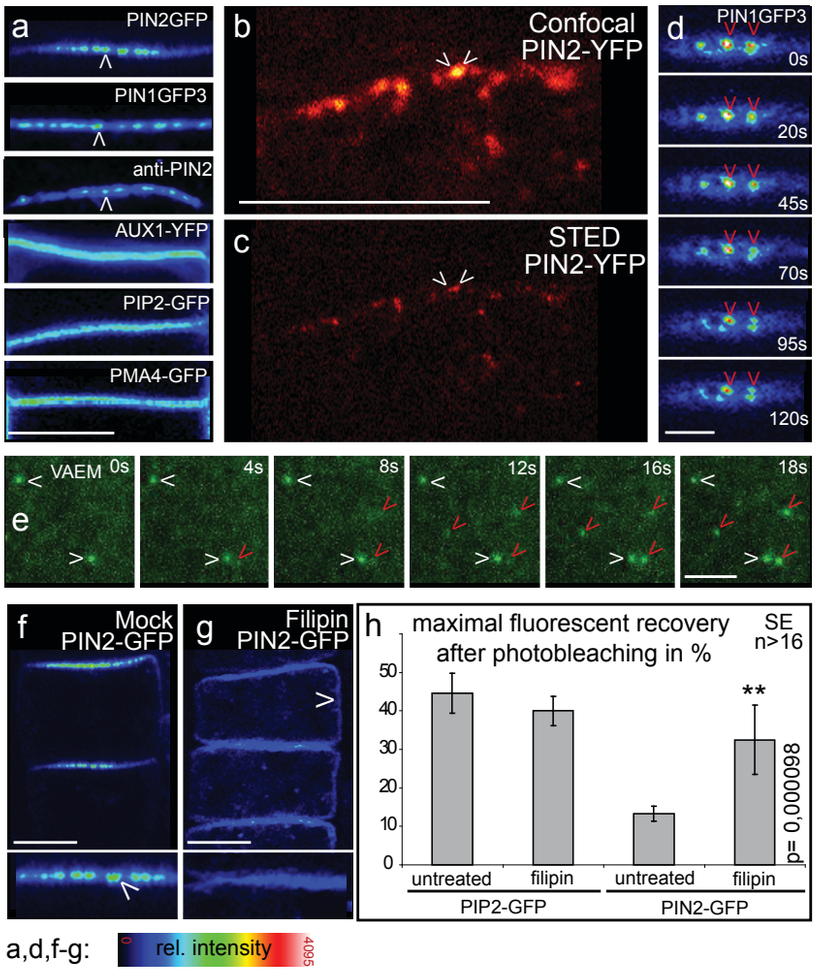

Figure 3 PIN proteins reside in non-mobile membrane clusters

(A) PIN proteins, but not non-polar AUX1, PIP2 or PMA4, are localized in membrane clusters (arrowheads). **(B, C)** Confocal (B) and super-resolution STED (C) microscopy of PIN2-YFP reveals PIN2 clusters in the apical plasma membrane (arrowhead) (see also Supplementary Figure 3 on cluster size evaluation). **(D)** pPIN2:PIN1-GFP (in epidermal cells) is non-mobile within membrane clusters (arrowheads) during 2 minute timelapse imaging (see also kymograph representation of 10 minutes time laps in Supplementary Figure 4). **(E)** VAEM imaging revealed non-mobile PIN2-GFP clusters (white arrowheads) and the gradual appearance of PIN2-GFP at the outer lateral plasma membrane of root epidermal cells (red arrowheads). **(F, G)** PIN2-GFP localization in membrane clusters (arrowhead) (F) is reduced after filipin [100µM, 3h] treatment (arrowhead depicts loss of PIN2 polarity) (G) (see also images with variable gain settings in Supplementary Figure 4). **(H)** Filipin treatment [100 µM; 20 minutes] results in a significant increase in membrane lateral mobility of PIN2-GFP, but not of PIP2;1-CFP (n>16 cells; * indicates p<0.0001). Error bars depict standard error.

Fluorescence intensity from 0 (black) to 4095 (brightest) is represented by the color code shown beneath the figure (A, D, F-G). Scale bar: 5 µm. All images are single scans.

In contrast, the auxin influx carrier AUX1 or other non-polar cargos, such as LTI6b, PIP2;1, Brassinosteroid receptor BRI1, or plasma membrane H+-ATPase PMA4 showed a very weak heterogeneity, but we did not detect any comparable clustering as for PIN proteins (Figure 3A; Supplementary Figure 1H). To improve resolution and to elaborate on the specificity of this finding, we employed sub-diffraction resolution STED microscopy (Hell and Wichmann, 1994; Willig *et al.*, 2006). While this method has been applied to mammalian cells before, here we established this method for the imaging of living plant cells. We observed PIN2-YFP accumulation in membrane clusters (Figure 3B and 3C), but we did not detect any AUX1-YFP proteins in plasma membrane subdomains (Figure 3A and 3B). Furthermore, STED microscopy revealed that the PIN2-containing membrane clusters vary in size and average between 100-200 nm in diameter (Supplementary Figure 3C and 3D).

These data illustrate that PIN proteins are distributed in distinct subdomains (clusters) in the nanometer range in the plasma membrane. This observation is in good accordance to our findings that PIN proteins reside in two distinct pools within the plasma membrane (majority in a relatively non-mobile and to a lesser extent in a mobile fractions).

3.7 MEMBRANE CLUSTERS REDUCE LATERAL DIFFUSION OF PIN PROTEINS

Next we analyzed whether PIN recruitment to the clusters in the plasma membrane could be related to the strongly reduced lateral diffusion of PIN proteins. Remarkably, PIN1 and PIN2 proteins associated clusters were largely non-mobile in the time window of at least 10 minutes (Supplementary Figure 4A). Variable angle epifluorescence microscopy (VAEM) revealed that also PIN2 proteins at the lateral cell side displayed non-mobile clustering in the plasma membrane (Figure 3E). In addition to non-mobile existing clusters at the lateral cell side, new PIN2 clusters appeared (Figure 3E), indicating either PIN protein delivery or recruitment to the membrane clusters. The gradual appearance of PIN2 clusters at the lateral cell side rather suggests a gradual recruitment scenario of free PIN2 proteins into membrane clusters at the lateral cell side, possibly reducing the lateral PIN2 diffusion.

In yeast, plasma membrane compartmentalization partially depends on its sterol composition (Bagnat and Simons, 2002; Grossmann *et al.*, 2008). However, lateral diffusion of PIN2 was not affected in sterol mutant cpi (Men *et al.*, 2008). Sterol-dependent cell functions can be furhtermore studied using the sterol-binding agents filipin and cyclodextrin which cause sterol desorption (Zidovetzki and Levitan, 2007) and modulates plant plasma membranes (Kleine-Vehn *et al.*, 2006; Men *et al.*, 2008). Filipin treatments

reduced both PIN2 association into membrane clusters (Figure 3F and 3G; Supplementary Figure 4B and 4C) and the polar localization of PIN2 after prolonged disruption of membrane sterols (Figure 3G).

Short-term fillipin treatment (20 minutes) was sufficient to enhance the fluorescence recovery rate of PIN proteins from 13% to 32% (Tukey test, $p<0,01$) (Figure 3H) but not that of the non-polar plasma membrane marker PIP2;1 (Figure 3H).

These findings suggest that PIN proteins display very limited lateral diffusion, due to constitutive recruitment to and residence in non-mobile membrane domains.

3.8 SUPER POLAR PIN DEPOSITION AND REDUCED LATERAL DIFFUSION ARE NOT SUFFICIENT FOR PIN POLARITY MAINTENANCE

The reduced lateral diffusion of PIN proteins (Dhonukshe *et al*., 2008; Men *et al*., 2008) might not rely on slower diffusion rates, but, in contrast, on immobilization of a large fraction of PIN proteins in the plasma membrane. To evaluate this assumption and to test its potential importance for PIN polarity maintenance we integrated this reduced PIN diffusion mechanism into our cmputer model (Figure 4A-4C).

Intriguingly, the combination of super polar exocytosis (Figure 1H) and reduced lateral diffusion due to PIN clustering in the membrane (Figure 4A) led to a preferential PIN polarization at the apical cell side in our model (Figure 4B). These findings are in accordance with our experimental findings and indicate that lateral diffusion is an important parameter for PIN polarity maintenance (Figure 2). However, compared to the experimental data (Figure 1A and 1B), the model simulation did not predict a steep decrease of PIN protein abundance at the lateral cell side (Figure 4C). Similarly, simulations of highly pronounced super polar exocytosis of PIN proteins, reduced lateral PIN diffusion (Supplementary Figure 5A-5H), or heir combination (Supplementary Figure 5I and 5J) did not result in realistic PIN distribution patterns (Figure 1A and 1B). Based on these *in silico* simulations, we suggest that super polar PIN deposition and reduced lateral mobility is not sufficient to explain PIN polarity maintenance *in planta*.

3.9 SPATIALLY DEFINED CLATHRIN-DEPENDENT PIN ENDOCYTOSIS IS REQUIRED FOR THE MAINTENANCE OF PIN POLARITY

The combination of super-polar deposition and reduced lateral mobility might not be sufficient for the observed steep decrease in intensity of PIN2-GFP at the lateral cell sides (Figure 4A and 4B; Figure 1A). Therefore, we assume that additional PIN retrieval

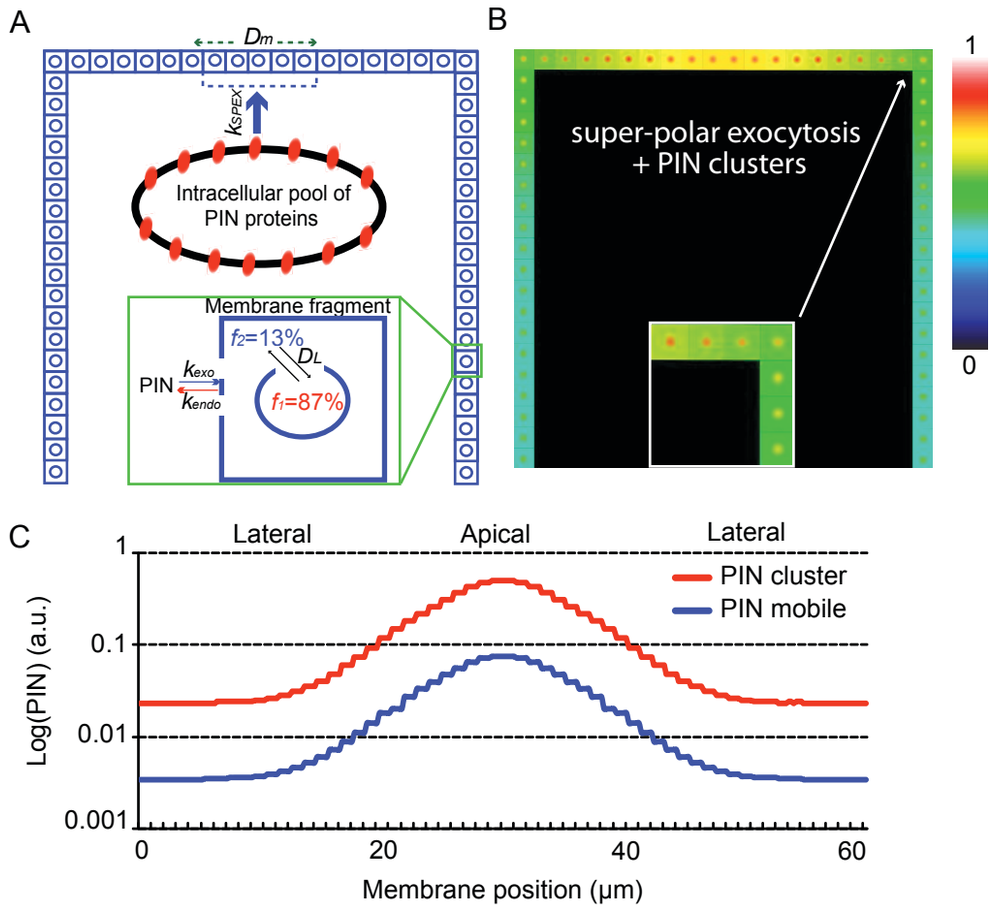

Figure 4 Integration of super-polar PIN delivery and membrane-associated PIN clusters for PIN polarity maintenance

(A) Schematics of the extended computer model. Inside each discrete membrane fragment PIN proteins are distributed in two groups (D_L) with non-mobile (f_1) and mobile (f_2) pool. Only the PIN proteins within the mobile pool (f_1) diffuse (D_m) to the adjacent membrane fragments. The remaining model assumption are as in Figure 1H. **(B, C)** A weak PIN polarization was predicted by computer model simulations assuming super-polar delivery of PIN proteins and PIN immobilization in membrane clusters (B) (Supplementary Movie 2). However, pronounced leakage of PIN proteins towards cell junctions was observed (white arrow). (C) Steady-state PIN distribution in the plasma membrane showed a shallow gradient-like profile. Color coding is the same as in Figure 1K.

mechanisms specifically at the lateral cell side might contribute to the regulation of PIN polarity maintenance. Hence, we subsequently investigated the requirement of endocytosis for PIN polarity maintenance.

PIN protein internalization is largely dependent on clathrin machinery (Dhonukshe *et al.*, 2007). To assess the spatial occurrence of clathrin, we examined clathrin light chain (CLC)-GFP localization at the plasma membrane by semi-quantitative confocal

imaging. CLC-GFP has a stronger localization at lateral cell sides as compared to apical or basal sides (Figure 5A). This clathrin enrichment at lateral cell sides appeared even more pronounced after onset of cellular elongation (Figure 5B). This finding indicates that plant cells can modulate the activity of clathrin at different cell sides, which could contribute to PIN polarity maintenance.

To address whether spatio-temporal activity of clathrin can directly influence PIN polarity, we selectively affected the clathrin-dependent PIN internalization by mutating a conserved tyrosin residue of PIN2 that is presumably required for its cargo-specific sorting into clathrin-coated pits (Supplementary Figure 6). While the majority of $PIN2^{Y505A}$-YFP still localized to the apical cell side in root epidermal cells, the mutation strongly enhanced PIN2 localization at the lateral cell side (Figure 5C and 5D). Notably, PIN2:$PIN2^{Y505A}$-YFP showed reduced PIN internalization and failed to fully rescue the *pin2* mutant phenotype (Supplementary Figure 6). These findings suggest that clathrin function is required for PIN polarity, possibly via PIN protein retrieval specifically from the lateral cell side.

Next, we invoked the temporal inhibition of the clathrin machinery by Tyrphostin23 treatments that affect tyrosine motif-dependent cargo recruitment to the clathrin coated pit (Dhonukshe *et al.*, 2007). The short-term treatment initially enhanced lateral PIN2 localization (Figure 5E) and in time led to the partial PIN2 mislocalization that is aparent from an apical-to-basal gradient in fluorescence intensity at the lateral cell side (Figure 5E). This is presumably the result of slow lateral diffusion of PIN2-YFP from the apical cell side. Notably, short-term Tyrphostin23 treatment had the most pronounced effect after the onset of cellular elongation.

Auxin itself negatively affects clathrin-dependent PIN endocytosis in a transient manner (Paciorek *et al.*, 2005; Robert *et al.*, 2010) and also enhanced PIN2 residence at the lateral cell side after 1-2 hours of exogenous application (Figure 5F). This provides a conceptual possibility that auxin affects polar PIN2 localization in root epidermal cells by spatial inhibition of clathrin-dependent endocytosis (Robert *et al.*, 2010; Wabnik *et al.*, 2010). Auxin perception has been suggested to feed back on PIN polarity (Wabnik *et al.*, 2010). In such a mechanism directional PIN-dependent auxin efflux could enhance PIN polarization and could explain the appearance of PIN protein gradients in the lateral cell side. In summary, independent genetic and pharmacological approaches revealed that clathrin-dependent PIN endocytosis at the lateral cell side is required for PIN polarity maintenance.

3.10 INTERWEAVING MECHANISM FOR PIN POLARITY MAINTENANCE

Next we used our computer model to analyze whether polar PIN deposition, reduced lat-

eral PIN mobility and spatially defined PIN internalization at the lateral cell sides might account for a robust PIN polarization mechanism (Figure 6A).

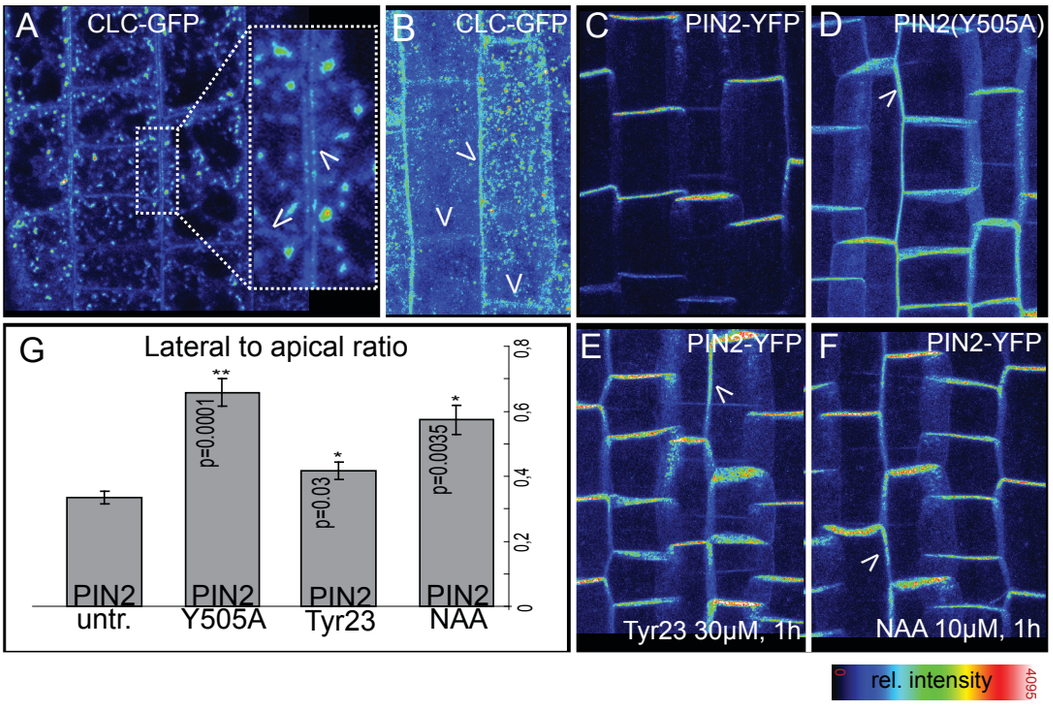

Figure 5 Clathrin-dependent PIN internalization at the lateral cell side for polarity maintenance

(A, B) Single scan (A) and 3D maximum projection (B) of clathrin light chain-GFP (CLC-GFP). Stonger clathrin activity occurs at the lateral cell side than at apical and basal sides, especially after onset of elongation (B). Arrowheads indicate basal and lateral cell margins. **(C-F)** Maximum projections depict polar localization of PIN2-YFP at the apical cell side (C). Polar localization is affected in tyrosine motif mutation $PIN2^{Y505A}$-YFP (D), or after short term tyrphostinA23 [30 µM; 1 hour] (E) and NAA [10 µM; 1 h] (F) treatments. Arrowheads indicate enhanced PIN2-YFP localisation at the lateral side of the cell.

(G) Grey value based evaluation of lateral PIN2-YFP localisation using lateral to apical ratio measurements (n>26 cells; measured in the transition zone).

Fluorescence intensity from 0 (black) to 4095 (brightest) is represented by the color code shown beneath the figure (A-F). Scale bar: 5 µm.

Model simulations predicted the formation of a sharp PIN concentration gradient (bell-shaped distribution curve) in the plasma membrane (Figure 6B). The asymmetric distribution of PIN proteins within the plasma membrane was characterized by an increase of PIN proteins in the polar domain and an exponential decrease of PIN levels at the lateral surfaces of the cell (Figure 6B and 6C). The predicted decrease of PIN abundance at the lateral cell side was in agreement with our quantitative confocal data

(approx. 1000-fold; Figure 6B and 6C; Figure 1A and 1B). Our model predicted a 5-fold decrease of PIN levels from the centre of the polar domain to its periphery (Figure 6B and 6C) which is in accordance with our experimental observations (Supplementary Figure 2). These findings illustrate that the computational model reproduces experimental observations (Figure 1A-1C) and indicate that plant cell polarity could be maintained by a general mechanism integrating (i) super-polar delivery, (ii) reduced lateral diffusion in the plasma membrane, and (iii) spatially restricted internalization. Furthermore, we tested whether super-polar delivery of PIN to the polar domain is strictly required for PIN polarity maintenance in our model and allowed PIN exocytosis to the whole polar domain (Figure 6D). We found that the shape of the PIN gradient in the plasma membrane and the bell-shaped distribution curve characteristic of the PIN polarity (Figure 6G) were similar to those in the control simulations (Figure 6C) and experiments (Figure 1A-1C). Next, we released the assumption of the polar PIN delivery in our model. By keeping endocytosis and exocytosis in balance, the model predicted an overall reduction of PIN levels in the plasma membrane and enhanced PIN labelling at the lateral surface of the cell (Figure 6E), but the preferential PIN polarity/asymmetry was preserved (Figure 6H). Interestingly, this finding was consistent with the experimental data that inhibition of the polar PIN recycling did not fully impair the preferential polar PIN localization (Figure 1G). Moreover, our model predictions were robust with respect to the model parameter manipulation in the biologically feasible range (Supplementary Figure 7).

These results demonstrate that super-polar delivery of PIN proteins might not sufficient to maintain PIN polarity in plant cells, but, instead, that the role of super-polar PIN targeting could be in focusing or separating directional auxin fluxes within a given tissue. Also, our hypothesis might explain why not all epidermal cells show super polar PIN localisation (Figure 1C).

Finally, to address the importance of PIN immobilization for PIN polarity maintenance, we gradually increased mobile (f_1=f_2) PIN fractions in our model (Figure 6F). Model predicted the substantial leakage of PIN proteins to the lateral membrane domains (Figure 6F and 6I), similar to experimental observations (Figure 3F-3H).
Both our experimental and *in silico* data suggest, that beside spatially defined PIN internalization (Figure 5), the reduced lateral PIN diffusion in the plasma membrane is strictly necessary to maintain polar PIN domains in plant cells.

3.11 DISCUSSION

Mechanisms of cell polarization (Chen *et al*., 2010; Humbert *et al*., 2006; Lu *et al*., 2005; Munro and Bowerman, 2009; Tepass *et al*., 2001; Wells *et al*., 2006)) are remarkably

well conserved in animal species (Shivas *et al.*, 2010). Three central polarity complexes,

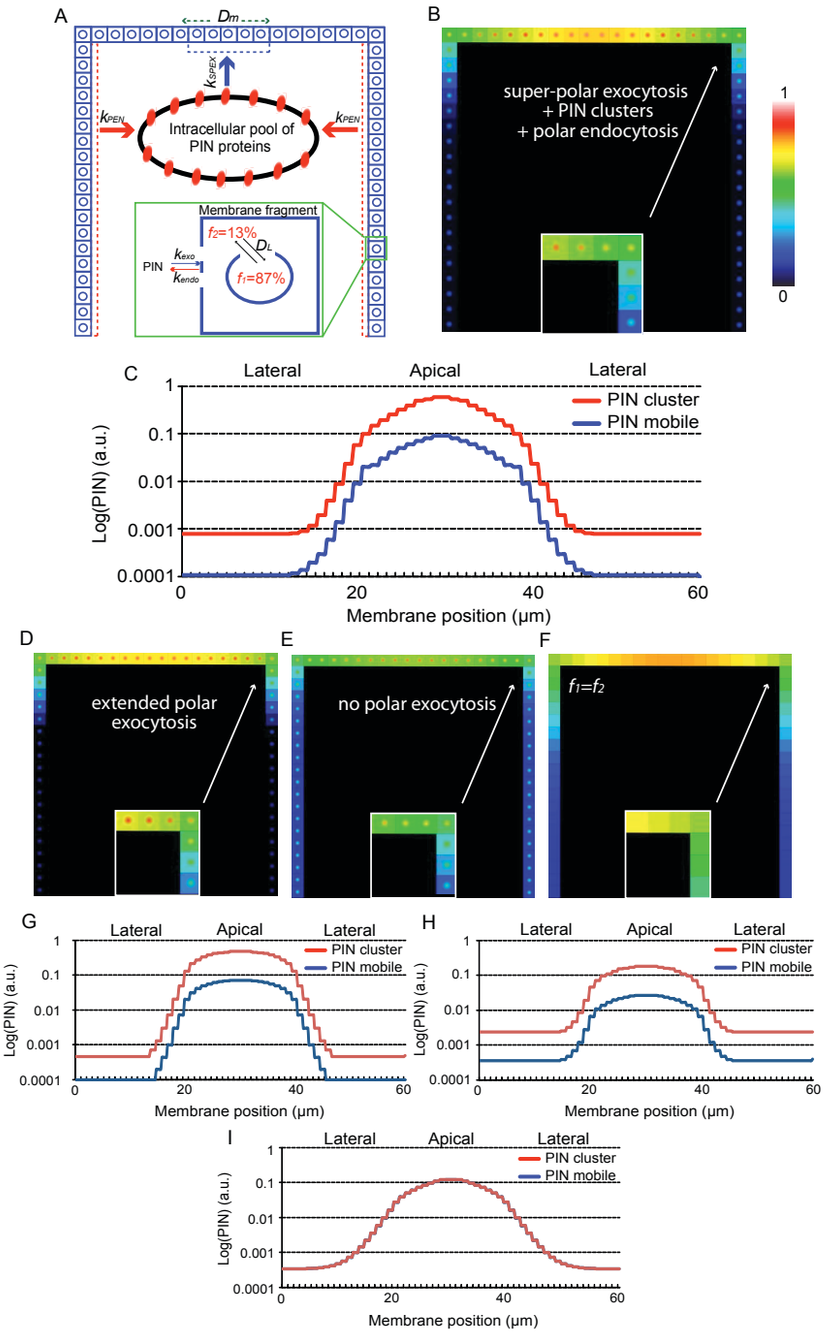

Figure 6 Conceptual model for interweaving polarity mechanism

(A) The model combines super-polar delivery of PIN proteins (Figure 1H), PIN immobilization in membrane clusters (Figure 4A) and spatially defined PIN endocytosis (k_{SPEX}; thick red arrow) at the whole lateral sides of the cell. **(B, C)** Simulations of the combined model predicted a bell-shaped, graded pattern of the PIN distribution in the plasma membrane (B), similar to the in planta observations (Figure 1A-1C) (Supplementary Movie 3).(C) Steady-state PIN distribution profiles display a highly defined apical PIN polar domain in the cell. **(D, E)** Model alterations either by polar PIN deposition along the whole apical cell side (D) or by assuming non-polar PIN exocytosis (e) do not affect qualitatively PIN polarization (Supplementary Movies 4 and 5). Although some minor effects on overall PIN distributions at cell edges were

observed (D and E white arrows). **(F)** Reduced PIN immobilization in membrane clusters (f_1=f_2) leads to enhanced PIN diffusion and ectopic PIN localisation at the lateral cell side. (F) (Supplementary Movie 6), as compared to non-altered model simulations (B). In silico findings are reminiscent with in planta filipin treatment (Figure 3F-3H). **(G-I)** Alterations in steady-state PIN distribution profiles for model simulations D, E and F.

Color coding scheme for simulations is as in Figure 1K.

such as Crumbs, Scribble and PAR modules, localize to and specify a distinct sub-domain of polarized cells (Shivas *et al.*, 2010). These polarity modules are by far best described in epithelial cells of mammals, but also operate in non epithelial cells such as in *C. elegans* embryos (Munro and Bowerman, 2009; Nelson and Beitel, 2009). Traditionally, polar delivery/exocytosis has drawn most attention for polarity establishment and maintenance (Altschuler *et al.*, 2008). However, studies in yeast and epithelial cells highlighted the importance of reduced lateral diffusion for polarity maintenance (Oh and Bi, 2011; teral diffusion for polarity maintenance (Oh and Bi, 2011; Valdez-Taubas and Pelham, 2003). The plasma membrane of epithelial cells is divided into apical and basolateral domains. Epithelial cells have tight cell-to-cell junctions (Giepmans and van Ijzendoorn, 2009) that that are functional diffusion barriers and separate the apical and basolateral membranes from each other and play important roles in polarity maintenance (Wells *et al.*, 2006). Recent growing evidences suggest that beside polar targeting and reduced lateral diffusion, the regulation of endocytosis is equally important for polarity maintenance cells (Dudu *et al.*, 2004; Shivas *et al.*, 2010). However, the underlying mechanism still needs to be unraveled. In budding yeast, the regulation of CDC42p exo- and endocytosis and the ring like, septin-based diffusion barriers (Oh and Bi, 2011) are similarly instructive for cell polarity establishment and maintenance (Orlando *et al.*, 2011).

On the contrary to animal or yeast models, cell wall encapsulated plant cells lack cell-to-cell junctions (Geldner, 2009) and ring-/septin-like diffusion barriers have been only reported in one particular cell type, the endodermis (Roppolo *et al.*, 2011). Moreover, the prominent molecular components of animal polarity complexes are absent in plants (Geldner, 2009) and, hence, the molecular mechanism underlying plant cell polarity are largely obscure. Here we revealed a mechanism for PIN polarity maintenance in plants, which depends on an interweaving mechanism of (i) super-polar delivery to the center of the polar plasma membrane domain, (ii) recruitment to clusters in the plasma membrane that limits lateral cargo diffusion, and (iii) a spatially restricted polar endocytosis. Previous work suggested that initial secretion of newly synthesized PIN proteins is non-polar, indicating that PIN recycling is crucial for PIN polarity establishment (Dhonukshe *et al.*, 2008). In this study we address how PIN proteins can maintain their polar localization within fluid membrane environment. Our results revealed that, similar

to the generation of PIN polarity after non-polar secretion, the constitutive endocytic recycling plays an important role also in the process of polarity maintenance. However, beside polar recycling, PIN polarity maintenance furthermore requires spatially defined regulation of clathrin-dependent PIN internalization and the recruitment of PIN proteins to the largely non-mobile membrane clusters.

Our findings indicate that filipin-sensitive PIN protein recruitment/exclusion to membrane clusters affects lateral mobility of PIN proteins, such as PIN1 and PIN2, and substantially contributes to PIN polarity maintenance.

Plant cells are not only competent to maintain but also to alter the polar PIN localization for complex tissue reprogramming - for instance during postembryonic organ formation (Benková and Bielach, 2010). Therefore, reduced PIN diffusion due to plasma membrane compartmentalization might have not only clear functional importance for PIN polarity maintenance, but might also have been key in the evolution of dynamic cell polarity alterations in plants. In plants, lateral diffusion in the plasma membrane appears to be limited by the cytoskeleton and the cell wall components (Feraru *et al.*, 2011; Martiniere *et al.*, 2011). Future work will address whether the non-mobile PIN clusters are eventually associated with the cytoskeleton or/and the cell wall.

Our study illustartes that plant cells have mechanisms to regulate polar PIN exocytosis (presumably by endosomal movement and spatially defined, short range vesicle trafficking), but also evolved a mechanism for spatially defined PIN endocytosis but also evolved a mechanism for spatially defined PIN endocytosis (Paciorek *et al.*, 2005; Robert *et al.*, 2010; Wabnik *et al.*, 2010). Notably, distinct regions for exocytosis and endocytosis to and from the plasma membrane have been reported in animal and plant cells, such as following cytokinesis, in plant root hairs, pollen tubes and in animal neuronal synapses (Boutte *et al.*, 2010; Kidokoro, 2006; Takeda *et al.*, 2008; Zhao *et al.*, 2010). Our findings further extend this view and are suggestive of an evolutionarily conserved mechanism of differentially active zones for exo- and endocytosis that would partially account for polarity maintenance.

Finally, our computer model simulations suggest that the partial loss of one of PIN polarity components can be counteracted by the remaining ones, leading to PIN protein enrichment at its designated position, thereby safeguarding directional auxin transport. We assume that the multi-component nature of the polar targeting mechanism proposed by the model can explain difficulties in genetically interfering with PIN polarity or more generally with cell polarity, which remains a challenge for plant cell and developmentally biology (Grunewald and Friml, 2010). Although this study focused on the apical polar domain, the principles of this model could be applied to any other polar domain that is manifest in plant cells.

3.12 EXPERIMENTAL METHODS

3.12.1 PLANT MATERIAL, GROWTH CONDITIONS AND DRUG TREATMENTS

Plant material: *PIN2::PIN2-GFP(*Xu and Scheres*, 2005)* , *PIN1::PIN1-GFP (*Benková *et al., 2003)* , *PIN2::PIN1-GFP-2;eir1-1 (*Wiśniewska *et al., 2006)*, *PIN2::PIN1-GFP-3 (*Wiśniewska *et al., 2006)*, *35S::GFP-PIP2a (*Cutler *et al., 2000)* and *35S::GFP-LTI6b (*Cutler *et al., 2000)*. Seedlings were grown vertically in Petri dishes on 0.8% agar 0.5x Murashige and Skoog (MS) medium with 1% sucrose (pH 5.9) at 21°C under continuous illumination.

3.12.2 IMMUNOLOCALIZATION

Immunolocalizations ware performed on 5-day-old seedlings by using Intavis in situ pro robot according to the published protocol (Sauer *et al*., 2006). Primary antibody: rabbit anti-PIN2 (Abas *et al*., 2006) 1:2000 and anti-PIN1 (Hein *et al*., 2008) 1:2000. Secondary antibody: Cy3 anti-rabbit (Sigma-Aldrich) 1:600.

3.12.3 QUANTIFICATION OF THE RELATIVE MOBILE FRACTION

Relative mobile fraction of PIN2-GFP was quantified by FRAP. A 100x objective (1.4 NA) was used at a digital zoom setting of 4. Pre-bleaching and post-bleaching imaging was done using a 488-nm beam set at 50% output and 5% transmission. Three scans were made to establish the pre-bleach intensity and then a circular region of interest (ROI) of 5.5 μm^2 was drawn in a median optical section of the fluorescence plasma membrane. 15 iterations of 488nm set at 100% transmission ware used for bleaching. Recovery of the fluorescence was recorded during 131.7 seconds with a delay of 2.5 seconds between frames. Images were 256*256 pixels and were made with a scan speed of 0.493 seconds per frame. We confirmed that the energy of 488 laser used to record post-bleach data had no bleaching effect by recording region unbleached ROI. To assess potential differences of lateral PIN2 diffusion within the apical cell side, we have bleached either 2um diameter in centre or in the periphery of the apical cell side. For FRAP analysis in stele cells (pPIN1:PIN1-GFP), we have used a 40x objective; zoom5; 512x512 images; scan speed 0.986 seconde; 22 scans for a total time of 102s so around 5.96s between each frames; ROI at 2µm diamters;laser set at 21%. All other setting as for the first set of experiments. Obviously, the results cannot be as reliable as with a 100x objective and bleaching was reduced by changing delay between frames. For analysis of the FRAP data to obtain the relative mobile fraction, we first normalised data by using the follow-

ing equation: I_n= [(I_t-I_{min}) / (I_{max}-I_{min})] x 100; where I_n is the normalised intensity, I_t is the intensity at any time t, I_{min} is the minimum post-photobleaching intensity and I_{max} is the mean pre-photobleaching intensity. Non-linear regression was used to model the normalised FRAP data. In this case, a two-phase exponential association equation was used: Y(t) = A + B (1+exp $^{(-K_1)(t)}$) + C (1-exp$^{(-K_2)(t)}$) ; where Y(t) is normalised intensity, A, B, C, K_1 and K_2 are parameters of the curve, and *t* is time. Then, the value of their Y(t=124s) was calculated and used as an approximation of the relative mobile fraction. 17 to 23 cells from at least 4 different 7-day-old seedlings were analyzed. The seedlings were immobilised to prevent focus-shift during scanning by mounting them in 1% low-melting-point agarose cooled down to room temperature. The cover slip was sealed with VALAP (Vaseline:lanolin:paraffin wax).

3.12.4 MICROSCOPY

For confocal laser scanning microscopy, a Leica TCS SP2 AOBS with upright microscope stand and an Olympus fluoview FV10 with inverted microcope stand were used. Semi quantitative confocal imaging was performed and analyse with FV10. Images were processed in Adobe Photoshop CS2 and assembled in Adobe Illustrater CS2 (Adobe Inc.). Fluorescence signal intensity was analyzed with Image J 1.37v (Rasband) and confocal software (Leica). Data were statistically evaluated with Excel 2003 (Microsoft). The STED microscopy setup was essentially as described previously (Hein *et al*., 2008). In short, Venus Fluorescence Protein was excited at 490 nm by a diffraction limited spot which was overlaid with a doughnut shaped STED beam of 590 nm. The STED focal doughnut was created by introducing a polymeric phase plate (RPC Photonics, Rochester, NY) applying imprinting a helical phase ramp of exp(iφ), with 0 < φ < 2π, inon the STED beam. The excitation and STED beams were overlapped by a dichroic mirror and then focused by a 1.3 NA objective lens (PL APO, 63x, glycerol, Leica, Germany). The epi-fluorescence was filtered with a 535/50 bandpass and detected by an avalanche photo diode. Images were recorded with resonant mirror scanning (15 kHz, SC-30; EOPC, Glendale, NY) along the x axis and stage scanning along the y axis (P-733, Physik Instrumente, Karlsruhe, Germany). For variable-angle epifluorescence microscopy (VAEM) observation, 5-days-old Arabidopsis root epidermal cells expressing PIN2-GFP was subjected to vital imaging by using fluorescence microscope (Nikon Eclipse TE2000-E and CFI Apo TIRF 100XH/1.49 numerical aperture objective) equipped with Nikon TIRF2 system. PIN2-GFP was excited with 488 nm Argon laser. In VAEM each frame was exposed for 100 milliseconds. Image was acquired with an Andor iXonEM EMCCD camera.

3.13 COMPUTER MODEL DETAILS

3.13.1 COMPUTER MODEL ASSUMPTIONS

The apical and neighboring lateral sides of root epidermis cell were modeled explicitly. For computational reasons, we represented the plasma membrane as a sequence of discrete membrane fragments each of 1x1 micron size (see Figures 1I, 4A and 6A). Each fragment was associated with either the apical or one of the two lateral cell sides (see Figures 1I, 4A and 6A). The intracellular membranes were approximated by one single endosomal compartment that represented the common intracellular pool of PIN proteins (see Figures 1I, 4A and 6A). The redistribution of PIN proteins between membrane fragments and endosomal compartments was determined by the basis of the PIN turnover rates (k_{exo} and k_{endo}) (see Figures 1I, 4A and 6A, thin blue and red arrows). This basal exo- and endocytosis rates are set to be constant for all cell sides. We considered that PIN proteins display lateral diffusion (D_m) within the plasma membrane (see Figures 1I, 4A and 6A).

The super polar delivery of PIN proteins occurs to a central region within one side of the cell, presumably via endosomal trafficking mechanisms and subsequent spatially defined protein recycling. We modeled this process by assuming an increased rate of PIN delivery (k_{SPEX}) to the center of the polar domain (see Figures 1I, 4A and 6A, thick blue arrow). Additionally, PIN proteins displayed specific distributions within the plasma membrane, namely recruitment into non-mobile plasma membrane clusters (Figure 3). Roughly, 87% of the plasma membrane-associated PIN proteins appeared to be non-mobile (PIN cluster) (f_1). The remaining 13% of PIN proteins (f_2) were considered to diffuse within the plasma membrane. In our model, a non-mobile (f_1) and mobile (f_2) PIN pools are associated with each discrete membrane fragment (Figures 4A and 6A). We consider a steady state exchange mechanism of the PIN material between the non-mobile and mobile pools via diffusion (D_L) (Figures 4A and 6A, black arrows).

As the increased clathrin-dependent PIN endocytosis at the lateral cell sides of epidermal root has been observed (Figure 5), we assumed an enhanced polar/spatially defined PIN endocytosis (k_{PEN}) along the whole lateral cell sides (Figure 6A, thick red arrow). The mathematical representation of the computer model is determined by coupled Ordinary Differential Equations (ODEs) and eight tunable parameters (k_{exo}, k_{endo}, f_1, f_2, D_m, D_L, k_{SPEX}, and k_{PEN}) that were biologically interpretable, and were estimated from experimental data.

All model simulations were performed until a steady-state emerged (on the average time scale of 3h (CPU)). The simulations were done by numerical computations of coupled ODE systems, with an adaptive-size, fifth-order Runge-Kutta method with monitoring of local truncation error to ensure accuracy and adjustment of the step size.

All figures were processed in Adobe Illustrator. Figures 1J, 4B and 6B, 6D-6F, Supplementary Figures 5 and 7 and Supplementary Movies 1-6 are screenshots from model simulations.

3.13.2 MATHEMATICAL DESCRIPTION

The diffusion of PIN proteins between membrane fragments follows Fick's law:

$$\frac{dPIN_{PMDi}}{dt} = \sum_{k \in N_j} \frac{D_m}{L} \cdot (PIN_{PMDk} - PIN_{PMDi}) \quad (1)$$

where a single discrete membrane fragment has exactly two neighbors (N_i=2); k represents the subsequent index of its neighbor; D_m describes the rate of lateral PIN diffusion and L is the length of membrane fragment (L=1). PIN_{PMDi} and PIN_{PMDk} are the mobile PIN pools in the i-th membrane fragment and the k-th neighboring membrane fragment, respectively.

The distribution of PIN proteins in each membrane fragment is governed by the following equations:

$$\frac{dPIN_{PMDi}}{dt} = D_L \cdot (f_2 \cdot PIN_{cluster} - f_1 \cdot PIN_{PMDi}) \quad (2)$$

$$\frac{dPIN_{cluster}}{dt} = D_L \cdot (f_1 \cdot PIN_{PMDi} - f_2 \cdot PIN_{cluster}) \quad (3)$$

where PIN_{PMDi} is the mobile PIN pool in the i-th membrane fragment and $PIN_{cluster}$ describes the non-mobile PIN pool. The parameter D_L defines the rate of PIN exchange between mobile and non-mobile pools of the i-th membrane fragment. f_1 and f_2 are the fractions of mobile and non-mobile PIN proteins in the membrane fragment, respectively.

The recycling of PIN proteins between the i-th discrete membrane fragment and endosomal compartment is calculated by following equations:

$$\frac{dPIN_{PMDi}}{dt} = PIN_{endosome} \cdot (k_{exo} + k_{SPEX}) - PIN_{PMDi} \cdot (k_{endo} + k_{PEN}) \quad (4)$$

$$\frac{dPIN_{endosome}}{dt} = \sum_{i=1}^{M} PIN_{PMDi} \cdot (k_{endo} + k_{PEN}) - PIN_{endosome} \cdot (k_{exo} + k_{SPEX}) \quad (5)$$

where PIN_{PMDi} is the mobile PIN pool in the i-th membrane fragment and $PIN_{endosome}$ represents a pool of PIN proteins in the endosomal compartment. The parameters k_{exo} and k_{endo} describe the basal rates of PIN turnover. M gives the total number of discrete membrane fragments of the plasma membrane. Note that parameter k_{SPEX} determines the rate of a super-polar delivery of PIN proteins at the center of the polar domain. We assumed $k_{SPEX} > 0$ for the j-th membrane fragment associated with the center of the polar domain and $k_{SPEX} = 0$ for any other plasma membrane fragment (Figures 1I, 4A and 6A). Similarly, parameter k_{PEN} determines the enhanced polar PIN endocytosis ($k_{PEN} > 0$) at the whole lateral surfaces of the cell (Figure 6A).

3.13.3 MODEL PARAMETERS

In the model simulations, the parameter values used were estimated from experimental data. From the fluorescent recovery after photobleaching (FRAP) experiments (Figures 2 and 3), the estimated non-mobile and mobile PIN fractions were $f_1 \sim 0.87$ and $f_2 \sim 0.13$, respectively. The parameter D_L was set to 1 $\mu m^2\ s^{-1}$ in all simulations. The basal PIN turnover rates were estimated for ~30 min half-time of PIN turnover and were $k_{exo} = k_{endo} = \ln(2)/T_{1/2} \sim 0.0005\ s^{-1}$. The vesicle delivery for the super-polar PIN delivery was of the order of ~20 s (Figures 1 and 6D). Therefore, we estimated the $k_{SPEX} \sim 0.04\ s^{-1}$. Similarly, as the experimental estimates for PIN retrieval from the plasma membrane was ~ 50 s (Figure 5), we approximated the value of k_{PEN} to ~ $0.02\ s^{-1}$. Parameter D_m was harder to estimate from experimental data, but a half-time recovery of the mobile PIN pool was of the order of ~ 10 s (Figure 2), which allowed us to approximate D_m to ~$0.1\ \mu m^2\ s^{-1}$.

In the model simulations presented in Figures 1J, parameter k_{PEN} was set to $0\ s^{-1}$ and equations (2) and (3) were neglected. For simulations in the Figures 4B, the parameter k_{PEN} was $0\ s^{-1}$. To simulate filipin treatment (Figure 3G and 3H) the gradual linear decrease of non-mobile PIN fraction (f_1) from 0.87 to 0.5 was introduced in simulations presented in Figures 6F. This resulted in change of mobile PIN fraction (f_2) from 0.13 to 0.5. In simulations of Figure 6E, parameter k_{SPEX} was set to $0.00001\ s^{-1}$. For model simulations presented in Supplementary Figure 5 the parameter setting as in Figure 4 with following modifications: (A) $k_{SPEX} \sim 0.4\ s^{-1}$ (C) $k_{SPEX} \sim 4\ s^{-1}$, (E) $D_m = 0.001\ \mu m^2\ s^{-1}$, (G) $D_m = 0.01\ \mu m^2\ s^{-1}$, (I) $k_{SPEX} \sim 0.4\ s^{-1}$, $D_m = 0.01\ \mu m^2\ s^{-1}$. For model simulations presented in Supplementary Figure 7 parameters were as in Figure 6B with the following changes: (A) $k_{SPEX} \sim 0.4\ s^{-1}$, (C) $k_{PEN} = 0.2\ s^{-1}$, (E) $D_m = 0.01\ \mu m^2\ s^{-1}$, (G) $D_m = 1\ \mu m^2\ s^{-1}$.

3.14 SUPPLEMENTARY FIGURES

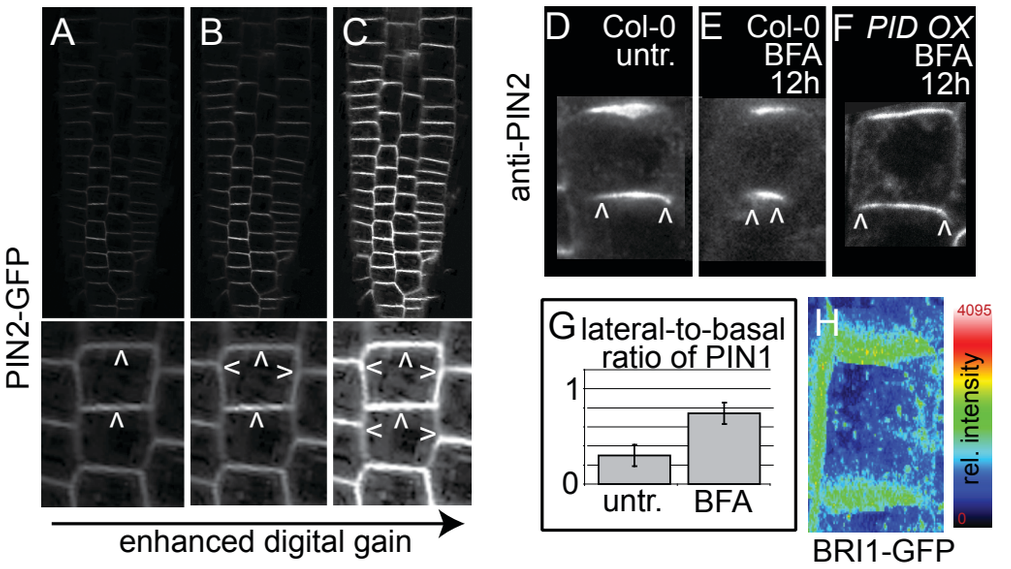

Supplementary Figure 1 Preferentially apical PIN2-GFP localization in root epidermal cells

(A-C) Gradual digital gain enhancement of PIN2-GFP signal. Arrowhead depict preferential PIN2-GFP localization. **(D-F)** Anti-PIN1 immunolocalisations in untreated (D) and BFA 12 hours treated (E-F) root stele cells. PIN targeting to a defined region at the apical side of the cell can be induced by prolonged treatment with the ARF-GEF subclass inhibitor Brefeldin A (BFA) (E). Notably, BFA leads to endosomal accumulations, so called BFA compartments, close to the plasma membrane (Figure 1G), eventually inducing super-polar PIN deposition by short range PIN exocytosis from the accumulating endosome to the adjacent region of the plasma membrane. Intriguingly, PID overexpression reduces PIN accumulation in BFA compartments and suppresses BFA-induced super apical PIN targeting (F). These findings are in agreement with our hypothesis that directional endosomal trafficking is important for spatially defined polar PIN targeting. In summary, these results are indicative of a polar deposition of PIN proteins by directional endosomal movement and positioning. **(G)** Lateral-to-basal ratio of anti-PIN1 staining in root stele cells in untreated (left) and BFA [50 µM, 1h] (right) treated seedlings (n=20 cells), indicating asymmetric PIN1 distribution (see also Figure 1H). **(H)** 3D xyz-projection (15 x 1-µm sections) of a epidermal cell expressing BRI1:BRI1-GFP (ca 20° view).

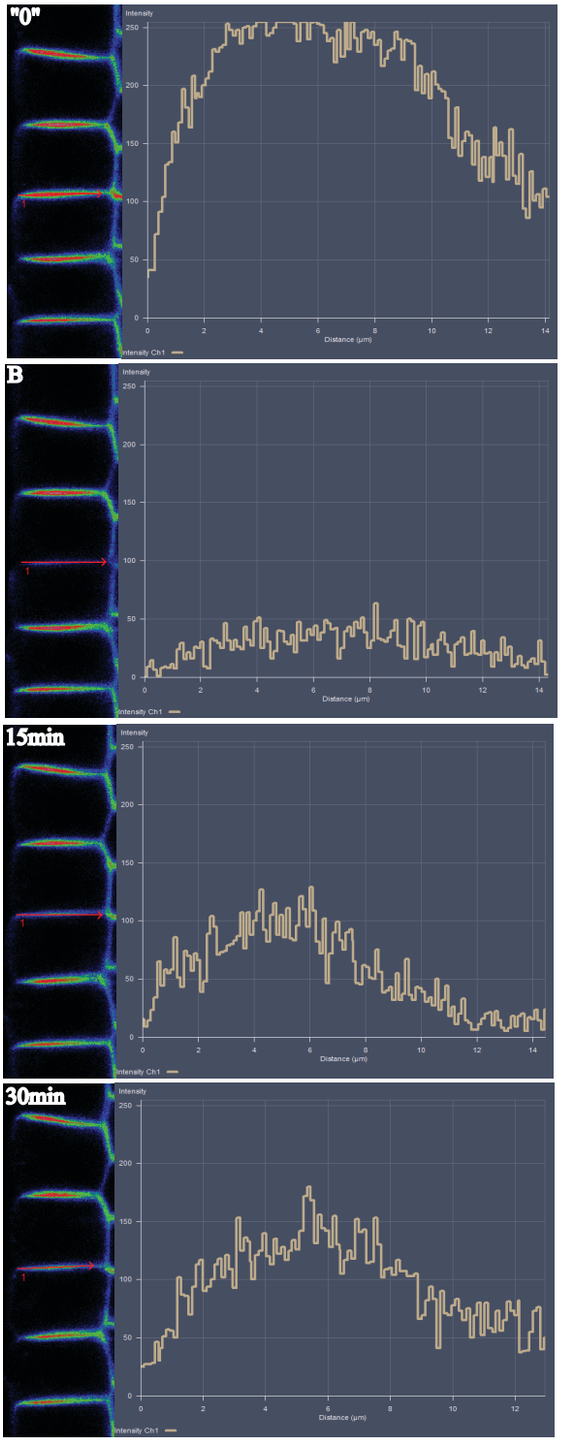

Supplementary Figure 2 Super polar PIN delivery

FRAP analysis of epidermal PIN2-GFP (median optical sections). Fluorescent profile analysis along the indicated red arrow indicates super polar PIN2 localisation and recovery after photo bleaching in the apical cell side. “0” depicts the pre bleached image; B shows post bleach; subsequent images illustrate recovery after 15min and 30min after photo bleaching.

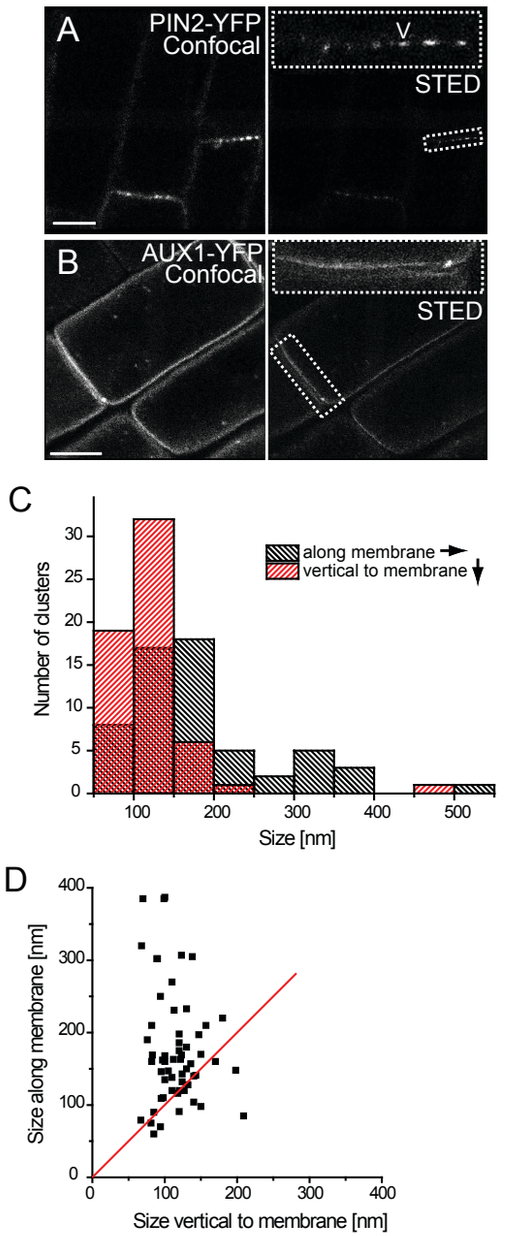

Supplementary Figure 3 STED microscopy size analysis of PIN2-Venus clusters

(A, B) Confocal (left panels) STED (right panels) microscopy visualizes PIN2-YFP (A), but not AUX1-YFP (B) in defined membrane clusters. **(C, D)** STED microscopy images of PIN2-YFP (24 in total) were recorded with a resolution of <70 nm. Clusters which were in focus and separately resolved were analyzed using ImageJ. A line summing up 3 pixels was drawn along and vertical to the plasma membrane to determine the cluster size (full width half maximum). (C) Histogram of the cluster size along and vertical to the plasma membrane. (D) Correlation of cluster size measured vertical and horizontal to the plasma membrane.

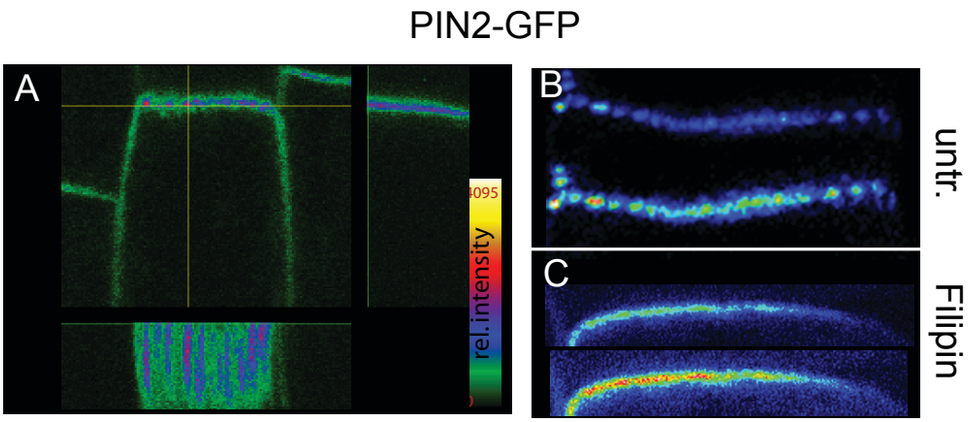

Supplementary Figure 4 PIN2 proteins reside in non-mobile membrane clusters

(A) Kymographic projection along the indicated yellow lines of PIN2-GFP time lapse (10s per frame/60 frames) imaging. **(B, C)** Untreated (B) and filipin (100µM; 2h) (C) treated PIN2-GFP. upper and lower images display the same sample with different gain settings.

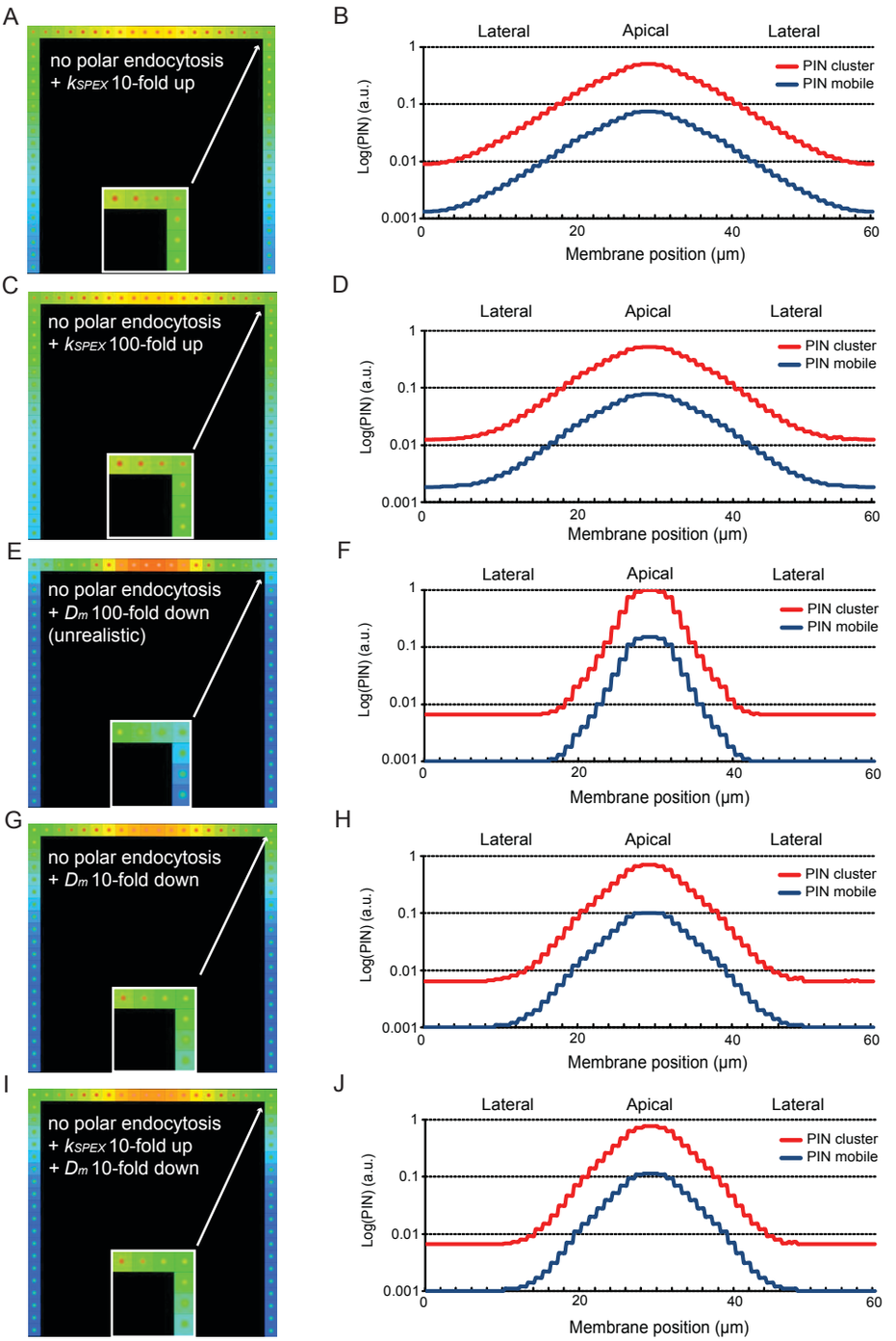

Supplementary Figure 5 Predictions of the model with no polar endocytosis (Figure 4) for the wide range of PIN diffusion and exocytosis rates.

(A-D) Simulations of the model presented in Figure 4 for up to a 100-fold increase of the rate of super-polar delivery of PIN2 proteins (k_{SPEX}) were similar to those shown in Figure 4B and 4C. Even significant boost of polar PIN2 delivery (two orders of magnitude) did not result in the realistic PIN polarization pattern (Figure 1A-1C), such as that demonstrated in Figure 6B and 6C. The pronounced lateral PIN2 signal was observed at peripheries of the polar domain and on lateral sides of the cell (B,D). **(E-F)** Predictions of the model for the severely reduced lateral diffusion of PIN2 proteins (a 100-fold decrease of D_m). The dramatic

and unrealistic reduction of PIN2 lateral diffusion (D_m to 0.001 $\mu m^2 s^{-1}$) had led to the sharp PIN gradient in the plasma membrane that was present in the polar domain. Notably, we reported relatively high PIN2 signal in the lateral membranes (F) as compared to the predictions of the model with polar PIN endocytosis (Figure 6B and 6C). **(G, H)** Similarly to simulations (A-D) and Figure 4B and 4c, model simulations for D_m = 0.01 μm^2 s-1 and no polar PIN endocytosis (G) predict the leakage of PIN2 proteins to the whole lateral membranes of the cell (G) and broad PIN2 distribution gradient (H). **(I, J)** Simulations of both reduced lateral diffusion (D_m = 0.01 $\mu m^2 s^{-1}$) and pronounced super polar PIN2 exocytosis (k_{SPEX}=0.4s^{-1}) did not produce a realistic PIN2 polar distribution (I, J) in comparison to the model simulations with spatially defined PIN2 endocytosis (Figure 6B and 6C).

Color coding scheme for simulations is as in Figure 1K.

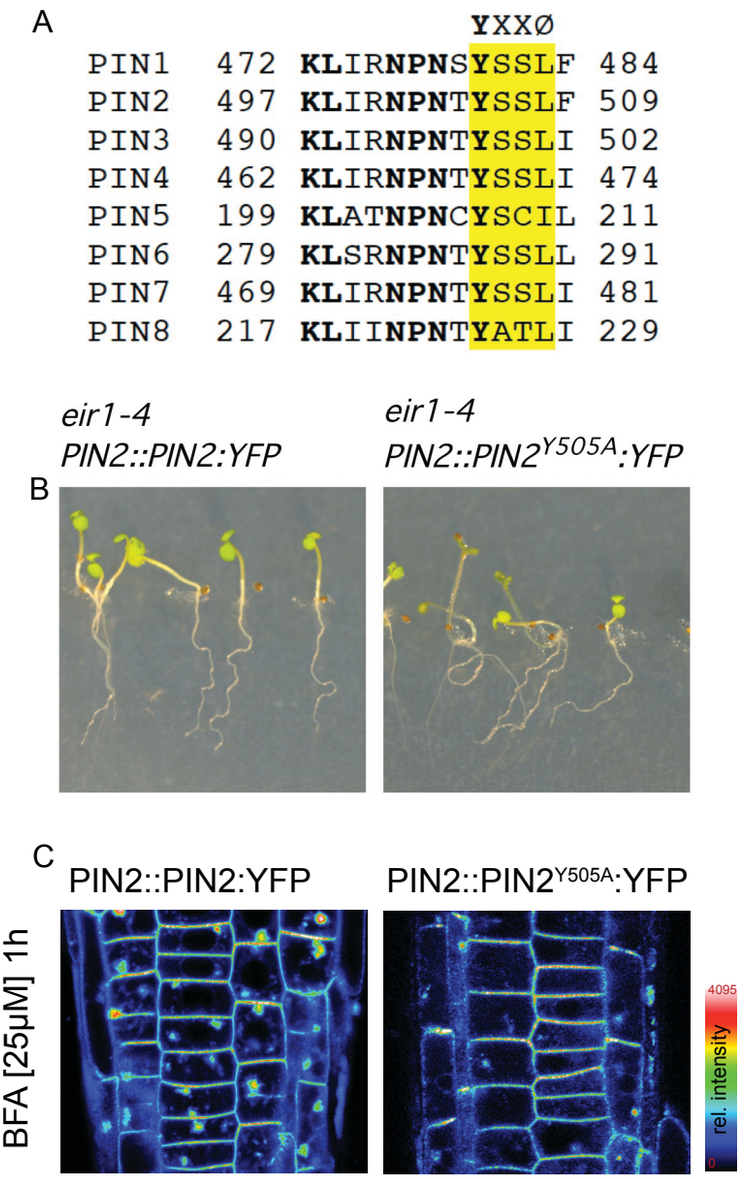

Supplementary Figure 6 Conserved tyrosin motif in PIN2

(A) Conserved, putative tyrosin motif in PIN1-PIN8. **(B)** PIN2:PIN2-YFP but not tyrosin motif mutated PIN2:PIN2Y505A-YFP rescues pin2 (eir1-4) mutant agravitropic phenotype. **(C)** PIN2:PIN2Y505A-YFP expressing seedlings show reduced PIN2 accumulation in BFA compartments (25µM; 1h) compared to PIN2:PIN2-YFP, indicating reduced PIN2 internalization.

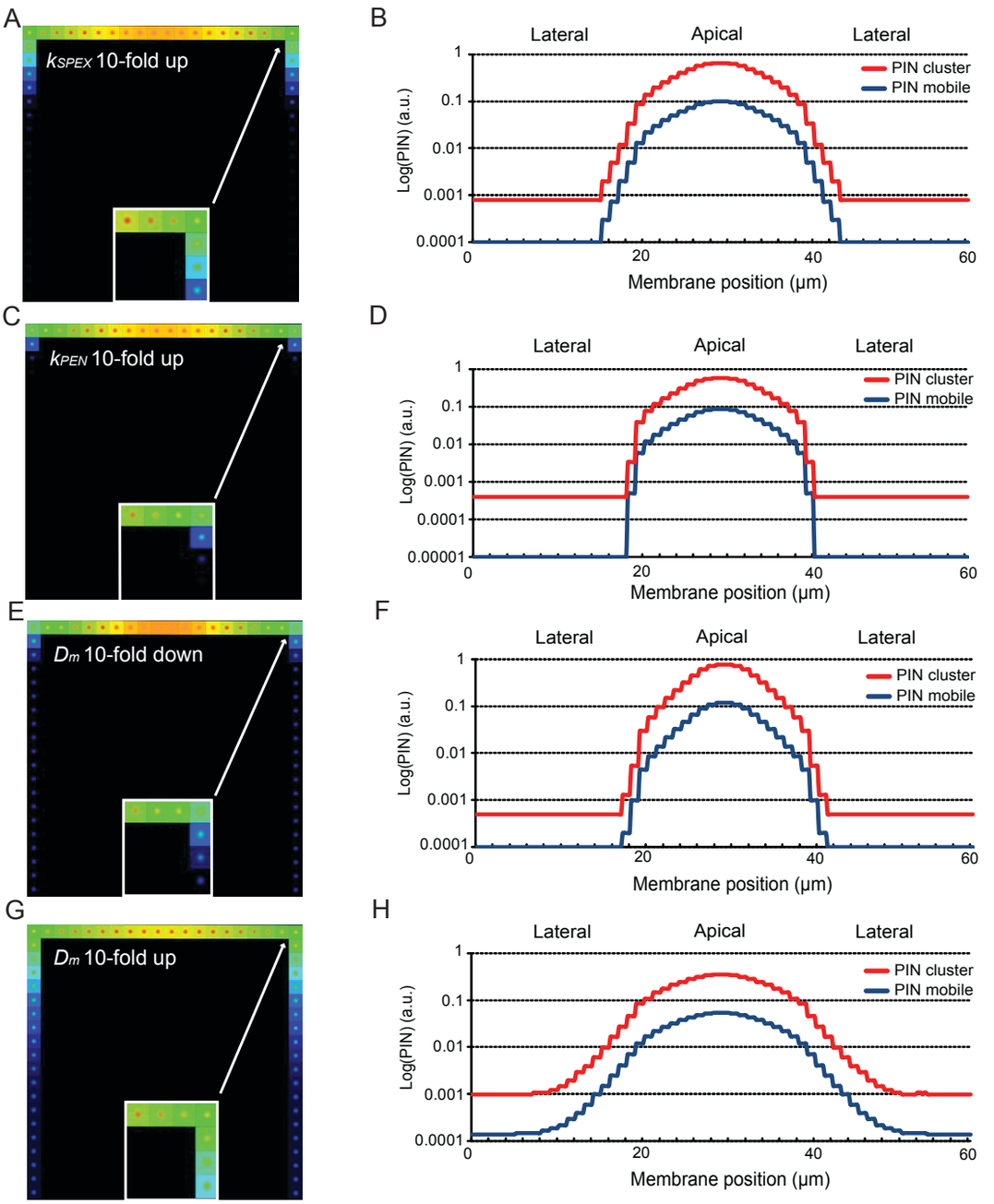

Supplementary Figure 7 Parameter sensitivity of the combined model (Figure 6A).

(A, B) Simulations of the model presented in Figure 6 for up to a 10-fold increase of the rate of super-polar delivery of PIN2 proteins (k_{SPEX}=0.4s^{-1}) were similar to those shown in Figure 6B and 6C indicating that model predictions are robust and do not depend on the choice of k_{SPEX}. **(C, D)** The higher rate of polar PIN2 endocytosis (k_{SPEX}=0.2s^{-1})(C) led to the sharper PIN2 distribution gradient (d) in the plasma membrane than that in the control simulations (Figure 6B and 6C). This highlights the importance of polar PIN2 endocytosis for the maintenance of PIN2 polar domains in the cell. **(E-H)** Model simulations predicts the relation between the rate of lateral PIN2 diffusion (D_m) and the steepness of the PIN2 gradient in the plasma membrane (F, H). If D_m was low (0.01 μm^2 s^{-1})(E) the steep PIN2 distributions were observed (F). Accordingly the high D_m (1 μm^2 s^{-1})(G) led to more broad PIN2 distributions (H), although, the qualitative PIN polarization profile was maintained, highlighting the model robustness for at least, one order of magnitude changes of lateral PIN2 diffusion rates.

Color coding scheme for simulations is as in Figure 1K.

3.15 SUPPLEMENTARY MOVIES

Supplementary Movie 1

The file contains Supplementary Movie 1 displaying the simulation of Figure 1J (super polar exocytosis). Color coding scheme used in the model simulations is as presented in Figure 1K.

Supplementary Movie 2

The file contains Supplementary Movie 2 displaying the simulation of Figure 4B (super polar exocytosis and PIN clusters). Color coding scheme used in the model simulations is as presented in Figure 1K.

Supplementary Movie 3

The file contains Supplementary Movie 3 displaying the simulation of Figure 6B (complete model). Color coding scheme used in the model simulations is as presented in Figure 1K.

Supplementary Movie 4

The file contains Supplementary Movie 4 displaying the simulation of Figure 6D (extended domain for polar PIN delivery). Color coding scheme used in the model simulations is as presented in Figure 1K.

Supplementary Movie 5

The file contains Supplementary Movie 5 showing the simulation of Figure 6E (no polar exocytosis). Color coding scheme used in the model simulations is as presented in Figure 1K.

Supplementary Movie 6

The file contains Supplementary Movie 6 showing the simulation of Figure 6F (the high mobility of PIN proteins). Color coding scheme used in the model simulations is as presented in Figure 1K.

ACKNOWLEGMENTS

We thank Ben Scheres and John Cuttler for sharing published material; Martine De Cock for assistance with the manuscript; and Markus Grebe for fruitful discussions. This work was supported by grants from the Research Foundation-Flanders (Odysseus to J.F. and project no. 3G006507 to W.G.), the EMBO Young Investigator Program (to J.F.) and the Vienna Science and Technology Fund (to J.K.-V.).

Chapter 4

Prototype cell-to-cell auxin transport mechanism by intracellular auxin compartmentization

"To produce a really good biological theory one must try to see through the clutter produced by evolution to the basic mechanisms lying beneath them, realizing that they are likely to be overlaid by other, secondary mechanisms. What seems to physicists to be a hopelessly complicated process may have been what nature found simplest, because nature could only build on what was already there."

—Francis Crick

PROTOTYPE CELL-TO-CELL AUXIN TRANSPORT MECHANISM BY INTRACELLULAR AUXIN COMPARTMENTIZATION

Krzysztof Wabnik[1,2,4,5], Jürgen Kleine-Vehn[1,2,3,5], Willy Govaerts[4] and Jiří Friml[1,2,5]

Contribution: Computation modeling work has been handled by K. Wabnik

Trends in Plant Science, 2011, in press

[1]Department of Plant Systems Biology, VIB, 9052 Gent, Belgium
[2]Department of Plant Biotechnology and Genetics, Ghent University, 9052 Gent, Belgium
[3]Department of Applied Genetics and Cell Biology, University of Applied Life Sciences and Natural Resources (BOKU), 1190 Vienna, Austria
[4]Department of Applied Mathematics and Computer Science, Ghent University, 9000 Gent, Belgium
[5]Department of Functional Genomics and Proteomics, Faculty of Science, and Central European Institute of Technology (CEITEC), Masaryk University, CZ-62500 Brno, Czech Republic
[5]These authors contributed equally to this work

ABSTRACT

Carrier-dependent, intercellular auxin transport is central to the developmental patterning of higher plants (tracheophytes). The evolution of this polar auxin transport might be linked to the translocation of some PIN auxin efflux carriers from their presumably ancestral localization at the endoplasmic reticulum (ER) to the polar domains at the plasma membrane. Here we propose an eventually ancient mechanism of intercellular auxin distribution by ER-localized auxin transporters involving intracellular auxin retention and switch-like release from the ER. The proposed model integrates feed-back circuits utilizing the conserved nuclear auxin signaling for the regulation of PIN transcription and a hypothetical ER-based signaling for the regulation of PIN-dependent transport activity at the ER. Computer simulations of the model revealed its plausibility for generating auxin channels and localized auxin maxima highlighting the possibility of this alternative mechanism for polar auxin transport.

4.1 AUXIN - AN ANCIENT SIGNALING MOLECULE IN LAND PLANT EVOLUTION

Plants evolved flexible developmental mechanisms to reorganize their comprehensive body plan in response to light, gravity and other environmental stimuli (Ding *et al.,* 2011; Friml *et al.,* 2002b; Kleine-Vehn *et al.,* 2010; Leyser, 2006). These developmental mechanisms are under the control of phytohormonal crosstalk. The phytohormone auxin plays an essential role in multiple developmental and physiological processes during the entire life cycle of plants.

Auxin signaling plays outstanding and evolutionarily conserved roles in the development of plant species (Christenson, 2000; Cooke *et al.,* 2002; Decker *et al.,* 2006; Fujita *et al.,* 2008; Hayashi *et al.,* 2008; Jenkins *et al.,* 1986; Johri and Desai, 1973; Lehnert and Bopp, 1983; Nyman and Cutter, 1981; Sakakibara *et al.,* 2003; Schumaker and Dietrich, 1998). Auxin coordinates plant development through transcriptional responses that are mediated by the evolutionarily conserved nuclear TIR1/AFB-dependent pathway (Chapman and Estelle, 2009; Lau *et al.,* 2009; Prigge *et al.,* 2010; Tromas *et al.,* 2010). This well-characterized TIR1/AFB-dependent mechanism presumably evolved > 500 million years ago in green algal lineages (Lau *et al.,* 2009). The auxin-induced gene expression is mediated by a family of auxin-responsive transcription factors, the auxin response factors (ARFs) (Gray *et al.,* 2001) and members of the auxin/indole-3-acetic acid (Aux/IAA) protein family that repress the ARF-dependent gene expression (Tan *et al.,* 2007). Auxin binds to the TIR1 subunit of the TIR1/AFB ubiquitin ligase to de-repress expression of auxin-responsive genes by ubiquitin-based targeting of Aux/IAAs for proteasome-dependent degradation (Dharmasiri and Estelle, 2004).

The auxin-binding protein 1 (ABP1) is another auxin receptor, encoded by a single-copy gene that is present in ancestral algal genomes (Tromas *et al.,* 2010), but its role in downstream auxin signaling in plants and its possibly conserved function in various plant species are poorly understood (Tromas *et al.,* 2010). ABP1 localizes preferentially to the ER and the outer side of the plasma membrane (cell wall) (Napier, 2002) and ABP1-dependent signaling is required for cell expansion/proliferation rates (Chen *et al.,* 2001; Jones *et al.,* 1998; Xu *et al.,* 2010), gene expression (Tromas *et al.,* 2010) and the regulation of clathrin-dependent endocytosis (Robert *et al.,* 2010).

4.2 POLAR AUXIN TRANSPORT

Among the plant hormones, auxin is unique because of its particular, polar distribution mechanism. It is asymmetrically distributed within tissues (auxin gradients) as a consequence of its directional intercellular transport and local biosynthesis (Benková *et al.,*

2003; Friml *et al.,* 2002a; Ikeda *et al.,* 2009; Reinhardt *et al.,* 2003; Sabatini *et al.,* 1999; Stepanova *et al.,* 2008). The directionality of cell-to-cell polar auxin transport correlates with and largely depends on the subcellular localization of PIN-formed (PIN) auxin efflux carriers at the plasma membrane (Petrášek *et al.,* 2006; Wiśniewska *et al.,* 2006). Additionally, the intracellular auxin transport is mediated by non-polar PGP/MDR/ABCB efflux carriers (Bandyopadhyay *et al.,* 2007; Geisler *et al.,* 2005; Galvan-Ampudia and Offringa, 2007) and the AUX/LAX family of auxin influx carriers (Bennett *et al.,* 1996; Marchant *et al.,* 1999; Swarup *et al.,* 2008; Swarup *et al.,* 2004). The PIN-dependent auxin flux within tissues plays a decisive role in almost every aspect of plant development, including embryogenesis (Friml *et al.,* 2003), *de novo* organ formation (Braybrook and Kuhlemeier, 2010; Heisler *et al.,* 2005; Reinhardt *et al.,* 2003) and tropism (Abas *et al.,* 2006; Ding *et al.,* 2011; Friml *et al.,* 2002b; Kleine-Vehn *et al.,* 2010).

4.3 PIN PROTEINS – EVOLUTIONARILY INSIGHTS

PIN proteins are crucial for the proper coordination of the cellular auxin homeostasis (Grunewald and Friml, 2010). The PIN protein family of *Arabidopsis thaliana* consists of eight members and can be classified in two major groups based on the sequence similarity, subcellular localization and expression patterns (Friml and Jones, 2010; Paponov *et al.,* 2005; Zažímolová *et al.,* 2010). The first group consists of PIN1, PIN2 PIN3, PIN4 and PIN7 proteins that contain a long, central hydrophilic loop, show similar expression domains and preferentially localize to the plasma membrane. The second group includes PIN5, PIN6 and PIN8 that, compared to the PIN1-type proteins, are characterized by a short hydrophilic loop (PIN5-like genes). Intriguingly, the PIN5-type proteins do not localize to the plasma membrane, but instead to the endoplasmic reticulum (ER), where they likely mediate the import of auxin into the ER lumen and largely contribute to the regulation of the cellular auxin homeostasis (Mravec *et al.,* 2009).

The moss *Physcomitrella patens* is a prominent comparative model to study the molecular evolution of land plants. Its genome contains the sequences of four PIN-like genes (designated PpPINA, PpPINB, PpPINC and PpPIND) with certain similarities to the PIN5-type genes (Mravec *et al.,* 2009). Additionally, intron sequences of these genes suggest the possibility of horizontal transfer of the PpPIND genomic sequence from monocots (Křeček *et al*., 2009; Mravec *et al*., 2009). Like the PIN5 protein, the isoform of PpPINA protein localizes to the ER when expressed in tobacco (*Nicotiana tabacum*) Bright Yellow-2 (BY-2) cells (Mravec *et al.,* 2009). Despite this, the localization and function of PIN5-like proteins in moss are yet to be experimentally demonstrated, based on this PpPINA localization in BY-2 cells, we hypothesize that the evolution of PIN auxin carriers in higher plants might involve their translocation from the original local-

ization at the ER to the polar domains at the plasma membrane.

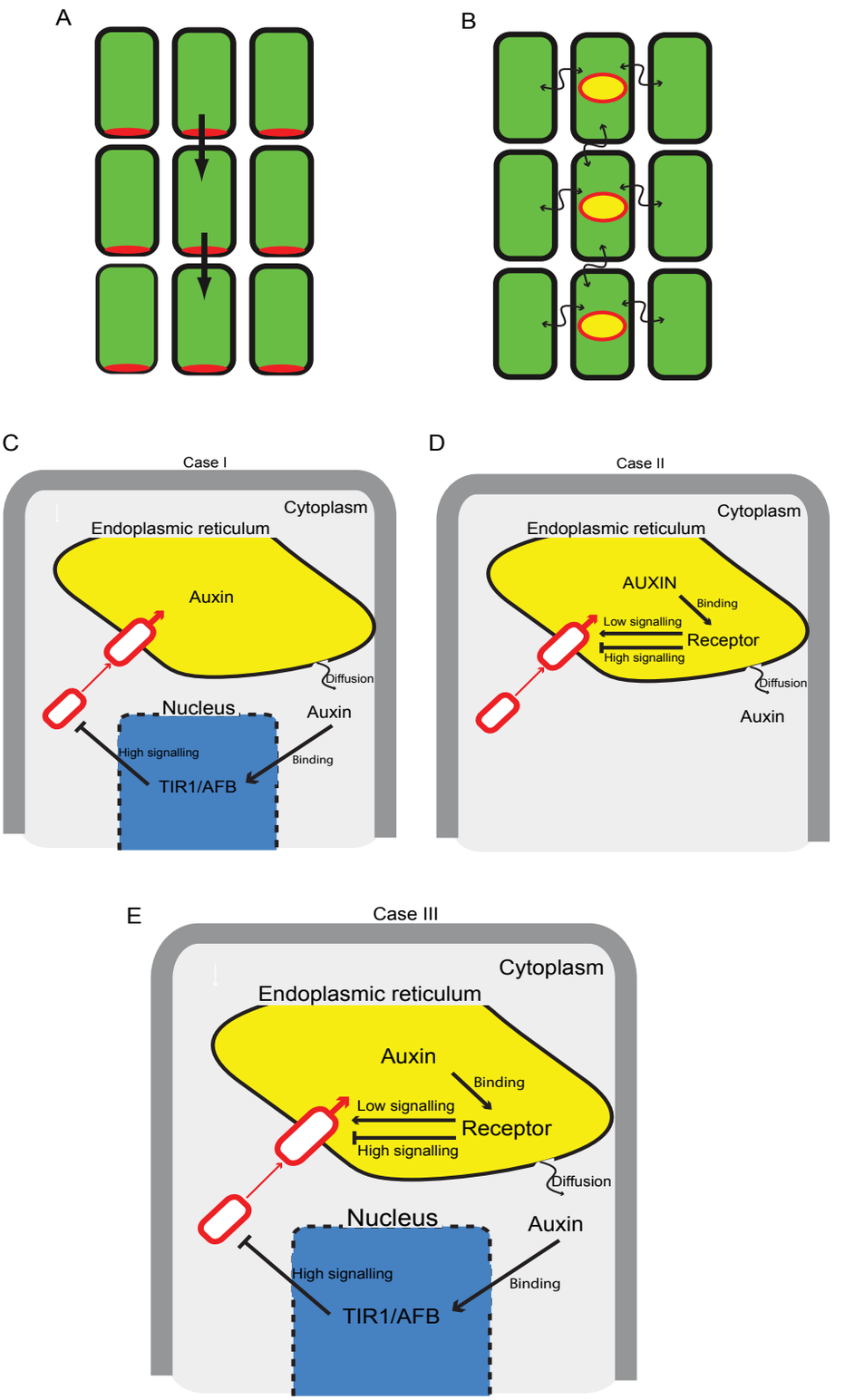

Figure 1 Insights in prototype for auxin transport mechanism.

(**A**) Schematics of PIN-dependent polar auxin transport in higher plants. PIN proteins preferentially localize to the specific polar plasma membrane domain. The directionality of cell-to-cell auxin transport (black arrows) within tissues is given by the preferential PIN polarization (in red). (**B**) Hypothetical auxin

transport mechanism in moss by carrier-dependent auxin storage in the ER. Auxin presumably accumulates in the ER lumen (yellow) of the PpPINA/PIN5-type-producing cell (red) that becomes the new source of auxin. The rapid release of auxin from the ER reservoir to the cytoplasmic pool enhanced non-polar intercellular auxin transport (thin black arrows). (**C**-**E**) The three plausible scenarios for auxin feedback on the PpPINA/PIN5-type protein activity at the ER (red). (**C**) TIR-dependent repression of PpPINA/PIN5-type transcription (thick black arrows) in the nucleus (Case I). (**D**) Receptor-mediated auxin signaling pathways (thick black arrows) for the regulation of the PpPINA/PIN5-type protein abundance/activity at the ER (Case II). (**E**) Model simulation that considers a combination of Case I (**C**) and Case II (**D**) (Case III). The ER compartment is shown in yellow and the cell nucleus in green. The wavy arrow depicts auxin diffusion.

4.4 NOVEL CONCEPT FOR ANCIENT CELL-TO-CELL AUXIN TRANSPORT

To address this possible prototype for PIN-dependent auxin transport mechanism we asked if and how PIN5-type, ER-localized auxin carriers could contribute to the auxin transport between cells in evolutionarily ancient organisms, such as mosses.

Although auxin transport has been suggested to contribute to sporophyte and gametophore development, apical dominance and axis elongation in moss (Christenson, 2000; Fujita and Hasebe, 2009; Fujita *et al.,* 2008; Jenkins *et al.,* 1986; Lehnert and Bopp, 1983; Nyman and Cutter, 1981), the involvement of the polar auxin transport in the development of *P. patens* still remains the subject of an open debate (Harrison *et al.,* 2009). In various moss species auxin appears to move between cells via diffusion in *Phaeoceros personii*, via apolar facilitated diffusion in *Pellia epiphylla*, and via polar auxin transport in the moss *Polytrichum ohioense* (Poli *et al*., 2003). Hence, the carrier-dependent mechanisms for the cell-to-cell auxin transport in early land plants remains an open question.

By assuming that the function of the PIN5-like proteins at the ER (Friml and Jones , 2010) might control the intracellular auxin availability for the cell-to-cell transport (Figure 1A and 1B), we tested whether these intracellular auxin carriers (Mravec *et al*., 2009), such as the PpPINA/PIN5-type proteins, could contribute to the distribution of auxin in a given tissue context. For that we hypothesized that the auxin content of cells expressing PpPINA/PIN5-type proteins increase due to subcellular compartmentalization. The ER auxin trapping and its further release from the ER could represent two subsequent states of auxin transport mechanism, auxin loading (source state) and auxin release (sink state), respectively. This non-trivial auxin transport dynamics could be realized by the feedback mechanisms similar to those regulating action of plasma membrane (PM) localized PIN proteins in higher plants (Leyser, 2006; Grunewald and Friml, 2010). This hypothetical, feedback-assisted transport mechanism (Figure 1B)

could be conceptualized as ancient and/or alternative machinery for the prominent PM carrier-based polar auxin transport in higher plants (Figure 1A). We explicitly inferred an feedback mechanism that negatively and/or positively regulates the activity of the Pp-PINA/PIN5-type proteins by auxin (Mravec *et al*., 2009). This signaling could occur via either conserved nuclear SCF/TIR1-dependent pathways (Chapman and Estelle, 2009) (Figure 1C), an hypothetical signaling from ER-resident auxin receptor (Tromas *et al*., 2009; Friml and Jones, 2010) (Figure 1D), or the combination of both (Figure 1E). To test the feasibility of our hypothesis, we used a computational approach to investigate whether auxin gradients could emerge from carrier-dependent intracellular auxin retention in the ER, controlled release of auxin into the cytosol and subsequent non-polar, intercellular auxin transport.

4.5 MODEL ASSUMPTIONS

Several general assumptions were made in our computer model, follow:
(**i**) Cell-to-cell auxin transport could occur by the activity of non-polar PGP/MDR/ABCB auxin efflux and AUX/LAX auxin influx carriers (Bandyopadhyay et al., 2007; Geisler et al., 2005; Bennett et al., 1996; Rensing *et al*., 2008) which are evolutionarily older than plasma membrane-associated PIN proteins (Rensing *et al*., 2008; Zažímolová *et al.,* 2010) as well as by passive diffusion and through the open cytoplasm-cytoplasm connections (plasmodesmata) (Rutschow *et al*., 2011). Carrier function, localisation and distribution have not been systematically addressed in mosses and therefore should be considered as hypothetical assumptions. Due to the lack of experimental data and for simplicity, we modeled the non-directional AUX1/LAX and PGP/MDR/ABCB-dependent auxin transport at the plasma membrane and passive auxin diffusion as one parameter that reflects the combined action of these processes;
(**ii**) The intracellular space is divided into two discrete subcellular compartments, the cytoplasm and ER and auxin can move between these compartments;
(**iii**) Due to the neutral pH in the cytoplasm (Supplementary Figure 1), deprotonated auxin (IAA-) would be transported actively to the internal “ER storage” (Mravec *et al*., 2009) by the PpPINA/PIN5 proteins (Figure 1C-1E), although a small auxin diffusion into the ER was considered as well;
(**iv**) Our model also considers a transport parameter that accounts for auxin transport from the ER lumen to the cytoplasm (Supplementary Figure 1; Figure 1C-1E). Because auxin flux mechanisms from the ER lumen to the cytosol are currently not known we hypothesized that such mechanism may rely on a carrier-dependent mechanism and/or on a diffusion-based transport (Supplementary Figure 1);
(**v**) Next, we considered three biologically plausible scenarios (Cases I-III) for the auxin

feedback on the presumed PpPINA/PIN5-type protein abundance or activity (Figure 1C and 1D).

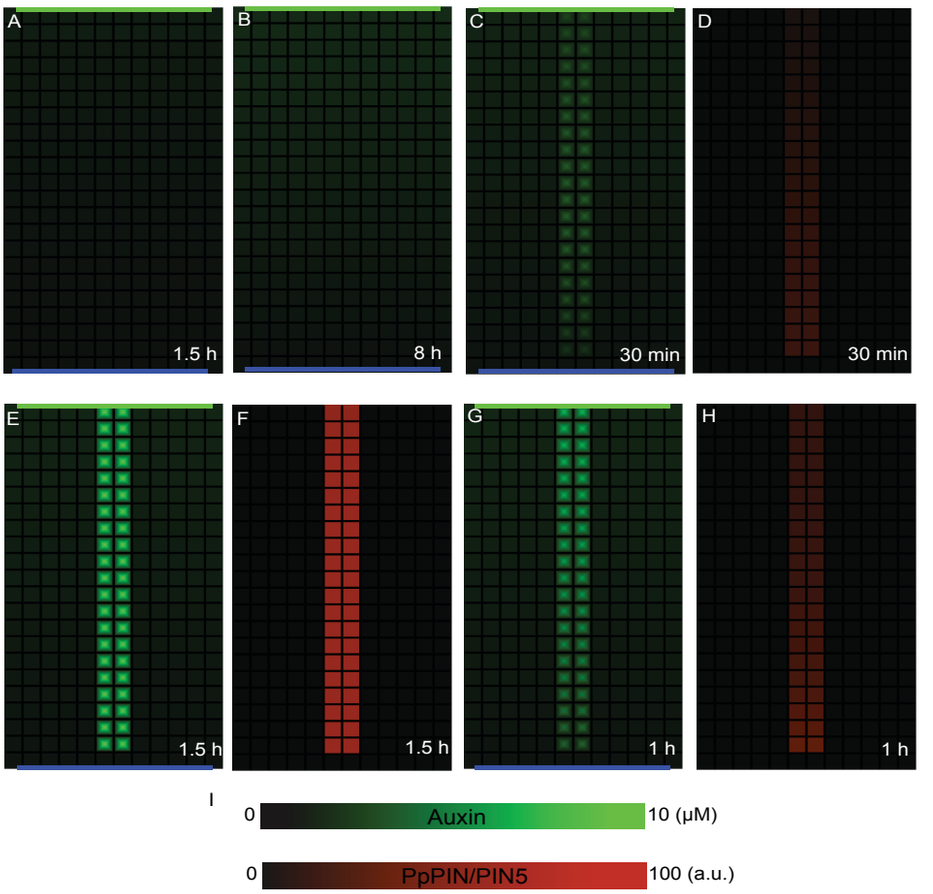

Figure 2 Progressive canalization of auxin flow by carrier-dependent ER retention mechanism

(A, B) Slow, purely diffusion-based, auxin distribution from an auxin source (green) to an auxin sink (blue) simulated on the rectangular cell grids after 1.5 h (A) and 8 h (B) (Supplementary Movie 1). **(C, D)** Computer simulations of auxin canalization for the model variant with SCF/TIR1-dependent downregulation of the PpPINA/PIN5-type activity (Figure 1C; Case I) (Supplementary Movie 2). Two layers of PpPINA/PIN5-type-producing cells were added to the grid. Auxin distribution is indicated in green (C) and PIN proteins in red (D) after 30 minutes of simulation. **(E, F)** Discrete auxin channels with high auxin concentrations predicted by simulations of the model variant that incorporates solely a receptor-based auxin signaling for the PpPINA/PIN5-type protein abundance at the ER (Figure 1D; Case II) (Supplementary Movie 3). Auxin distribution is indicated in green (E) and PIN proteins in red (F) after 90 minutes of simulation. **(G, H)** The integration of two feedback signaling pathways for the regulation of PpPINA/PIN5-type protein activity in the model (Figure 1E; Case III) (Supplementary Movie 4) predicted the accelerated progression of conductive auxin channels between the auxin source (green) and the auxin sink (blue) within 1 hour. Similarly to (E and F), the auxin concentrations in the PpPINA/PIN5-type-producing

cells (H) were elevated, both in the ER and cytoplasm (G). **(I)** Color mapping for auxin and PpPINA/PIN5-type levels in the model simulations. In all simulations, central color intensity displays mean auxin level in the ER and peripheral intensity shows mean cytosolic auxin concentration.

Case I is when auxin at high concentrations in the cytoplasm down regulate the PpPINA/PIN5-type activity (Mravec *et al*., 2009). That could occur via the conserved SCF/TIR1-dependent signaling pathway at the level of transcriptional regulation that is known to control PM PIN expression in higher plants (Kepinski and Leyser, 2005; Dharmasiri *et al*., 2005) (Figure 1C). Case II is when, at low and high concentrations, the internally stored (ER) auxin promotes and inhibits the activity or abundance of the PpPIN/PIN5-type proteins at the ER membrane, respectively. This might be realized by ABP1-dependent signaling in the ER (Figure 1D) (Friml and Jones, 2010), since majority of ABP1 proteins are present in the ER (Napier, 2002; Tromas *et al*., 2010). Case III was where both mechanisms are combined (Case I and Case II) (Figure 1E).

4.6 CELL-TO-CELL TRANSPORT BY PIN-DEPENDENT INTRACELLULAR AUXIN RETENTION AND RELEASE

The PIN1-type-dependent polar auxin transport is crucial for patterning of vascular systems in higher plants (Berleth and Sachs, 2001; Rolland-Lagan and Prusinkiewicz, 2005; Sauer *et al.,* 2006; Scarpella *et al.,* 2006). To assess whether the proposed prototype model for auxin transport in ancient organisms, such as *P. patens*, might explain the directional auxin movement within tissues, we used dynamic computer simulations on rectangular cell grids with an auxin source and a distal auxin sink (Figure 2). We found that model considering the ubiquitous PpPINA/PIN5-type activity in the tissues did not predict well defined and spatially-restricted auxin transport canals but they were broad and less defined (Supplementary Figure 2; Case III). This hints at the possibility of cell-type-specific regulators of PpPINA/PIN5 expression which would increase the efficiency of the proposed auxin transport mechanism (Poli *et al*., 2003). Therefore, we proposed that the expression of the PpPINA/PIN5-type proteins could be restricted to the specific region of the cellular grids by a cell-type specific factors thus determining the auxin transport routes (Figure 2C-2H).

All three model scenarios (Cases I-III) predicted the formation of a PpPINA/PIN5-type-dependent conductive auxin channel, connecting an auxin source to an auxin sink (Figure 2C, 2E and 2G). Remarkably, for all three simulated cases, auxin translocation emerged on average a 10-fold faster (Figure 2C, 2E and 2G) than in models that exclude the auxin carriers at the ER and, hence, solely relied on non-polar cell-to-cell auxin transport (Figure 2A and 2B). When the ER-localized auxin signaling was present (Cases II and III), the auxin concentrations in the conductive auxin channel were

particularly elevated (Figure 2C, 2E and 2G). This auxin accumulation in the transport route coincided with enhanced PpPINA/PIN5-type protein activities (Figure 2D, 2F and 2H), leading to auxin depletion from neighboring tissues (Figure 2C, 2E and 2G).

In conclusion, our *in silico* model simulations illustrate that this hypothetical non-polar, intercellular auxin transport mechanism could lead to auxin drainage from neighboring tissue, auxin accumulation in competent cells and finally to the formation

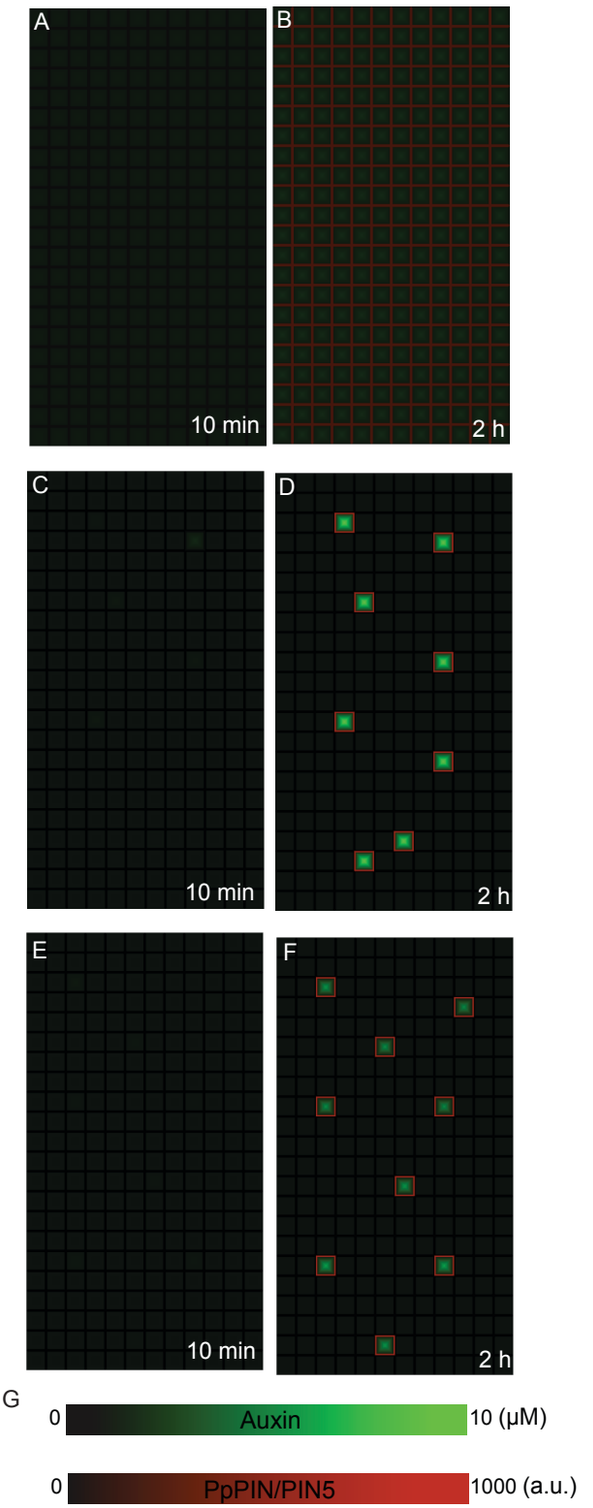

Figure 3 Spatio-temporal auxin patterning in model simulations

Model simulations on cell grids and initial perturbations in auxin concentrations. Auxin levels in the ER and cytoplasm are represented by cell centers and cell borders, respectively. For simplicity, domains of PpPINA/PIN5-type protein activity are shown in red on the rim of each cell. **(A, B)** Spatially homogenous auxin patterns in the model simulations that incorporated solely SCF/TIR1-dependent auxin signaling on the PpPINA/PIN5-type activity (Figure 1C; Case I) (Supplementary Movie 5). **(C, D)** Model variant with a hypothetical auxin signaling on PpPINA/PIN5-type protein abundance at the ER (Figure 1D; Case II) (Supplementary Movie 6), predicting spatially restricted auxin accumulation patterns (D). **(E, F)** Model simulations for the combined auxin signaling pathways (Figure 1E; Case III) (Supplementary Movie 7), demonstrating the plausibility of the model for the spatial organization of the auxin patterning (F). **(G)** Color map of auxin and PpPINA/PIN5-type levels.

of preferred auxin transport routes. The observed dynamics in auxin uptake and release in PIN expressing cells is a self-emerging property of our model and enables to create the steep auxin gradients in the tissue (see Figure 2, auxin content in the channels and neighbouring tissue). Thus, our model might hint at a simpler prototype for the known polar auxin transport mechanism in flowering plants. This cell-to-cell auxin transport mechanism could account for the spatio-temporal distribution of auxin in nonvascular plants, but could similarly contribute to the spatial auxin distribution in higher plants by acting in parallel to the well-characterized polar auxin transport mechanism.

4.7 SPATIAL AUXIN DISTRIBUTIONS

In flowering plants, polarized auxin transport is associated with the formation of asymmetric auxin distributions (auxin maxima) during organogenesis (Benjamins and Scheres, 2008; Heisler *et al.,* 2005; Jonsson *et al.,* 2006; Reinhardt *et al.,* 2003; Smith *et al.,* 2006). To investigate whether the proposed non-polar, but conductive; cell-to-cell auxin transport models (Figure 1C and 1D, Cases I-III) are capable of generating spatial auxin accumulation patterns, we tested the model simulations on the cell grids, assuming an initial auxin concentration (noise) in each cell (Figure 3) as well as a basal auxin production and auxin degradation. Additionally, all cells were allowed to produce PpPIN/PIN5-type proteins. Only the model that incorporated the receptor-based auxin signaling on PpPIN/PIN5-type protein abundance at the ER (Cases II and III) could generate spatially organized patterns (Figure 3A-3F). These auxin patterns were apparently the consequence of feedback-based reinforcement of original fluctuations in auxin concentrations. Notably, the individual auxin maxima differed in the auxin levels (Figure 3D and 3F).

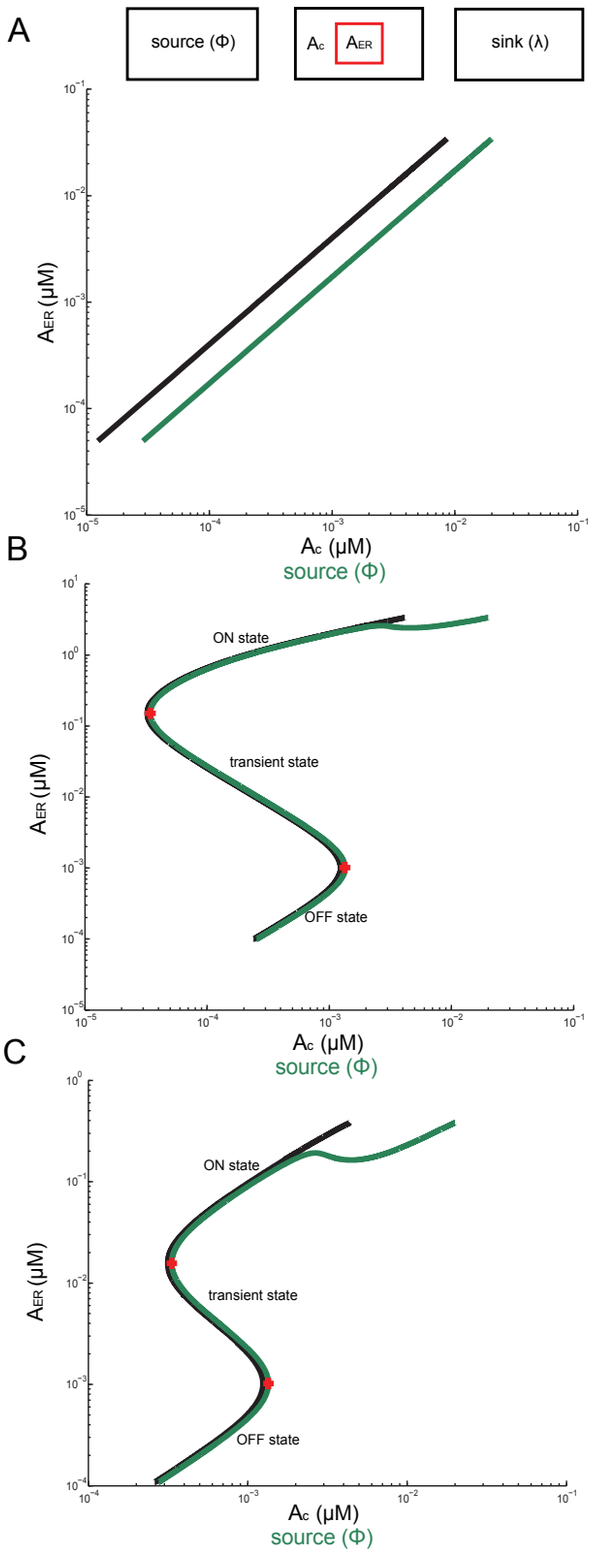

Figure 4 Dynamics of the proposed auxin transport mechanism

Simplified model simulation on the PpPINA/PIN5-type-producing cell (source, cell and sink). A_C and A_{ER} represent mean auxin concentrations in the ER lumen and cytoplasm, respectively. The parameter source is a variable signal (free bifurcation parameter) and A_C and A_{ER} represent preferential model responses (black line) to this signal (green line). **(A)** Monotonic dynamics in the model that incorporates solely SCF/

TIR1-dependent auxin signaling for the regulation of PpPINA/PIN5-type transcription (Figure 1C; Case I). **(B, C)** Model that includes either receptor-based auxin signaling on PpPINA/PIN5-type abundance at the ER (Figure 1D; Case II) or the combination of both possibilities (Figure 1E; Case III), revealing a switch-like (bistable) behavior in response to the variable signal, characterized by three possible states: (1) OFF state in which auxin concentration is higher in the cytoplasm than that in the ER lumen (auxin loading state), (2) transient unstable state and (3) ON state that mimics the formation of a new auxin reservoir (auxin storage) in the ER and subsequent release of auxin to the cytoplasmic pool.

Collectively, the model simulations revealed that at least two variants of the proposed model (Cases II and III), for an ancient PIN-dependent auxin transport mechanism facilitated the simple spatial pattern formation.

4.8 DYNAMICS OF THE MODEL

To understand the underlying dynamics of the proposed model (Figure 1C and 1D), we analyzed how the models responded to parameter deviations (input signal) (Figure 4). To this end, we used the bifurcation theory that is a useful tool to analyze dynamics of biological systems (Govaerts and Sautois, 2005; Tyson and Novak, 2008).

Solely, the model that incorporated a SCF/TIR1-dependent auxin signaling on the PpPINA/PIN5-type protein activity (Case I) showed monotonic dynamics described by the linear increase of cellular auxin accumulation (Figure 4A). Remarkably, non-trivial dynamics were observed for the models that combined the ER-localized auxin signaling pathway for the modulation of the PpPINA/PIN5-type protein activity (Cases II and III) (Figure 4B and 4C). These model dynamics can be conceptualized as a hysteresis or on/off switch mechanism in which auxin is loaded into the ER and subsequently released into the cytoplasm (Figure 4B and 4C, green line). Accordingly, highly abundant auxin temporarily blocks its release from the ER (OFF or auxin loading state) and triggers the transient PpPINA/PIN5-type-dependent formation of the local auxin source in the ER (Figure 4B and 4C, green line). After the auxin accumulation in the ER reaches a threshold level, auxin is transported back to the cytoplasm and is eventually to the adjacent cells (ON or auxin release state) (Figure 4B and 4C, green line). These findings provided a mechanistic explanation for our model predictions (Figure 2 and 3).

Our analysis of the model dynamics revealed that each cell capable of PpPINA/PIN5-type-dependent auxin retention in the ER can act both as auxin sink (local auxin loading) or auxin source (local release), ultimately enabling aa facilitated, non-polar intercellular auxin transport.

4.9 CONCLUSION AND FUTURE DIRECTIONS

In flowering plants, polar auxin transport, localized auxin biosynthesis and auxin homeostasis play important roles in various developmental processes including embryogenesis, de novo organ formation and tropism (Benjamins and Scheres, 2008; Vanneste and Friml, 2009). In evolutionarily older, nonvascular plants, such as the moss *P. patens*, auxins have similarly profound developmental functions (Christenson, 2000; Cooke *et al.,* 2002; Decker *et al.,* 2006; Fujita *et al.,* 2008; Hayashi *et al.,* 2008; Jenkins *et al.,* 1986; Johri and Desai, 1973; Lehnert and Bopp, 1983; Nyman and Cutter, 1981; Sakakibara *et al.,* 2003; Schumaker and Dietrich, 1998). However, the presence of the polar auxin transport in the development of nonvascular plants remains controversial. The PIN1-type protein function at the plasma membrane is generally considered to control the polar auxin transport, but only PIN5-like genes have been found in the genomic sequence of *P. patens* with hypothetical functions at the ER (Mravec *et al.,* 2009). Even though the molecular function of the PIN proteins in nonvascular plants is unknown, here, an hypothetical mechanism is proposed for the ancient, yet simpler prototype of the PIN-dependent polar auxin transport

We suggest a conceptually novel, plausible mechanism for cell-to-cell auxin transport via carrier-dependent intracellular auxin exchange between the ER and the cytoplasm. These mechanism hypothesizes on PpPINA/PIN5-type-dependent auxin storage in the ER that, in turn, represents the source of a non directional cell-to-cell auxin transport. Consistently, we demonstrated that this mechanism is capable of generating channel-like auxin transport routes, similar to those observed during development in mosses (*Phaeoceros personii*, *Pellia epiphylla*) (Poli *et al*., 2003) , as well as spatiopatterns of auxin accumulation. Hence, this model could forecast an ancient auxin transport machinery for spatiotemporal auxin distribution in the earliest land plants, such as mosses. Future research in mosses or other more ancient plant species will provide further molecular and mechanistic insight into the fascinating evolution of polar auxin transport mechanisms.

Recent report shows that extracellular ABP1 regulates PIN protein activity at the plasma membrane by regulating its abundance (Robert *et al*., 2010; Wabnik *et al*., 2010). We hypothesize that ABP1 in the ER could similarly regulate the residence/activity of PIN5-type proteins at the ER membrane. Intriguingly, the evolution of PIN proteins in higher plants might have evolved a sorting process from the ER to the plasma membrane, likely by the involvement of a tyrosin motif in the PIN1-type proteins (Mravec *et al*., 2009). Whether such a mechanism could have co-evolved further in flowering plants with the co-function of the ER export and extracellular role of ABP1 in the trafficking of membrane-localized PIN proteins remains a fascinating subject of further research.

4.10 COMPUTATIONAL METHODS

4.10.1 MODEL SIMULATIONS

The cellular grid tissue template for the model was created using the version of VV (Vertex-Vertex) programming language (Smith *et al.,* 2003; Smith *et al.,* 2006) and in the L-system-based modeling software L-studio (Karwowski and Prusinkiewicz, 2004) (http://algorithmicbotany.org/lstudio). The simulations were done by numerical computations of coupled ODE systems, with an adaptive-size, fifth-order Runge-Kutta method. For the bifurcation analysis, we used MATCONT - graphical Matlab package for numerical bifurcation analysis (Dhooge *et al.,* 2003). All figures were processed in Adobe Illustrator (Adobe Inc. CS2). Figures 2 and 3 are screenshots from model simulations.

4.10.2 MATHEMATICAL DESCRIPTION OF THE MODEL

In the computer model, each cells consisted of a two discrete intracellular compartments: cytoplasm and endoplasmic reticulum (ER) (Figure 1). Cell-to-cell auxin transport is modeled as follows:

$$\frac{dAC_i}{dt} = \phi - \lambda \cdot AC_i + \frac{1}{V_c} \cdot p_{IAAH} \cdot \sum_{k \in N_j} l_{i->k} \cdot (AC_k - AC_i)) \quad (1)$$

where AC_i is the average auxin concentration in the cytoplasm of the i-th cell and AC_k represents auxin concentration in the cytoplasm of adjacent cell (k). The parameter p_{IAAH} is the plasma membrane permeability for non-polar auxin transport . V_c is the average volume of the cell and $l_{i->k}$ is crossing area, respectively. For simplicity, each cell has the same volume ($V_c \sim 100\ \mu m^2$) and crossing area $l_{i->k} = l = 10\ \mu m^2$. Φ is auxin production (source, Figure 4) term and λ regulates auxin degradation (sink, Figure 4) term.

Auxin transport between cytoplasm and ER compartment is expressed as follows:

$$\frac{dAC_i}{dt} = \frac{1}{V_c} \cdot (D_{ER} \cdot AER_i - D_C \cdot AC_i - p_{pin} \cdot PpPIN_i \cdot \frac{AC_i}{K_A + AC_i}) \quad (2)$$

$$\frac{dAER_i}{dt} = \frac{1}{V_{ER}} \cdot (D_C \cdot AC_i - D_{ER} \cdot AER_i + p_{pin} \cdot PpPIN_i \cdot \frac{AC_i}{K_A + AC_i}) \quad (3)$$

where $V_{ER}/V_c = 0.1$ is a ratio of average area for cytoplasm and ER compartments. AC_i and AER_i are the average auxin concentrations in cytoplasm and ER, respectively. D_C and D_{ER} are diffusion constants for auxin transport between cytoplasm and ER compartment. We assumed that $D_C << D_{ER}$ and that auxin transport into ER is largely dependent on $PpPIN_i$ expression. The parameter p_{PIN} represents transport capacity for PpPIN proteins and K_A is saturation constant for PpPIN-dependent auxin transport.

Case I

In the first model variant, PpPINA/PIN5 protein expression is modeled as follows:

$$\frac{dPpPIN_i}{dt} = \alpha_b + \alpha_r \cdot \frac{1}{K_m^N + AC_i^N} - \delta_b \cdot PpPIN_i \tag{4}$$

where α_b and δ_b are basal rates of $PpPIN_i$ expression and degradation, respectively. The parameter αr controls $PpPIN_i$ transcriptional repression by auxin and K_m is auxin concentration threshold.

Case II

In the second scenario, PpPINA/PIN5 protein expression is given by:

$$\frac{dPpPIN_i}{dt} = \alpha_b + \alpha_r \cdot \frac{R \cdot AER_i^N}{K_R^N + AER_i^N} - \delta_b \cdot PpPIN_i - \delta_r \cdot \frac{R \cdot AER_i^N}{K_I^N + AER_i^N} \tag{5}$$

where α_r is an auxin-inducible $PpPIN_i$ expression and R represents number of ER-resident auxin receptors. Parameter δ_r is an auxin-dependent PpPIN/PIN5 protein degradation. Terms K_R and K_I are auxin concentration thresholds for auxin-induced PpPIN/PIN5 expression and degradation, respectively. The remaining terms are as in Case I.

Case III

The combination of both model variants (Cases I and II):

$$\frac{dPpPIN_i}{dt} = \alpha_b + \alpha_r \cdot \frac{R \cdot AER_i^N}{K_R^N + AER_i^N + AC_i^N} - \delta_b \cdot PpPIN_i - \delta_r \cdot \frac{R \cdot AER_i^N}{K_I^N + AER_i^N} \tag{6}$$

The terms in equation (6) are as in Cases I and II.

4.10.3 MODEL PARAMETERS

Parameter	Case I	Case II	Case III	units
p_{IAAH}	10	10	10	$\mu m s^{-1}$
p_{PIN}	20	20	20	$\mu m s^{-1}$
D_C	5	5	5	$\mu m^2 s^{-1}$
D_{ER}	500	500	500	$\mu m^2 s^{-1}$
α_b	0.0001	0.0001	0.0001	s^{-1}
δ_b	0.1 (Fig. 2), 0.005 (Fig. 3)	0.0001	0.0001	s^{-1}
α_r	1	1	1	s^{-1}
δ_r	-	0.1 (Fig.2), 0.005 (Fig. 3)	0.1 (Fig. 2, Fig. S2), 0.005 (Fig. 3)	s^{-1}
R	-	100	100	μM
K_A	1	1	1	μM
K_m	1	1	1	μM
K_R	-	1	1	μM
K_I	-	5	5	μM
N	2	2	2	-
Φ	0.02 (Fig. 2), 0.002 (Fig. 3)	0.02 (Fig. 2), 0.002 (Fig. 3)	0.02 (Fig. 2, Fig. S2), 0.002 (Fig. 3)	$\mu M s^{-1}$
λ	1(sink) (Fig. 2), 0.001 (Fig. 3)	1 (sink) (Fig. 2), 0.001 (Fig. 3)	1 (sink) (Fig. 2, Fig. S2), 0.001 (Fig. 3)	s^{-1}

4.11 SUPPLEMENTARY FIGURES

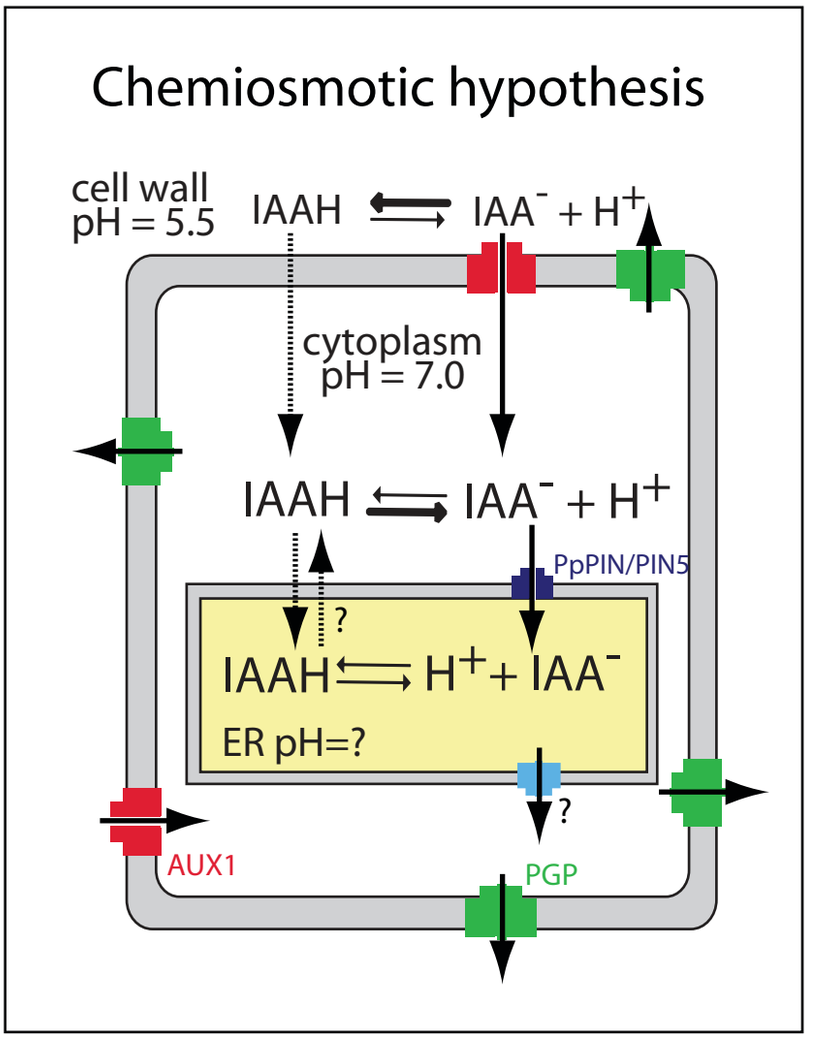

Supplementary Figure 1 Chemiosomotic hypothesis for inter- and intracellular auxin transport in moss In the cell wall (pH of 5.5) auxin is mostly protonated and can easily enter the cell via diffusion (dashed black arrow) or cross-membrane transport by AUX/LAX influx carriers (in red). Due to neutral pH of cytoplasm (~7.0), auxin is largely deprotonated and thus requires active transport mediated by PGP/MDR/ABCB efflux transporters (in green) to exit the cell. PpPINA/PIN5 proteins (in dark blue) sit at the endoplasmic reticulum (ER) membrane where they presumably mediated auxin import into ER lumen.. Since the exact pH of ER is not know as well as transport machinery out of the ER membrane, auxin could simply diffuse in/out of the ER (dashed arrows) and/or be pumped out via hypothetical transporter depending on the actual pH of the ER compartment (in blue).

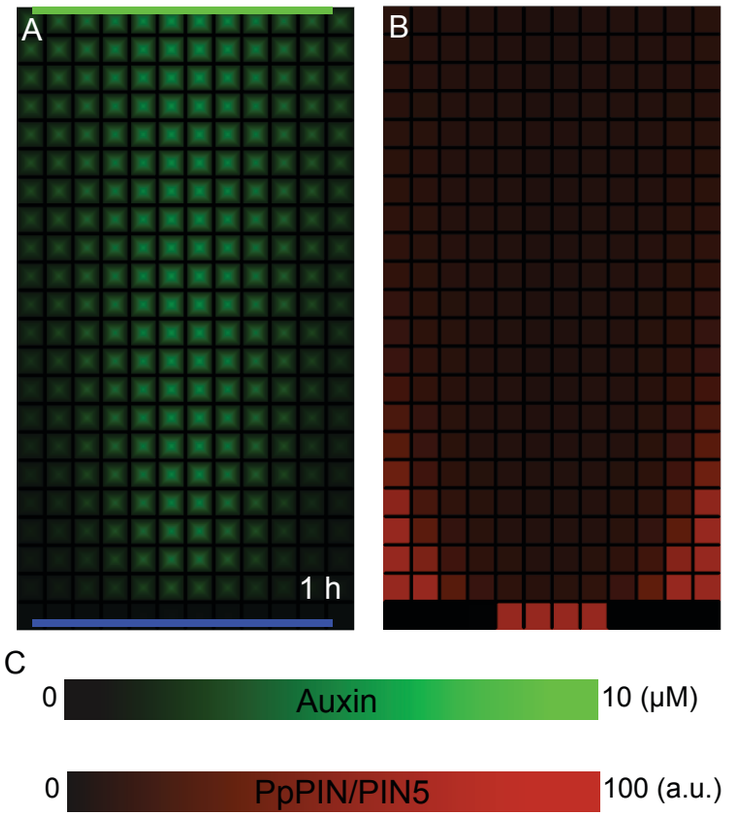

Supplementary Figure 2 Model with ubiquitous PpPINA/PIN5 expression predicts the widening of auxin canal

(A, B) The integration of two feedback signaling pathways for the regulation of PpPINA/PIN5 protein activity in the model (Figure 1E; Case III) and ubiquitous PpPINA/PIN5 expression in the tissue resulted in a broad auxin channel, spanning towards neighboring tissues (A). (B) PpPINA/PIN5 expression pattern coincides with the broad auxin transport route (A). Model parameters are as in simulations of Figure 2G-2H. (C) Color mapping for auxin and PpPINA/PIN5 levels in model simulations.

4.13 SUPPLEMENTARY MOVIES

Supplementary Movie 1

The file contains Supplementary Movie 1 displaying the simulations of Figure 2A-2B (diffusion). Color coding scheme used in the model simulations is as presented in Figure 2I.

Supplementary Movie 2

The file contains Supplementary Movie 2 displaying the simulations of Figure 2C-2D (Case I). Color coding scheme used in the model simulations is as presented in Figure 2I.

Supplementary Movie 3
The file contains Supplementary Movie 3 displaying the simulations of Figure 2E-2F (Case II). Color coding scheme used in the model simulations is as presented in Figure 2I.

Supplementary Movie 4
The file contains Supplementary Movie 4 displaying the simulations of Figure 2G-2H (Case III). Color coding scheme used in the model simulations is as presented in Figure 2I.

Supplementary Movie 5
The file contains Supplementary Movie 5 displaying the simulations of Figure 3A-2B (Case I, homogenous auxin distribution). Color coding scheme used in the model simulations is as presented in Figure 3G.

Supplementary Movie 6
The file contains Supplementary Movie 6 displaying the simulations of Figure 3C-2D (Case II, auxin patterning). Color coding scheme used in the model simulations is as presented in Figure 3G.

Supplementary Movie 7
The file contains Supplementary Movie 6 displaying the simulations of Figure 3E-2F (Case III, auxin patterning). Color coding scheme used in the model simulations is as presented in Figure 3G.

ACKNOWLEDGMENTS

This work was supported by grants from the Research Foundation-Flanders (Odysseus to J.F. and project no. 3G006507 to W.G.), the EMBO Young Investigator Program (to J.F), and and the Vienna Science and Technology Fund (to J.K.-V.).

CHAPTER 5

WOX5-AUXIN FEEDBACK SIGNALLING MODULATES AUX-IN GRADIENT-GUIDED PATTERNING OF THE *ARABIDOPSIS* ROOT

"What is important is the gradual development of a theory, based on a careful analysis of the ... facts. ... Its first applications are necessarily to elementary problems where the result has never been in doubt and no theory is actually required. At this early stage the application serves to corroborate the theory. The next stage develops when the theory is applied to somewhat more complicated situations in which it may already lead to a certain extent beyond the obvious and familiar. Here theory and application corroborate each other mutually. Beyond lies the field of real success: genuine prediction by theory. It is well known that all mathematized sciences have gone through these successive stages of evolution."

— John von Neumann

WOX5-AUXIN FEEDBACK SIGNALLING MODULATES AUXIN GRADIENT-GUIDED PATTERNING OF THE *ARABIDOPSIS* ROOT

Zhaojun Ding[1,2,8], Krzysztof Wabnik[1,2,3,8], Stephan Pollmann[4,5], Willy Govaerts[4], Steffen Vanneste[1,2], Marcus Geisler[6,7], and Jiří Friml[1,2]

under review, 2011
Contribution: Computation modeling work has been handled by K. Wabnik

[1]Department of Plant Systems Biology, VIB, 9052 Gent, Belgium
[2]Department of Plant Biotechnology and Genetics, Ghent University, 9052 Gent, Belgium
[3]Department of Applied Mathematics and Computer Science, Ghent University, 9000 Gent, Belgium
[4]Department of Plant Physiology, Ruhr-University Bochum, 44780 Bochum, Germany
[5]Centro de Biotecnología y Genómica de Plantas (UPM - INIA), Campus de Montegancedo, 28223 Pozuelo de Alarcón, Madrid, Spain
[6]Institute of Plant Biology, University of Zurich and Zurich–Basel Plant Science Center, CH- 8008 Zurich, Switzerland
[7]Department of Biology, Plant Biology, CH-1700 Fribourg, Switzerland
[8] These authors contributed equally to this work

ABSTRACT

Cell production in plants mostly occurs at the extremities of the plant body, called meristems. The mechanism underlying the patterning and maintenance of meristems was elusive. In the primary root meristem there is a critical involvement for a gradient of the phytohormone auxin across the root stem cell niche. This auxin gradient depends largely on polar cell-to-cell auxin transport. Recently, the transcription factor WUSCHEL-RELATED HOMEOBOX 5 (WOX5) was identified as a master regulator of root stem cell niche patterning. Here, our experimental and computational studies demonstrate that WOX5 is required for spatial restriction and maintenance of the maximum of phytohormone auxin in the quiescent center of the root. In turn, this root-associated auxin maximum feeds back on the WOX5 expression via the AUXIN-RESISTANT3-dependent regulation of auxin responses. Our results suggest that this feedback circuit is critical for the auxin-guided root patterning.

5.1 INTRODUCTION

The small signalling molecule auxin is a versatile regulator of plant growth and development including root patterning (Bennett and Scheres, 2010; Chapman and Estelle, 2009; Ding and Friml, 2010; Dolan, 1998; Kepinski and Leyser, 2005; Overvoorde *et al*., 2010; Sabatini *et al*., 1999; Santner *et al*., 2009; Sundberg and Ostergaard, 2009; Swarup *et al*., 2005; Tsukagoshi *et al*., 2010). In the roots of *Arabidopsis thaliana,* a gradient-guided auxin maximum is maintained by concerted action of auxin metabolic processes (del Pozo and Estelle, 2000; Fischer *et al*., 2006; Ljung *et al*., 2005; Petersson *et al*., 2009; Stepanova *et al*., 2008; Tao *et al*., 2008; Woodward and Bartel, 2005) and cell-to-cell polar auxin transport (Blilou *et al*., 2005; Friml *et al*., 2002; Grieneisen *et al*., 2007). The acropetal and basipetal auxin flows in the root are largely coordinated by PIN-FORMED (PIN) proteins that determine the direction of polar auxin transport (Luschnig *et al*., 1998; Petrášek et al., 2006; Wiśniewska *et al*., 2006), and by AUXIN/LIKE-AUXIN (AUX/LAX) influx carriers (Swarup *et al*., 2005; Yang and Murphy, 2009) and the P-GLYCOPROTEIN/MULTIDRUG-RESISTANCE/ABCB (PGP/MDR/ACBC) auxin efflux carriers (Geisler and Murphy, 2006). These auxin flows result in root-associated auxin maximum that is spatially restricted to the distal root tip as demonstrated by the activity of a synthetic *DR5* auxin-responsive promoter (Blilou *et al*., 2005; Friml *et al*., 2002; Sabatini *et al*., 1999). This auxin maximum guides root growth and development by influencing cell division, cell expansion and stem cell differentiation (Blilou *et al*., 2005; Ding and Friml, 2010; Sabatini *et al*., 1999).

The transcription factor WOX5 has been identified as a major organizer of the root stem cell niche that can be functionally replaced by WUSCHEL (Sarkar *et al*., 2007). Interestingly, WOX5 is specifically expressed in the QC to maintain the surrounding stem cell identities (Sarkar *et al*., 2007). Notably, auxin promotes distal stem cell (DSC) differentiation via the restriction of WOX5 transcription in the QC through the downstream AXR3-dependent auxin signaling pathway (Ding and Friml, 2010).

Here we used independently, experimental and computer modeling approaches to reveal the unexpected feedback loop between the WOX5 activity and the maintenance of auxin maximum in the root tip. We demonstrated that a novel WOX5-auxin feedback circuit is critical to maintain the sharp auxin gradient in the root tip which associates with the proper patterning of root stem cell niches.

5.2 AUXIN MAXIMUM AND LOCAL AUXIN GRADIENT IN THE ROOT TIP GUIDE ROOT STEM CELL PATTERNING

Previous studies based on the artificial auxin signaling response reporter *DR5::GUS* im-

plied that the auxin maximum might be located mainly in the root columella cells (Friml *et al.*, 2002; Sabatini *et al.*, 1999), but direct auxin measurements (Petersson *et al.*, 2009) and theoretical predictions (Benjamins and Scheres, 2008; Grieneisen *et al.*, 2007) suggest that the highest auxin content should be spatially restricted to the quiescent center (QC). When the alternative artificial auxin response reporter *DR5rev::GFP* was used (Friml *et al.*, 2003), the auxin signaling maximum was indeed in the QC of the root apex (Figure 1A).

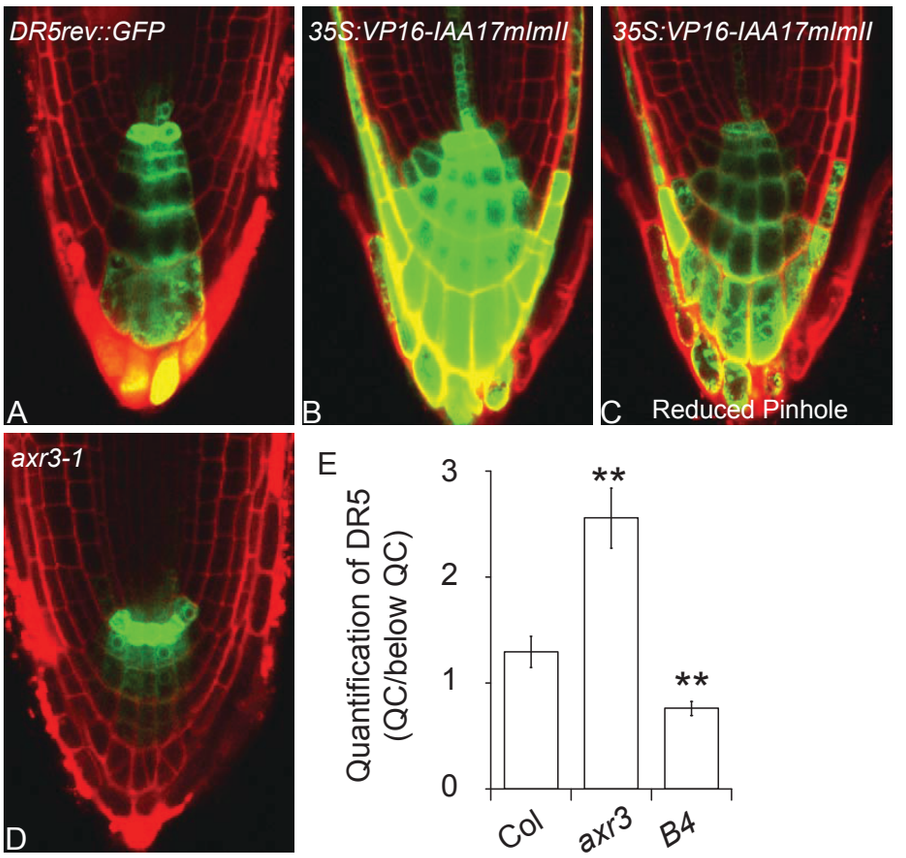

Fig.ure 1 Regulation of the auxin signaling maximum in the QC through IAA17

(A) Localization of the auxin signaling maximum in the QC, which is shown via *DR5rev::GFP*. (**B**, **C**) Lack of the auxin signaling maximum in the QC from the dominant active IAA17 line (*35S:VP16-IAA-17mImII*), although the whole auxin signaling in *35S:VP16-IAA17mImII (B) is much stronger than that of the wild-type control (A). The same root was scanned with reduced pinhole settings (C).* **(C)** The auxin signaling maximum in the QC in *axr3-1*, shown by *DR5rev::GFP*. **(D)** Quantification of *DR5rev::GFP* signals, shown in (A, B, and C). Error bars depict standard deviation, n>15.

To assess the underlying mechanism of the auxin signaling maximum in QC cells (Fig. 1), we analyzed the effect of an engineered version of indole-3-acetic acid 17 (IAA17; *35S:VP16-IAA17mImII*) (Li *et al.*, 2009) that enhanced the auxin response independently of the auxin content and the dominant negative mutant AUXIN RESIS-

TANT3/IAA17 (*axr3-1*) with inhibited auxin responses due to the increased IAA17 protein stability (Tiwari *et al*., 2003). In the *35S:VP16-IAA17mImII* mutant, the quantitative *DR5rev::GFP* auxin response in the root tips was on avarage stronger than that of the wild-type control (Figure 1A, 1B and 1E), but, remarkably, the auxin signaling maximum was not spatially restricted to QC cells (Figure 1C and 1E), indicating the absence of an auxin signaling maximum in the QC. Moreover, the root distal stem cells (DSCs) of this mutant were all differentiated as demonstrated by the pronounced starch accumulation (Supplementary Figure 1A and 1C). In contrast, the *axr3-1* mutant (Rouse *et al*., 1998) showed a decreased DR5 signaling in roots (Ouellet *et al*., 2001), while maintaining the auxin signaling maximum in the QC region (Figure 1A, 1D and 1E). Live-cell imaging revealed a steeper gradient of *DR5rev::GFP* activity between QC cells and root apical cells below the QC (Figure 1A, 1D and 1E) that was associated with a severely impaired DSC differentiation marked by starch accumulation only in the most distal root cap cells (Supplementary Figure 1A and 1B). Collectively, our investigations indicated that the QC specific auxin maximum is essential for maintaining DSC identity.

5.3 WOX5 ACTIVITY MODULATES FREE AUXIN CONTENT OF THE QC CELLS

Auxin has recently been shown to promote DSC differentiaton via the restriction of *WOX5* transcription in the QC through the downstream AXR3-dependent auxin signaling pathway (Ding and Friml, 2010). This observation highlights the possibility for a feedback regulation between auxin signaling and WOX5 activity. To address this question, we analyzed the *DR5rev:GFP* marker in the *wox5* mutant (Figure 2) and found that the auxin signaling maximum restricted to QC cells was absent (Figure 2A-2C) as similarly in *35S:VP16-IAA17mImII* plants (Figure 1B, 1C, and 1E). Furthermore, the *wox5* mutant phenocopied the *35S:VP16-IAA17mImII* mutant in the context of enhanced terminal differentiation of DSCs (Sarkar *et al*., 2007) (Figure 1). Moreover, the ratio of *DR5rev::GFP* activity between QC cells and root apical cells below the QC was lower than that of the control (Figure 2C), hinting at a possible role of WOX5 in the maintenance of the auxin maximum in the QC.

To test this hypothesis, we measured free IAA levels in the *wox5* mutant and in the dexamethasone (DEX)-inducible *35S::WOX5-GR* plants (Figure 2D). However, the free IAA levels did not change in the *wox5* mutant compared with the wild type controls (Fig.ure 2D), but, after induction of the *WOX5* expression (Figure 2D), they were significantly increased (Figure 2D), indicating a role of WOX5 in free IAA production/deconjugation. The free IAA data measured in the DEX-inducible *35S::WOX5-GR* line were also confirmed with another auxin response reporter, *DR5::GUS*. After DEX in-

duction, the *DR5::GUS* signals were enhanced both in roots and cotyledon leaves of the *35S::WOX5-GR* line (Supplementary Figure 3).

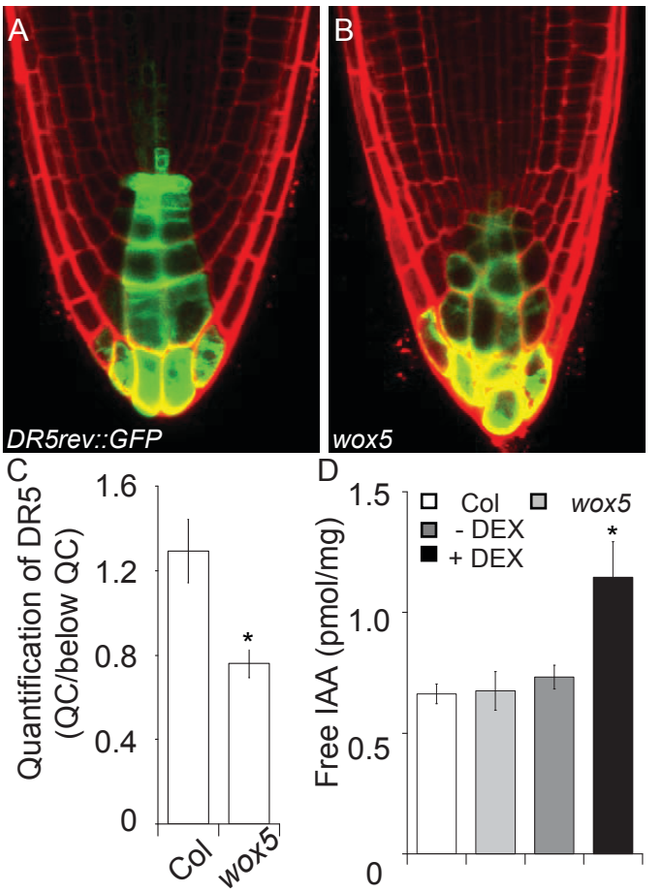

Figure 2 Involvement of WOX5 in the auxin maximum generation in the QC

(A) Localization of the normal auxin signaling maximum in the QC, which is shown via *DR5rev::GFP*. **(B)** Lack of the auxin signaling maximum in the QC in *wox5*. **(C)** Quantification of DR5rev::GFP signals shown in (A and B). Error bars depict standard deviation, n>20. **(D)** Increase in the free IAA level in *35S::WOX5-GR* after DEX inductions (black column). Error bars depict standard deviation, n=4.

Previously, the *wox5* mutant had been reported to show an increase in conjugated IAA (Gonzali *et al.*, 2005), implying that WOX5 might regulate free IAA production through the manipulation of the IAA deconjugation. To assess the involvement of WOX5 in free IAA production, we analyzed the expression level of auxin deconjugation-related genes in the *35S::WOX5-GR* line and found that they were highly induced in the presence of DEX (Supplementary Figure 2). Taken together, our results suggest that WOX5 might contribute to gradient-guided root patterning by modulating the auxin (free IAA) content of QC cells.

5.4 WOX5-AUXIN FEEDBACK REGULATION FOR THE ROOT PATTERNING

As our studies imply a feedback mechanism that links the WOX5 activity to the auxin maximum in QC cells, we examined the *WOX5::ERGFP* marker expression in the background of the *35S:VP16-IAA17mImII* and *axr3-1* auxin signaling mutants (Figure 3). The *axr3-1* mutant displayed a slightly broader *WOX5::ERGFP* expression domain that extended to the endodermis/cortex initials (Figure 3B) than that of the wild-type control (Figure 3A). Notably, the *WOX5* misexpression correlated with reminiscent, ectopic *DR5* upregulation in endodermis/cortex initials of the *axr3-1* mutant (Figure 1A and 1D), but the *WOX5::ERGFP* expression was severely repressed in the *35S:VP16-IAA17mImII* mutant (Figure 3C), corresponding with the lack of an auxin gradient across the QC and an enhanced DSC differentiation (Figure 1B; Supplementary Figure 1). Thus, *wox5* and *axr3-1* mutants have opposite DSC phenotypes that correlate with effects on the steepness of the auxin signaling gradient. Our genetic analysis demonstrated that WOX5 and AXR3 seem to act in the same regulatory pathway, because the *wox5 axr3-1* double mutant showed an inhibited root DSC differentiation as seen in the *axr3-1* single mutant (Figure 3D-3G). Our studies indicate that, to generate or maintain the root auxin maximum in QC cells, plants need to maintain *WOX5* expression to a certain level through AXR3-dependent auxin responses.

5.5 *IN SILICO* COMPUTER MODEL ACCURATELY PREDICTS EXPERIMENTAL OBSERVATIONS

To test the plausibility of the proposed WOX5-auxin feedback mechanism, we used *in silico* computer simulations (Figure 4). The previously suggested *in silico* root model was shown to reproduce the establishement of auxin maximum in the root tip based solely on the auxin transport reflux loop, realized by the necessary assumption of lateral inward PIN2 polarization in root epidermis and cortex (Grieneisen *et al.*, 2007). In contrast, the experimantal data pin-point as slightly different scenario in which acropetal and basipetal auxin flows are separated by partial lateralization of the PIN2 protein to the outer lateral cell side in the cortex versus the inner lateral PIN1 polarization in endodermis cells (Kleine-Vehn and Friml, 2008; Sauer *et al.*, 2006). This indicates the possibility for the actual sparation of bidirectional auxin flows as an experimentally validated alternative for the proposed “reflux loop” (Grieneisen *et al.*, 2007). Therefore, this experimentally derived topology of the PIN polarity network (Kleine-Vehn and Friml, 2008; Sauer *et al.*, 2006) has been incorporated in our model (Figure 4A). Besides the experimental PIN protein localizations, the model incorporates both the WOX5-depen-

dent regulation of free auxin levels in QC cells (Figure 2) and the auxin-mediated repression of the WOX5 activity (Figure 3) at high auxin concentrations (saturated auxin transport) (Goldsmith *et al.*, 1981) (Figure 4A). For the full model description, we refer to the Computational methods.

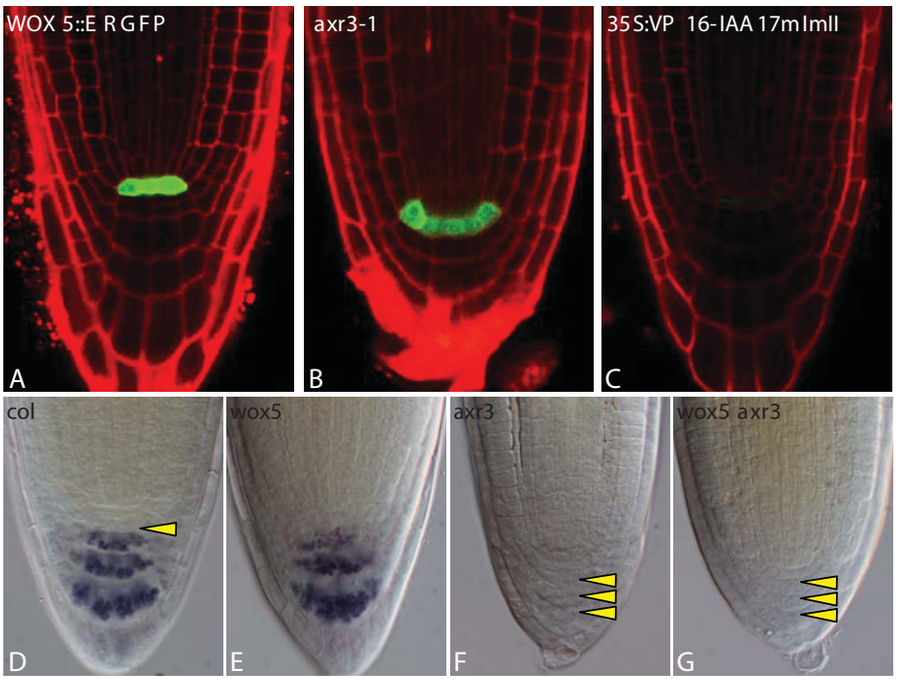

Figure 3 IAA17 action upstream of WOX5 and restriction of *WOX5* expression in the QC
(A) *WOX5::ERGFP* signal visible only in the QC in the wild-type control. **(B)** Expanded *WOX5::ERGFP* signals into the endodermis/cortex initials in *axr3-1*. **(C)** Highly repressed *WOX5::ERGFP* signals in *35S:VP16-IAA17mImII*. (**D**-**G**) Differentiation status of distal stem cells (DSCs; yellow arrowhead) below the QC (red arrowhead) in 4-day-old seedlings as inferred from the lugol staining. Wild-type roots show typically one tier of DSCs (D), *wox5* terminal DSC differentiation (E), both *axr3-1* (F) and *wox5 axr3* (G) the same defects in DSC differentiation as revealed by multiple tiers of DSCs.

In silico model simulations based solely on the PIN-dependent polar auxin transport with the PIN polarity obtained from experimental observations do not predict an auxin maximum spatially restricted to the QC. In fact, the model predicted the appearance of auxin maximum in columella initials just below the QC cells (Figure 4C). Consistently, the normal PIN protein localizaton pattern was observed both in the *wox5* mutant which lacks the auxin signaling maximum in the QC cells, and in the *WOX5* overexpression line *35S::WOX5-GR* (Supplementray Figures 4 and 5). This indicates that the realistic PIN polarization network incorporated in our model might not explain the maintenance of auxin maximum in the QC cells and thus other factors such as local auxin biosynthesis or deconjugation might be required (Ikeda *et al.*, 2009). Remarkably, we found the combination of the WOX5-auxin feedback loop and the PIN-dependent auxin transport

in our model could correctly predict the maintenance of auxin maximum in the QC (Figure 4B). Moreover, the highest auxin accumulation was noted in the QC cells and decreased exponetially toward more distal columella cells, indicating the presence of a local auxin gradient in the root tip (Figure 4B and 4F).

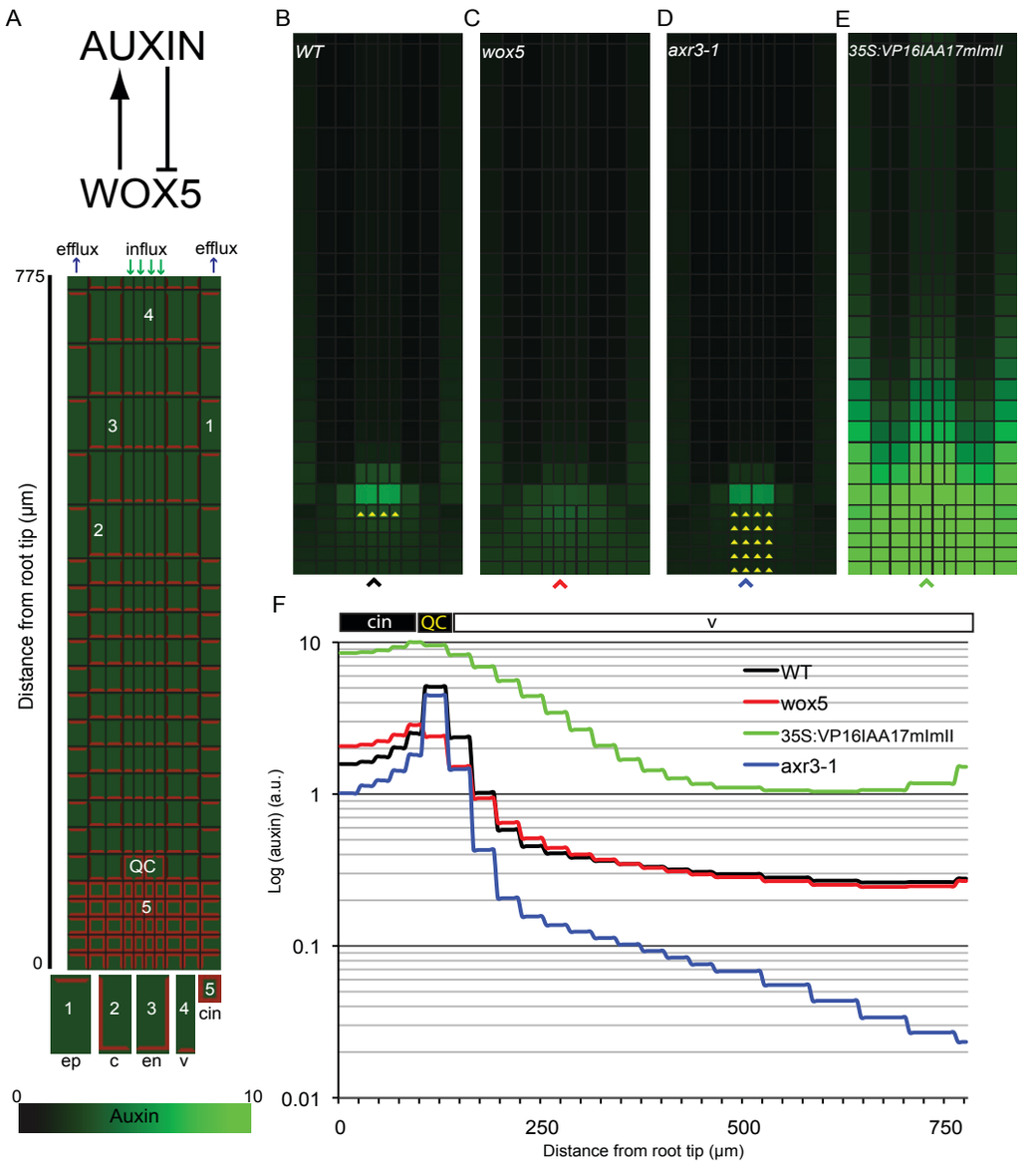

Fig.ure 4 Integrated computer model for the root auxin maximum establishment

(A) Schematic WOX5-auxin feedback regulation and *in silico* computer model of the root meristem. The five distinct regions of the root meristem were incorporated into the model: one layer of root epidermis (1), one layer for both root cortex and endodermis (2 and 3), four central layers of vascular cells (4); and columella initials (5). Two QC cells (yellow) correspond to the most distal vascular cells (4). For each cell type (1 to 5) in the model, only experimentally observed PIN distributions patterns were considered. The *WOX5* expression was restricted to the QC cells. Color coding scheme for auxin concentrations in the root simulations is given in green. (**B**-**E**) Compatible *in silico* wild-type simulations of the model that integrates the WOX5-auxin feedback and the polar auxin transport (B)(Supplementary Movie 1) and the

computer simulations of the *in silico wox5* mutant (C)(Supplementary Movie 2), low auxin signaling (*axr3-1*) (D)(Supplementary Movie 3), and high auxin signaling (*35S:VP16-IAA17mImII*) (E)(Supplementary Movie 4) mutants to experimental observations (Figure 1A-1D and 2A and 2B). The predicted stem cell layers depicted by yellow triangles below the QC correspond to those observed experimentally (Figure 3D-3F; Supplementary Figure 1). **(F)** Steady-state graded concentration profiles along longitudinal sections through the vascular and columella tissues for wild-type and mutant simulations (distance from root tip in μm). Steep exponential auxin gradients were observed between QC cells (yellow) and columella initials (cin) in wild-type (black) and *axr3-1* (blue) simulations and were largely absent in the simulations of *wox5* (red) and *35S:VP16-IAA17mImII* (green) mutants, similarly to those in experimental measurements (Figures 1E and 2C).

For detailed model descriptions and model parameters used in the simulations, see Computational methods and Supplementary Table 2.

The steepness of this gradient corresponded to the experimentally observed pattern of root stem cell niche (Figures 4B and 3D) and was severely reduced in the *wox5* mutant (Figures 4C and 3D). Thus, the model predictions are fully consistent with the experimental observations of auxin distributions, and columella differentiation patterns with no need for additional assumptions or modifications (Figure 2A and 2B). These findings could be explained in a following manner: the WOX5-auxin circuit locally increases the free auxin content of QC cells. Consequently, high auxin concentrations are built up in QC cells such that threshold concentrations of the saturated auxin transport are reached (~ 3 [a.u.]; Figure 4F). Because of the limited capacity of auxin transport, an auxin maximum can be efficiently maintained in the QC region through the self-organizing WOX5-auxin feedback loop (Figure 4F, black curve). Subsequently, this leads to the formation of steep auxin signaling gradient in the root tip with instructive properties for the root meristem patterning (Figure 4B and 4D).

Next, we simulated *in silico* auxin signaling and polar transport mutants. Through manipulation of the WOX5-auxin feedback mechanism (for full description of the methods used, we refer to Computational methods), a clearly local auxin gradient with the highest auxin accumulation was noted in QC cells to maintain DSC identities in wild-type simulations (Figure 4B and 4F), but was strongly affected in simulations of both the *axr3-1* and *35S:VP16-IAA17mImII* mutants that are defective in auxin signaling. The *axr3-1* shows a highly pronounced local auxin gradient and less DSC differentiation, whereas the *35S:VP16-IAA17mImII* mutant displays no auxin signaling maximum in QC cells and more DSC differentiation that is due to pronounced overall auxin responses (independent of free auxin content) (Figure 4D-4F). Similar results were obtained by simulating mutants that lack either the acropetal (stele domain) or the basipetal auxin transport (epidermis and cortex). Both local auxin gradient and DSC differentiation were affected in each case (Supplementary Figure 6). Additionally, an increased lateralization

of PIN2 proteins in the cortex/endodermis leads to a broader auxin accumulation, spanning outside of the QC, and an enhanced DSC differentiations (Supplementary Figure 7).

The *in silico* manipulations of the auxin-mediated WOX5 repression had minor effects on the auxin distribution pattern in the root tips (Supplementary Figures 8 and 9). However, a highly pronounced repression of the WOX5 activity resulted in stem cell and auxin patterning defects (Supplementary Figure 10) that virtually reproduced the experimental observations of the *wox5* mutant (Figure 4C), indicating that the WOX5 activity provides a stabilizing factor for establishing/maintaining the auxin maximum in the QC and the correct DSC differentiation pattern.

5.6 CONCLUSIONS

The experimental data on the WOX5-auxin feedback circuit supported by computer model simulations demonstrate that the polar auxin transport might act in parallel with the revealed WOX5-auxin feedback signaling to coordinate the auxin-dependent patterning of roots. By using independent experimental and modeling approaches, we demonstrated that WOX5 modulates the free auxin content of QC cells and that this WOX5 activity is repressed by AXR3-dependent auxin responses. The underlying feedback mechanism might mechanistically link WOX5, auxin signaling, and polar auxin transport to facilitate the auxin gradient-guided patterning of roots. We speculate that a similar mechanism might be involved in the auxin-dependent patterning of shoots, because WOX5 belongs to the conserved family of plant stem cell regulators. Recently, *WOX5* has been shown to be repressed by the CLE40/ACR4 signaling cascade derived from the columella cells (De Smet *et al*., 2008; Stahl *et al*., 2009). It will be interesting to see how this additional layer of regulation can be integrated into our model.

5.7 EXPERIMENTAL METHODS

5.7.1 PLANT MATERIALS AND GROWTH CONDITIONS

Published transgenic and mutant lines: *wox5-1*, *35S::WOX5-GR* (Sarkar *et al.*, 2007), *WOX5::ERGFP* (Xu *et al.*, 2006), *DR5rev::GFP* (Friml *et al.*, 2003), *axr3-1 (*Sabatini *et al., 1999)*, *35S*:*VP16-IAA17mImII (*Li *et al., 2009), PIN3::PIN3::GFP (*Dello Ioio *et al., 2008), DR5::GUS* (Ulmasov *et al.*, 1997). The *wox5 axr3*, double mutant was generated by crossing *wox5-1* with *axr3-1*. *DR5::GUS 35S::WOX5-GR* was generated by crossing *DR5::GUS* with *35S::WOX5-GR*. *DR5rev::GFP/wox5* and *DR5rev::GFP*/*35S*:*VP16-IAA17mImII* were generated through crossing *DR5rev::GFP* with *wox5-1* or *35S*:*VP16-IAA17mImII.* Seeds were surface sterilized with chlorine gas and incubated for 3 days after being plated onto Murashige and Skoog (MS) medium before transferred to a growth room with 16 LL/8 DD at 19°C for 5 days.

5.7.2 PHENOTYPE ANALYSIS

Starch granules in root tips were stained with Lugol's solution for 1-2 minutes then mounted onto the slides with chloral hydrate and checked them immediately. Histochemical analysis of β-glucuronidase (GUS) activity was carried out by incubation of seedling roots in GUS staining solution [0.05 M $NaPO_4$ buffer (pH 7.0), 5 mM $K_3Fe(CN)_6$, 5 mM $K_4Fe(CN)_6$, 10 mM X-glucuronide at 37°C until blue staining was visible, followed by two washes in distilled water and mounting in 70% (w/v) chloral hydrate, 10% (v/v) glycerol for microscopy. Image acquisition was carried out with an Axiocam HR camera attached to a Olympus microscope. For confocal microscopy images, Zeiss LMS 510 or Olympus FV10 ASW confocal scanning microscopes were used. Counterstaining of cell walls was achieved by mounting seedling roots in 10 μM propidium iodide.

5.7.3 IMMUNODETECTIONS

The antibodies were diluted as follows: rabbit anti-PIN1 (1:1000), rabbit anti-PIN2 (1:1000; generously provided by C. Luschnig) , Cy3 488-conjugated secondary anti-mouse (1:600; Dianova and Sigma).

5.7.4 FREE IAA MEASUREMENTS

Free IAA contents were quantified as described (Pollmann *et al.*, 2009). For the extraction of plant metabolites, three samples (replicates) of each were incubated at 60 °C under constant shaking over 1 hr in 1 ml methanol supplemented with 30 pmol of $[^2H]_2$-IAA (internal standard). Supernatants and residual plant material was separated by centrifugation, and the cell-free extracts dried under vacuum. Residues were dissolved in

30 µl methanol to which 200 µl diethyl ether was added. If necessary, dissolving was forced by ultrasonic treatment (Sonorex RK510S, Bandelin, Berlin, Germany). Particle-free samples were then loaded onto a custom-made micro-scale aminopropyl solid-phase extraction cartridge. Columns were washed with 250 µl of $CHCl_3$:2-propanol, 2:1 (v/v), and IAA containing fractions then eluted with 400 µl acidified diethyl ether (2% acetic acid (v/v)). Eluates were dried, re-dissolved in 20 µl methanol, and finally derivatized by treatment with 100 µl ethereal diazomethane. Thereafter, samples were transferred into autosampler vials, dried under a gentle stream of nitrogen, and taken up in 15 µl of chloroform. For IAA quantification, 1 µl of the methylated samples was injected into the GC-MS system. The spectra were recorded on a Varian Saturn 2000 ion-trap mass spectrometer coupled with a Varian CP-3800 gas chromatograph (Varian, Walnut Creek, CA, USA). Separation of compounds was achieved by chromatography on a ZB-50 fused silica capillary column (Phenomenex, Torrence, CA, USA). The mass spectrometer was used in CI-MRM positive ion detection mode with methanol as the reactant gas. The setting for endogenous IAA was as follows: IAA m/z = 190 $[M+H]^+$, 0.50 V. In a second channel using the same excitation amplitude, the $[^2H]_2$-IAA standard was analysed. Here, the setting for the parent ion was: $[^2H]_2$-IAA m/z = 192 $[M+H]^+$. The amount of endogenous IAA in the samples was calculated from the signal ratio of the unlabelled over the stable isotope-labelled mass fragment observed in the two analysed channels.

5.7.5 QUANTITATIVE PCR ANALYSIS

RNA was extracted with the RNeasy kit (Qiagen). Poly(dT) cDNA was prepared from total RNA 5 day old seedlings. Superscript III reverse transcription (Invitrogen) and quantification were done on an LightCycler 480 apparatus (Roche Diagnostics) with the SYBR Green I Master kit (Roche Diagnostics) according to the manufacturer's instructions. All individual reactions were done in triplicate. Data were analyzed with qBase (Hellemans *et al.*, 2007). Expression levels were normalized to those of TUBULIN, which showed no clear systematic changes in Ct value. The primers used to quantify gene expression levels are described in Supplemental Table 1.

5.8 COMPUTATIONAL METHODS

5.8.1 COMPUTER SIMULATIONS

The cellular grid tissue template for the model was created using the version of VV (Vertex-Vertex) programming language (Smith *et al.*, 2003) and and the L-system-based modeling software L-studio (Karwowski and Prusinkiewicz, 2004)(http://algorithmicbotany.org/lstudio) The simulations were done by numerical computations of coupled ODE systems, with an adaptive-size, fifth-order Runge-Kutta method. All figures were processed

in Adobe Illustrator. Figure 4 and Supplementary Figures 6-10 demonstrate the outcome from model simulations.

5.8.2 MATHEMATICAL DESCRIPTION

In the computer model, each cells consists of two compartments, namely the cytoplasm and the plasma membrane (Figure 4A). The plasma membrane was divided into four discrete fragments, each associated with one side of the cell. Non-polar cell-to-cell auxin transport was modeled as follows:

$$\frac{dAUXIN_i}{dt} = \frac{1}{V_i} \cdot \left\{ \phi + p_{IAAH} \cdot \sum_{j \in N_i} l_{i->j} \cdot (AUXIN_j - AUXIN_i) \right\} - \mu \cdot AUXIN_i \quad (1)$$

where $AUXIN_i$ and $AUXIN_j$ are mean auxin concentration in the cytoplasm of *i*-th cell. V_i and $l_{i->j}$ are *i*-th cell volume and crossing areas between *i*-th cell and adjacent *j*-th cells, respectively. The parameter P_{IAAH} represents plasma membrane permeability for non-polar auxin transport. The parameter Φ is the auxin source term (auxin influx to the root meristem; Figure 4A) and parameter μ is auxin sink (auxin efflux from the root via epidermis; Figure 4A). To account for realistic root tissue layout, cell length varies along main root axis (60 µm, 30 µm, 20 µm). Also differences in the cell width are incorporated in our model: 30 µm for root epidermis and QC cells, 25 µm for cortex and endodermis cells and 15 µm for vascular cells (Figure 4A).
The PIN-dependent polar auxin transport was modeled as follows:

$$\frac{dAUXIN_i}{dt} = \frac{1}{V_i} \cdot \left\{ p_{PIN} \cdot \sum_{j \in N_i} l_{i->j} \cdot \left(\frac{AUXIN_j}{1 + AUXIN_j} - \frac{AUXIN_i}{1 + AUXIN_i} \right) \right\} \quad (2)$$

where P_{PIN} controls PIN-dependent auxin transport across the plasma membrane. We assumed a similar expression strength for PIN1, PIN2 and PIN3 and PIN4 by setting P_{PIN} to its typical value of 20 (μms^{-1}) (Goldsmith *et al.*, 1981; Swarup *et al.*, 2005; Kramer *et al.*, 2007; Grieneisen *et al.*, 2007) but to account for weaker lateral PIN2 polarization that is restricted to cortex and endodermis cells, P_{PIN} was set to 10 (μms^{-1}) by default. Additionally, we assumed that polar auxin transport mediated by PIN proteins is saturated (1 µM concentration) (Goldmith *et al.*, 1981; Mitchison, 1980).

In the model, endogenous WOX5 expression was spatially restricted to QC root cells (Sarkar *et al.*, 2007; Ding *et al.*, 2010). We modeled an auxin-mediated repression of WOX5 transcription (Ding *et al.*, 2009) as follows:

$$\frac{dWOX5_{QC}}{dt} = \alpha_{WOX} \cdot (\frac{1}{1 + K_A \cdot AUXIN_{QC}}) - \delta_{WOX} \cdot WOX5_{QC} \quad (3)$$

where $WOX5_{QC}$ represents WOX5 levels in the QC cells. The parameters α_{WOX} and δ_{WOX} describe the basal rates of WOX5 transcription. $AUXIN_{QC}$ is mean auxin concentration in QC root cell. The parameter K_A defines the strength of WOX5 repression by auxin. Similarly, WOX5-depenent feedback up-regulation of free auxin levels (deconjugation/ production) in QC cells was described by the following equation:

$$\frac{dAUXIN_{QC}}{dt} = \beta_{WOX} \cdot (\frac{WOX5_{QC}}{1 + K_{WOX} \cdot WOX5_{QC}}) \quad (4)$$

where β_{WOX} defines the rate of WOX5-dependent free auxin deconjugation and K_{WOX} is the saturation constant.

5.8.3 LOCAL AUXIN GRADIENT AND STEM CELL MAINTENANCE

To connect the local auxin gradient in the root tip to the pattern of DSC niche, we developed the linear formula that utilizes the slope of this gradient and the actual auxin concentration of columella cells laying beneath the QC region:

$$SCT = a \cdot AUXIN_i$$
$$a = \frac{AUXIN_{QC} - \min\{AUXIN_i\}}{\min\{AUXIN_i\}^2} \quad (5)$$

where, a is the slope of auxin gradient between QC cells and the most distal columella cells measured along the y-axis. $AUXIN_{QC}$ is the auxin concentration in QC cell and $AUXIN_i$ is the auxin concentration in columella cell, respectively.
If SCT (stem cell threshold) for a given columella cell is larger than a fixed threshold value (THR) then this cell does not differentiate and keeps its stem cell identity.
We used the THR value of 3 in all model simulations that resulted in the observed patterns of stem cells (Figure 4B-4E; Figure 3D-3F).

5.8.4 PARAMETER SENSITIVITY

The model sensitivity was analyzed with respect to the variation of some critical parameters, that were crucial for WOX5-auxin feedback regulation (K_A, K_{WOX}, δ_{WOX}) and polar auxin transport (P_{PIN}). In general we found the model was qualitatively robust.

For more details on this analysis we refer to Supplementary Figures 6-10. All model parameter used in model simulations are listed in Supplementary Table 2.

5.9 SUPPLEMENTARY TABLES

Supplementary Table 1 Primers for q-PCR analysis

TUBF: ACTCGTTGGGAGGAGGAACT
TUBR: ACACCAGACATAGTAGCAGAAATCAAG
IAR3F: AGGCAAGCGAGCGTGAAT
IAR3R: GCATGAAGGGAAGCACCATAA
ILR1F: GCGGAAGCGATGATTGGA
ILR1R: TGGCTATGACCATGTTCGTCC
ILL1F: CGATGCCACCAACTGTGAAC
ILL1R: TGGTGAATGAGACGACGCATA
ILL2F: CCAATGCCACCAACAGTGAA
ILL2R: CCGTACGGAAGCACATCCTC
DFL1F: ACACGCCAATTCCTCCCTC
DFL1R: CCATTGCTTGTGACCAGGG

Supplementary Table 2 Model parameters

Parameter	**Figure 4B**	**Figure 4C**	**Figure 4D**	**Figure 4E**	**Supp Fig 6**	**Supp Fig 7**	**Supp Fig 8**	**Supp Fig 9**	**Supp Fig 10**	**units**
p_{IAAH}	10	10	10	10	10	10	10	10	10	μms^{-1}
p_{PIN}	20	20	20	20	1 (PIN1 vascular); 1 (PIN2 cortex, endodermis, epidermis);	20	20	20	20	μms^{-1}
$p_{PIN\ (lateral)}$	10	10	10	10	10 ; 1 (PIN2 cortex, endodermis, epidermis);	0; 20	10	10	10	μms^{-1}
α_{WOX}	1	0	1	1	1	1	1	1	1	s^{-1}
δ_{WOX}	0.01	0	0.01	0.1	0.01	0.01	0.01	0.01	1	s^{-1}
K_A	2	0	0.2	200	2	2	0.2; 20	2	2	μM
β_{WOX}	0.06	0	0.15	0.06	0.06	0.06	0.06	0.06	0.06	s^{-1}
K_{WOX}	1	0	1	1	1	1	1	0.1; 10	1	μM
Φ	0.3	0.3	0.03	1	0.3	0.3	0.3	0.3	0.3	μMs^{-1}
μ	1	1	1	1	1	1	1	1	1	s^{-1}

5.10 SUPPLEMENTARY FIGURES

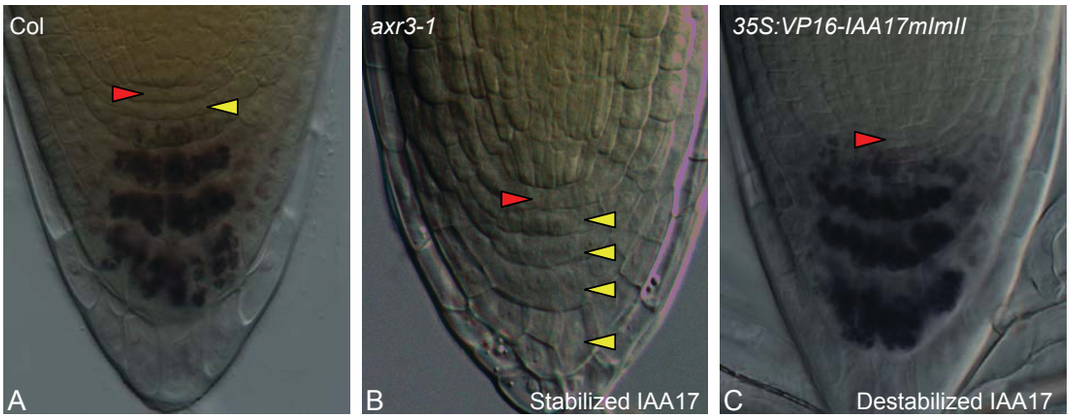

Supplementary Figure 1 IAA17 is crucial for root distal stem cells (DSCs) differentiation

Differentiation status of DSCs (yellow arrowhead) below the QC (red arrowhead) in 4-day-old seedlings as inferred from the lugol staining. Wild-type roots show typically one tier of DSCs **(A)**, *axr3-1* defects in DSC differentiation as revealed by multiple tiers of DSCs **(B)**, and *35S:VP16-IAA17mI* terminal DSC differentiation **(C)**.

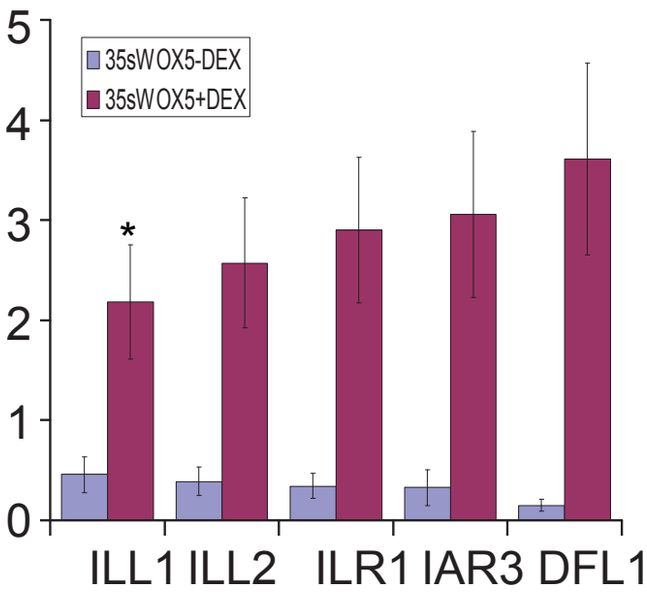

Supplementary Figure 2 IAA deconjugation related genes induced in 35S::WOX5-GR after DEX treatment

IAA deconjugation-related genes expression was analyzed by Q-PCR analysis. Tubulin was used as the relative control. RNA was isolated from roots of 5-day-old *35S::WOX5-GR* seedlings with and without DEX induction. Error bars represent standard errors (Student's *t* test, * $P < 0.05$). The experiment was repeated twice with similar results.

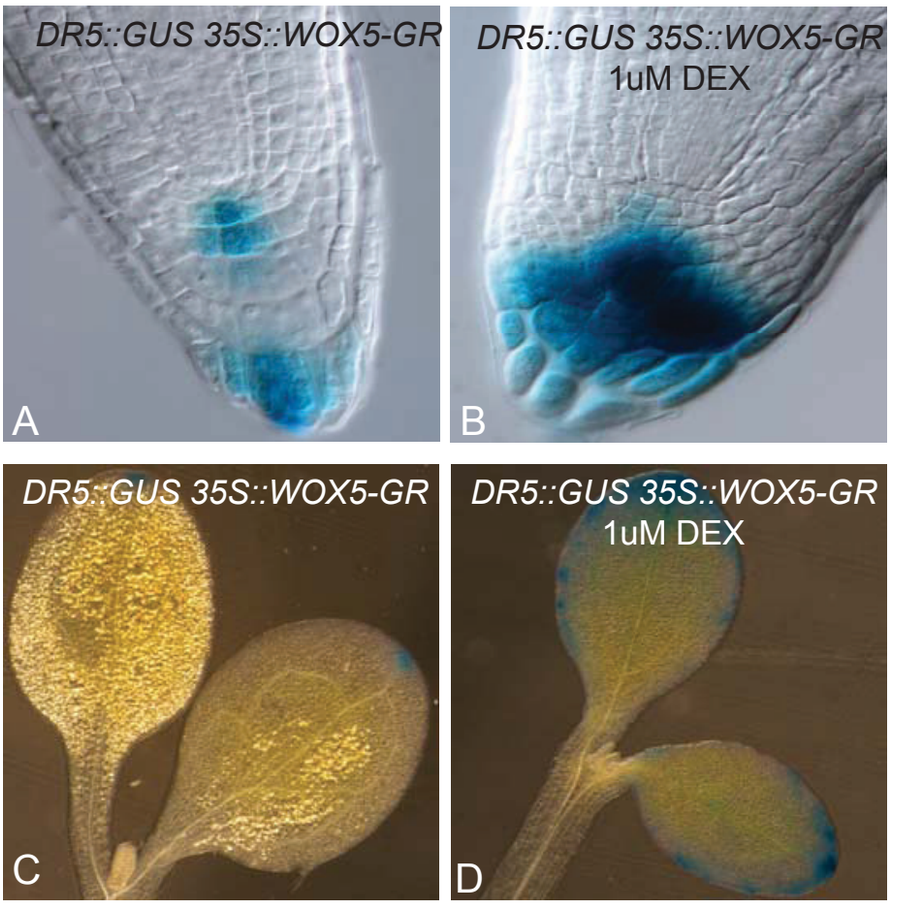

Supplementary Figure 3 Increased auxin signalling in 35S::WOX5-GR after DEX induction shown by expression of *DR5::GUS* auxin response reporter was increased in *35S::WOX5-GR* after 1uM DEX induction **(B,D)** as compared to noninduced controls **(A,C)**.

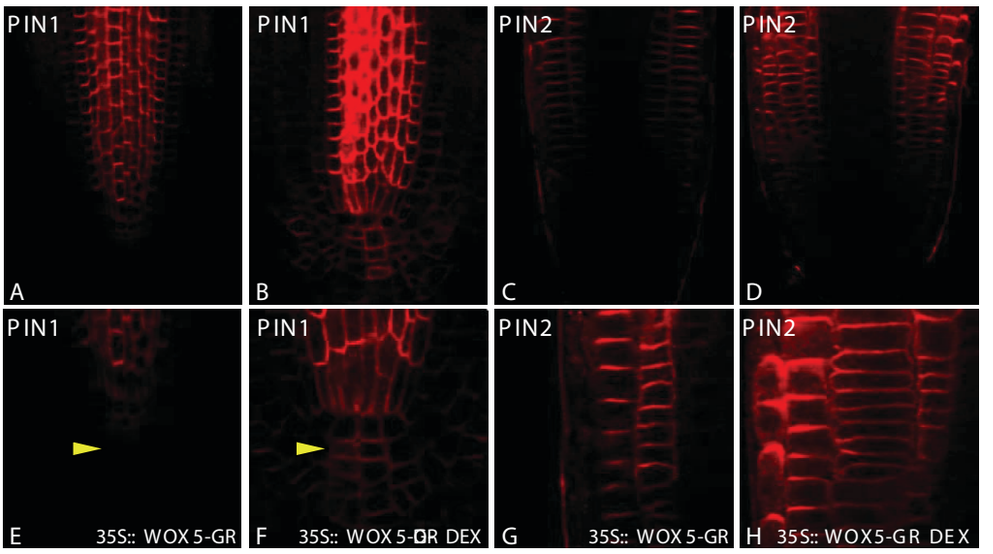

Supplementary Figure 4 PIN1 and PIN2 expression in 35S::WOX5-GR after DEX inductions

Immunostaining was done with anti-PIN1 and anti-PIN2 antibody with 4 day old *35S::WOX5-GR* seedlings with 1uM DEX **(A, C, E and G)** and without DEX induction **(B, D, F and H)**. The PIN1 and PIN2 proteins had normal localization patterns after the induction of WOX5. The increased PIN1 and PIN2 signals might be result from the higher auxin level in *35S::WOX5-GR* seedlings.

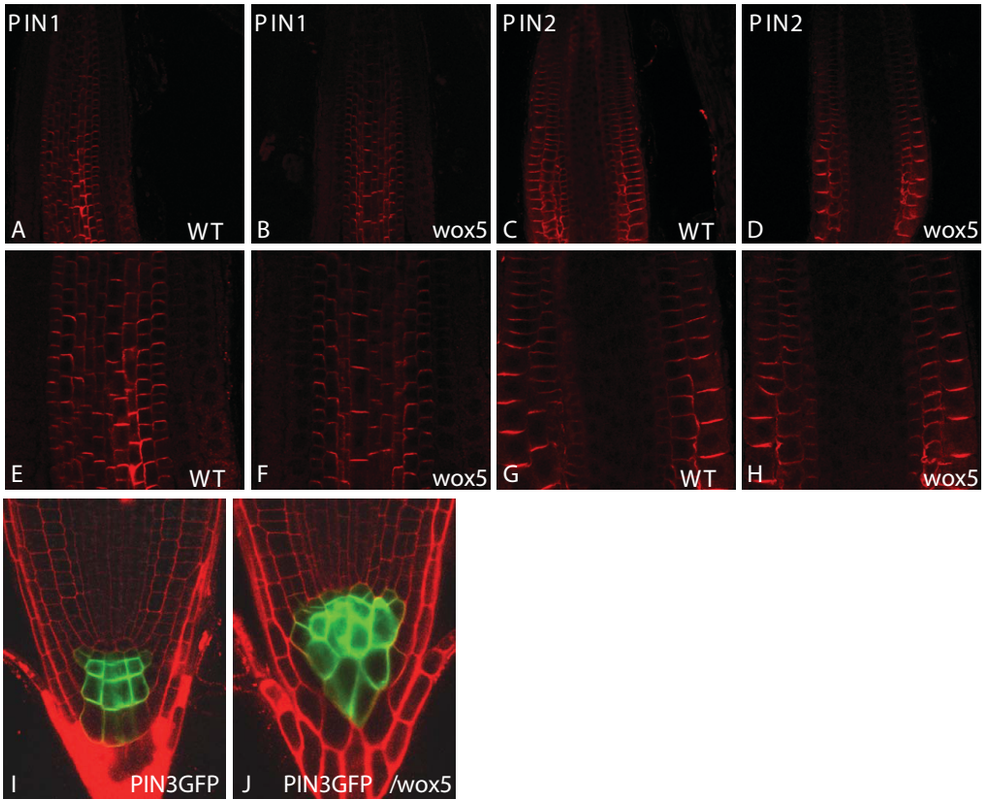

Suppplementary Figure 5 PIN protein analysis in wox5

PIN1 and PIN2 expression was analyzed in wild-type **(A, C, E and G)** and *wox5* **(B, D, F and H)** by im-

munostaining with anti-PIN1 and anti-PIN2 antibodies. PIN3::PIN3::GFP in WT **(I)** and *wox5* **(J)**. PIN1, PIN2 and PIN3 have normal localization patterns in *wox5* compared to those of wild-type controls.

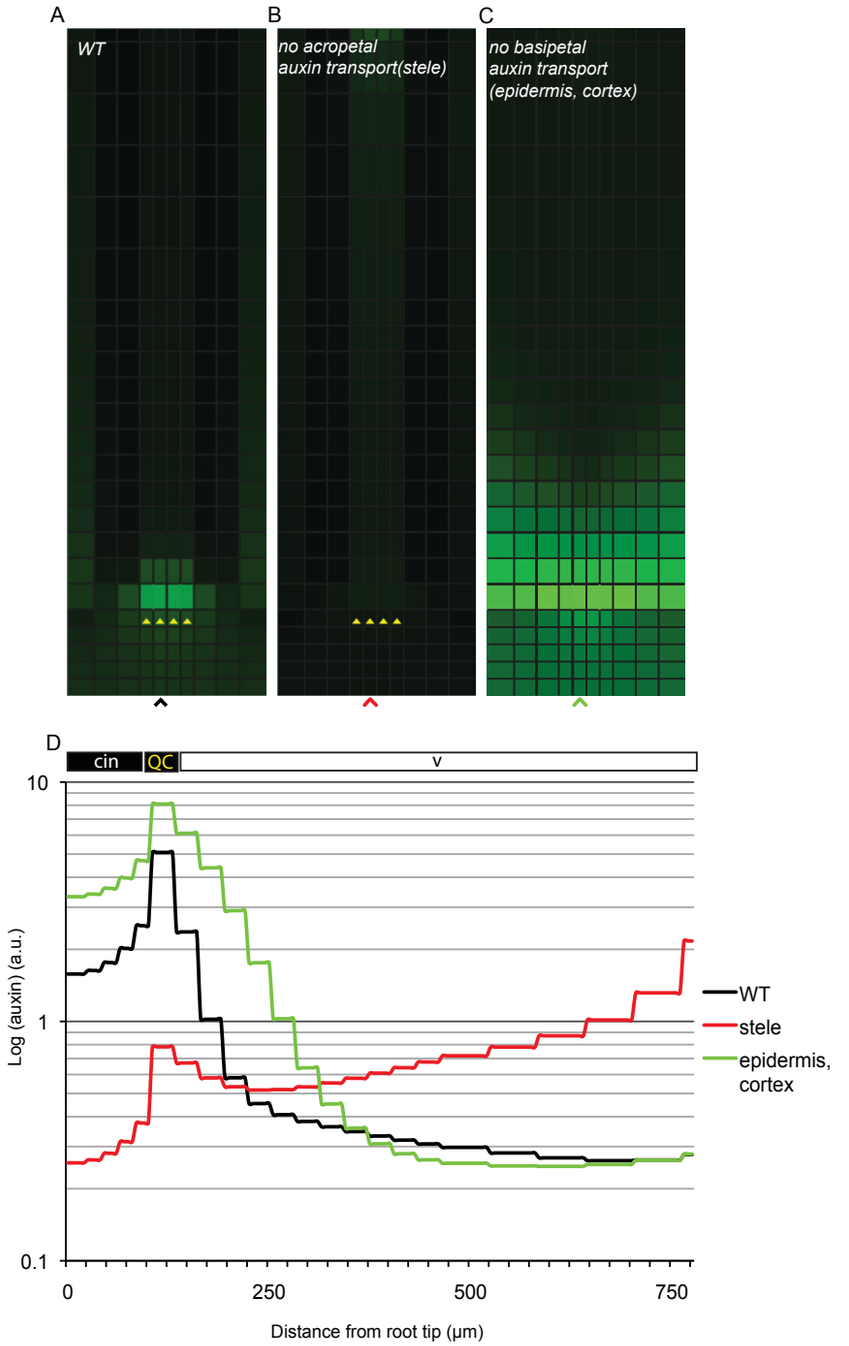

Supplementary Figure 6 Computer model sensitivity with respect to manipulations of the polar auxin transport

(A-C) Results of model manipulations: control situation (A), (B, C) the removal of acropetal auxin flow (pin1) (B) or basipetal auxin flow (pin2) (C) *in silico* mutants. **(D)** Steady state auxin concentration profiles illustrating that the auxin gradients between QC cells and columella initials (cin) are qualitatively robust with respect to various manipulations in the polar auxin transport mechanism. However, the quantitative auxin pattern in the root tip was disturbed in both acropetal auxin flow (pin1) (B) or basipetal auxin flow

(pin2) (C) *in silico* mutants. Color coding scheme and symbols are as in Figure 4A.

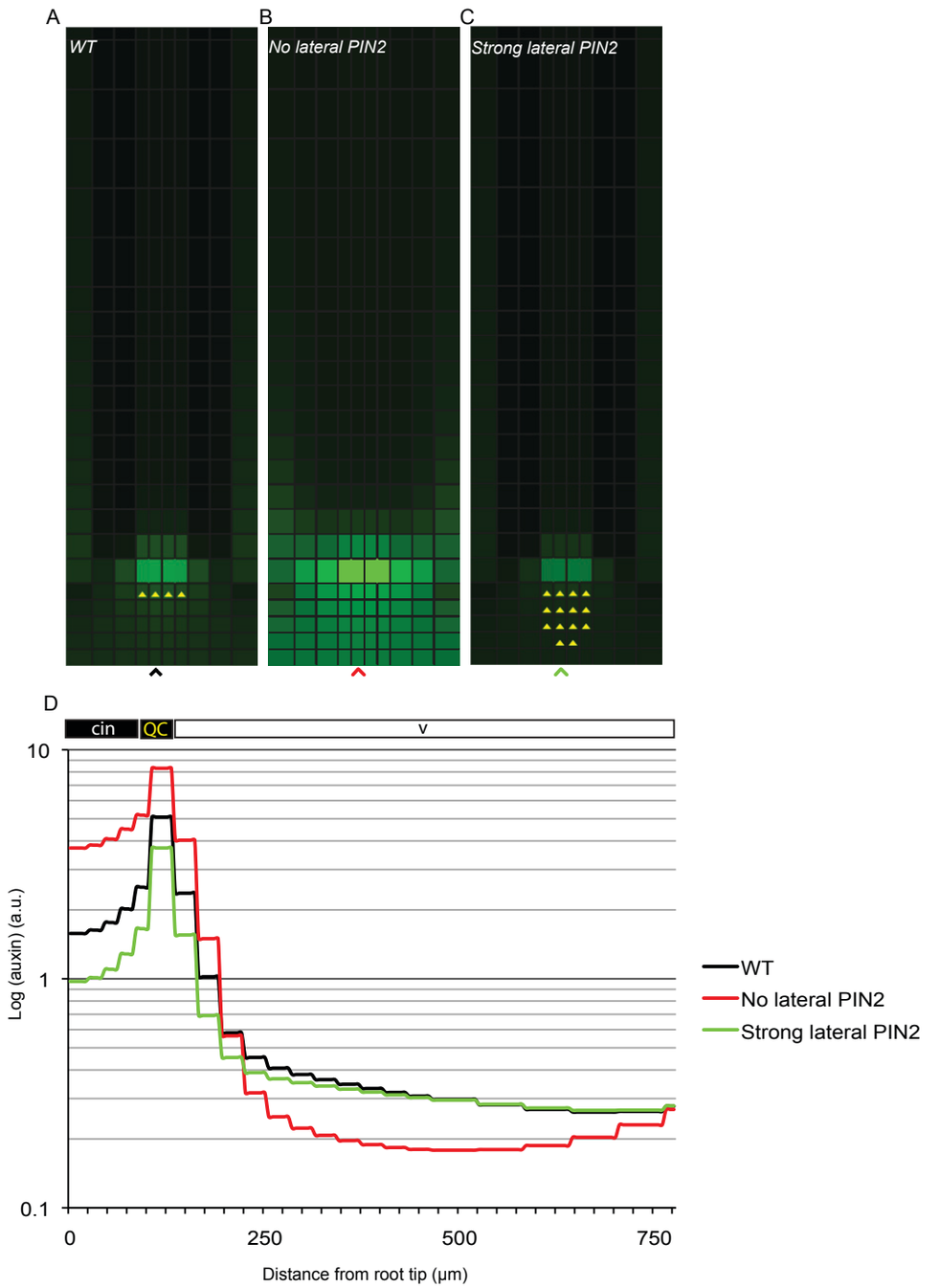

Supplementary Figure 7 The role of PIN2 lateralization in cortex and endodermis

(A) The control simulation with by default weak PIN2 lateralization in cortex and endodermis. **(B-C)** Simulations of the model without lateral PIN2 polarization predicting the more broad auxin maximum as compared to that of control simulations (A). Interestingly, the model with strong PIN2 lateralization in cortex and endodermis predicts a sharp auxin maximum in QC cells (C). **(D)** The steady state auxin concentration profiles illustrating that auxin gradients between QC cells and columella are robustly maintained either in the presence or absence of lateral PIN2 polarization in cortex and endodermis. Color cod-

ing scheme and symbols are as for auxin concentrations is the same as in Figure 4.

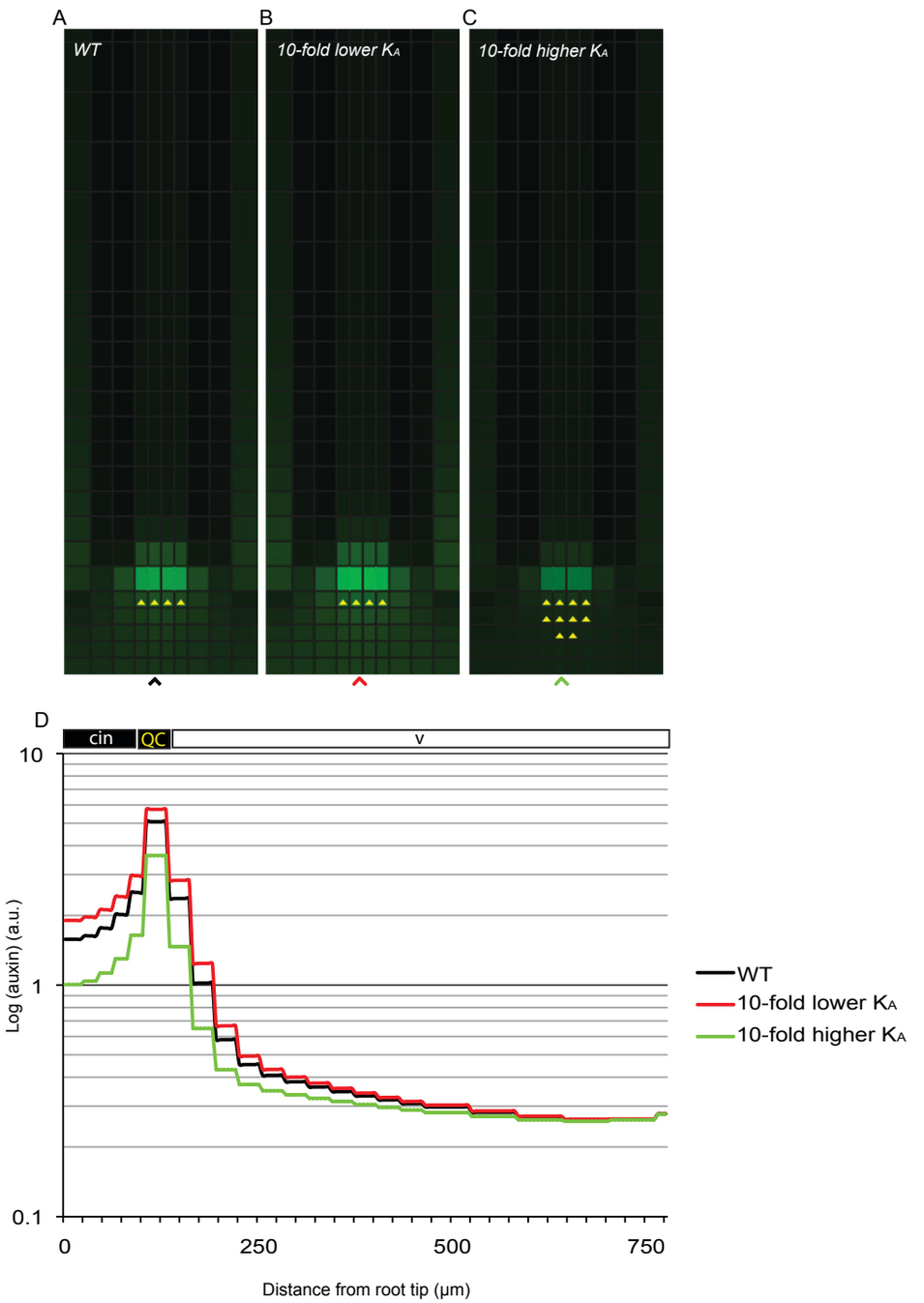

Suppplementary Figure 8 Model robustness with respect to the auxin-mediated repression of WOX5 **(A)** The control simulation with default value of K_A (eq. 3, Supplementary Table 2). **(B-D)** Simulations of the model with either a 10-fold decrease (B) or a 10-fold increase (C) in value of K_A were virtually similar to those of the control model (A). (D) The steady state auxin concentration profiles illustrating the maintenance of steep auxin gradients between QC cells and columella that are crucial to pattern the stem cell niche. Color coding scheme and symbols are as in Figure 4.

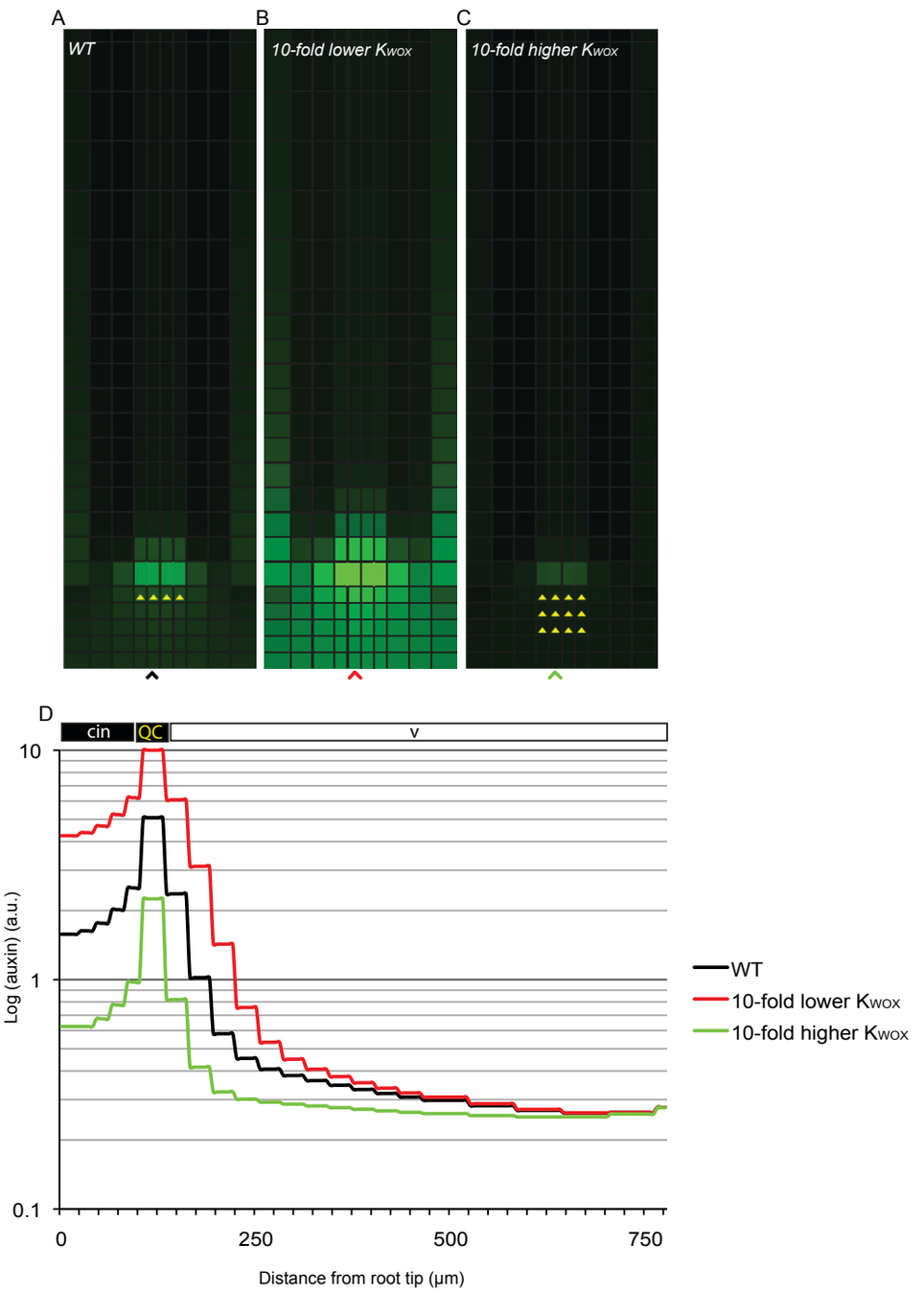

Supplementary Figure 9 *In silico* testing of WOX5-dependent regulation of free auxin levels

(A) The control simulation with default value of K_{WOX} (eq. 4, Supplementary Table 2). **(B-D)** Simulations of the model with either a 10-fold decrease (B) or a 10-fold increase (C) in value of K_{WOX} showing either decrease or elevation of auxin levels along the whole root meristem. (D) Auxin concentration profiles display the maintenance of steep auxin gradients in the root (C). Color coding scheme and symbols are as in Figure 4.

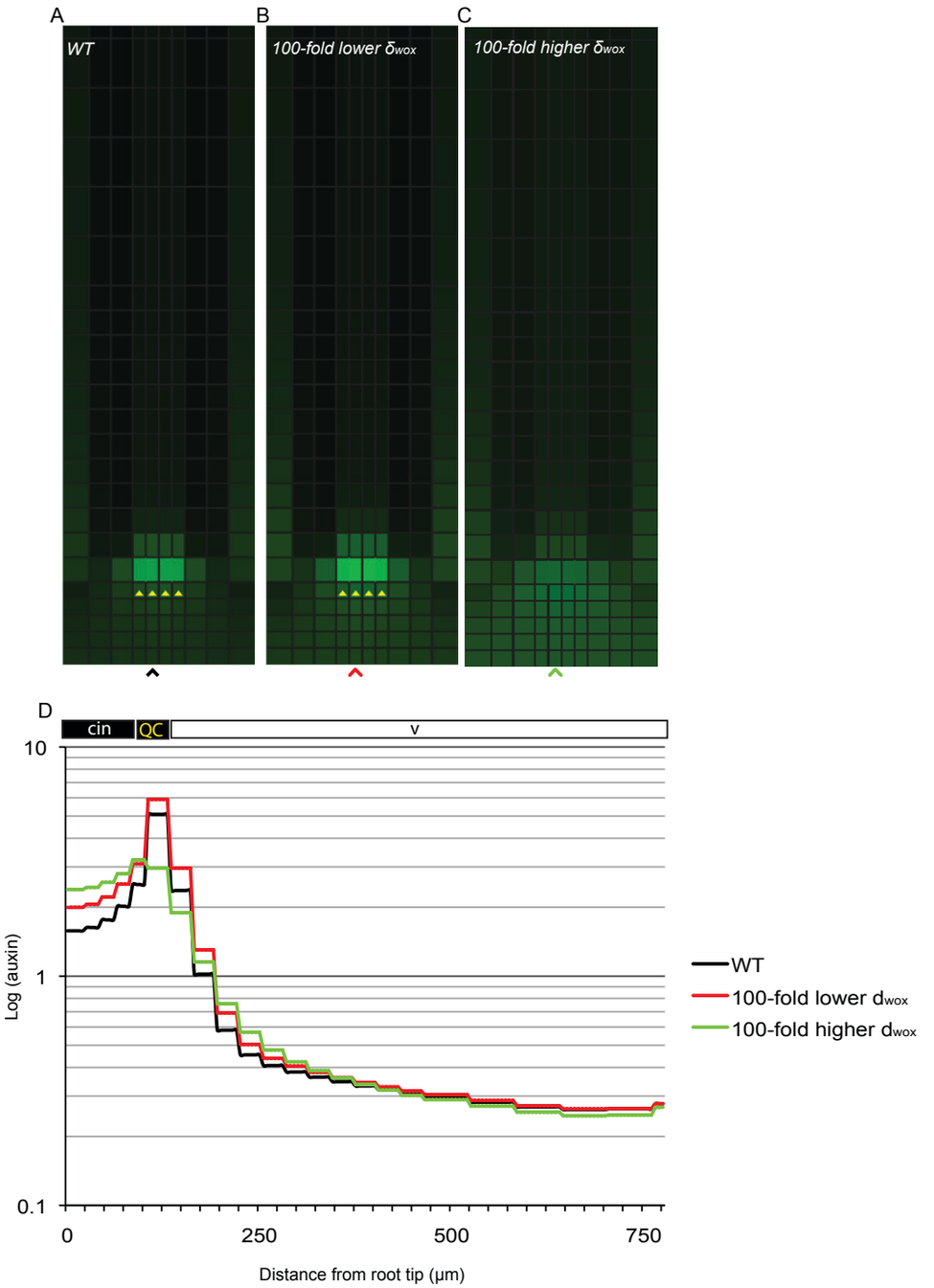

Supplementary Figure 10 *In silico* testing of auxin-independent repression of WOX5 activity

(A) The control simulation with default setting of WOX5 degradation (δ_{WOX}) (eq. 3, Supplementary Table 2). **(B)** Simulations of the model with either a 100-fold decrease of δ_{WOX} (B). **(C-D)** A 100-fold increase in δ_{WOX} resulting in severely reduced auxin gradient between QC cells and columella similar to that from the *wox5* mutant simulation (Figure 4C and 4F), suggesting that negligible levels of *WOX5* expression (analogous to the *wox5* mutant) might have a strong impact on the maintenance of the auxin maximum in the QC and stem cell differentiation pattern (Figure 2) and, thus proper patterning of the root (Figure 3). Color coding scheme and symbols are as in Figure 4.

5.11 SUPPLEMENTARY MOVIES

Supplementary Movie 1
The file contains Supplementary Movie 1 displaying the simulation of Figure 4B (*in silico* WT root). Color coding scheme used in the model simulations is as presented in Figure 4A.

Supplementary Movie 2
The file contains Supplementary Movie 2 displaying the simulation of Figure 4C (*in silico* wox5 mutant). Color coding scheme used in the model simulations is as presented in Figure 4A.

Supplementary Movie 3
The file contains Supplementary Movie 3 displaying the simulation of Figure 4D (*in silico axr3-1* mutant). Color coding scheme used in the model simulations is as presented in Figure 4A.

Supplementary Movie 4
The file contains Supplementary Movie 4 displaying the simulation of Figure 4E (*in silico 35S:VP16IAA17mImII* mutant). Color coding scheme used in the model simulations is as presented in Figure 4A.

ACKNOWLEDGEMENTS

We acknowledge Ben Scheres, Thomas Laux and Tom J. Guilfoyle for sharing published materials, Eva Benková for helpful discussions, Jürgen Kleine-Vehn and Xu Chen for critical reading of the manuscript, and Martine De Cock for help in preparing it. This work was supported by grants from the Research Foundation-Flanders (Odysseus and project no. 3G006507 to W.G.) and the EMBO Young Investigator Program to J.F., from DFG-SFB480/A-10 to S.P., and from Swiss National Science Foundation (Grant Nr. 31003A-125001) to M.G. S.V. is a postdoctoral fellow of the Research Foundation-Flanders.

Chapter 6

Conclusions and perspectives

The combination of computational modeling and experimental studies presented in this thesis addresses classical and emerging problems underlying the feedback regulation in auxin-driven plant development. Through multi-scale (molecular, cellular and tissue levels) models that integrate state-of-the-art experimental data and local feedback mechanisms, one could explore and comprehend seemingly unrelated processes such as subcellular dynamics and intercellular communication, and thus capture the essential principles of pattern formation in plants.

In the summarizing discussion of this thesis I will bridge the gap between different modeling studies performed herein by pinpointing common regulatory principles as well as evolutionary insights into the modeled mechanisms, and propose some of the future directions for the model design that are indicated by present and ongoing research in the area of auxin biology.

6.1 FEEDBACK-DRIVEN PIN POLARIZATION: FROM CELLS TO TISSUES

The understanding of mechanisms underlying tissue polarization in plants is one of most challenging problems in developmental biology. In plants, polar, cell-to-cell auxin transport provides means to coordinate the polarity of growth and the tissue remodeling through the establishment of local auxin gradients (Grunewald and Friml, 2010). Remarkably, auxin controls its own transport from cells by modulating both trafficking and transcription of its carrier proteins including PIN auxin efflux carrier, and AUX/LAX auxin influx carriers (Paciorek *et al.*, 2005; Chapman and Estelle, 2008; Robert *et al.*, 2010; Leyser, 2011). In **Chapter 2** of this thesis, we demonstrated that a general feedback mechanism on subcellular PIN protein dynamics could be realized locally, inside and outside of the cell by several feedback loops working in concert (**Chapter 1**; Figure 3). This local feedback regulation could involve coupled receptor-mediated signaling pathways. In the model, the hypothetical, extracellular auxin signaling largely contributes to the PIN polarity establishment through competitive utilization of extracellular auxin receptors. Subsequently, the intracellular auxin signaling is used to reinforce and ultimately maintain the PIN polarization within the tissue. However, the proposed Extracellular receptor-based polarization (ERP) model predicts the emergence of extracellular auxin gradients that, as those inside the cell, have yet not been experimentally observed (**Chapter 1**). Nevertheless, given a slow diffusion of auxin in the cell wall (Kramer *et al.*, 2007) and the compactness of the plant cell wall, the presence of auxin gradients in the cell wall might be biologically reasonable.

The novel concept for spatial perception of extracellular auxin gradients by cells provides means to locally activate signaling cues and thus transfer a globally polarizing

signal within the tissue. This could be seen as an analogy to the substrate-depletion paradigm of classical patterning mechanism in the reaction-diffusion systems (Meinhardt, 1996). In the ERP model, auxin promotes the signaling cascade for inhibition of PIN internalization (local activator) and depletes free receptors from the intercellular pools (substrate depletion). Similarly to reaction-diffusion concept the crucial requirement for patterning in the ERP model is that diffusion of activated receptors is reduced compared to the diffusion of inactive receptors (**Chapter 2**).

Recent experimental studies demonstrate that ABP1 protein could be an extracellular auxin receptor that regulates trafficking processes at the plasma membrane (Robert *et al.*, 2010; Xu *et al.*, 2010). Nonetheless, this effect is not specific for PIN proteins (as suggested by the ERP model) but applies to all plasma membrane proteins (Robert *et al.*, 2010), indicating the possibility for the general, ABP1-dependent mechanism for the regulation of protein trafficking that to be inherited through the evolution of the plant species (Tromas *et al.*, 2010; Friml and Jones, 2010). In **Chapter 3** of this thesis, we propose a plant-specific mechanism for the maintenance of PIN polarity in the plant cell. The proposed mechanism is unique to PINs and could operate in parallel to the general ABP1-dependent mechanism for the regulation of internalization of plasma membrane proteins (**Chapter 2**; Robert *et al.*, 2010). Therefore, a combined model that incorporates PIN protein recruitment, its subsequent clustering in the plasma membrane domains (**Chapter 3**) and the auxin feedback on PIN protein internalization (**Chapter 2**) could possibly explain subtle differences in the subcellular dynamics of various auxin carriers.

Interestingly, the activity of PIN auxin carriers is not restricted to the plasma membrane of the plant cell. Importantly, the PIN5 protein that is a member of the PIN protein family, has been shown to act at the membrane of Endoplasmic Reticulum (ER) to mediate auxin import into ER lumen (Mravec *et al.*, 2009), and thus largely contributing to the regulation of intracellular auxin homeostasis (Mravec *et al.*, 2009). In **Chapter 4** of this thesis, the PIN-dependent mechanism for auxin retention in the ER was proposed. Firstly, this model highlights the importance of intracellular auxin compartmentization for the regulation of free auxin levels in the cells during plant development and patterning. Secondly, it suggests how the ER-associated PIN proteins could feed back on cytosolic auxin reservoir and eventually alter both intracellular and extracellular auxin signaling cues (**Chapter 2**). To address this particular issue one would require future experimentation by combining PIN polarization models presented in **Chapters 2-3** with the ER-based auxin retention mechanism presented in **Chapter 4** into an executive model and test the feasibility of the this model for developmental patterning in plants.

6.2 LOCAL FEEDBACK LOOPS AND CELL-TYPE SPECIFIC FACTORS THAT COORDINATE PLANT DEVELOPMENT

The central focus of this thesis was given to the utilization of local feedback mechanisms and their presumably centralized role in developmental patterning of plants. However, some additional requirements for cell-specific factors have been discussed in **Chapters 3-5.** Given the great importance of feedback regulation in developmental patterning (Leyser *et al*., 2006; Benjamins and Scheres, 2008; Vanneste and Friml, 2009), one can see that cell-type specific regulators (i.e local source of hormone production or local protein expression) would also play important roles, for instance in the local coordination of feedback cues.

In **Chapter 3** of this thesis, several cell-specific regulators of PIN polarization were proposed to help in maintaining PIN polar domains at the plasma membrane. These include the spatial recruitment of proteins to the polar domains and their clustering in specific regions at the plasma membrane. Similarly, the model proposed in **Chapter 4** introduces hypothetical, most likely molecular factors that could restrict PIN protein expression to the particular domain within a given tissue. Moreover, model simulations suggest that these additional factors might be required to narrow down the facilitated auxin transport in early land plants (**Chapter 4**). Finally, in **Chapter 5** of this thesis, we illustrated that the cell-type specific expression of master regulator of root stem cell niche could feed on the auxin signaling gradients in the root tip, to ultimately regulate stem cell differentiation.

These three studies demonstrate that cell-type specific factors can play a role in restricting the feedback-dependent control of patterning processes to the selective/specialized tissues such as meristem, epidermal or vascular tissues. Given this, one might consider to integrate cell-type specific factors at different levels of regulation to increase precision and realisticity of the existing models for auxin-dependent patterning in plants.

6.3 GO BEYOND - EVOLUTIONARY INSIGHTS

The research in this thesis brings to light an important aspect of pattern adaptability in plant development through the evolution and inheritance of feedback mechanisms. In **Chapter 4**, we discussed the possible evolution of auxin transport machinery that could encompass the translocation of PIN proteins from their presumably ancestral localization at the endoplasmic reticulum (ER) to the polar domains at the plasma membrane. Next we proposed that such a mechanism could have co-evolved further in flowering plants with the co-function of the ER export and extracellular role of ABP1 in the trafficking of membrane-localized PIN proteins (**Chapter 2**). The verification of this hy-

pothesis is a fascinating subject for future research.

In **Chapter 5**, we proposed that the principles of WOX5-auxin feedback regulation involved in patterning of the root meristem could, to some degree, overlap with auxin-dependent patterning of plant shoots, since WOX5 belongs to the evolutionary conserved family of WUSCHEL transcription factors that are involved in maintenance of stem cell niches in plants (Sarkar *et al*., 2008; De Smet *et al*., 2008; Stahl *et al*., 2009). Indeed, it would be interesting to test whether the cell-type activity of WUSCHEL-like genes would serve as a general principle for maintaining local auxin gradients in roots and shoots.

In **Chapter 3** of this thesis we compared the PIN-specific mechanism for polarity in the plant cell by comparing it to known determinants of polarity in animal or yeast cells such as diffusion barriers or prominent polarity regulators (Dudu *et al*., 2004; Giepmans and van Ijzendoorn, 2009; Nelson and Beitel, 2009). We found that plant cells could compensate the lack of diffusion barriers by an alternative mechanism that involves cargo clustering in the plasma membrane domains and pronounced cargo internalization at the edges of the polar domain.

6.4 SUMMARY

To conclude: the work presented in this thesis provides several, novel and interesting insights in the auxin feedback regulation in plant development. The results of this work were gathered in a number of consecutive chapters which together illustrate that local feedbacks accompanied by cell-type-specific factors can serve as common modules for developmental patterning in plants. Moreover, this work hints on the evolvability of auxin signaling pathways and their roles in the regulation of subcellular dynamics and the coordination of cell-to-cell communication through polarized auxin transport.

Finally, this research proposes some future directions for model development and highlights a continuous need for the adaption of models to the most recent experimental data.

General remarks

CONTRIBUTION TO MANUSCRIPTS

Wabnik, K., Hvidsten, TR., Kedzierska, A., Van Leene, J., De Jaeger, G., Beemster, GT., Komorowski, J. and Kuiper, MT. (2009) Gene expression trends and protein features effectively complement each other in gene function prediction.. *Bioinformatics* **25:** 322-330.

KW and TRH and MTK initiated the project, KW designed most of the experiments and carried out most of the experiments.KW, TRH and MTK wrote the paper.

Wabnik, K.*, Kleine-Vehn, J.*, Balla, J., Sauer, J., Naramoto, S., Reinöhl, V., Merks, R.M.H., Govaerts, W., and Friml, J. (2010). Emergence of tissue polarization from synergy of intracellular and extracellular auxin signaling. *Mol. Syst. Biol* **6**: 447.

KW, JKV and JF initiated the project, KW and JKV designed most of the experiments and K.W carried out the modelling study. KW, JKV and JF wrote the paper.

Kleine-Vehn, J.*, Wabnik, K.*, Martinière, A., Tanaka, H., Willig, K., Naramoto, S., Leitner, J., Jakobs, S., Robert, S., Luschnig, C., Govaerts, W., Hell, S., Runions, J., and Friml, J. (2011). Mechanistic framework for generation and maintenance of PIN auxin efflux carrier polarity in plant cells, *under review.*

JKV and JF and KW initiated the project, KW and JKV designed most of the experiments and K.W carried out the computational part of this work. JKV, KW and JF wrote the paper.

Wabnik, K., Govaerts, W., Friml, J. and Kleine-Vehn, J., (2011). Feedback models for polar auxin transport: an emerging trend, *Molecular BioSystems, DOI:10.1039/C1MB05109A.*

KW and JKV and JF prepared and wrote the manuscript.

Wabnik, K.*, Kleine-Vehn, J.*, Govaerts, W., and Friml, J. (2011). Prototype cell-to-cell auxin transport mechanism by intracellular auxin compartmentization, *Trends in Plant Science, DOI: 10.1016/J.TPLANTS.2011.05.002.*

KW and JKV initiated the project, KW and JKV designed most of the experiments and carried out most of the experiments. KW, JKV and JF wrote the paper.

Ding, Z.*, Wabnik, K*., Pollemann, S., Govaerts, Vanneste, S., W., Geisler, M., and Friml, J. (2011). WOX5-auxin feedback modulates auxin gradient-guided patterning of the *Arabidopsis* root, *under review.*

ZD, KW and JF initiated the project, ZD and KW designed most of the experiments and K.W carried out the computer modeling experiments. ZD, KW and JF wrote the paper.

* Equal contributions

COMMONLY USED ABBREVIATIONS

ABP auxin binding protein 1
ARF Adenosyl ribosylation factor
AUX1 AUXIN-RESISTANT1
AXR3 AUXIN RESISTANT3/IAA17
BFA Brefeldin A
CLC clathrin light chain
DSC distal stem cells
ER Endoplasmatic reticulum
ERP Extracellar receptor-based polarization
FRAP Fluorescence recovery after photobleaching
GEF Guanine nucleotide exchange factor
GFP GREEN FLUORESCENT PROTEIN
GH Generalized-Hopf bifurcation
GUS Glucuronidase
H Andronow-Hopf bifurcation
HH Double-Hopf bifurcation
IAA Indolacetic acid
LAX LIKE-AUX1
LP Limit point
LPC Limit point cycle
LTI6 LOW-TEMPERATURE-INDUCED6b
MDR multiple drug resistance/P-glycoproteins
NAA Naphthalenacetic acid
1-NOA 1-naphthoxy acetic acid
NPA 1-N-naphtylphtalamic acid
ODE Ordinary differential equations

PGP phosphoglycoprotein
PI Polarization Index
PID PINOID
PIN PIN-FORMED
PIP2 PLASMA MEMBRANE INTRINSIC2
PM Plasma membrane
PMA4 H+-ATPase
PP2A PP2A-1 protein serine/threonine phosphatase
PpPIN *Physcomitrella patens* PIN
QC Quiescent centre
SA Signaling Asymmetry
SCFTIR1 Skp1, cdc53p/cullin, F-box protein TIR1
STED sub-diffraction resolution microscopy
TIR1 TRANSPORT INHIBITOR RESPONSE 1
TIBA 2,3,5-triiodobenzoic acid
WOX5 WUSCHEL-RELATED HOMEOBOX 5
VAEM Variable angle epifluorescence microscopy
YFP YELLOW FLUORESCENT PROTEIN
ZH Zero-Hopf bifurcation

CURRICULUM VITAE

PERSONAL INFORMATION

Name:	Krzysztof Teodor Wabnik
Date of birth:	25.12.1982
Place of Birth:	Gliwice
Nationality:	Polish

EDUCATION

1989-1996	Elementary school and gimnasium no. 5, Gliwice
1997-2001	High School no. 2 im. Wrobleskiego, Gliwice (mathematcis and computer science)
2001-2006	Master of Science, Silesian University of Technology, Gliwice (Automatics and Robotics, Engineering)
2007-2011	PhD student at Ghent University (Biotechnology), Gent, Belgium
since 2009 VIB,	Member of Auxin group, Plant Systems Biology Department, Univeristy of Gent, Belgium

STUDY ABROAD

02/2006-	Socrates/Erasmus student at University of Gent (Bioinformatics)
06/2006	Exchange project (3 months), Computation Biology Group, VIB
06/2007	Visiting student, The Linnaeus Centre for Bioinformatics Uppsala University, Sweden
07/2010	Visiting student, The Biological Modeling and Visualization research group, Department of Computer Science, Univeristy of Calgary, Calgary, Canada

FUNDINGS

2007-2009	ECT* Marie Curie fellowship
2009-2011	The Research Foundation Flanders (FWO) project no. 3G006507

INVITED SPEECH

10/2009	Seminar lecture in Plant Physiology, Department of Biology, Plant Science, IPS Institut für Pflanzenwissenschaften Universität Bern, Switzerland Title: "A unifying model for cell and tissue polarisation predicts extracellular perception of auxin gradient"
07/2009	Auxins and Cytokinins in Plant Development - International Sym posium. Prague, Czech Republic (ACPD) Title:"Modelling of positive-feedback mechanism for auxin carrier polarization during auxin-dependent plant development"
04/2009	PepCon 2009, Seul, South Korea Title: "Gene Expression Profiles and Protein Features Effectively Complement Each Other in Gene Function Prediction"

CONFERENCE POSTERS

06/2008	7th ESMTB Conference, Edinburgh, Scotland Title:"Predicting cell cycle control genes using integrative bioinfor matics"
03/2009	CSHL Meeting, Computational Cell Biology Title:"Modeling PIN polarization for auxin canalization and accumulation"

PUBLICATIONS

Ding, Z., Wabnik, K., Pollemann, S., Govaerts, Vanneste, S., W., Geisler, M., and Friml, J. (2011). WOX5-auxin feedback modulates auxin gradient-guided patterning of the *Arabidopsis* root, under review.

Kleine-Vehn, J., Wabnik, K., Martinière, A., Tanaka, H., Willig, K., Naramoto, S., Leitner, J., Jakobs, S., Robert, S., Luschnig, C., Govaerts, W., Hell, S., Runions, J., and Friml, J. (2011). Mechanistic framework for generation and maintenance of PIN auxin efflux carrier polarity in plant cells, under review.

Wabnik, K., Kleine-Vehn, J., Govaerts, W., and Friml, J. (2011). Prototype cell-to-cell auxin transport mechanism by intracellular auxin compartmentization, *Trends in Plant Science*, DOI: 10.1016/J.TPLANTS.2011.05.002.

Wabnik, K., Govaerts, W., Friml, J., Kleine-Vehn, J., (2011). Feedback models for polar auxin transport: an emerging trend, *Molecular BioSystems, DOI:10.1039/C1MB05109A*.

Wabnik, K., Kleine-Vehn, J., Balla, J., Sauer, J., Naramoto, S., Reinöhl, V., Merks, R.M.H., Govaerts, W., and Friml, J. (2010). Emergence of tissue polarization from synergy of intracellular and extracellular auxin signaling. *Mol. Syst. Biol* **6**: 447.

Wabnik, K., Hvidsten, TR., Kedzierska, A., Van Leene, J., De Jaeger, G., Beemster, GT., Komorowski, J. and Kuiper, MT. (2009) Gene expression trends and protein features effectively complement each other in gene function prediction.. *Bioinformatics* **25:** 322-330.

Bibliography

Abas L, Benjamins R, Malenica N, Paciorek T, Wiśniewska J, Moulinier-Anzola JC, Sieberer T, Friml J, Luschnig C (2006) Intracellular trafficking and proteolysis of the *Arabidopsis* auxin-efflux facilitator PIN2 are involved in root gravitropism. *Nat Cell Biol* **8:** 249-256

Altschuler SJ, Angenent SB, Wang Y, Wu LF (2008) On the spontaneous emergence of cell polarity. *Nature* **454**: 886-889.

Alassimone J, Naseer S, Geldner N (2010) A developmental framework for endodermal differentiation and polarity. *Proc Natl Acad Sci U S A* **107**: 5214-5219

Bagnat M, Simons K (2002) Cell surface polarization during yeast mating. *Proc Natl Acad Sci U S A* **99**: 14183-14188

Balla, J, Kalousek, P, Reinöhl, V, Friml, J and Procházka, S (2011) Competitive canalization of PIN-dependent auxin flow from axillary buds controls pea bud outgrowth. *Plant J* **65**: 571-577.

Bainbridge K, Guyomarc'h S, Bayer E, Swarup R, Bennett M, Mandel T, Kuhlemeier C (2008) Auxin influx carriers stabilize phyllotactic patterning. *Genes Dev* **22:** 810-823

Bandyopadhyay A, Blakeslee JJ, Lee OR, Mravec J, Sauer M, Titapiwatanakun B, Makam SN, Bouchard R, Geisler M, Martinoia E, Friml J, Peer WA, Murphy AS (2007) Interactions of PIN and PGP auxin transport mechanisms. *Biochem Soc Trans* **35:** 137-141

Bayer EM, Smith RS, Mandel T, Nakayama N, Sauer M, Prusinkiewicz P, Kuhlemeier C (2009) Integration of transport-based models for phyllotaxis and midvein formation. *Genes Dev* **23:** 373-384

Benjamins R, Scheres B (2008) Auxin: the looping star in plant development. *Annu Rev Plant Biol* **59:** 443-465

Benková E, Bielach A (2010) Lateral root organogenesis - from cell to organ. *Curr Opin Plant Biol* **13**: 677-683

Benková E, Michniewicz M, Sauer M, Teichmann T, Seifertová D, Jürgens G, Friml J (2003) Local, efflux-dependent auxin gradients as a common module for plant organ formation. *Cell* **115:** 591-602

Bennett MJ, Marchant A, Green HG, May ST, Ward SP, Millner PA, Walker AR, Schulz B, Feldmann KA (1996) Arabidopsis AUX1 gene: a permease-like regulator of root gravitropism. *Science* **273:** 948-950

Bennett T, Scheres B (2010) Root development-two meristems for the price of one? *Curr Top Dev Biol* **91**: 67-102

Berleth T, Sachs T (2001) Plant morphogenesis: long-distance coordination and local

patterning. *Curr Opin Plant Biol* **4:** 57-62

Bilsborough GD, Runions A, Barkoulas M, Jenkins HW, Hasson A, Galinha C, Laufs P, Hay A, Prusinkiewicz P, Tsiantis M (2011) Model for the regulation of Arabidopsis thaliana leaf margin development. *Proc Natl Acad Sci U S A* **108***:3424-3429*

Blilou I, Xu J, Wildwater M, Willemsen V, Paponov I, Friml J, Heidstra R, Aida M, Palme K, Scheres B (2005) The PIN auxin efflux facilitator network controls growth and patterning in Arabidopsis roots. *Nature* **433**: 39-44

Boutte Y, Frescatada-Rosa M, Men S, Chow CM, Ebine K, Gustavsson A, Johansson L, Ueda T, Moore I, Jurgens G, Grebe M (2010) Endocytosis restricts Arabidopsis KNOLLE syntaxin to the cell division plane during late cytokinesis. *EMBO J* **29**: 546-558

Braybrook SA, Kuhlemeier C (2010) How a plant builds leaves. *Plant Cell* **22:** 1006-1018

Chapman EJ, Estelle M (2009) Mechanism of auxin-regulated gene expression in plants. *Annu Rev Genet* **43:** 265-285

Chen CL, Gajewski KM, Hamaratoglu F, Bossuyt W, Sansores-Garcia L, Tao C, Halder G (2010) The apical-basal cell polarity determinant Crumbs regulates Hippo signaling in Drosophila. *Proc Natl Acad Sci U S A* **107:** 15810-15815

Chen JG, Shimomura S, Sitbon F, Sandberg G, Jones AM (2001) The role of auxin-binding protein 1 in the expansion of tobacco leaf cells. *Plant J* **28:** 607-617

Chen JG, Ullah H, Young JC, Sussman MR, Jones AM (2001) ABP1 is required for organized cell elongation and division in Arabidopsis embryogenesis. *Genes Dev* **15**: 902-911

Chen Y, Lagerholm BC, Yang B, Jacobson K (2006) Methods to measure the lateral diffusion of membrane lipids and proteins. *Methods* **39**: 147-153

Christenson M (ed) (2000) *Control of morphogenesis in bryophytes*. Cambridge: Cambridge University Press, 199–224pp

Cooke TJ, Poli D, Sztein AE, Cohen JD (2002) Evolutionary patterns in auxin action. *Plant Mol Biol* **49:** 319-338

Cutler SR, Ehrhardt DW, Griffitts JS, Somerville CR (2000) Random GFP::cDNA fusions enable visualization of subcellular structures in cells of Arabidopsis at a high frequency. *Proc Natl Acad Sci U S A* **97**: 3718-3723

Darwin C, Darwin F (1880) *The Power of Movement in Plants*. London, John Murray, 592 pp

De Smet I, Jürgens G (2007) Patterning the axis in plants--auxin in control. *Curr Opin Genet Dev* **17**: 337-343

Decker EL, Frank W, Sarnighausen E, Reski R (2006) Moss systems biology en route: phytohormones in Physcomitrella development. *Plant Biol (Stuttg)* **8:** 397-405

del Pozo JC, Estelle M (1999) The Arabidopsis cullin AtCUL1 is modified by the ubiquitin-related protein RUB1. *Proc Natl Acad Sci U S A* **96:** 15342-15347

Dello Ioio R, Nakamura K, Moubayidin L, Perilli S, Taniguchi M, Morita MT, Aoyama T, Costantino P, Sabatini S (2008) A genetic framework for the control of cell division and differentiation in the root meristem. *Science* **322:** 1380-1384

Dharmasiri N, Dharmasiri S, Estelle M (2005) The F-box protein TIR1 is an auxin receptor. *Nature* **435:** 441-445

Dharmasiri N, Dharmasiri S, Weijers D, Lechner E, Yamada M, Hobbie L, Ehrismann JS, Jurgens G, Estelle M (2005) Plant development is regulated by a family of auxin receptor F box proteins. *Dev Cell* **9:** 109-119

Dharmasiri N, Estelle M (2004) Auxin signaling and regulated protein degradation. *Trends Plant Sci* **9:** 302-308

Dhonukshe P, Aniento F, Hwang I, Robinson DG, Mravec J, Stierhof Y-D, Friml J (2007) Clathrin-mediated constitutive endocytosis of PIN auxin efflux carriers in *Arabidopsis*. *Curr Biol* **17:** 520-527

Dhonukshe P, Huang F, Galvan-Ampudia CS, Mahonen AP, Kleine-Vehn J, Xu J, Quint A, Prasad K, Friml J, Scheres B, Offringa R (2010) Plasma membrane-bound AGC3 kinases phosphorylate PIN auxin carriers at TPRXS(N/S) motifs to direct apical PIN recycling. *Development* **137**: 3245-3255

Dhonukshe P, Tanaka H, Goh T, Ebine K, Mähönen AP, Prasad K, Blilou I, Geldner N, Xu J, Uemura T, Chory J, Ueda T, Nakano A, Scheres B, Friml J (2008) Generation of cell polarity in plants links endocytosis, auxin distribution and cell fate decisions. *Nature* **456:** 962-966

Dhooge A, Govaerts W, Kuznetsov YA (2003) MATCONT: A MATLAB package for numerical bifurcation analysis of ODEs. *Acm T Math Software* **29**: 141-164

Ding Z, Demarsy, E., Galván Ampudia, CS., Łangowski, Ł. , Kleine-Vehn, J., Fan, Y., Morita, MT., Tasaka, M., Offringa, R., Fankhauser, C. and Friml, J. (2011) Light-mediated polarization of an auxin efflux carrier transport for phototropic response in Arabidopsis. *Nat Cell Biol,* in press

Ding Z, Friml J (2010) Auxin regulates distal stem cell differentiation in Arabidopsis roots. *Proc Natl Acad Sci U S A* **107:** 12046-12051

Dolan L (1998) Pointing roots in the right direction: the role of auxin transport in response to gravity. *Genes Dev* **12**: 2091-2095

Dubrovsky JG, Sauer M, Napsucialy-Mendivil S, Ivanchenko MG, Friml J, Shishkova S,

Celenza J, Benková E (2008) Auxin acts as a local morphogenetic trigger to specify lateral root founder cells. *Proc Natl Acad Sci USA* **105:** 8790-8794

Dudu V, Pantazis P, Gonzalez-Gaitan M (2004) Membrane traffic during embryonic development: epithelial formation, cell fate decisions and differentiation. *Curr Opin Cell Biol* **16**: 407-414

Feugier FG, Mochizuki A, Iwasa Y (2005) Self-organization of the vascular system in plant leaves: inter-dependent dynamics of auxin flux and carrier proteins. *J Theor Biol* **236:** 366-375

Feraru E, Feraru MI, Kleine-Vehn J, Martiniere A, Mouille G, Vanneste S, Vernhettes S, Runions J, Friml J (2011) PIN polarity maintenance by the cell wall in Arabidopsis. *Curr Biol* **21:** 338-343

Fischer U, Ikeda Y, Ljung K, Serralbo O, Singh M, Heidstra R, Palme K, Scheres B, Grebe M (2006) Vectorial information for Arabidopsis planar polarity is mediated by combined AUX1, EIN2, and GNOM activity. *Current Biology* **16:** 2143-2149

Friml J, Benkova E, Blilou I, Wisniewska J, Hamann T, Ljung K, Woody S, Sandberg G, Scheres B, Jurgens G, Palme K (2002a) AtPIN4 mediates sink-driven auxin gradients and root patterning in Arabidopsis. *Cell* **108:** 661-673

Friml J, Jones AR (2010) Endoplasmic reticulum: the rising compartment in auxin biology. *Plant Physiol* **154:** 458-462

Friml J, Vieten A, Sauer M, Weijers D, Schwarz H, Hamann T, Offringa R, Jürgens G (2003) Efflux-dependent auxin gradients establish the apical--basal axis of *Arabidopsis*. *Nature* **426:** 147-153

Friml J, Wiśniewska J, Benková E, Mendgen K, Palme K (2002b) Lateral relocation of auxin efflux regulator PIN3 mediates tropism in *Arabidopsis*. *Nature* **415:** 806-809

Friml J, Yang X, Michniewicz M, Weijers D, Quint A, Tietz O, Benjamins R, Ouwerkerk PB, Ljung K, Sandberg G, Hooykaas PJ, Palme K, Offringa R (2004) A PINOID-dependent binary switch in apical-basal PIN polar targeting directs auxin efflux. *Science* **306**: 862-865

Fujita H, Mochizuki A (2006) Pattern formation of leaf veins by the positive feedback regulation between auxin flow and auxin efflux carrier. *J Theor Biol* **241**: 541-551

Fujita T, Hasebe M (2009) Convergences and divergences in polar auxin transport and shoot development in land plant evolution. *Plant Signal Behav* **4:** 313-315

Fujita T, Sakaguchi H, Hiwatashi Y, Wagstaff SJ, Ito M, Deguchi H, Sato T, Hasebe M (2008) Convergent evolution of shoots in land plants: lack of auxin polar transport in moss shoots. *Evol Dev* **10:** 176-186

Galvan-Ampudia CS, Offringa R (2007) Plant evolution: AGC kinases tell the auxin

tale. *Trends Plant Sci* **12:** 541-547

Galweiler L, Guan C, Muller A, Wisman E, Mendgen K, Yephremov A, Palme K (1998) Regulation of polar auxin transport by AtPIN1 in Arabidopsis vascular tissue. *Science* **282**: 2226-2230

Geisler M, Blakeslee JJ, Bouchard R, Lee OR, Vincenzetti V, Bandyopadhyay A, Titapiwatanakun B, Peer WA, Bailly A, Richards EL, Ejendal KF, Smith AP, Baroux C, Grossniklaus U, Muller A, Hrycyna CA, Dudler R, Murphy AS, Martinoia E (2005) Cellular efflux of auxin catalyzed by the Arabidopsis MDR/PGP transporter AtPGP1. *Plant J* **44:** 179-194

Geisler M, Murphy AS (2006) The ABC of auxin transport: the role of p-glycoproteins in plant development. *FEBS Lett* **580**: 1094-1102

Geldner N (2009) Cell polarity in plants: a PARspective on PINs. *Curr Opin Plant Biol* **12**: 42-48

Geldner N, Friml J, Stierhof Y-D, Jürgens G, Palme K (2001) Auxin transport inhibitors block PIN1 cycling and vesicle trafficking. *Nature* **413:** 425-428

Giepmans BN, van Ijzendoorn SC (2009) Epithelial cell-cell junctions and plasma membrane domains. *Biochim Biophys Acta* **1788**: 820-831

Goldsmith MHM, Goldsmith TH, Martin MH (1981) Mathematical analysis of the chemosmotic polar diffusion of auxin through plant tissues. *Proc Natl Acad Sci USA* **78:** 976-980

Gonzali S, Novi G, Loreti E, Paolicchi F, Poggi A, Alpi A, Perata P (2005) A turanose-insensitive mutant suggests a role for WOX5 in auxin homeostasis in Arabidopsis thaliana. *Plant J* **44:** 633-645

Govaerts W, Sautois B (2005) The onset and extinction of neural spiking: a numerical bifurcation approach. *J Comput Neurosci* **18:** 265-274

Gray WM, Kepinski S, Rouse D, Leyser O, Estelle M (2001) Auxin regulates SCF(TIR1)-dependent degradation of AUX/IAA proteins. *Nature* **414:** 271-276

Grieneisen VA, Xu J, Maree AF, Hogeweg P, Scheres B (2007) Auxin transport is sufficient to generate a maximum and gradient guiding root growth. *Nature* **449:** 1008-1013

Grossmann G, Malinsky J, Stahlschmidt W, Loibl M, Weig-Meckl I, Frommer WB, Opekarova M, Tanner W (2008) Plasma membrane microdomains regulate turnover of transport proteins in yeast. *J Cell Biol* **183**: 1075-1088

Grunewald W, Friml J (2010) The march of the PINs: developmental plasticity by dynamic polar targeting in plant cells. *EMBO J* **29:** 2700-2714

Haagen-Smit AJ, Dandliker WB, Wittwer SH, Murneek AE (1946) Isolation of

3-indoleacetic acid from immature corn kernels. *Amer J Bot* **33**: 118-120

Harrison CJ, Roeder AH, Meyerowitz EM, Langdale JA (2009) Local cues and asymmetric cell divisions underpin body plan transitions in the moss Physcomitrella patens. *Curr Biol* **19:** 461-471

Hayashi K, Tan X, Zheng N, Hatate T, Kimura Y, Kepinski S, Nozaki H (2008) Small-molecule agonists and antagonists of F-box protein-substrate interactions in auxin perception and signaling. *Proc Natl Acad Sci U S A* **105:** 5632-5637

Hein B, Willig KI, Hell SW (2008) Stimulated emission depletion (STED) nanoscopy of a fluorescent protein-labeled organelle inside a living cell. *Proc Natl Acad Sci U S A* **105**: 14271-14276

Heisler M, Jonsson H (2006) Modeling auxin transport and plant development. *Journal of Plant Growth Regulation* **25**: 302-312

Heisler MG, Hamant O, Krupinski P, Uyttewaal M, Ohno C, Jonsson H, Traas J, Meyerowitz EM (2010) Alignment between PIN1 polarity and microtubule orientation in the shoot apical meristem reveals a tight coupling between morphogenesis and auxin transport. *PLoS Biol* **8**: e1000516

Heisler MG, Ohno C, Das P, Sieber P, Reddy GV, Long JA, Meyerowitz EM (2005) Patterns of auxin transport and gene expression during primordium development revealed by live imaging of the *Arabidopsis* inflorescence meristem. *Curr Biol* **15:** 1899-1911

Hell SW, Wichmann J (1994) Breaking the diffraction resolution limit by stimulated emission: stimulated-emission-depletion fluorescence microscopy. *Opt Lett* **19**: 780-782

Hellemans J, Mortier G, De Paepe A, Speleman F, Vandesompele J (2007) qBase relative quantification framework and software for management and automated analysis of real-time quantitative PCR data. *Genome Biol* **8**: R19

Huang F, Zago MK, Abas L, van Marion A, Galvan-Ampudia CS, Offringa R (2010) Phosphorylation of conserved PIN motifs directs Arabidopsis PIN1 polarity and auxin transport. *Plant Cell* **22**: 1129-1142

Ibañes M, Fàbregas N, Chory J, Caño-Delgado AI (2009) Brassinosteroid signaling and auxin transport are required to establish the periodic pattern of *Arabidopsis* shoot vascular bundles. *Proc Natl Acad Sci USA* **106:** 13630-13635

Ikeda Y, Men S, Fischer U, Stepanova AN, Alonso JM, Ljung K, Grebe M (2009) Local auxin biosynthesis modulates gradient-directed planar polarity in Arabidopsis. *Nat Cell Biol* **11:** 731-738

Jenkins GI, Courtice GRM, Cove DJ (1986) Gravitropic Responses of Wild-Type and

Mutant Strains of the Moss Physcomitrella-Patens. *Plant Cell Environ* **9:** 637-644

Johri MM, Desai S (1973) Auxin regulation of caulonema formation in moss protonema. *Nat New Biol* **245:** 223-224

Jones AM, Im KH, Savka MA, Wu MJ, DeWitt NG, Shillito R, Binns AN (1998) Auxin-dependent cell expansion mediated by overexpressed auxin-binding protein 1. *Science* **282:** 1114-1117

Jones AR, Kramer EM, Knox K, Swarup R, Bennett MJ, Lazarus CM, Leyser HM, Grierson CS (2009) Auxin transport through non-hair cells sustains root-hair development. *Nat Cell Biol* **11:** 78-84

Jönsson H, Heisler MG, Shapiro BE, Meyerowitz EM, Mjolsness E (2006) An auxin-driven polarized transport model for phyllotaxis. *Proc Natl Acad Sci USA* **103:** 1633-1638

Karwowski R, Prusinkiewicz P (2004) The L-system-based plant-modeling environment L-studio 4.0. In Proceedings of the 4th International Workshop on Functiona-Structural Plant Models, pp 403-405

Kepinski S, Leyser O (2005) Plant development: auxin in loops. *Curr Biol* **15:** R208-210

Kepinski S, Leyser O (2005) The *Arabidopsis* F-box protein TIR1 is an auxin receptor. *Nature* **435:** 446-451

Kidokoro Y (2006) Vesicle trafficking and recycling at the neuromuscular junction: two pathways for endocytosis. *Int Rev Neurobiol* **75**: 145-164

Kleine-Vehn J, Dhonukshe P, Sauer M, Brewer P, Wiśniewka J, Paciorek T, Benková E, Friml J (2008a) ARF GEF-dependent transcytosis and polar delivery of PIN auxin carriers in *Arabidopsis*. *Curr Biol* **18:** 526-531

Kleine-Vehn J, Dhonukshe P, Swarup R, Bennett M, Friml J (2006) Subcellular trafficking of the *Arabidopsis* auxin influx carrier AUX1 uses a novel pathway distinct from PIN1. *Plant Cell* **18:** 3171-3181

Kleine-Vehn J, Ding Z, Jones AR, Tasaka M, Morita MT, Friml J (2010) Gravity-induced PIN transcytosis for polarization of auxin fluxes in gravity-sensing root cells. *Proc Natl Acad Sci U S A* **107:** 22344-22349

Kleine-Vehn J, Friml J (2008) Polar targeting and endocytic recycling in auxin-dependent plant development. *Annu Rev Cell Dev Biol* **24:** 447-473

Kleine-Vehn J, Huang F, Naramoto S, Zhang J, Michniewicz M, Offringa R, Friml J (2009) PIN auxin efflux carrier polarity is regulated by PINOID kinase-mediated recruitment into GNOM-independent trafficking in Arabidopsis. *Plant Cell* **21**: 3839-3849

Kleine-Vehn J, Leitner J, Zwiewka M, Sauer M, Abas L, Luschnig C, Friml J (2008b)

Differential degradation of PIN2 auxin efflux carrier by retromer-dependent vacuolar targeting. *Proc Natl Acad Sci USA* **105:** 17812-17817

Kögl F, Kostermans DGFR (1934) Hetero-Auxin als Stoffwechselprodukt niederer pflanzlicher Organismen. Isolierung aus Hefe. Hoppe Seyler' s *Z Physiol Chem* **228**: 113-121

Kramer EM (2004) PIN and AUX/LAX proteins: their role in auxin accumulation. *Trends Plant Sci* **9:** 578-582

Kramer EM (2006) How far can a molecule of weak acid travel in the apoplast or xylem? *Plant Physiol* **141**: 1233-1236

Kramer EM (2008) Computer models of auxin transport: a review and commentary. *J Exp Bot* **59**: 45-53

Kramer EM (2009) Auxin-regulated cell polarity: an inside job? *Trends Plant Sci* **14:** 242-247

Kramer EM, Frazer NL, Baskin TI (2007) Measurement of diffusion within the cell wall in living roots of *Arabidopsis thaliana*. *J Exp Bot* **58:** 3005-3015

Křeček P, Skupa P, Libus J, Naramoto S, Tejos R, Friml J, Zažímolová E (2009) The PIN-FORMED (PIN) protein family of auxin transporters. *Genome Biol* **10:** 249

Kuhlemeier C (2007) Phyllotaxis. *Trends Plant Sci* **12**: 143-150

Kwon C, Neu C, Pajonk S, Yun HS, Lipka U, Humphry M, Bau S, Straus M, Kwaaitaal M, Rampelt H, El Kasmi F, Jurgens G, Parker J, Panstruga R, Lipka V, Schulze-Lefert P (2008) Co-option of a default secretory pathway for plant immune responses. *Nature* **451**: 835-840

Langowski L, Ruzicka K, Naramoto S, Kleine-Vehn J, Friml J (2010) Trafficking to the outer polar domain defines the root-soil interface. *Curr Biol* **20**: 904-908

Lau S, Shao N, Bock R, Jurgens G, De Smet I (2009) Auxin signaling in algal lineages: fact or myth? *Trends Plant Sci* **14:** 182-188

Laxmi A, Pan J, Morsy M, Chen R (2008) Light plays an essential role in intracellular distribution of auxin efflux carrier PIN2 in Arabidopsis thaliana. *PLoS One* **3:** e1510

Leblanc N, David K, Grosclaude J, Pradier J-M, Barbier-Brygoo H, Labiau S, Perrot-Rechenmann C (1999) A novel immunological approach establishes that the auxin-binding protein, Nt-abp1, is an element involved in auxin signaling at the plasma membrane. *J Biol Chem* **274:** 28314-28320

Lehnert B, Bopp M (1983) The Hormonal-Regulation of Protonema Development in Mosses .1. Auxin-Cytokinin Interaction. *Z Pflanzenphysiol* **110:** 379-391

Leyser O (2006) Dynamic integration of auxin transport and signalling. *Curr Biol* **16:**

R424-433

Leyser O (2011) Auxin, self-organisation, and the colonial nature of plants. *Curr Biol* **21:** R331-337

Li H, Cheng Y, Murphy A, Hagen G, Guilfoyle TJ (2009) Constitutive repression and activation of auxin signaling in Arabidopsis. *Plant Physiol* **149**: 1277-1288

Li H, Tiwari SB, Hagen G, Guilfoyle TJ (2011) Identical amino Acid substitutions in the repression domain of auxin/indole-3-acetic Acid proteins have contrasting effects on auxin signaling. *Plant Physiol* **155**: 1252-1263

Ljung K, Hull AK, Celenza J, Yamada M, Estelle M, Normanly J, Sandberg G (2005) Sites and regulation of auxin biosynthesis in Arabidopsis roots. *Plant Cell* **17:** 1090-1104

Lomax, TL, Muday, GK and Rubery, P. H., Auxin transport. In Plant Hormones and Their Role in Plant Growth Development, P., J., Davies: Kluwer, Dordrecht, Netherlands, 1995.

Lu H, Bilder D (2005) Endocytic control of epithelial polarity and proliferation in Drosophila. *Nat Cell Biol* **7:** 1232-1239

Luschnig C, Gaxiola RA, Grisafi P, Fink GR (1998) EIR1, a root-specific protein involved in auxin transport, is required for gravitropism in Arabidopsis thaliana. *Genes Dev* **12**: 2175-2187

Marchant A, Kargul J, May ST, Muller P, Delbarre A, Perrot-Rechenmann C, Bennett MJ (1999) AUX1 regulates root gravitropism in Arabidopsis by facilitating auxin uptake within root apical tissues. *EMBO J* **18:** 2066-2073

Martiniere A, Gayral P, Hawes C, Runions J (2011) Building bridges: formin1 of Arabidopsis forms a connection between the cell wall and the actin cytoskeleton. *Plant J* **66:** 354-365

Meinhardt H (1996) Models of biological pattern formation: common mechanism in plant and animal development. *Int J Dev Biol* **40:** 123-134

Men S, Boutte Y, Ikeda Y, Li X, Palme K, Stierhof YD, Hartmann MA, Moritz T, Grebe M (2008) Sterol-dependent endocytosis mediates post-cytokinetic acquisition of PIN2 auxin efflux carrier polarity. *Nat Cell Biol* **10**: 237-244

Merks RMH, Van de Peer Y, Inzé D, Beemster GTS (2007) Canalization without flux sensors: a traveling-wave hypothesis. *Trends Plant Sci* **12:** 384-390

Merks, RMH, Guravage, M, Inzé, D and Beemster, GT (2011) VirtualLeaf: An Open-Source Framework for Cell-Based Modeling of Plant Tissue Growth and Development. *Plant Physiol* **155**: 656-666

Michniewicz M, Zago MK, Abas L, Weijers D, Schweighofer A, Meskiene I, Heisler MG, Ohno C, Zhang J, Huang F, Schwab R, Weigel D, Meyerowitz EM, Luschnig C, Offringa R, Friml J (2007) Antagonistic regulation of PIN phosphorylation by PP2A and PINOID directs auxin flux. *Cell* **130**: 1044-1056

Mitchison GJ (1980) The dynamics of auxin transport. *Proc R Soc Lond B* **209:** 489-511

Mitchison GJ (1981) The Polar Transport of Auxin and Vein Patterns in Plants. *Philos T Roy Soc B* **295**: 461-&

Mravec J, Skupa P, Bailly A, Hoyerova K, Krecek P, Bielach A, Petrášek J, Zhang J, Gaykova V, Stierhof YD, Dobrev PI, Schwarzerova K, Rolcik J, Seifertova D, Luschnig C, Benkova E, Zazimalova E, Geisler M, Friml J (2009) Subcellular homeostasis of phytohormone auxin is mediated by the ER-localized PIN5 transporter. *Nature* **459:** 1136-1140

Munro E, Bowerman B (2009) Cellular symmetry breaking during Caenorhabditis elegans development. *Cold Spring Harb Perspect Biol* **1:** a003400

Napier RM, David KM, Perrot-Rechenmann C (2002) A short history of auxin-binding proteins. *Plant Mol Biol* **49:** 339-348

Nelson KS, Beitel GJ (2009) Cell junctions: lessons from a broken heart. *Curr Biol* **19**: R122-123

Nyman LP, Cutter EG (1981) Auxin-Cytokinin Interaction in the Inhibition, Release, and Morphology of Gametophore Buds of Plagiomnium-Cuspidatum from Apical Dominance. *Can J Bot* **59:** 750-762

Oh Y, Bi E (2011) Septin structure and function in yeast and beyond. *Trends Cell Biol* **21:** 141-148

Okada K, Ueda J, Komaki MK, Bell CJ, Shimura Y (1991) Requirement of the Auxin Polar Transport System in Early Stages of Arabidopsis Floral Bud Formation. *Plant Cell* **3**: 677-684

Orlando K, Sun X, Zhang J, Lu T, Yokomizo L, Wang P, Guo W (2011) Exo-endocytic trafficking and the septin-based diffusion barrier are required for the maintenance of Cdc42p polarization during budding yeast asymmetric growth. *Mol Biol Cell* **22:** 624-633

Ouellet F, Overvoorde PJ, Theologis A (2001) IAA17/AXR3: Biochemical insight into an auxin mutant phenotype. *Plant Cell* **13:** 829-841

Overvoorde P, Fukaki H, Beeckman T (2010) Auxin control of root development. *Cold Spring Harb Perspect Biol* **2**: a001537

Paciorek T, Zažímalová E, Ruthardt N, Petrášek J, Stierhof Y-D, Kleine-Vehn J, Morris DA, Emans N, Jürgens G, Geldner N, Friml J (2005) Auxin inhibits endocytosis and

promotes its own efflux from cells. *Nature* **435:** 1251-1256

Paponov IA, Teale WD, Trebar M, Blilou I, Palme K (2005) The PIN auxin efflux facilitators: evolutionary and functional perspectives. *Trends Plant Sci* **10:** 170-177

Peer WA, Bandyopadhyay A, Blakeslee JJ, Makam SN, Chen RJ, Masson PH, Murphy AS (2004) Variation in expression and protein localization of the PIN family of auxin efflux facilitator proteins in flavonoid mutants with altered auxin transport in *Arabidopsis thaliana*. *Plant Cell* **16:** 1898-1911

Petersson SV, Johansson AI, Kowalczyk M, Makoveychuk A, Wang JY, Moritz T, Grebe M, Benfey PN, Sandberg G, Ljung K (2009) An auxin gradient and maximum in the Arabidopsis root apex shown by high-resolution cell-specific analysis of IAA distribution and synthesis. *Plant Cell* **21:** 1659-1668

Petrášek J, Mravec J, Bouchard R, Blakeslee JJ, Abas M, Seifertová D, Wiśniewska J, Tadele Z, Kubeš M, Čovanová M, Dhonukshe P, Skůpa P, Benková E, Perry L, Křeček P, Lee OR, Fink GR, Geisler M, Murphy AS, Luschnig C, Zažímalová E, Friml J (2006) PIN proteins perform a rate-limiting function in cellular auxin efflux. *Science* **312:** 914-918

Poli DB, Jacobs M, Cooke TJ (2003) Auxin regulation of axial growth in bryophyte sporophytes: Its potential significance for the evolution of early land plants. *Am J Bot* **90:** 1405-1415

Pollmann S, Duchting P, Weiler EW (2009) Tryptophan-dependent indole-3-acetic acid biosynthesis by 'IAA-synthase' proceeds via indole-3-acetamide. *Phytochemistry* **70**: 523-531

Prigge MJ, Lavy M, Ashton NW, Estelle M (2010) Physcomitrella patens auxin-resistant mutants affect conserved elements of an auxin-signaling pathway. *Curr Biol* **20:** 1907-1912

Prusinkiewicz P, Crawford S, Smith RS, Ljung K, Bennett T, Ongaro V, Leyser O (2009) Control of bud activation by an auxin transport switch. *Proc Natl Acad Sci USA* **106:** 17431-17436

Raven JA (1975) Transport of Indoleacetic-Acid in Plant-Cells in Relation to Ph and Electrical Potential Gradients, and Its Significance for Polar Iaa Transport. *New Phytologist* **74**: 163-172

Reinhardt D, Pesce ER, Stieger P, Mandel T, Baltensperger K, Bennett M, Traas J, Friml J, Kuhlemeier C (2003) Regulation of phyllotaxis by polar auxin transport. *Nature* **426:** 255-260

Rensing SA, Lang D, Zimmer AD, Terry A, Salamov A, Shapiro H, Nishiyama T, Perroud

PF, Lindquist EA, Kamisugi Y, Tanahashi T, Sakakibara K, Fujita T, Oishi K, Shin IT, Kuroki Y, Toyoda A, Suzuki Y, Hashimoto S, Yamaguchi K *et al* (2008) The Physcomitrella genome reveals evolutionary insights into the conquest of land by plants. *Science* **319:** 64-69

Robert S, Kleine-Vehn J, Barbez E, Sauer M, Paciorek T, Baster P, Vanneste S, Zhang J, Simon S, Hayashi K, Dhonukshe P, Yang Z, Bednarek SY, Jones AM, Aniento F, Zažímolová E, Friml J (2010) ABP1 mediates auxin inhibition of clathrin-dependent endocytosis in Arabidopsis. *Cell* **143:** 111-121

Rolland-Lagan AG, Prusinkiewicz P (2005) Reviewing models of auxin canalization in the context of leaf vein pattern formation in Arabidopsis. *Plant J* **44:** 854-865

Roppolo D, De Rybel B, Tendon VD, Pfister A, Alassimone J, Vermeer JE, Yamazaki M, Stierhof YD, Beeckman T, Geldner N (2011) A novel protein family mediates Casparian strip formation in the endodermis. *Nature* **473:** 380-383

Rouse D, Mackay P, Stirnberg P, Estelle M, Leyser O (1998) Changes in auxin response from mutations in an AUX/IAA gene. *Science* **279**: 1371-1373

Rubery PH, Sheldrak.Ar (1974) Carrier-Mediated Auxin Transport. *Planta* **118**: 101-121

Rutschow HL, Baskin TI, Kramer EM (2011) Regulation of Solute Flux through Plasmodesmata in the Root Meristem. *Plant Physiol* **155:** 1817-1826

Sabatini S, Beis D, Wolkenfelt H, Murfett J, Guilfoyle T, Malamy J, Benfey P, Leyser O, Bechtold N, Weisbeek P, Scheres B (1999) An auxin-dependent distal organizer of pattern and polarity in the Arabidopsis root. *Cell* **99:** 463-472

Sachs T (1969) Polarity and the induction of organized vascular tissues. *Ann Bot (Lond)* **33**: 263

Sachs T (1981) The control of the patterned differentiation of vascular tissues. *Adv Bot Res* **9:** 151-262

Sahlin P, Söderberg B, Jönsson H (2009) Regulated transport as a mechanism for pattern generation: capabilities for phyllotaxis and beyond. *J Theor Biol* **258:** 60-70

Sakakibara K, Nishiyama T, Sumikawa N, Kofuji R, Murata T, Hasebe M (2003) Involvement of auxin and a homeodomain-leucine zipper I gene in rhizoid development of the moss Physcomitrella patens. *Development* **130:** 4835-4846

Santos F, Teale W, Fleck C, Volpers M, Ruperti B, Palme K (2010) Modelling polar auxin transport in developmental patterning. *Plant Biol (Stuttg) 12 Suppl* **1**: 3-14

Santner A, Calderon-Villalobos LI, Estelle M (2009) Plant hormones are versatile chemical regulators of plant growth. *Nat Chem Biol* **5**: 301-307

Sarkar AK, Luijten M, Miyashima S, Lenhard M, Hashimoto T, Nakajima K, Scheres

B, Heidstra R, Laux T (2007) Conserved factors regulate signalling in Arabidopsis thaliana shoot and root stem cell organizers. *Nature* **446:** 811-814

Sauer M, Balla J, Luschnig C, Wišniewska J, Reinöhl V, Friml J, Benková E (2006) Canalization of auxin flow by Aux/IAA-ARF-dependent feed-back regulation of PIN polarity. *Genes Dev* **20:** 2902–2911

Scarpella E, Barkoulas M, Tsiantis M (2010) Control of leaf and vein development by auxin. *Cold Spring Harb Perspect Biol* **2:** a001511

Scarpella E, Marcos D, Friml J, Berleth T (2006) Control of leaf vascular patterning by polar auxin transport. *Genes Dev* **20:** 1015-1027

Shivas JM, Morrison HA, Bilder D, Skop AR (2010) Polarity and endocytosis: reciprocal regulation. *Trends Cell Biol* **20:** 445-452

Schumaker KS, Dietrich MA (1998) Hormone-Induced Signaling during Moss Development. *Annu Rev Plant Physiol Plant Mol Biol* **49:** 501-523

Sorefan K, Girin T, Liljegren SJ, Ljung K, Robles P, Galvan-Ampudia CS, Offringa R, Friml J, Yanofsky MF, Ostergaard L (2009) A regulated auxin minimum is required for seed dispersal in Arabidopsis. *Nature* **459:** 583-586

Smith C, Prusinkiewicz P, Samavati F (2003) Local specification of surface subdivision algorithms. Lect Notes Comput Sc 3062: 313-327

Smith RS, Guyomarc'h S, Mandel T, Reinhardt D, Kuhlemeier C, Prusinkiewicz P (2006) A plausible model of phyllotaxis. *Proc Natl Acad Sci U S A* **103:** 1301-1306

Stahl Y, Wink RH, Ingram GC, Simon R (2009) A signaling module controlling the stem cell niche in Arabidopsis root meristems. *Curr Biol* **19**: 909-914

Steffens B, Feckler C, Palme K, Christian M, Böttger M, Lüthen H (2001) The auxin signal for protoplast swelling is perceived by extracellular ABP1. *Plant J* **27:** 591-599

Steinmann T, Geldner N, Grebe M, Mangold S, Jackson CL, Paris S, Galweiler L, Palme K, Jurgens G (1999) Coordinated polar localization of auxin efflux carrier PIN1 by GNOM ARF GEF. *Science* **286**: 316-318

Stepanova AN, Robertson-Hoyt J, Yun J, Benavente LM, Xie DY, Dolezal K, Schlereth A, Jurgens G, Alonso JM (2008) TAA1-mediated auxin biosynthesis is essential for hormone crosstalk and plant development. *Cell* **133:** 177-191

Stoma S, Lucas M, Chopard J, Schaedel M, Traas J, Godin C (2008) Flux-based transport enhancement as a plausible unifying mechanism for auxin transport in meristem development. *PLoS Comput Biol* **4**: e1000207

Sundberg E, Ostergaard L (2009) Distinct and dynamic auxin activities during reproductive development. *Cold Spring Harb Perspect Biol* **1**: a001628

Swarup K, Benková E, Swarup R, Casimiro I, Peret B, Yang Y, Parry G, Nielsen E, De

Smet I, Vanneste S, Levesque MP, Carrier D, James N, Calvo V, Ljung K, Kramer E, Roberts R, Graham N, Marillonnet S, Patel K et al (2008) The auxin influx carrier LAX3 promotes lateral root emergence. *Nat Cell Biol* **10:** 946-954

Swarup R, Kargul J, Marchant A, Zadik D, Rahman A, Mills R, Yemm A, May S, Williams L, Millner P, Tsurumi S, Moore I, Napier R, Kerr ID, Bennett MJ (2004) Structure-function analysis of the presumptive Arabidopsis auxin permease AUX1. *Plant Cell* **16:** 3069-3083

Swarup R, Kramer EM, Perry P, Knox K, Leyser HMO, Haseloff J, Beemster GTS, Bhalerao R, Bennett MJ (2005) Root gravitropism requires lateral root cap and epidermal cells for transport and response to a mobile auxin signal. *Nat Cell Biol* **7:** 1057-1065

Takano J, Tanaka M, Toyoda A, Miwa K, Kasai K, Fuji K, Onouchi H, Naito S, Fujiwara T (2010) Polar localization and degradation of Arabidopsis boron transporters through distinct trafficking pathways. *Proc Natl Acad Sci U S A* **107**: 5220-5225

Takeda S, Gapper C, Kaya H, Bell E, Kuchitsu K, Dolan L (2008) Local positive feedback regulation determines cell shape in root hair cells. *Science* **319**: 1241-1244

Tan X, Calderon-Villalobos LI, Sharon M, Zheng C, Robinson CV, Estelle M, Zheng N (2007) Mechanism of auxin perception by the TIR1 ubiquitin ligase. *Nature* **446:** 640-645

Tanaka H, Kitakura S, De Rycke R, De Groodt R, Friml J (2009) Fluorescence imaging-based screen identifies ARF GEF component of early endosomal trafficking. *Curr Biol* **19:** 391-397

Tao Y, Ferrer JL, Ljung K, Pojer F, Hong F, Long JA, Li L, Moreno JE, Bowman ME, Ivans LJ, Cheng Y, Lim J, Zhao Y, Ballare CL, Sandberg G, Noel JP, Chory J (2008) Rapid synthesis of auxin via a new tryptophan-dependent pathway is required for shade avoidance in plants. *Cell* **133**: 164-176

Tepass U, Tanentzapf G, Ward R, Fehon R (2001) Epithelial cell polarity and cell junctions in Drosophila. *Annu Rev Genet* **35:** 747-784

Thimann KV, Skoog F (1933) Studies on the growth hormone of plants. III. The inhibiting action of the growth substance on bud development. *Proc Natl Acad Sci USA* **19:** 714-716

Tiwari SB, Hagen G, Guilfoyle T (2003) The roles of auxin response factor domains in auxin-responsive transcription. *Plant Cell* **15**: 533-543

Tromas A, Braun N, Muller P, Khodus T, Paponov IA, Palme K, Ljung K, Lee J-Y, Benfey P, Murray JAH, Scheres B, Perrot-Rechenmann C (2009) The AUXIN BINDING PROTEIN 1 is required for differential auxin responses mediating root growth.

PLoS One **4:** e6648

Tromas A, Paponov I, Perrot-Rechenmann C (2010) AUXIN BINDING PROTEIN 1: functional and evolutionary aspects. *Trends Plant Sci* **15:** 436-446

Tsukagoshi H, Busch W, Benfey PN (2010) Transcriptional regulation of ROS controls transition from proliferation to differentiation in the root. *Cell* **143**: 606-616

Tyson JJ, Novak B (2008) Temporal organization of the cell cycle. *Curr Biol* **18:** R759-R768

Ulmasov T, Murfett J, Hagen G, Guilfoyle TJ (1997) Aux/IAA proteins repress expression of reporter genes containing natural and highly active synthetic auxin response elements. *Plant Cell* **9:** 1963-1971

Valdez-Taubas J, Pelham HR (2003) Slow diffusion of proteins in the yeast plasma membrane allows polarity to be maintained by endocytic cycling. *Curr Biol* **13**: 1636-1640

Vanneste S, Friml J (2009) Auxin: a trigger for change in plant development. *Cell* **136:** 1005-1016

Vieten A, Vanneste S, Wiśniewska J, Benková E, Benjamins R, Beeckman T, Luschnig C, Friml J (2005) Functional redundancy of PIN proteins is accompanied by auxin-dependent cross-regulation of PIN expression. *Development* **132:** 4521-4531

Wabnik K, Kleine-Vehn J, Balla J, Sauer M, Naramoto S, Reinohl V, Merks RM, Govaerts W, Friml J (2010) Emergence of tissue polarization from synergy of intracellular and extracellular auxin signaling. *Mol Syst Biol* **6:** 447

Wabnik K, Kleine-Vehn J, Govaerts W, and Friml J (2011) Cell-to-cell auxin transport mechanism by intracellular auxin compartmentization, *Trends in Plant Science*, DOI: 10.1016/J.TPLANTS.2011.05.002.

Wabnik K, Govaerts W, Friml J, Kleine-Vehn J, (2011) Feedback models for polar auxin transport: an emerging trend, *Molecular BioSystems,* DOI:10.1039/C1MB05109A.

Wells CD, Fawcett JP, Traweger A, Yamanaka Y, Goudreault M, Elder K, Kulkarni S, Gish G, Virag C, Lim C, Colwill K, Starostine A, Metalnikov P, Pawson T (2006) A Rich1/Amot complex regulates the Cdc42 GTPase and apical-polarity proteins in epithelial cells. *Cell* **125**: 535-548

Went FW (1974) Reflections and Speculations. *Annu Rev Plant Phys* **25**: 1-26

Willemsen V, Friml J, Grebe M, van den Toorn A, Palme K, Scheres B (2003) Cell polarity and PIN protein positioning in Arabidopsis require STEROL METHYLTRANSFERASE1 function. *Plant Cell* **15**: 612-625

Willig KI, Kellner RR, Medda R, Hein B, Jakobs S, Hell SW (2006) Nanoscale resolution in GFP-based microscopy. *Nat Methods* **3**: 721-723

Wiśniewska J, Xu J, Seifertová D, Brewer PB, Růžička K, Blilou I, Rouquié D, Benková E, Scheres B, Friml J (2006) Polar PIN localization directs auxin flow in plants. *Science* **312:** 883

Woodward AW, Bartel B (2005) Auxin: regulation, action, and interaction. *Ann Bot* **95:** 707-735Xu J, Hofhuis H, Heidstra R, Sauer M, Friml J, Scheres B (2006) A molecular framework for plant regeneration. *Science* **311:** 385-388

Xu J, Hofhuis H, Heidstra R, Sauer M, Friml J, Scheres B (2006) A molecular framework for plant regeneration. *Science* **311**: 385-388

Xu J, Scheres B (2005) Dissection of Arabidopsis ADP-RIBOSYLATION FACTOR 1 function in epidermal cell polarity. *Plant Cell* **17**: 525-536

Xu T, Wen M, Nagawa S, Fu Y, Chen JG, Wu MJ, Perrot-Rechenmann C, Friml J, Jones AM, Yang Z (2010) Cell surface- and rho GTPase-based auxin signaling controls cellular interdigitation in Arabidopsis. *Cell* **143:** 99-110

Yang H, Murphy AS (2009) Functional expression and characterization of Arabidopsis ABCB, AUX 1 and PIN auxin transporters in Schizosaccharomyces pombe. *Plant J* **59**: 179-191

Ye ZH (2002) Vascular tissue differentiation and pattern formation in plants. *Annu Rev Plant Biol* **53**: 183-202

Zažímolová E, Murphy AS, Yang H, Hoyerova K, Hosek P (2010) Auxin transporters--why so many? *Cold Spring Harb Perspect Biol* **2:** a001552

Zhang J, Nodzynski T, Pencik A, Rolcik J, Friml J (2010) PIN phosphorylation is sufficient to mediate PIN polarity and direct auxin transport. *Proc Natl Acad Sci U S A* **107**: 918-922

Zhao Y, Yan A, Feijo JA, Furutani M, Takenawa T, Hwang I, Fu Y, Yang Z (2010) Phosphoinositides regulate clathrin-dependent endocytosis at the tip of pollen tubes in Arabidopsis and tobacco. *Plant Cell* **22:** 4031-4044

Zidovetzki R, Levitan I (2007) Use of cyclodextrins to manipulate plasma membrane cholesterol content: evidence, misconceptions and control strategies. *Biochim Biophys Acta* **1768**: 1311 1324

Acknowledgments

I'm all over it now,
And I can't say how glad I am about that…

My four years long PhD journey reaches its final destination. Taking steps in studying plant biology as a bioinformatician/theoretical biologist was from the very beginning difficult and challenging. I came to University of Ghent in Belgium as a naive post-graduate student with strong background in engineering and mathematics but a little knowledge of plant biology. During my research performed at VIB, Plant Systems Biology Department and University of Ghent, I encountered many friendly and inspiring people coming from different research fields and having different scientific expertise. Therefore, I am grateful to all of them for showing me how to approach scientifically challenging problems from various perspectives.

My initial credits go to my first supervisor Martin Kuiper how introduced me to the multidisciplinary field of Systems Biology and Bioinformatics. I thank Torgeir R. Hividsten and Jan Komorowski for giving me much support and sharing their scientific expertise during first two years of my doctoral path. Erick Antezana and Vladimir Mironov for all these fruitful discussion that certainly stimulated and accelerated the progress of my research. I am also very grateful to my second supervisor Roeland Merks that uncovered the modeling curtain and showed me the direction to the truly fascinating and challenging field of auxin biology.

Roughly two years ago, I safely landed in my current research group led by Czech 'king-PIN' - Jiri Friml, and I have been gone through so far the most exiting and inspiring time of my research career. However it is just a beginning, so much awaits to be done…

…I remember well the day in which I met Jiri. By that time I was frustrated by the fact that my two previous supervisors have to leave their labs due to personal reasons so I had to face unexpected problems. Being a fresh plant modeler, I approach Jiri's office with a ray of hope that he could provide me with new home for remaining years of my PhD, and, yes he did!. Especially, I thank you Jiri for this opportunity to work as independent student in your lab that I believe, is a full of great scientific potential. I am grateful for your understanding:) and patience to my mathematical reasoning in biology. I am still learning so many things from you, for instance how to be critical, pragmatic and diplomatic :). Moreover, I would like to thank for the possibility to meet and work back-to-back with your excellent postdocs!, Jurgen, Helen, Zhaojun. Jurgie - you are my scientific soulmate, every discussion we had and every work that we did together was not only fun but a never-ending inspiration. I especially admire your enthusiasm to do science and your healthy scientific criticism. I hope we will join forces in the near future-wish you a lot of luck in your new scientific journey in Vienna. Helen, it is a pleasure to work with you, having all these challenging and stimulating discussions that improved

my biological understanding of plant embryogenesis. Thank you Zhaojun for your willingness to include me in your interesting project, it was extraordinary fun to combine your experiments with my modeling to sharpen some of root-related scientific issues. I am grateful to Eva, Tomek, Stephanie, Steffen, Wim, Elena, Elke, Mugur, Harry, Sathoshi, Yunlong, for friendly and fruitful discussions and their interest in my work. Special thanks go to the polish-czech-slovak community which helped me to feel a bit like home. I would like to give a bunch of thanks to Przemysław Prusinkiewicz, Richard Smith, and Adam Runions, who have suited me with necessary tools to do my research and have tought me not only how to do modeling but also how to use it to approach scientific problems.

I give big credits go to my promoter Willy Govaerts for his constitutive support whatever I faced any mathematical or technical problems. Willy, I am grateful for all discussions that we had and all help I have received from you. Finally I would like to thank all members of my PhD panel for their efforts and willingness to evaluate this thesis - I am truly honoured.

Chciałbym złożyć wielkie podziękowania mojej pięknej, przyszłej żonie Ani za jej pomoc, nadzwyczajną kuchnie i nigdy nie gasnące wsparcie!!! Jak również całej mojej rodzinie za wsparcie i doping, bez Was osiągnięcie stopnia pierwszego doktora w rodzinie:) nie byłoby możliwe!